STUDY OF FERROMAGNETIC LIQUID

By R.E. Rosensweig and R. Kaiser

March 1967

Prepared under Contract No. NASW-1219 by
AVCO CORPORATION
Space Systems Division
Wilmington, Massachusetts

Office of Advanced Research and Technology

NATIONAL AERONAUTICS AND SPACE ADMINISTRATION

ABSTRACT

The existence of a strongly ferromagnetic fluid (ferrofluid) offers possibilities of a multitude of technological applications. This work describes studies in the synthesis and modification of stable colloidal dispersions with strong magnetic response and Newtonian viscosity. It proves possible to produce magnetic fluid that is characterized by a saturation magnetization greater than 700 gauss concomitant with a viscosity that is less than 30 centistokes. Determination is made of magnetization versus applied field, viscosity at various temperatures and fluid compositions, particle size and size distribution, surface tension, and other physical parameters. The experimental data are inter-correlated and yield estimates of various physicochemical parameters. Modification by reversible flocculation-peptization and other means yields ferromagnetic fluids with accented properties. An instability phenomenon is encountered when a uniform magnetic field is applied normal to the surface of the more highly magnetic fluids. A linearized perturbation analysis satisfactorily predicts critical parameters characterizing the transition of the smooth fluid surface to a new equilibrium state in which the surface possesses small scale deflections having a definite periodicity.

CONTENTS

CONTENTS (Cont'd)

CONTENTS (Cont'd)

CONTENTS (Cont'd)

CONTENTS (Concl'd)

LIST OF FIGURES

LIST OF FIGURES (Cont'd)

LIST OF FIGURES (Cont'd)

LIST OF FIGURES (Cont'd)

LIST OF FIGURES (Cont'd)

LIST OF FIGURES (Concl'd)

LIST OF TABLES

LIST OF TABLES (Cont'd)

LIST OF TABLES (Cont'd)

LIST OF TABLES (Concl'd)

STUDY OF FERROMAGNETIC LIQUID

by Ronald E. Rosensweig and Robert Kaiser

Avco Corporation

Wilmington, Massachusetts

SUMMARY

The existence of a strongly ferromagnetic fluid offers a multitude of technological applications. Any device or process utilizing ordinary liquids must be reconsidered in the knowledge that magnetic forces may be induced in the medium.

Utilizing the technique of grinding ferrites in hydrocarbon media in the presence of a surfactant, colloidal dispersions are produced having ferromagnetic properties simultaneous with Newtonian fluid behavior even in the presence of an applied magnetic field. The studied variables include length of grinding time, colloid formation amount, nature of the initial magnetic powder, nature of dispersant material and its concentration, nature of carrier fluid, and equipment effects. Over 60 long term grinds are conducted with durations from 120 to 2900 hours in tests involving over 25 different dispersants. A technique of sedimentation testing is developed for efficient selection of the surfactant material.

Successful colloids are produced with oleic acid, Aerosol OT, Aerosol TR, Tenlo 70, aluminum naphthanate, dodecylamine, and other dispersants. Data are reported of the amount of colloid formed as a function of time. The buildup of colloid concentration follows an s-shaped curve which is interpreted by a simple grinding law. The translation of saturation magnetization from bulk solid to property of the ferromagnetic fluid varies from 35 to 99 percent.

The most highly magnetic fluid is characterized by a saturation magnetization of more than 700 gauss concomitant with viscosity less than 30 centistokes. Volumetric loading of the solid, magnetic constituent is as high as 20 percent.

It is found that the addition of an excess of a polar solvent that is miscible with the carrier fluid results in flocculation in which particles separate from the liquid phase. After separation of the solids from the

supernatant, it is observed that the solids redisperse spontaneously (peptize) in fresh solvent in a number of cases. It is thus possible to isothermally concentrate the colloid and interchange the carrier solvent. Other means studied for the modification of the ferrofluids include ultracentrifugation and magnetodialysis.

Magnetic properties are determined as a function of the applied field and also of temperature. Initial permeability is found to be mainly a function of the saturation magnetization with the permeability ranging between 1 and 3 times that of a vacuum.

Study is also devoted to viscosity relationships, thermal stability, surface tension, and particle size by electron microscopy. Colloid prepared by electrodeposition into mercury is characterized.

Concomitant with the production of the very highly magnetic fluids a striking phenomenon is observed, the surface instability of the fluid in the presence of a uniform magnetic field. A linearized perturbation analysis is presented which satisfactorily predicts the critical parameters.

Finally, the present state-of-the-art is reviewed and goals are established for future research in magnetic fluids.

INTRODUCTION

This is a report on continuing work under contract with the National Aeronautics and Space Administration to provide research in the synthesis and characterization of ferrohydrodynamic fluids.

The ferrohydrodynamic fluids (ferrofluids) are strongly polarizable, extremely stable dispersions of magnetic media in a fluid carrier. In the presence of magnetic fields these fluids experience appreciable forces which then give rise to a number of unique fluid-dynamic and fluid-static phenomena. These phenomena, in turn, are of broad interest in instrumentation, energy conversion, medical neurosurgery, frictionless bearings, ferrofluid characterization, and other applications.

The ferrofluids, which are colloidal suspensions, are a far different material from the magnetic clutch materials of the 1940's. These were suspensions of fairly large (micron) sized particles in oil, and proved useful in clutches, brakes, and dashpots, because their viscosities were highly dependent upon the applied magnetic field. Ferrofluids, by contrast, are produced with very fine (submicron) sized particles so as to retain their fluid properties under all applied fields and field gradients.

Experience with ordinary colloids teaches that particles that are sufficiently fine can be suspended indefinitely in a liquid even though the particles' specific gravity differs greatly from that of the liquid. The mechanism that makes this possible is Brownian motion -- the random thermal agitation produced by impact with molecules of the fluid. Should the particles be magnetic, however, there is an energy of attraction to be overcome if they are not to flocculate and then settle. Although calculations made on colloidal phenomena often suffer from considerable uncertainty, it is nonetheless worthwhile by way of review to sketch a rough picture. Quantitative treatment of the theory of the colloid stabilization mechanism is given in reference 1.

To begin with, the magnetic energy of uniformly magnetized, tangent spheres (which the particles will be taken to be) is proportional to the square of the magnetization and to the cube of the particle radius. Thus, by making the particles very small, the magnetic flocculating effect is reduced. At some size, then, thermal agitation alone should prevent flocculation -- provided that the magnetic energy is less than the thermal energy kT (where k is the Boltzmann constant, and T is the absolute temperature). Computations show that particles 25 to 100 angstroms in diameter should be stable on this basis, for the range of magnetic materials available. Calculation of the sedimentation equilibrium for particles of this size show also that even a magnetic force field cannot separate the particles from the fluid. (Such a field can, however, create a particle density gradient much the way the earth's gravitational field helps create such a gradient in the atmosphere.)

However, there is another factor that looms in the realm of particles as small as those in ferrofluids. This is the attractive van der Waals force, whose origin is the attraction of a fluctuating electric dipole for a neighboring induced dipole. According to London's model, the energy for two distant particles is proportional to the inverse sixth power of distance. For equal sized spheres, this attractive energy equals the thermal energy kT when the two surfaces are about one sphere radius apart -- a result which is valid for any size sphere. As the spheres approach each other closer than this, the attractive energy increases rapidly, and theoretically becomes very large upon contact. Hence, to avoid flocculation, it becomes essential to prevent such close approach of the particles.

It turns out that the necessary separation can be achieved by coating each particle during its manufacture, with an elastic cushion which thus acts as a dispersing agent. This was effectively the approach taken by Papell of NASA in his early work on ferrofluids (refs. 2 and 3). The ferromagnetic particles are produced by tumbling ferrite materials with steel balls in the

presence of a carrier fluid such as kerosene which has dissolved in it a dispersing agent such as oleic acid. During the course of this program we have further studied this technique and have learned how to increase the magnetic strength of the fluid by a factor of nearly 10 while incorporating flexibility in the choice of magnetic solid, carrier fluid, and dispersant material.

The presently reported studies mainly address the topics of ferrofluid preparation, the modification of a ferrofluid once prepared, and characterization of ferrofluid properties. Inferences concerning the microscopic structure of the material are presented which are based on the factual information, largely of a quantitative nature, which is evolved from the experimental program. A bibliography is included as a guide to related studies which have already reached the stage of publication.

Acknowledgments

At the outset, special appreciation is due Mr. Macon Ellis of NASA Langley Research Center for his active encouragement of this work at the initial stage.

Avco's seminal interest in synthesizing a ferromagnetically responsive liquid originated with the energy conversion concept of E. L. Resler and R. E. Rosensweig. Since ferromagnetism is unknown in true liquids it was decided at an early stage to attempt the dispersion of tiny, solid, ferromagnetic particles in a liquid medium. During the course of an experimental and theoretical quest for a magnetic liquid the discovery of Mr. S. Stephen Papell, of NASA Lewis Research Center came to the fore. By means of the size reduction technique, Papell had been able to produce the material that was envisioned. Most important to the energy conversion work, the technique readily lent itself to incorporation of alternate component materials. This is to acknowledge the helpful communication at the time of the preprogram effort.

A major fascination of this work has been the occasional appearance of a totally unexpected phenomenon. A prime example is the spontaneous instability of a magnetic fluid interface in the presence of a normally applied magnetic field. The interface becomes stabilized at another equilibrium configuration which displays a regular pattern of "liquid spikes". The theoretical treatment of the phenomenon is developed in this report. The theoretical treatment is adapted from original work of Martin D. Cowley, Visiting Associate Professor at the Massachusetts Institute of Technology, while the experimental confirmation represents a collaborative effort. A

corresponding theory of the phenomenon seems inherent in the monograph of James R. Melcher (ref. 4), see his category MH-I interaction.

Finally, it is noted that Dr. John W. Nestor contributed invaluably to the establishment of an operative laboratory as well as in other respects while Mr. Norman Sheppard was of great assistance throughout all experimental aspects of the program.

PREPARATION OF NONMETALLIC FERROFLUIDS BY GRINDING

Ferrofluids consisting of stable colloidal suspensions of a ferrite in kerosene have been produced in tests by ball milling the ferrite and kerosene mixture in the presence of a suitable surfactant. The objectives of the grinding tests were to produce a wide number of magnetic fluid types for further testing, characterization, and general use. At the same time these tests yielded quantitative information concerning the effect of process parameters on the rate of colloid formation in successful grinds.

The Grinding Technique

Laboratory Equipment. - The laboratory grinding operations were performed in nine mill jar facilities operated in conjunction with an equal number of ball mills, electric timers, and ancillary equipment including a vented sound proof enclosure. The jars were standard, baffled stainless steel jars manufactured by Paul Abbe Inc. Jars of nominal 4.7 pint and 1.6 gallon capacity were used in these studies. They were operated, as is standard in grinding practice, at about 60 percent of critical speed, the rotational speed at which the centrifugal force acting on the charge is equal to its weight.

In addition, a high speed laboratory Szegvari attritor was also used. The attritor consists of an upright, stationary cylindrical water-jacketed grinding tank filled with small steel balls, as in a regular ball mill. However, in the attritor, agitation is supplied by six arms attached at right angles to a vertical rotating shaft which is centralized in the grinding tank. The rotation of these arms agitates the ball charge, which in turn, provides the continuous shearing action necessary for dispersion.

The specifications of the grinding equipment are presented in table 1.

TABLE 1. – GRINDING EQUIPMENT USED

Manufacturer	Manufacturer's designation	Outside dimensions		Nominal capacity	Size of balls, inches	Total ball load		rpm
		Height, inches	Diameter, inches			Weight, pounds	Volume of mill, percent	
Paul Abbe	S.S. Specimen Jar	5.50	5.13	4.7 pt.	1/4 to 1/2[a]	16	50	90
Paul Abbe	S.S. Assay Jar	9.00	8.75	1.6 gal.	1/4 to 1/2[a]	32	50	60
Union Process Inc.	Szegvari Attritor Research Model 01	4.0	3.0	600 cm^3	3/16	---	50	0 to 500

[a]Ball size distribution, in. | Weight, %

one-half | 7.8

three-eighths | 15

one-quarter | 7

Procedure and Analysis. - Premeasured quantities of carrier liquid, stabilizing agent and magnetic powder were charged to a ball mill that was half filled with carbon-steel balls. This mixture was then subjected to continuous grinding.

Unless otherwise indicated a standard starting quantity of ingredients was used in each piece of equipment, as indicated in table 2.

TABLE 2. – THE INGREDIENTS OF STANDARD FERROFLUIDS

Grinding facility	Magnetic powder, grams	Carrier liquid, cc	Surfactant, cc
Large mill	200	1250	100
Small mill	100	625	50
Attritor	40	300	20

The mixture was sampled periodically to determine the rate of colloid formation.

In-process analysis consisted of the removal of a 15 cc sample which was then centrifuged in an International Clinical Centrifuge for 10 minutes, at 5100 rpm. This nominally removed all particles greater than 1000 Å. The density and the saturation magnetization of the supernatant liquid were then measured. This gave an indication of the cumulative amount of solids present in the liquid. The sample was returned to the vessel after analysis.

Grinding was allowed to proceed until it became evident that further grinding would not result in a further change in fluid properties. The jar was then removed from the mill and emptied.

Three criteria were used to stop a run:

i. If there was no measurable colloid formation within the first few hundred hours. In this case, the product was discarded.

ii. If the volumetric loading of solids in suspension reached a plateau indicating that substantially all the solid material charged to the mill had been reduced to colloidal dimensions. In this case the raw suspension was centrifuged with a Lourdes LCA-1 Centrifuge that provided the 17 000 g

acceleration necessary to remove particles larger than 350 Å in nominal diameter. The resulting product was a primary ferrofluid which could then be modified by techniques such as evaporation to produce fluids of varying physical properties.

iii. If the material had been transformed into a gel which would not liquify by addition of further liquid or dispersing agent. In this case a sample was saved, the rest of the material being discarded.

Parameters Studied. - In preprogram tests, ferrofluids had been formed by grinding magnetite in the presence of kerosene and oleic acid in a ball mill. This was the point of departure for these studies. Here, the parameters investigated include nature of the surfactant used, nature of the solid being ground, viscosity and nature of the solvent, concentration effects, and equipment effects. A list of runs is presented in tables 3 and 4.

Hydrocarbon Base Ferrofluids

Selection of Dispersants by Screening Techniques. - A screening technique was developed that would permit selection of favorable combinations of solid/solvent/surfactant that would result in a stable ferromagnetic dispersion when ground in a ball mill. Such a technique is needed because of the long period of time required in the mill before any measurable effects become apparent.

Any technique chosen had to be rapid and as experimentally simple as possible. It had to be applicable to the raw materials as received now used in the synthesis of the ferrofluids.

Fortunately, the ferromagnetic powders that are used (magnetite, ferrites, metal powders) as starting materials are already finally divided when received. These materials range in particle size from about 0.1 μ to 5 μ in diameter. This is the range of most paint pigments. A technique now being used in paint technology to characterize the state of dispersion of a pigment in a solvent was therefore given consideration.

The effect of a number of surfactants on the sedimentation of magnetite in kerosene was scheduled in 50 ml color comparison tubes. One-half gram of synthetic magnetite (Pfizer IRN 100, Lot 1207) with a surface area of 12.5 m^2/gram was dispersed in 50 ml of kerosene which contains about 0.015 gram of surfactant. The powder was used as received from the

TABLE 3. – SERIES OF GRINDING RUNS

Key to Comments

I. Successful ferrofluid formed with initial mixture of ingredients

II. Successful ferrofluid formed with the addition of extra carrier liquid to break transient gel formation

III. Successful ferrofluid formed with the addition of extra surfactant to break transient gel formation

IV. Successful ferrofluid formation with the addition of extra surfactant and carrier liquid to break gel formation

V. Unsuccessful run, initial colloid formation followed by formation of intractable gel

VI. Unsuccessful run, no initial colloid formation

A. Strong fluid formed $M_s > 150$ gauss

B. Medium fluid formed $75 < M_s < 150$ gauss

C. Weak fluid formed $M_s < 75$ gauss

TABLE 3

TABLE 3. – (Cont'd)

Charge	Carrier fluid	Dispersant	Dispersant formula	Magnetic powder	Time	Comments*
G-1 through G-12 1.6 gal	Kerosene	Oleic acid (0.5 cc/gm solids)	$CH_3(CH_2)_7CH{=}CH(CH_2)_7COOH$	Magnetite $FeO \cdot Fe_2O_3$	3 to 6 weeks	IIC Production Runs
G-13 4.7pint	Kerosene	Oleic acid (0.5 cc/gm solids)	$CH_3(CH_2)CH{=}CH(CH_2)_7COOH$	Iron, Fe	1220 hrs	IC
G-14 4.7 pint	Kerosene	Emulphor EL-620 (0.5 cc/gm solids)	Polyoxyethylated vegetable oil	Iron, Fe		VI
G-15 1.6 gal	Heptane	Oleic acid (0.5 cc/gm solids)	$CH_3(CH_2)_7CH{=}CH(CH_2)_7COOH$	Magnetite, $FeO \cdot Fe_2O_3$	4 weeks	IA
G-16 1.6 gal	Heptane	Caproic acid (0.5 cc/gm solids)	$CH_3(CH_2)_4COOH$	Magnetite $FeO \cdot Fe_2O_3$	4 weeks	VI
G-17 4.7 pint	Kerosene	10-undecenoic acid (0.5 cc/gm solids)	$CH_2{=}CH(CH_2)_8COOH$	Magnetite $FeO \cdot Fe_2O_3$	3 days	VI

*See key at end of table.

Table 3 cont

TABLE 3. – (Cont'd)

Charge	Carrier fluid	Dispersant	Dispersant formula	Magnetic powder	Time	Comments
G-18 4.7 pint	Kerosene	Sorbic acid (0.5 cc/gm solids)	$CH_3CH=CHCH=CHCOOH$	Magnetite $FeO \cdot Fe_2O_3$	4 days	VI
G-19 4.7 pint	n-octane	Octanoic acid (0.5 cc/gm solids)	$CH_3(CH_2)_6COOH$	Magnetite $FeO \cdot Fe_2O_3$	8 weeks	V
G-20 4.7 pint	Kerosene	Ethylhexanoic acid (0.5 cc/gm solids)	$CH_3(CH_2)_3CH(C_2H_5)COOH$	Magnetite $FeO \cdot Fe_2O_3$	6 weeks	VI
G-21 1.6 gal	Kerosene	Oleic acid (0.25 cc/gm solids)	$CH_3(CH_2)_7CH=CH(CH_2)_7COOH$	Magnetite $FeO \cdot Fe_2O_3$	2726 hrs	IVA
G-22 1.6 gal	Kerosene	Oleic acid (0.25 cc/gm solids)	$CH_3(CH_2)_7CH=(CH_2)_7COOH$	Manganese-zinc ferrite Curie temp. 90 to 100° C	12 weeks	IC
G-23 4.7 pint	Water	Perfluoro-octanoic acid (0.5 gm/gm solids)	$CF_3(CF_2)_6COOH$	Magnetite $FeO \cdot Fe_2O_3$	5 days	VI

Table 3 Cont'd

TABLE 3. – (Cont'd)

Charge	Carrier fluid	Dispersant	Dispersant formula	Magnetic powder	Time	Comments
G-24 1.6 gal	Kerosene	Oleic acid (1.0 cc/gm solids)	$CH_3(CH_2)_7CH=CH(CH_2)_7COOH$	Manganese-zinc ferrite Curie temp. 90 to 100° C	10 weeks	II
G-25 4.7 pint	Water	Trifluor-acetic acid (0.5 cc/gm solids)	CF_3COOH	Magnetite $FeO \cdot Fe_2O_3$	10 days	VI
G-26 4.7 pint	Kerosene	Oleic acid (0.5 cc/gm solids)	$CH_3(CH_2)_7CH=CH(CH_2)_7COOH$	Magnetite (Wright Industries)	2629 hrs.	IA
G-27 4.7 pint	Water	Cobalt Sulfate (1.0 gm salt/gm solid)	$CoSO_4.7H_2O$	Magnetite $FeO.Fe_2O_3$	4 weeks	VI
G-28 4.7 pint	Kerosene	Cobalt sulfate (1 gm/gm solids)	$CoSO_4.7H_2O$	Magnetite $FeO.Fe_2O_3$	4 weeks	VI

Table 3 Cont'd

TABLE 3. – (Cont'd)

Charge	Carrier fluid	Dispersant	Dispersant formula	Magnetic powder	Time	Commnets
G-29 4. 7 pint	Heptane	FC-170 (0. 05 cc/gm solids)	---	Magnetite $FeO \cdot Fe_2O_3$	1 week	VI
G-30 4. 7 pint	Kerosene	Oleic acid (0. 5 cc/gm solids)	$CH_3(CH_2)_7CH=CH(CH_2)_7COOH$	Magnetite $FeO \cdot Fe_2O_3$	16 weeks	IA
G-31a 4. 7 pint	Dow-Corning 510 silicone fluid; 50 centistokes	---	---	Magnetite $FeO. Fe_2O_3$	1100 hrs	VI
G-31b 4. 7 pint	---	Union Carbide A 1100γ-amino-propyl triethoxy-silane. Add 35 grams	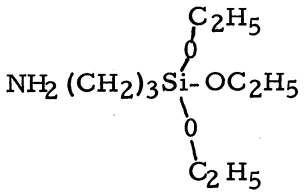	Magnetite $FeO. Fe_2O_3$	300 hrs	VI
G-32 1. 1 gal	Kerosene	(Aerosol OT) Sodium di-2-ethyl-hexyl sulfosuccinate (0. 5 gm/gm solids)	$CH_2COOCH_2CH(C_2H_5)(CH_2)_3CH_3$ $CH_2COOCH_2CH(C_2H_5)(CH_2)_3CH_3$ SO_3Na	Manganese-zinc ferrite Curie temp. 90 to 100° C	12 weeks	V

TABLE 3 CONT

TABLE 3. – (Cont'd)

Charge	Carrier fluid	Dispersant	Dispersant formula	Magnetic powder	Time	Comments
G-33 1.6 gal	Kerosene	(Aerosol AY) Sodium diamyl sulfosuccinate (0.5 gm/gm solids)	$CH_2COO\ C_5H_{11}$ $CH\ COO\ C_5H_{11}$ SO_3Na	Manganese-zinc ferrite Curie temp 90 to 100° C	12 weeks	V
G-34 1.6 gal	Kerosene	(Aerosol MA) Sodium dihexyl sulfosuccinate (0.5 gm/gm solids)	$CH_2COOC_6H_{13}$ $CH\ COOC_6H_{13}$ SO_3Na	Manganese-zinc ferrite Curie temp 90 to 100° C	11 weeks	V
G-35 1.6 gal	Water	Cerous nitrate (0.25 gm/gm solids)	$Ce(NO_3)_3 \cdot 6H_2O$	Magnetite $FeO \cdot Fe_2O_3$	2 weeks	VI
G-36 1.6 gal	15 - 10 Octane decane mixture	(Aerosol OT) sodium di-2-ethyl-hexyl sulfosuccinate (0.5 gm/gm solids)	$CH_2COOCH_2CH(C_2H_5)(CH_2)_3CH_3$ $CH\ COOCH_2CH(C_2H_5)(CH_2)_3CH_3$ SO_3Na	Magnetite $FeO \cdot Fe_2O_3$	1000 hrs	V
G-37 1.6 gal	Oleic acid	---	---	Magnetite $FeO \cdot Fe_2O_3$	5 weeks	VI

TABLE 3. – (Cont'd)

Charge	Carrier fluid	Dispersant	Dispersant formula	Magnetic powder	Time	Comments
G-38 1.6 gal	Kerosene	(Aerosol MA) Sodium dihexyl sulfosuccinate (0.5 gm/gm solids)	$CH_2COOC_6H_{13}$ $CH\ COOC_6H_{13}$ SO_3Na	Magnetite $FeO \cdot Fe_2O_3$	5 weeks	V
G-39 1.6 gal	Dow-Corning 510 silicone fluid; 50 centistokes	Pentacosanoic acid (0.05 gm/gm solids)	$CH_3(CH_2)_{23}COOH$	Magnetite $FeO \cdot Fe_2O_3$	4 weeks	VI
G-40 1.6 gal	Decane	Oleic acid (0.5 cc/gm solids)	$CH_3(CH_2)_7CH=CH(CH_2)_7COOH$	Magnetite $FeO \cdot Fe_2O_3$	2000	IIB
G-41 1.6 gal	Kerosene	Octadecylamine (0.175 gm/gm solids) will add to 0.35 gm/gm	$CH_3(CH_2)_{16}CH_2NH_2$	Magnetite $FeO \cdot Fe_2O_3$	2500 hrs	IVC
G-42A 4.7 pint	Kerosene	---	---	Magnetite $FeO \cdot Fe_2O_3$	800 hrs	VI

TABLE 3 CONT.

TABLE 3. – (Cont'd)

Charge	Carrier fluid	Dispersant	Dispersant formula	Magnetic powder	Time	Comments
G-42B 4.7 pint	Kerosene	Oleic acid added to G-42A at 0800 hrs (0.5 cc/gm solids)	---	Magnetite $FeO \cdot Fe_2O_3$	1450 hrs	IVC
G-43 4.7 pint	Kerosene	Aerosol OT sodium di-2-ethyl-hexyl-sulfosuccinate (aqueous) (0.50 cc aq/ gm solids)	$CH_2COOCH_2CH(C_2H_5)(CH_2)_3CH_3$ $CH\ COOCH_2\ CH(C_2H_5)(CH_2)_3CH_3$ SO_3Na	Manganese-zinc ferrite Curie temp. 90 to 100° C	2175 hrs	IVC small amounts of water have no effect on process
G-44 1.6 gal	Kerosene	Tenlo 70 (0.5 cc/gm solids)	Oil soluble nonionic surfactant. Condensation product of an amino ester of a fatty acid	Magnetite $FeO \cdot Fe_2O_3$	1475 hrs	IA
G-45 1.6 gal	Kerosene	Soya lecithin (0.5 cc/gm solids)	Phosphorous-containing lipide	Magnetite $FeO \cdot Fe_2O_3$	1500 hrs	V
G-46 1.6 gal	Kerosene	Span 80 (sorbitan monooleate (0.5 cc/gm solids)	$OCH\ CH_2OCO(CH_2)_7CH=$ $CH(CH\ )_7\ CH_3(CHOH)_3CH_2$	Magnetite $FeO \cdot Fe_2O_3$	1920 hrs	IV

TABLE 3 cont'd

TABLE 3. – (Cont'd)

Charge	Carrier fluid	Dispersant	Dispersant formula	Magnetic powder	Time	Comments
G-47 4.7 pint	Kerosene	Aerosol TR (sodium di-tridecyl-sulphosuc-cinate)	$CH_2COOC_{13}H_{27}$ $CHCOOC_{13}H_{27}$ SO_2Na	Magnetite $FeO.Fe_2O_3$	2492 hrs	IA Fluid thickened upon stand-ing
G-48 1.6 gal	Kerosene	Tenlo 70 (0.5 cc/gm solids)	Oil soluble nonionic surfactant, condensation product of an amino ester of a fatty acid	Manganese-zinc ferrite curie temp. 90 to 100° C	4447 hrs	IIC
G-49 1.6 gal	Kerosene	Dodecylamine (0.4 gm/gm solids)	$CH_3(CH_2)_{11}NH_2$	Magnetite $FeO\cdot Fe_2O_3$	3639 hrs	IC Short chain sur-factant used.
G-50 1.6 gal	Kerosene	Aluminum naphthanate (0.4 gm/gm solids)	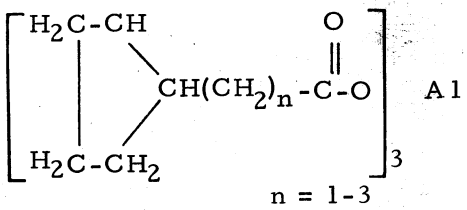 A1 n = 1-3	Magnetite $FeO.Fe_2O_3$	3219 hrs	IIC
G-51 1.6 gal	Kerosene	Oleic acid (1.0 cc/gm solids)	$CH_3(CH_2)_7CH{=}CH(CH_2)_7COOH$	Magnetite $FeO.Fe_2O_3$	3088 hrs	IIA
G-52	Open number					

Table 3

TABLE 3. – (Concl'd)

Charge	Carrier fluid	Dispersant	Dispersant formula	Magnetic powder	Time	Comments
G-53 1.6 gal	Kerosene (deoxy-genated)	Tenlo 70 (0.5 cc/gm solids)	See G-48	Carbonyl iron	---	IC decomposition of surfactant noted
G-54	Open number					
G-55 4.7 pint	Kerosene	Octylamine (0.5 cc/gm solids)	$CH_3(CH_2)_7NH_2$	Magnetite $FeO.Fe_2O_3$	879 hrs	VI

TABLE 4. – ATTRITOR GRINDS

Test No.	Carrier fluid	Carrier quantity, cc	Solid	Amount Solids, gm	Dispersant	Dispersant formula	Dispersant quantity	Attritor speed, rpm	Cumulative time of grind, hours	Comments
A-7	Decane	365	Lodex* Fe-Co round	50.0	Oleic acid	$CH_3(CH_2)_7 CH = CH(CH_2)_7 COOH$	25 cc	450	360	Gel which broke into nonmagnetic fluid
A-9	Toluene	300	Magnetite	50.0	Aluminum stearate	$[CH_3-(CH_2)_{16}-C-0]_3 AL$	25 gm	450	120	Nonmagnetic
A-10	Kerosene	300	Magnetite	50.0	Oleic acid	See A-7	25 cc	450	120	Magnetic fluid
A-11	Kerosene	300	Magnetite	50.0	Oleic acid	See A-7	25 cc	505	360	Magnetic fluid
A-12	Kerosene	240	Vitro $Fe_2 0_3$	40.0	Oleic acid	See A-7	20 cc	450	672	Magnetic fluid magnetization peaked at about 360 hrs
A-13	Kerosene	240	Vitro $Fe_2 0_3$	40.0	Oleic acid	See A-7	20 cc	450	366	Repeat of A-12 stopped run at peak magnetization
A-14	Fluorolube FS-5	240	Magnetite	40	Perfluoro-octanoic acid	$CF_3-(CF_2)_6 COOH$ (isomer mixture)	40 gm	450	120	Nonmagnetic
A-16	Perfluoro tributyl amine	240	Magnetite	40	Perfluoro-octanoic acid	See A-14	40 gm	450	120	Nonmagnetic

*Registered trademark General Electric Co.

manufacturer. Kerosene used was of reagent grade. No particular drying steps were taken. Each tube was shaken by hand individually one-hundred times and then placed in a tube rack. To compare surfactants, in order to have comparable agitation, the whole rack was shaken by hand by lifting it on arc motion twenty-five times over the operator's head. A board was placed across the top of the tubes to prevent them from falling out. The rack was then placed on a table while the powder settled to the bottom of the tubes. The relative degrees of dispersion were determined qualitatively by observing the opacity of the solution in the different tubes.

The photograph in figure 1 was taken about 5 to 10 minutes after shaking. The tubes contained the additives described in table 5.

TABLE 5 – IDENTIFICATION OF SPECIMENS IN SEDIMENTATION TESTS ILLUSTRATED IN FIGURE 3

1. Blank	No additive
2. Brij 92	Polyoxyethylene (2) oleyl ether (Atlas Chem.)
3. Octanoic acid	---
4. Span 80	Sorbitan mono-oleate (Atlas Chem.)
5. Tween 80	Polyoxyethylene (20) sorbitan mono-oleate (Atlas Chem.)
6. Oleic acid	---
7. Oleic acid	0.1 gm surfactant
8. Lanolin	---
9. Aerosol OT	Sodium di-2-ethyl-hexyl sulfosuccinate
10. Aerosol MA	Sodium di-hexyl sulfosuccinate
11. Aerosol TR	Sodium di-tridecyl sulfosuccinate
12. Brij 98	Polyoxyethylene (20) oleyl ether (Atlas Chem.)

Figure 1. – Sedimentation Tests Illustrating the Variation of Opacity with Nature of the Dispersant Species.
(The dispersants are identified in the text.)

FIG 1

By far, the best results were obtained with Aerosol OT (Tube 9). This additive appears to be a very effective dispersant. Some dispersion was also obtained with Span 80 (Tube 4), Aerosol TR (Tube 11), and oleic acid of the higher concentration. Lesser dispersion was obtained with Brij 98 and Aerosol MA. Poor dispersion was obtained with the Blank, which settled rapidly, Brij 92, octanoic acid, oleic acid at the low level, and lanolin.

Grinding tests had been previously performed on magnetite-kerosene mixtures which contained no additive, Aerosol OT, Aerosol MA, Aerosol TR, oleic acid and octanoic acid. Good magnetic fluids were obtained with Aerosol OT, Aerosol TR and oleic acid. Poor results were obtained with no surfactant and octanoic acid. Intermediate results were obtained with Aerosol MA.

Based on the above, there is a correlation between these simple dispersion tests and the long term grinding tests. Additives that result in good dispersion of the powder generally resulted in stable colloidal suspensions.

The effect of concentration of Aerosol OT on the dispersion of the suspensions was also studied. The levels studied were zero, 0.004, 0.012, 0.024, 0.072, 0.12, 0.24, 0.50, and 1.30 grams Aerosol OT per 0.50 gram of magnetite in 50 cc of kerosene. All the solutions which contained any additive were much stabler than the blank. There appeared to be very little effect of surfactant concentration except for the solution which contained 1.3 gm. It could be that the settling of coarser aggregates was masked by the intense color caused by the dispersed particles. These results do indicate that Aerosol OT is an effective dispersant in very small concentrations. At the lowest level added (0.004 gm/0.50 gm powder), Aerosol OT would be present at a surface concentration of about 130 $\AA^2$/molecule, if all absorbed. This is less than monomolecular coverage.

Further sedimentation tests on magnetite suspensions were carried out, using an Erlenbach reciprocating agitator to disperse magnetite particles in a systematic and reproducible fashion. (See figure 2.) In these tests, 1.0 gram of standard magnetite (IRN 100) was added to 65 cc liquid which contained a predetermined amount of surface agent in an 8 x 1 inch flat bottom test tube which was then stoppered. Twenty tubes were then placed on the shaker. The tubes were shaken for 1 hour at 280 cycles/min. The tubes were removed from the shaker as quickly as possible, placed in a vertical rack and the rate of settling of magnetite was then observed.

Tests were carried out with magnetite-kerosene suspensions in the presence of numerous surfactants. The results are listed in table 6.

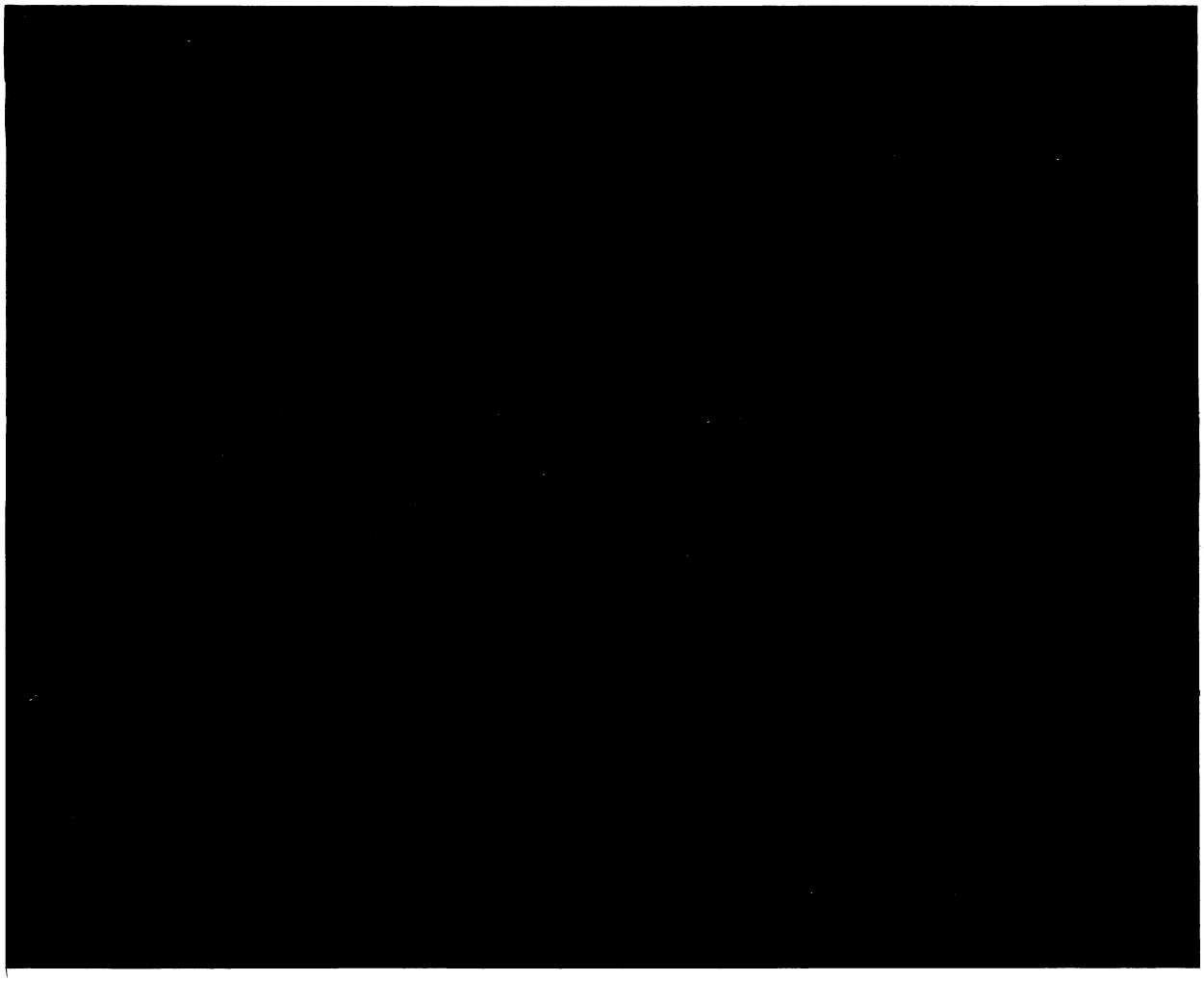

Figure 2. – Reciprocating Agitator Employed in Screening Tests to Determine Candidate Dispersing Agents for Various Magnetic Powders and Carrier Liquid Combinations

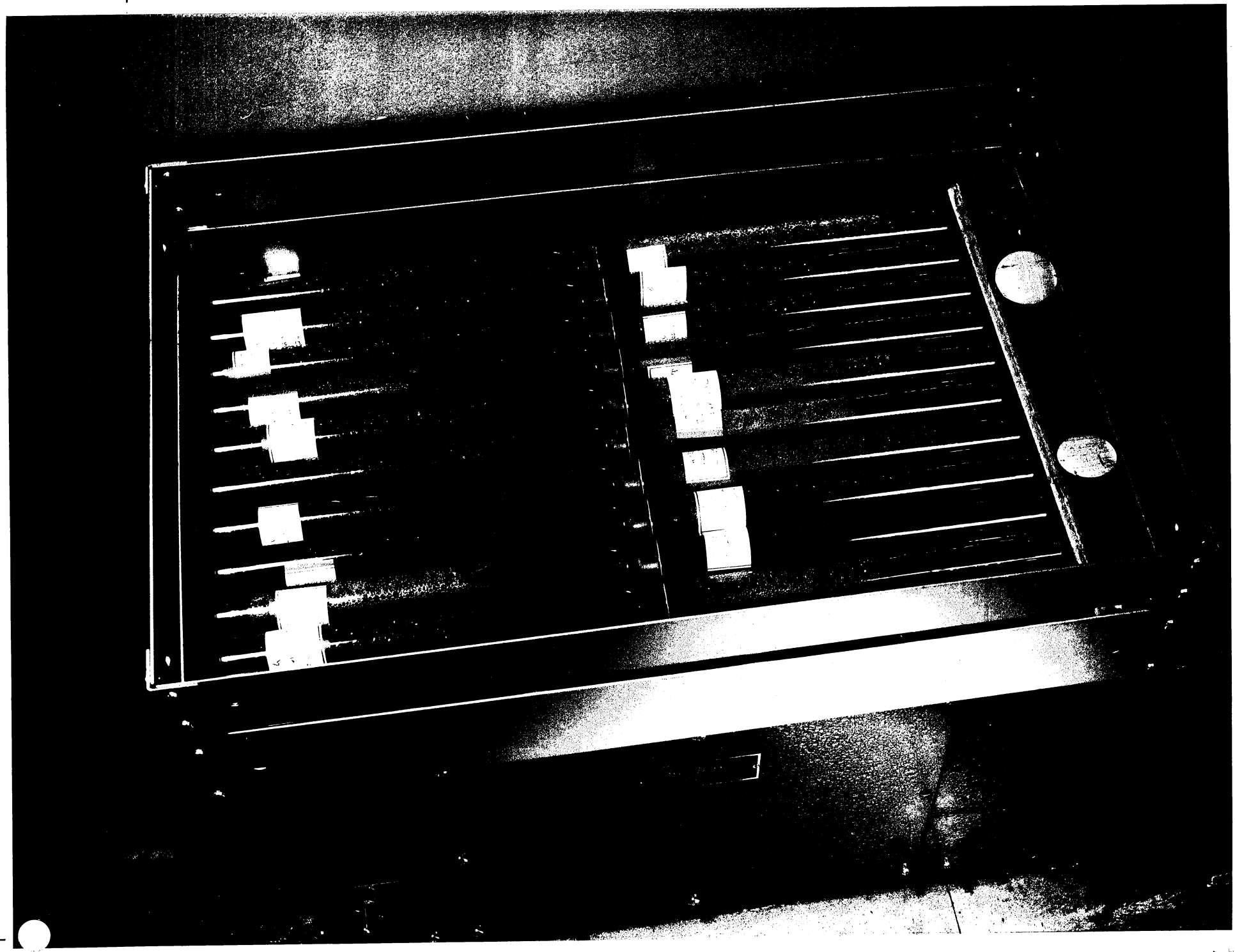

FIGURE 2 Pg 23

FIG 2

TABLE 6. – FURTHER SEDIMENTATION SCREENING TESTS IN KEROSENE SOLVENT

Sample No.	Surfactant	Amount added	Poor	Good	Excellent
A-1	Lecithin	0.05 gm			x
A-2	Sodium lauryl sulfate	.05 gm	x		
A-3	Sodium stearate	.05 gm		x	
A-4	Sodium alkyl-aryl Sulfonate	.05 gm		x	
A-5	Sodium laurate	.05 gm	x		
A-6	Sodium oleate	.05 gm	x		
A-7	Aluminum stearate	.05 gm	x		
A-8	Aluminum oleate	.05 gm		x	
A-9	Aluminum naphthanate	.10 gm			x
A-10	Aluminum naphthanate	.05 gm		x	
A-11	Hexadecyl trimethyl ammonium bromide	.05 gm	x		
A-12	Hexadecylamine	.05 gm		x	
A-13	Dodecylamine	.05 gm		x	
A-14	Octadecylamine	.05 gm			x
A-15	Arquad 2 HT-100 (Armour)	.05 gm	x		
A-16	Aerosol TR (American Cyanamid)	.05 gm		x	
A-17	Aerosol OT (American Cyanamid)	.05 gm		x	
A-18	EDTA (Ethylenediamine tetra acetic acid)	.05 gm	x		
A-19	Trisodium nitrilotriacetate, monohydrate (NTA)	.05 gm	x		
A-20	Blank	---	x		
A-21	Cobalt naphthanate (6% solution)	1.00 cc		x	
A-22	Calcium naphthanate (4% solution)	1.6 cc		x	

TABLE 6. (Concl'd)

Sample No.	Surfactant	Amount added	Poor	Good	Excellent
A-23	Lead naphthanate (24% solution)	0.30 cc		x	
A-24	Zinc naphthanate (8% solution)	.80 cc		x	
A-25	Tenlo 70 (Nopco Chem.)	.08 cc			x
A-26	Oleic acid	.07 cc		x	
A-27	Oleic acid	.22 cc		x	
A-28	10-undecenoic acid	.07 cx	x		
A-29	10-undecenoic acid	.22 cc	x		
A-30	Blank	---	x		
A-31	L-79 Silicone (Union Carbide Chem)	.10 cc	x		
A-32	Brij 98, 5% solution[a] (Atlas Chem)	1.0 cc	x		
A-33	Tween 80, 5% solution[a] (Atlas Chem)	1.0 cc	x		
A-34	Brij 92, 5% solution[a] (Atlas Chem)	1.0 cc	x		
A-35	Span 80, 5% solution[a] (Atlas Chem)	1.0 cc		x	
A-36	Octanoic acid, 5% solution[a]	1.0 cc	x		
A-37	Linoleic acid	0.07 cc		x	
A-38	Caproic acid	.07 cc	x		
A-39	Proprionic acid	.07 cc	x		
A-40	Di-2-ethyl-hexyl phosphoric acid	.07 cc	x		

[a]In kerosene

Settling time of less than 2 minutes = poor.

Settling time of less than 5 minutes = good.

Settling time of more than 5 minutes = excellent.

A family of chemicals that appear to be good suspending agents are the heavy metal naphthanates (A-9, A-10, A-21, A-24). There is an increased settling time which was especially noticeable with aluminum naphthanate, especially at a level of 0.10 gram of additive. The fatty amines (A-12 to A-15) also appear to be good suspending agents, as are the fatty acids, oleic acid, and linoleic acid.

A number of miscellaneous compounds such as lecithin, Tenlo 70, Span 80, and the Aerosols OT and TR appeared quite satisfactory. They are all products with high lipophile values.

The ionized surfactants in general do not appear to be good suspending agents. This is not surprising in that they should have a limited solubility in a nonpolar solvent such as kerosene. The cationics were represented by quarternary ammonium compounds (A-11, A-15, and A-31). The anionics were represented by sodium salts of a number of fatty acids. In this case, there was some variation in settling time. In general, settling time increased with increasing chain length of the organic part of the molecules. Sodium laurate was less effective than sodium stearate. This will vary with molecular structure since sodium oleate is also a very poor stabling agent.

All the short chain compounds, including EDTA (A-18), NTA (A-19), and the carboxylic acids of shorter chain lengths (A-28, A-29, A-36, A-38, and A-39) were poor suspending agents.

Other compounds that were not satisfactory were Brij 92 and Brij 98 (A-32 and A-34) and di-2-ethyl-hexyl phosphoric acid.

As two general groups from these tests, the fatty amines and the heavy metal naphthanates appear to be promising candidate surfactants.

Grinding Tests with Different Surfactants. - There was no colloid formation unless a proper stabilizing agent was present. Grinding magnetite in kerosene without any additives (G-42a) did not result in colloid formation. Grinding magnetite in a number of hydrocarbons in the presence of small organic molecules such as caproic acid (G-16) octanoic acid (G-19) ethyl hexanoic acid (G-20), 10-undecanoic acid (G-17), sorbic acid (G-18) and octylamine (G-55), did not result in the formation of ferrofluid. Similarly inorganic salts as exemplified by cobalt sulfate heptahydrate (G-28) were not satisfactory stabilizing agents. Neither was a commercial perfluorinated surfactant FC-170, manufactured by Minnesota Mining and Manufacturing Company (G-29).

Additives that resulted in stable colloid formation in magnetic solid/hydrocarbon systems were all polar organic molecules that contained at least 12 carbon atoms that are soluble in the hydrocarbon. This is a necessary but not sufficient characteristic since some compounds which have this characteristic structure did not yield colloids. Thus, grinding tests in the presence of saturated straight chain carboxylic acids were not successful. In tests preliminary to this program, it was found that lauric acid (CH_3-$(CH_2)_{10}COOH$) and stearic acid (CH_3-$(CH_2)_{16}$-COOH) yielded little or no colloid. Similar poor results were obtained with aluminum stearate in kerosene (A-9).

Successful results were obtained with 18 unsaturated carbon fatty acids. Thus oleic acid and linoleic acid both resulted in magnetite based ferrofluids in preprogram tests. Oleic acid was used in this series of tests as a standard grinding agent.

A number of magnetic-solid hydrocarbon-solvent oleic-acid runs were carried out to study the effects of the different solids, solvents, equipment and concentration of surfactant on the rate of formation and properties of ferrofluids. These will be discussed in subsequent sections. In addition a standard magnetite-oleic acid-kerosene mixture was used in a series of production runs in order to have sufficient material for general evaluation (G-1 to -12).

Referring to Run G-42, it had been previously pointed out that no magnetic colloid had formed after eight hundred hours of grind. At this point, oleic acid was then added (0.5 cc oleic acid/gram of magnetite) with the subsequent formation of colloid dispersion.

It should also be noted that grinding in pure oleic acid (Run G-37) does not result in the formation of a colloidal dispersion.

A class of surfactants which resulted in the formation of some colloidal ferrite in the grinding runs were a number of succinic acid derivatives manufactured by American Cyanamid Corp. These were:

Aerosol TR (Sodium di-tridecyl sulfosuccinate)
Aerosol OT (Sodium di - 2-ethyl-hexyl sulfosuccinate)
Aerosol MA (Sodium di-hexyl sulfosuccinate)
Aerosol AY (Sodium diamyl sulfosuccinate)

Aerosol TR formed a ferrofluid (G-47). Aerosol OT, Aerosol MA, and Aerosol AY initially formed a magnetically responsive colloidal suspension. These suspensions later gelled with prolonged grinding (Runs G-32,

-33, -34, -36, -38, and -43). These gels were not broken by the addition of further solvent and the runs were discontinued. Subsequently, however, it was found that further addition of surfactant resulted in the liquification of these gels, yielding a stable colloidal dispersion.

Other surfactants that behaved in an analogous manner were sorbitan monooleate (G-45) (Span 80 manufactured by Atlas Chemical Co) and soya lecithin (G-46) a natural phosphorous containing lipid. In both these cases, there was initial formation of a colloid-containing liquid followed by the formation of a gel that further addition of solvent did not disrupt so the run was discarded. With these two products, it was found that additional surfactant resulted in the liquification of the gel. This gel phenomenon will be discussed in more detail in a later section on the stability of colloidal dispersions.

Dodecylamine (G-49) and octadecylamine (G-41) both produced a stable colloid dispersion. Run G-49 is still in process. The rate of colloid formation is much slower than with oleic acid at an equal concentration. As pointed out before, octylamine (G-55) does not form a stable dispersion. In all three cases a waxy film forms at the surface of the suspensions which upon standing increases in thickness with time. This characteristic is a definite disadvantage.

Excellent results were obtained with Tenlo 70 a proprietary surfactant manufactured by the NOPCO Chemical Corp. This material is a nonionic surfactant used in paint manufacturing as a dispersant. It has been found to be an extremely effective wetting agent for iron oxide pigments in vinyl solutions employed in the manufacture of magnetic inks. Infrared analysis showed the presence of amine and alcohol groups. Tenlo 70 proved to be the dispersant yielding the fastest grinding rates. As discussed in subsequent sections the resulting ferrofluid had good physical properties.

Aluminum naphthanate was also used as a dispersant. This material differs from the surfactant used in that aluminum naphthanate is a gelling agent for hydrocarbons. Run G-50 was started with the standard ratio of components. This mixture formed a gel which was broken by dilution with kerosene. Once this gel was broken, the run resulted in the formation of a colloidal dispersion at a slower rate than oleic acid.

Kinetics of Colloid Formation. - The formation of magnetic colloid as a function of time is presented in figures 3 through 11 as a function of a number of operating parameters:

Figure 3 Effect of Operating Equipment, Using Magnetization as Index of Colloid Formation

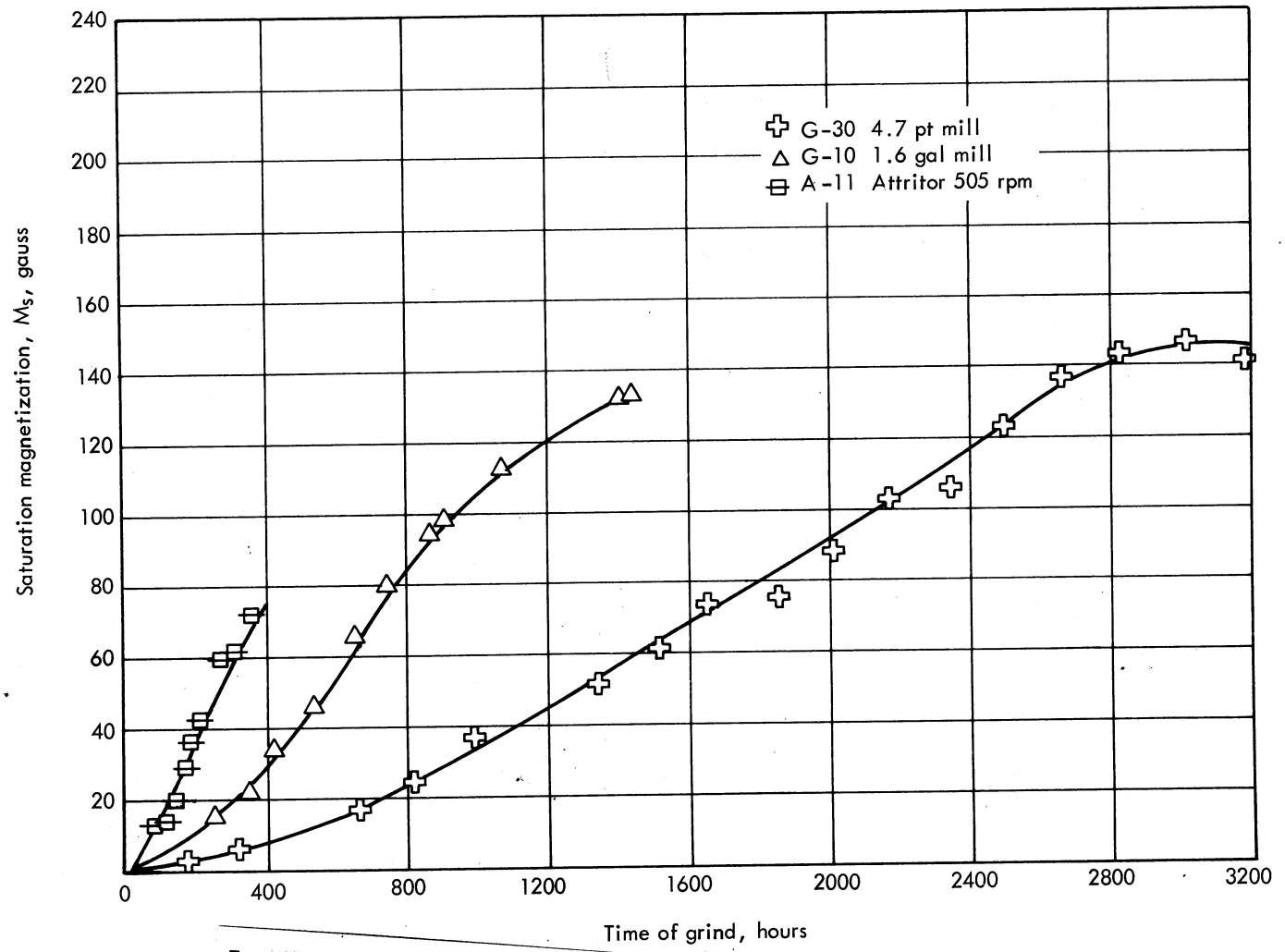

87-2765

Figure 3. – Effect of Operating Equipment, Using Magnetization as Index of Colloid Formation

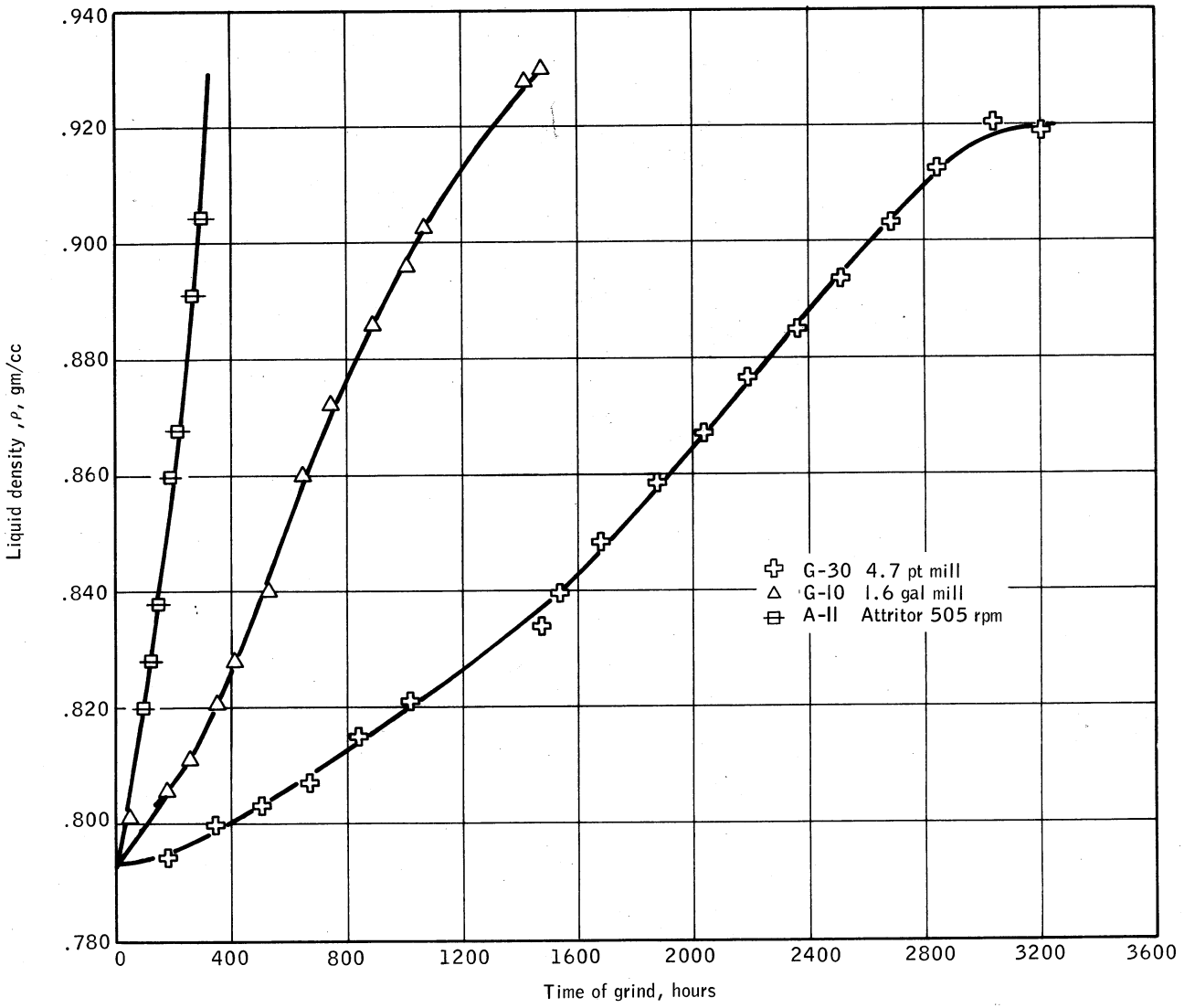

Figure 4. – Effect of Operating Equipment, Using Liquid Density as Index of Colloid Formation

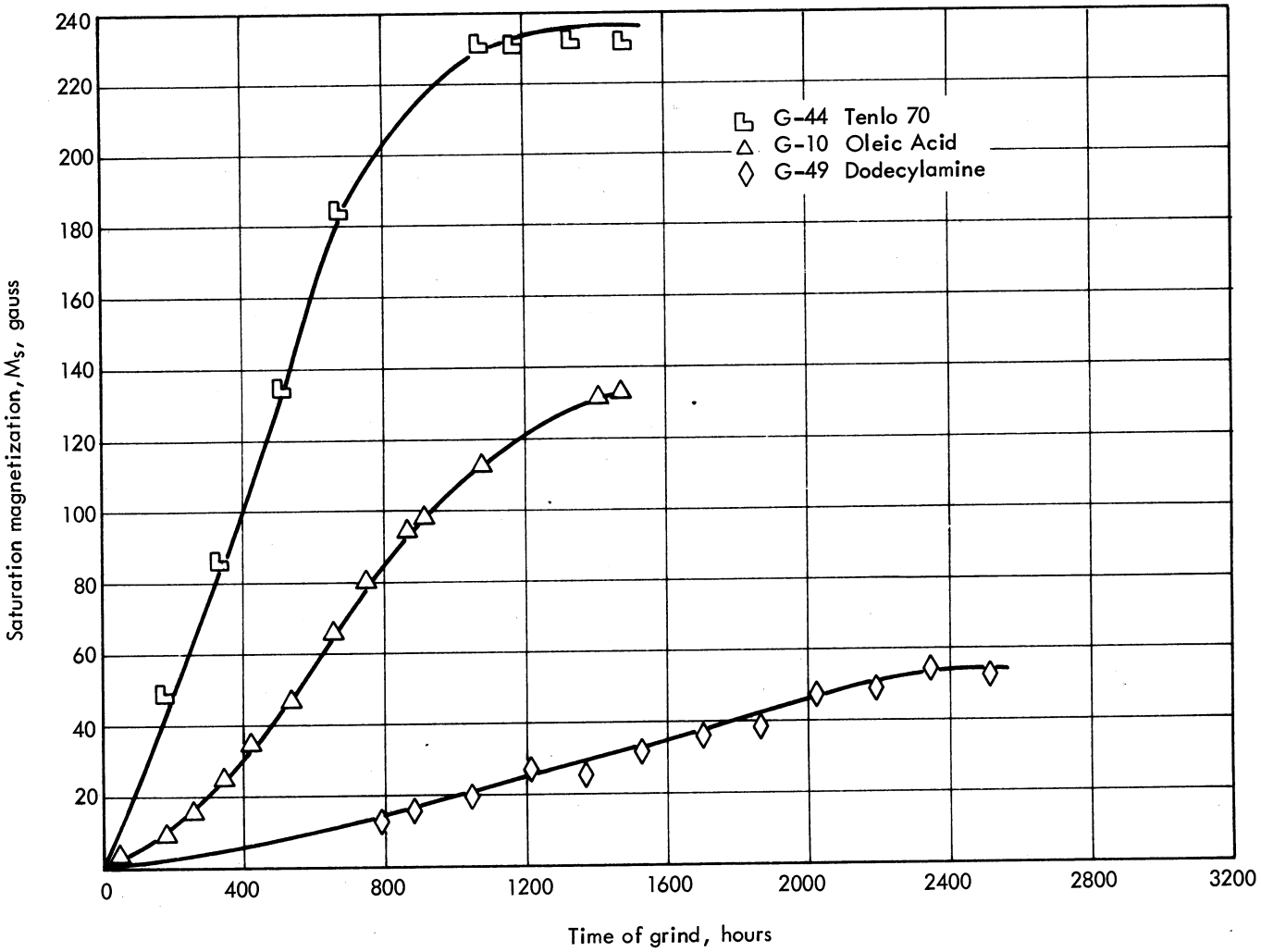

87-2767

Figure 5. – Effect of Surfactant Type, Using Magnetization as Index of Colloid Formation

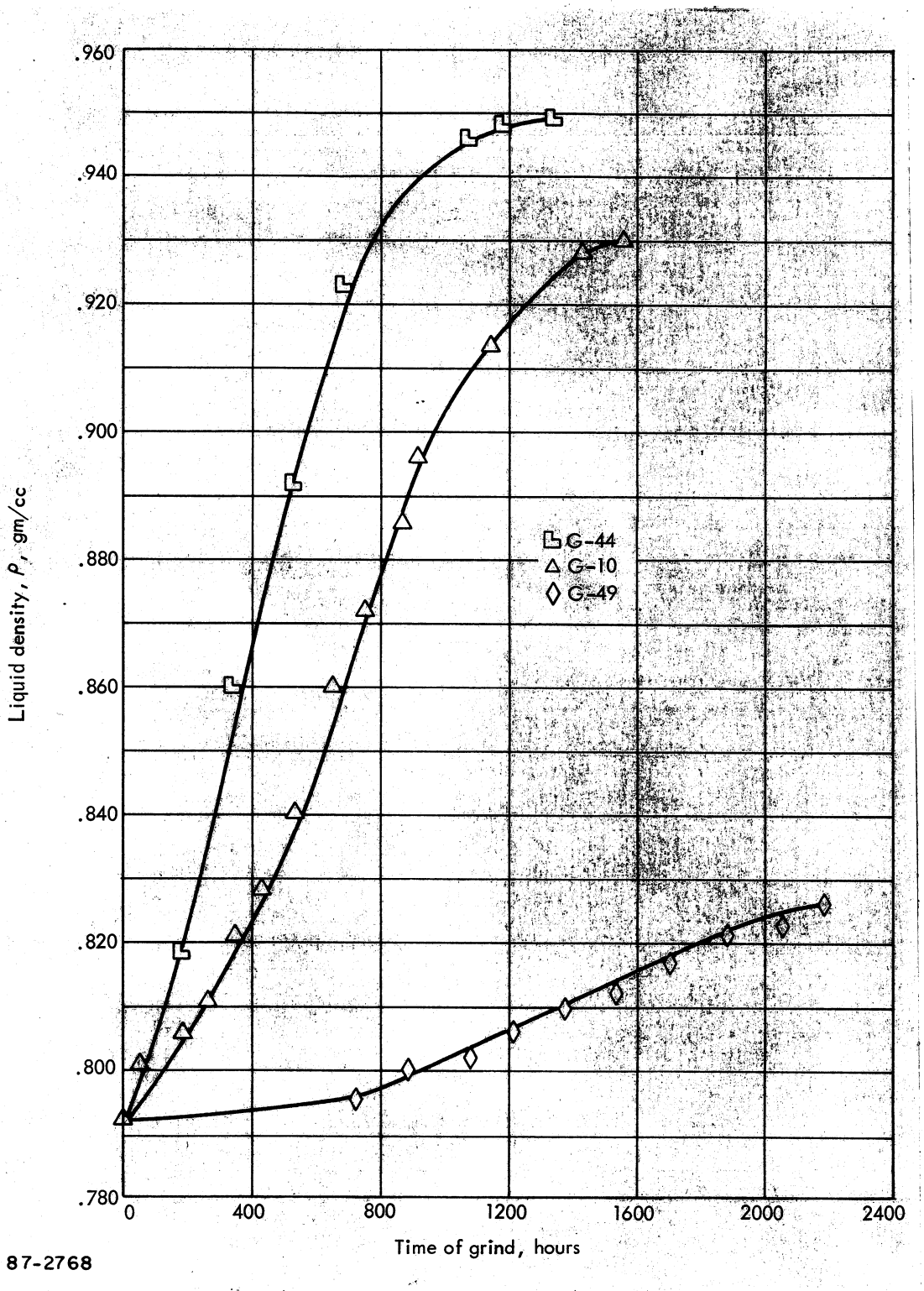

Figure 6. – Effect of Surfactant Type, Using Liquid Density as Index of Colloid Formation

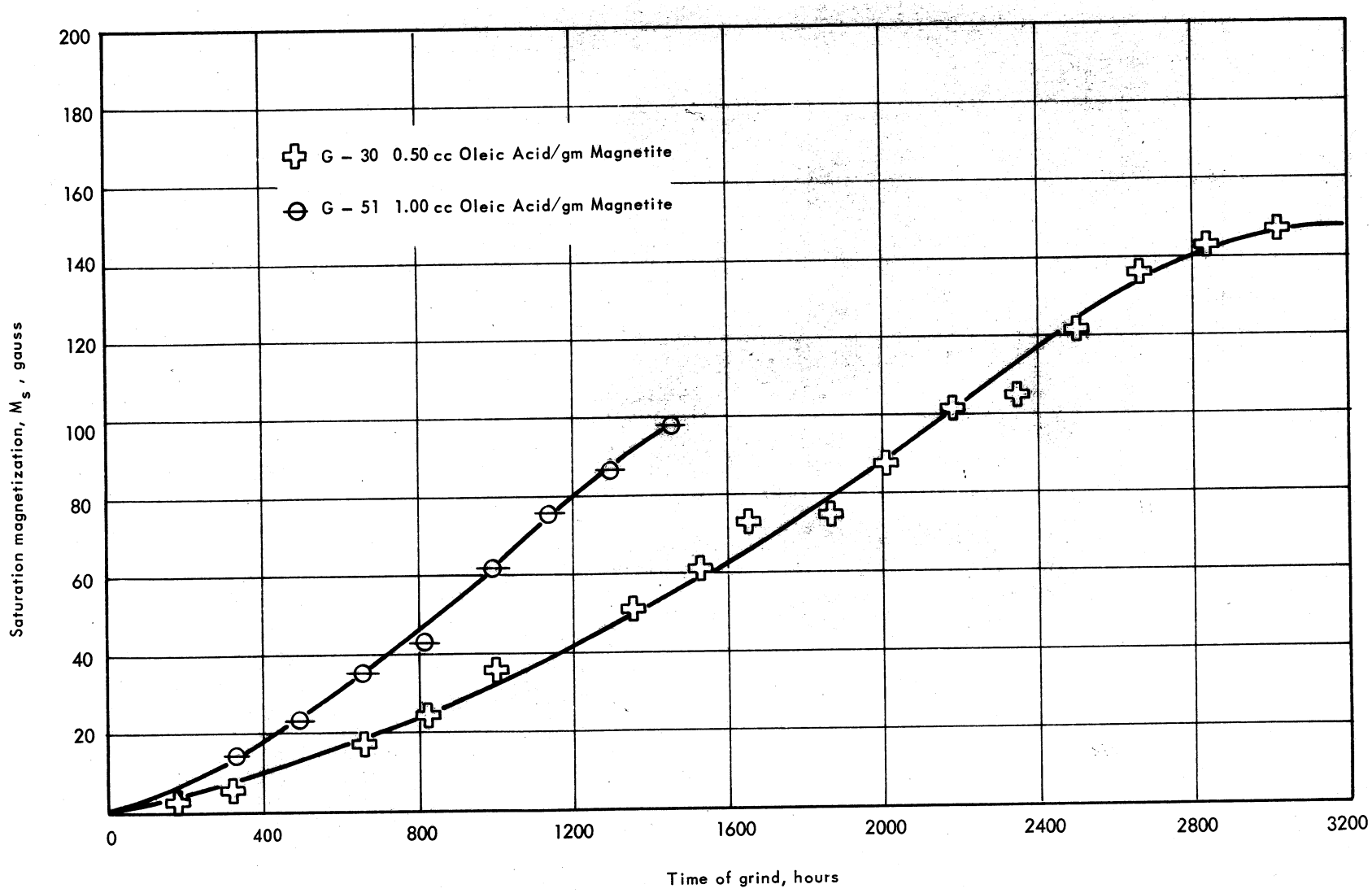

87-2769

Figure 7. – Effect of Surfactant Concentration, Using Magnetization as Index of Colloid Formation

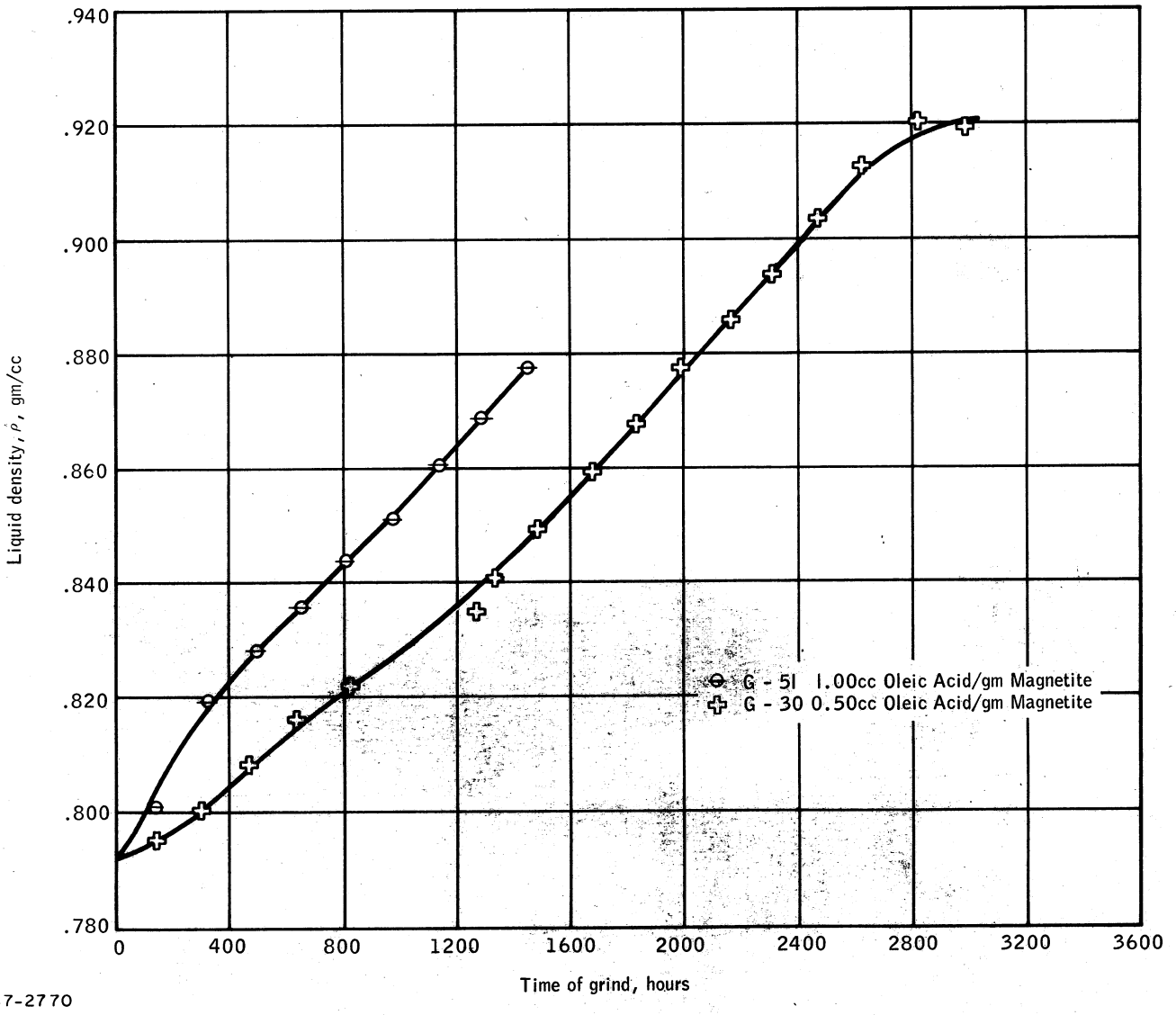

Figure 8. – Effect of Surfactant Concentration, Using Liquid Density as Index of Colloid Formation

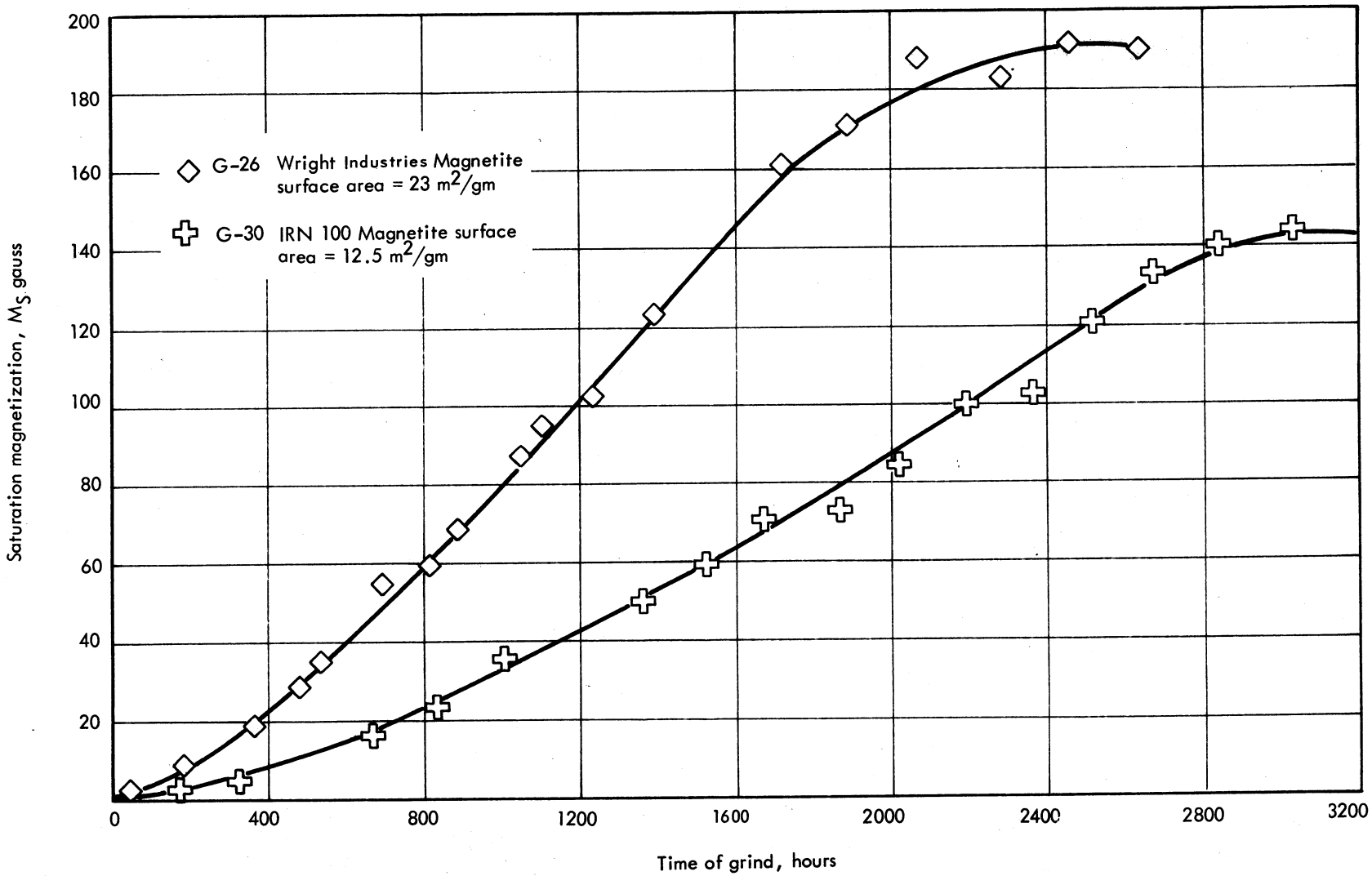

87-2771

Figure 9. – Effect of Initial Particle Size, Using Magnetization as Index of Colloid Formation

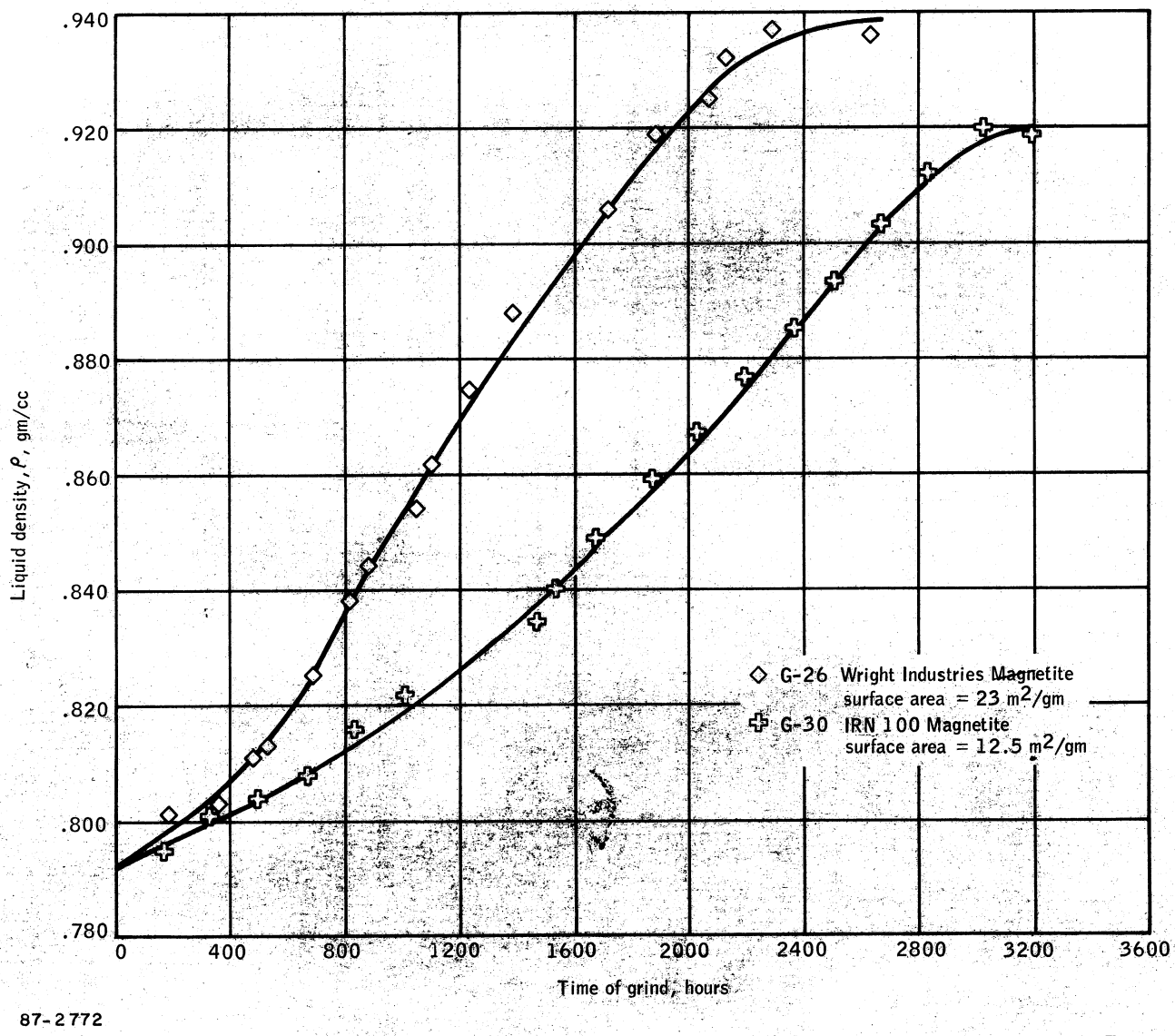

Figure 10. – Effect of Initial Particle Size, Using Liquid Density as Index of Colloid Formation

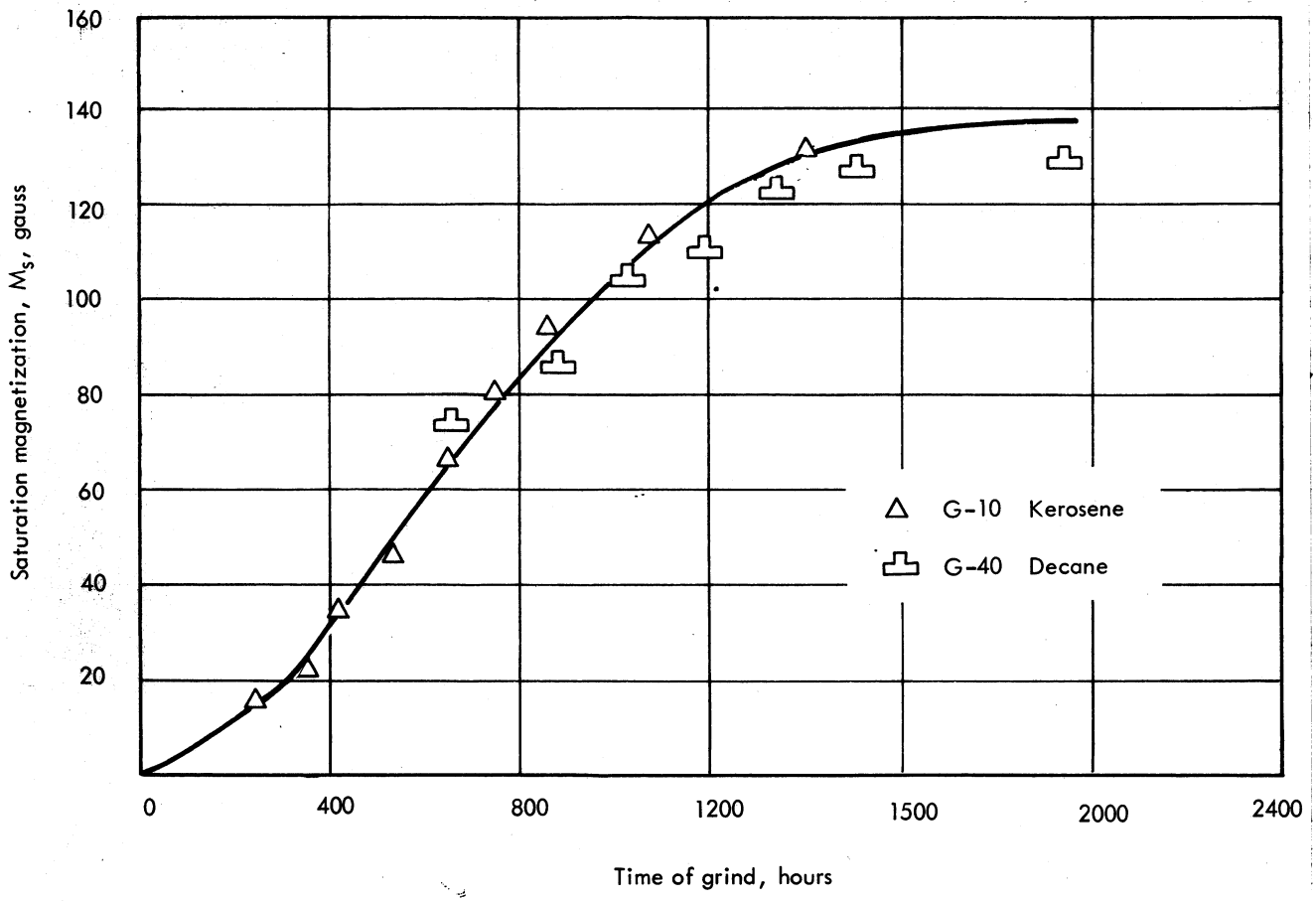

87-2773

Figure 11. – Effect of Carrier Fluid, Using Magnetization as Index of Colloid Formation

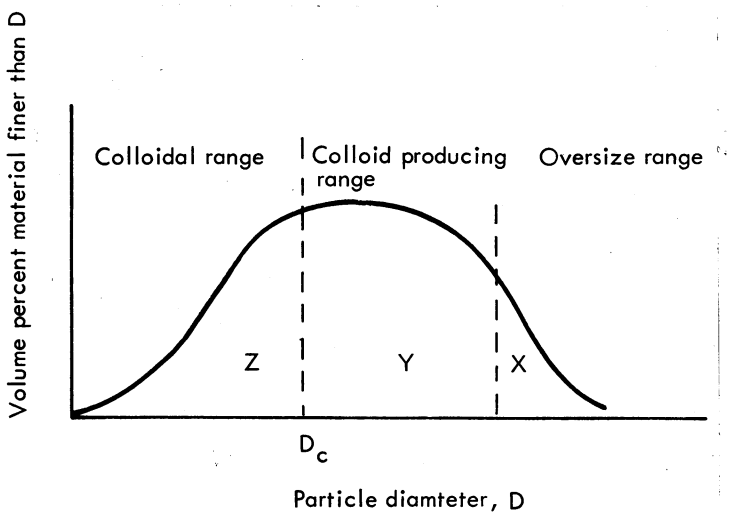

87-2774

Figure 12. – Schematic Size Distribution of Powder for Development of Grinding Model

Figure 4 Effect of Operating Equipment, Using Liquid Density as Index of Colloid Formation

Figure 5 Effect of Surfactant Type (Magnetization)

Figure 6 Effect of Surfactant Type (Density)

Figure 7 Effect of Surfactant Concentration (Magnetization)

Figure 8 Effect of Surfactant Concentration (Density)

Figure 9 Effect of Initial Particle Size (Magnetization)

Figure 10 Effect of Initial Particle Size (Density)

Figure 11 Effect of Carrier Fluid (Magnetization)

An s-shaped curve results in each case. Magnetic characteristics appear after an initial induction period, rise fairly quickly with time and then level off to an asymptotic value.

The rate of colloid formation was analyzed in terms of a first order cascade. The size distribution of material that is being ground was arbitrarily divided into three zones as shown in figure 12.

Consider the rate of change of x, y and z with time, assuming particle-size independent first order kinetics.

i. Rate of change of X with time

$$dX/dt = - K_1 X \qquad (1)$$

by integration:

$$X = X_0 \, e^{-K_1 t} \qquad (2)$$

where, X_0 = initial value of X ($t = 0$)

K_1 = rate constant, hr^{-1}

ii. Rate of change of Y with time

There is both formation of Y from X and disappearance of Y to Z during grinding:

$$dY/dt = K_1 X - K_1 Y \tag{3}$$

Substituting for X and transposing:

$$dY/dt + K_1 Y = K_1 X_0 e^{-K_1 t} \tag{4}$$

Integration of this first order equation with the following initial boundary conditions:

$$t = 0,\ Y = Y_0,\ Z_0 = 0 \text{ so that } X_0 + Y_0 = 1$$

yields the following expression for Y as a function of time:

$$Y = [K_1 X_0 t + 1 - X_0] e^{-K_1 t} \tag{5}$$

iii. Rate of change of Z with time

$$dZ/dt = K_1 Y \tag{6}$$

Substituting equation (5) for (4) and transposing terms:

$$dZ = K_1 e^{-K_1 t} [K_1 X_0 t + 1 - X_0] dt$$

Integrating with the boundary condition $t = 0\ Z = 0$ yields:

$$Z = 1 - e^{-K_1 t} (1 + K_1 X_0 t) \tag{7}$$

If the starting material is much coarser than the colloidal range then $X_0 \approx 1$ and equation (7) reduces to:

$$Z = 1 - e^{-K_1 t} (1 + K_1 t) \tag{8}$$

According to this equation the rate of colloid formation is an exponential decay process with a linear term superimposed. Note that when $X_0 = 0$ the equation reduces to a single exponential decay relationship. Plotting Z as

a function of t for a finite value of K_1 yields an S-shaped curve. Initially when $Kt << 1$ the product $e^{-K_1 t}(1 + K_1 t)$ is approximately equal to 1 so that Z changes slowly and remains near zero. Only when exponential term swamps the linear term as t increases does Z increase as an exponential function to an asymptotic value.

Physically in terms of the grinding operation, the initial powder can be considered to consist of boulders which first have to be broken into much smaller units which then break up into colloidal size particles.

The rate of colloid formation obtained experimentally in the grinding tests is described by this model. The results can be described mathematically by equation (8), each run having a characteristic rate constant which is a function of the process conditions.

Effect of Operating Equipment. - A standard mixture of magnetite oleic-acid kerosene was ground in a large mill (Run G-10), a small mill (G-30) and in the attritor at two speeds (A-10 and A-11). This mixture was of the proportions:

$$\frac{\text{cc kerosene}}{\text{gm magnetite}} = 6.25 \qquad \frac{\text{cc oleic acid}}{\text{gm magnetite}} = 0.50$$

The grinding data for these runs are presented in figure 13. This is a plot of the cumulative volume fraction solids, Z, that remains in suspension after centrifuging as a function of time. This nominally consists of particles smaller than 600 Å. Z is equal experimentally to the ratio of the magnetization saturation, M_s, at time, t, to the ultimate magnetization at infinite time, $M_{s\infty}$ when all the solids have been ground.

The solid curves represent the values of Z predicted by equation (8), using a value of the coefficient K_1 that best fits the data in each case. These values of K_1 and the saturation magnetization for each run after 500 hours of grind are presented in table 7.

The rate of grind is a function of the equipment used. Under otherwise equal conditions the rate of grind is faster in the attritor than in a standard ball mill. In the attritor, the rate constant appears to vary as the

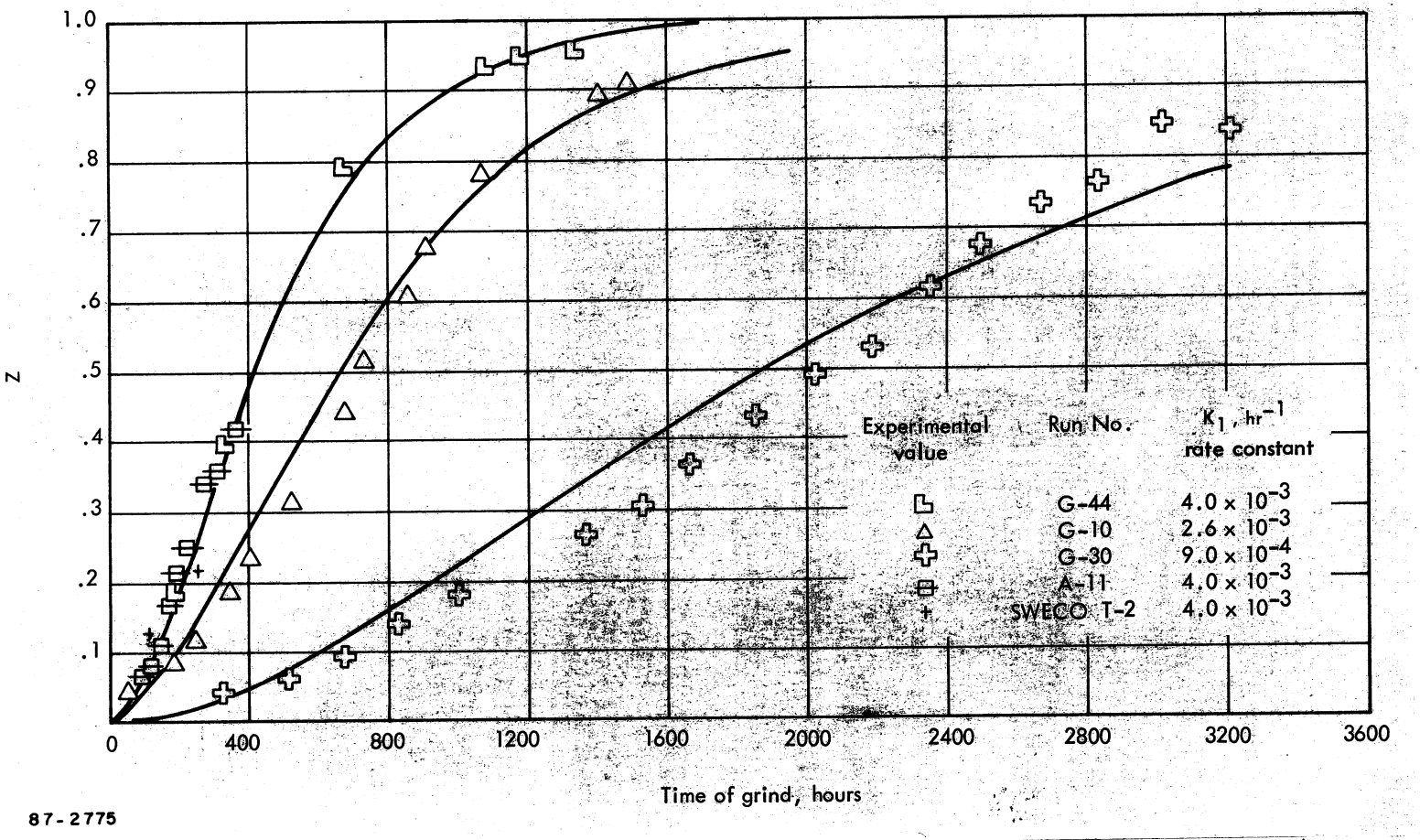

Figure 13. – Comparison of Experimental Colloid Formation versus Values Predicted by $Z = 1 - e^{-K_1 t}(1 + K_1 t)$ Based on Volumetric Solids Content.

TABLE 7. – VALUES OF THE SATURATION MAGNETIZATION AFTER 500 HOURS OF GRINDING AND THE GRINDING RATE CONSTANT, K_1, FOR DIFFERENT GRINDS

Grind No.	500 hour saturation magnetization, gauss	Grinding rate constant K_1, inverse hours
G-10	45	2.6×10^{-3}
G-26	30	2.0×10^{-3}
G-30	12	9.0×10^{-4}
G-40	45	2.6×10^{-3}
G-42	0	0
G-44	130	4.0×10^{-3}
G-49	8	6.0×10^{-4}
G-51	24	1.6×10^{-3}
A-11	over 100 (extrapolated)	4.0×10^{-3}
SWECO T-2	---	4.0×10^{-3}

square of the speed of rotation of the impeller. Run A-11 was operated at 600 rpm. Run A-10 at 505 rpm. The rate constant in large ball mill is about three times the rate constant obtained in a small mill. This is approximately equal to the ratio of the mill diameter squared.

These results that can be interpreted in terms of the kinetic energy of the balls in the mills. In the attritor the velocity of the balls should increase with the rotational speed of the impeller. In the ball mills the velocity of the free falling balls increases with the path length of the falling balls which is proportional to the mill diameter.

Effect of Surfactant Concentration. - In a number of runs, at a fixed kerosene-to-magnetite ratio of 6.25 cc/gm, the oleic acid concentration was varied between 0 and 1.0 cc/gm magnetite. (See table 8.)

TABLE 8. – GRINDING TESTS IN WHICH CONCENTRATION OF OLEIC ACID WAS VARIED

Run No.	Mill size	Oleic acid concentration
G-42	4.7 pint	0
G-21	1.6 gal	.25 cc/gm
G-30	4.7 pint	.50 cc/gm
G-10	1.6 gal	.50 cc/gm
G-51	4.7 pint	1.0 cc/gm

The rate constants and saturation magnetization values at 500 hours for these runs are also presented in table 7. Since two mill sizes were used the data are not directly comparable. For each size mill, doubling the surfactant concentration results in a proportional increase in the rate of colloid formation. Translating the small mill results into equivalent large mill results by using the ratios of rate constants of Runs G-10 and G-30 it is found that the rate constant varies as the oleic concentration to 0.7 power.

Effect of Solvent Viscosity. - Solvent viscosity was varied from 0.4 to 1.8 cp by grinding a magnetite/oleic acid blend in heptane (G-15), decane (G-40), and kerosene (G-10). No noticeable differences in the rate of colloid formation were noted when the material was ground in decane as compared to kerosene. The heptane data was not amenable to rate analysis because it had

formed a gel during processing which was later broken. Thus, in the limited range of 1.0 to 1.8 cp solvent viscosity had no effect.

Effect of Surfactant Type. - The surfactant used had a strong effect on the rate of grind, e.g., Tenlo 70 (G-44) as compared to the standard, oleic acid. The reduced rate data for G-44 are also presented in figure 5 and table 7. The specific grinding rate of Tenlo 70 is 50 percent higher than that of oleic acid.

Similarly, octadecyl amine is not as effective a grinding agent as oleic acid.

Effect of Magnetic Solids Type. - All the solids that could be used in these studies are members of a small family of metals or closely related metal oxides that are magnetic. To be of use in these grinding tests they must also be available as a relatively fine powder.

The principal material examined was a powdered synthetic magnetite. ($FeO \cdot Fe_2O_3$) manufactured by the Minerals, Pigments and Metals Division of Chas. Pfizer & Co. Inc. This material is marketed under the codes IRN 100 and MO 4332. Physical properties of this material are listed in table 9. Figure 14 is an electron photomicrograph of this powder obtained through the courtesy of the manufacturer.

A number of tests were performed with a manganese-zinc ferrite with a nominal Curie point of 90 to 100° C manufactured by Krystinel Corp. This powder was of interest in order to prepare a ferrofluid suitable for energy conversion studies, due to its low Curie point and high pyromagnetic coefficient in the temperature range of 20 to 150° C. Figure 15 is a photomicrograph of this powder. In-house studies of the temperature-magnetization properties of this powder indicated that this material had a Curie point of about 195° C, however. Saturation magnetization at 22° C was found to be 4600 gauss. The true density of this powder is 5.0 gm/cm^3.

A run was made with magnetic pigment 4000 manufactured by Wright Industries, Inc., Brooklyn, N.Y. This material is magnetite powder with a specific surface area of 23 m^2/gm.

It was also possible to obtain an extremely finely divided grade of magnetic ferric oxide (γFe_2O_3) from Vitro Laboratories, West Orange, N.J. This material had a specific surface area of 56 m^2/gm which corresponds to an average particle size of 210 Å. The saturation magnetization was 5400 gauss. This material was synthesized in an electric arc so that the particles are fairly spherical in shape.

FIG 15 — Tab 1-1

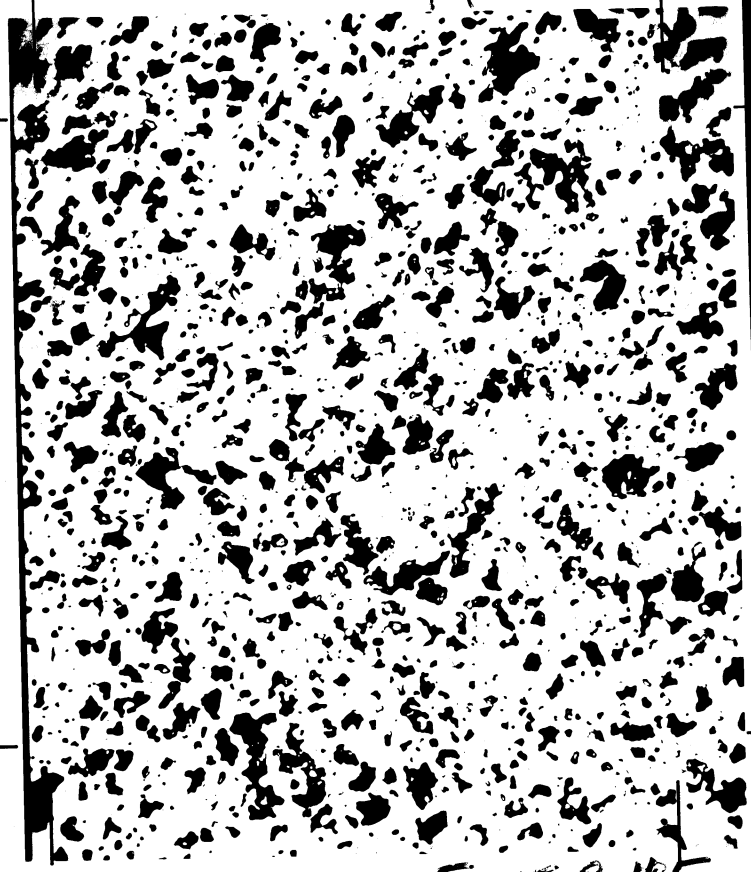

Fig 15 Pg 45

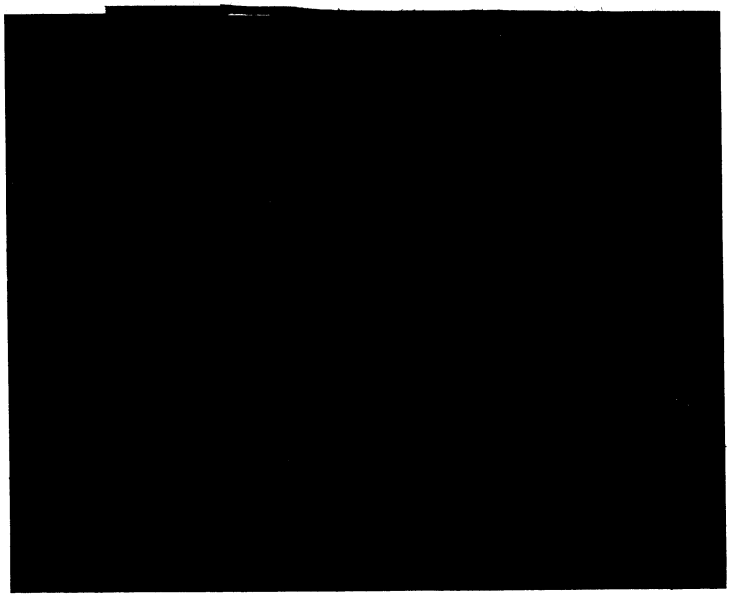

IRN 100

17,500X

PFIZER MINERALS PIGMENTS
& METALS DIVISION

87-2776

MO-4232

Figure 14. – Electron Micrograph of Raw Magnetite, IRN 100

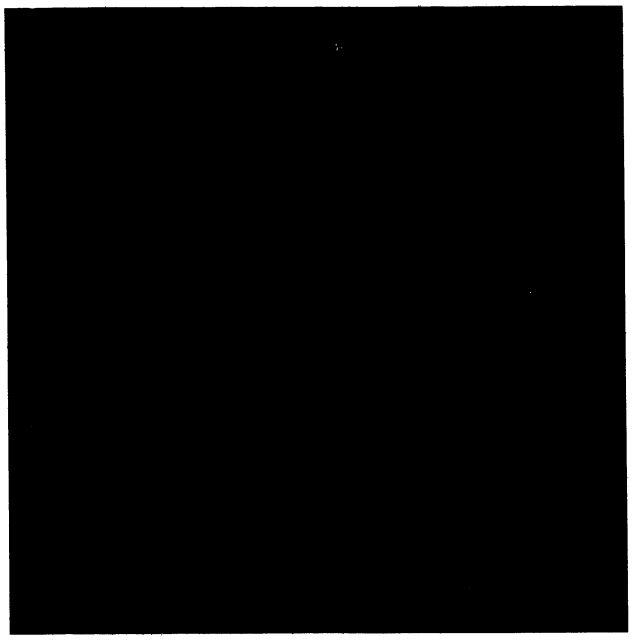

10 μ

87-2777

Figure 15. – Micrograph (500X) of Raw 90 to 100° C Curie Temperature, Manganese-Zinc Ferrite (Krystinel Corp.)

Top

(17,500X IRN-100)

C.K. WILLIAMS & CO.

MO-4232

17,500
~~35,000x~~

ONE MICRON

T-50

FIG 14

Fig 14 Pg 45

TABLE 9. – PROPERTIES OF IRN 100 MAGNETIC OXIDE

Chemical composition	Fe_3O_4
Particle shape	Acicular
Average particle length	0.55 micron
Average particle width	.08 micron
Surface area (BET)	12.5 m^2/gram
Oil adsorption	50 ± 5
Apparent density	6 ± 0.5 gm/$in.^3$
Specific gravity	5.0 gm/cc
Magnetic properties	
Saturation magnetization	5660 gauss
Curie point	570° C
Initial permeability	70

Table 9

[a]Manufacturer: Pfizer Minerals, Pigments and Metals Division

17 500X

All these oxides formed colloidal dispersions when ground in kerosene in a ball mill in the presence of a stabilizing agent such as oleic acid. This is not surprising since the stability and colloidal properties of the ferrofluids should be insensitive to the specific nature of these closely related solids used in their preparation.

The rate of colloid formation, however, should be a function of the solid used. Important variables should be average particle size, particle size distribution, and friability of the material.

IRN 100 magnetite and Wright Industries magnetite can be compared from rate constants for runs G-30 and G-26 shown in table 10.

TABLE 10. – GRINDING RATE CONSTANTS FOR ALTERNATE MAGNETIC POWDERS

Run No.	Powder	Initial specific surface area, m^2/gram	Rate constant, hr^{-1}
G-30	IRN 100	12.5	0.8 to 0.9×10^{-3}
G-26	Wright Ind. 4000	23 to 24	2.0×10^{-3}

The shape of the curve is the same for both powders. (See fig. 9.)

Not surprisingly, the finer starting material results in a faster appearance of colloid and therefore a higher apparent rate constant. It is difficult to go into more detailed comparisons since particle shape and size distributions are different for the two powders.

The results of the grinding runs for the 90 to 100° C ferrite did not lend themselves to a quantitative comparison. There were difficulties with gelling. With this material there was a large discrepancy between the volume fraction solids obtained from density and magnetic measurements. This will be discussed later in more detail.

Qualitatively in comparing runs G-10 and G-21 (IRN 100 magnetite) with runs G-22 and G-24 (900 to 100° C ferrite) it was found that the rate of colloid formation was much lower for the 90 to 100° C ferrite. Partially, this is due to the much coarser size of the initial material as is evidenced by

figure 15. There is also most probably a difference in the grindability of two materials which has not been evaluated per se.

Some unusual results were obtained with the finely divided Vitro ferric oxide. This was the only material in which there was first an increase in the magnetic moment with grinding time followed by a decrease with further grinding time, even though the solid content is asymptotic to a fixed value. (See fig. 16.)

A number of factors should be noted:

i. There is no induction period with this powder. The solids density curve, which is an exponential function, and the magnetization curve do not have an upward inflection point.

In terms of the grinding model presented, this indicates a value of $X_0 \rightarrow 0$, with the rate of grinding following an exponential decay:

$$Z = 1 - e^{-K_1 t}$$

In this case, $K = 6.7 \times 10^{-3}\ hr^{-1}$ using density data.

ii. The asymptotic density value is higher than the value corresponding to the initial loading of powder -- indicating that contamination due to mill wear occurs here also.

iii. The fact that the magnetic moment decreases is most interesting and puzzling. This was only solid material tested that exhibited this behavior. In this case there has to be a stress-induced change in the structure of the powder. One possible explanation is that with very small particles one introduces enough mechanical energy to have the following reaction:

$$\gamma Fe_2O_3 \xrightarrow[\text{energy}]{} \alpha Fe_2O_3$$

γFe_2O_3 is a magnetic material, αFe_2O_3 is nonmagnetic. αFe_2O_3 is the stable phase at room temperature.

The decrease in magnetic moment can also be explained in terms of superparamegnetic effects, see discussion of results of the magnetic properties of ferrorfluids.

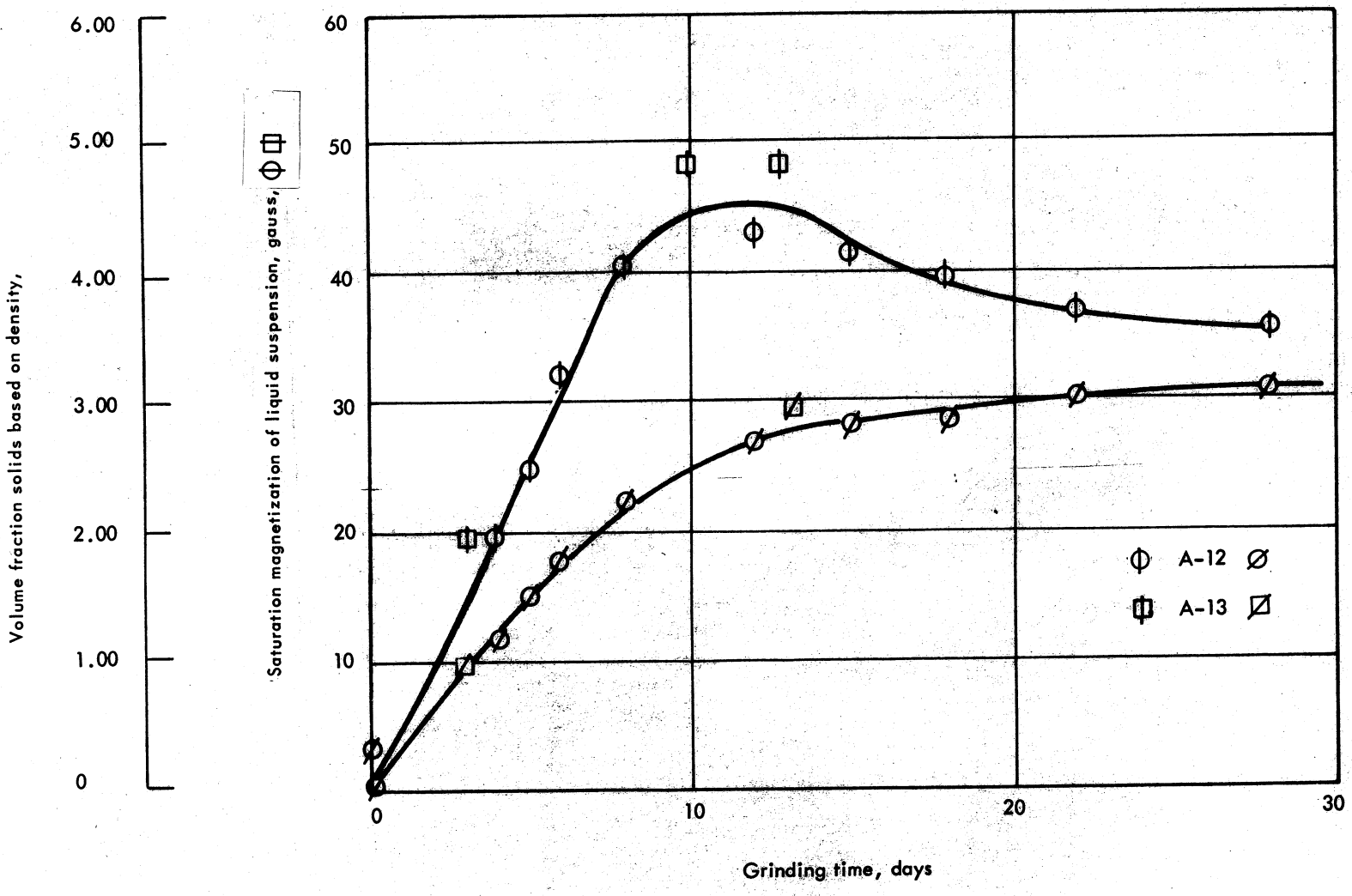

87-2778

Figure 16. – Magnetization and Density of Vitro Powder Ferrofluid Grinds (A-12 and A-13) as a Function of Time of Grinding

Still another possibility for the decrease in magnetic moment might be the destruction of the magnetic domains by systematic grinding without any accompanying change in crystal structure. There would be a minimum particle size below which no material exhibit ferromagnetic properties.

Translation of Magnetic Property into the Ferrofluid. - The volume fraction solids in suspension is calculated from density measurements by the equation

$$\epsilon = \frac{\rho - \rho_L}{\rho_s - \rho_L} \tag{9}$$

was not always in a one to one accord with the volume fraction solids calculated from magnetization measurements

$$\epsilon = \frac{M_s}{M_{ss}} \tag{10}$$

where

ϵ = volume fraction solids

ρ = density of the suspension

ρ_L = density of the base liquid

ρ_s = solids density

M_s = saturation magnetization of the sample

M_{ss} = saturation magnetization of the pure solid.

Both the density and magnetization measurements were found to increase monotonically with time when ferrites were ground. It was found that the volume fraction solids calculated from density measurements was equal to or higher than the value obtained from magnetization measurements. (See table 11.)

It was noted that from the density measurements of runs G-26 and G-24, the volume fraction solids were higher than would be obtained from the standard amount of powder normally charged.

It had been previously postulated that the reason why colloids whose magnetic constituent is the manganese-zinc ferrite were much weaker magnetically than those containing magnetite at a given volume fraction solids,

TABLE 11. – CONVERSION FOR DIFFERENT GRINDS

Run No.	Hours of Grind	Solids fraction density, ϵ_D	Solids fraction magnetization, ϵ_M	Conversion, $K = \frac{\epsilon_M}{\epsilon_D}$
A-10	360	2.38	0.87	0.36
A-11	360	3.78	1.33	.35
G-4, -5, -6[a]	500	1.52	1.11	.74
G-10[a]	1478	2.50	2.28	.89
G-15	618	3.40	2.19	.65
G-21[a]	2726	---	---	.71
G-22	1800	2.28	.75	.33
G-24	1680	1.78	.63	.35
G-26	2629	3.56	3.35	.94
G-30	3195	2.93	2.44	.83
G-40	1997	2.36	2.28	.97
G-41	3271	2.04	.83	.40
G-42	2596	1.52	.61	.40
G-43	2086	1.26	.83	.66
G-44[a]	1329	3.77	3.74	.99
G-47[a]	2492	2.42	2.39	.98
G-48	3638	2.67	1.09	.41
G-49	2829	0.96	.83	.86
G-50	2240	1.28	.87	.68
G-51	1455	1.99	1.74	.88

[a]After ultracentrifuging.

was due to the destruction of a portion of the magnetic properties by grinding, due to a stress-induced crystalline rearrangement. A more likely possibility is that of nonmagnetic contaminants being introduced into the suspension due to wear of balls and mills. The stainless steel shells of the standard mill jars and the shell and shaft of the attritor all showed signs of wear. The carbon steel balls themselves were abraded with time. In addition to the ferrite originally added, the colloid suspension formed in a ball mill should also contain:

i. Stainless steel fragments which are nonmagnetic

ii. Carbon steel fragments from the balls which are magnetic

iii. Oxidation products of the above such as $\alpha\, Fe_2O_3$ which in general are nonmagnetic

In run G-10, the initial charge contained 200 gm or 200/5 = 40 cc of magnetite as well as 100 cc of oleic acid and 1250 cc of kerosene. The volume fraction solids in suspension can be no higher than $\frac{40}{1250 + 100 + 40} = 0.029$ or 2.9 percent. The volume fraction solids from density measurements at the end of the run was found to be 3.3 percent. The maximum magnetization of the liquid should be equal to (0.029) (5660) = 168 gauss, since the saturation magnetization of the pure magnetite was 5660 gauss. The experimentally found value for the liquid ground 1478 hours was 174 gauss, which is in good agreement with the expected value. From the above we can conclude that nonmagnetic fragments certainly were present. This is supported further by the observation that in washing the balls after the end of a run, small metallic fragments are found in the washings.

In the attritor, there is a greater divergence. After 380 hours of grind at 600 rpm, the volume fraction solids from density measurements was 3.77 percent. Measured magnetization was 75 gauss which corresponds to 75/5660 = 1.32 percent solids content. The concentration solids in the initial charge was 3.0 percent. There was evidently some nonmagnetic material also present in the suspension which could only come from the shell, the balls, and the driving arm.

The greater apparent loss in magnetization that occurs when the 90 to 100° C ferrite rather than magnetite is ground in a ball mill can be interpreted by differences in grindability. The ferrite can be considered to be more abrasive and harder to grind than magnetite under similar conditions so that for a given period of time of grind, less ferrite than magnetite is ground while at the same time there is greater wear of the grinding media. Measurement of the weight change of the grinding media is needed to examine this point.

Other Grinding and Dispersing Tests

Vibratory Mill. - Special arrangements were made with Southwestern Engineering Company (SWECO) to conduct milling tests in their vibratory mills. This type of mill generally leads to faster grinding than is obtained in ordinary ball mills.

The charge supplied to SWECO was of the proportions:

$$\frac{\text{cc kerosene}}{\text{gm magnetite}} = 4.75 \qquad \frac{\text{cc oleic acid}}{\text{gm magnetite}} = 0.50$$

The results of these tests may be compared with our run G-10 in which the corresponding proportions were:

$$\frac{\text{cc kerosene}}{\text{gm magnetite}} = 6.25 \qquad \frac{\text{cc oleic acid}}{\text{gm magnetite}} = 0.50$$

In all these tests, the strength of magnetic colloid was determined as a function of grinding time. Test T-1 was conducted in an M18 stainless steel Vibro-Energy Mill with 166 pounds of cylindrical alumina media and 1-1/2 gallons of charge while T-2 was done in the same type of mill using 150 pounds of case-hardened steel cylinders and 1 gallon of charge. All colloidal fluid removed from the mills was centrifuged for 10 minutes at approximately 2000 g, prior to magnetic measurement, in order to remove oversize material. Results of these tests are summarized in table 12.

TABLE 12. – COMPARATIVE GRINDING RATES IN BALL MILLS
(Saturation Magnetization in Gauss for H = 10 000 Oersted)

Time, hours	SWECO T-1	SWECO T-2	G-10
120	0	25	6
240	0	46	14
360	---	---	25
560	---	---	26

The grinding data obtained by SWECO yield a rate constant of 4.0×10^{-3} hr^{-1}. The reduced rate data are presented in figure 13 and table 12.

In order to compare the efficiency of the SWECO mill to the ball mills used in our work, the effect of the higher oleic acid concentration had to be taken into consideration. There is a higher oleic acid concentration in the SWECO solvent than there was in the in-house tests. The equivalent rate constant at an oleic acid concentration of 1.0 cc oleic acid/12.5 cc solvent is 3.0×10^{-3} hr^{-1}. This is comparable to 2.6×10^{-3} hr^{-1} for the rate constant in a 1.6 gallon mill. The SWECO mill, therefore, grinds only about 20 percent more quickly than 1.6 gallon mill. The mill effect is less than the effect of changing surfactants.

Grinding in Other Solvents. - The major problem underlying all of the work in the preparation of ferrofluids is one of stabilizing the colloidal sol under a variety of physical conditions. It has been possible to prepare a kerosene-based ferrofluid which is stable under a relatively narrow temperature range. While this fluid is novel and has many useful properties, it also has inherent limitations. Many suggestions have been made which would use ferromagnetic fluid dispersions but with requirements on the fluid that cannot be met if kerosene or a similar hydrocarbon is used as the basic solvent. Attempts were made to prepare ferrofluids in such different liquid bases as water, phenyl methyl silicone oil (Dow-Corning Fluid 510) and fluorocarbons.

Grinding magnetite in water in the presence of perfluoro-octanoic acid (G-23) perfluoro-acetic acid (G-25) cobalt sulfate heptahydrate (G-27) and cerous nitrate hexahydrate (G-35) did not result in the formation of a colloid.

Similarly, there was no colloid formation when magnetite was ground in either 50 centistoke Dow-Corning 510 fluid, with no surfactant (G-31a) or in the presence of pentacosanoic acid (G-39).

Sedimentation studies were run in a low viscosity fluorolube as a preliminary test to grinding magnetite in this type of liquid.

Fluorolubes are addition polymers of trifluorovinyl chloride. They are linear polymers built up of a recurring unit which is

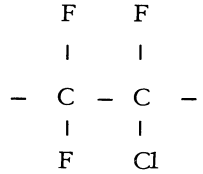

The Fluorolubes whose end groups are fluorinated are manufactured by the Hooker Chemical Company. They are very stable chemically. They are extremely stable to oxidation and they are noncorrosive. They are thermally stable to approximately 300° C. They are nonflammable and nontoxic. They have a low surface tension. All these properties have made them useful instrument lubricants.

The sedimentation studies were run with the most fluid grade of Fluorolube commercially available, Fluorolube FS-5. Physical properties of this material are presented in table 13.

TABLE 13. – PROPERTIES OF FLUOROLUBE FS-5

Average molecular weight	560
Pour point, °C	-60
Density at 100° F, gm/cc	1.858
Vapor pressure at 100° F, mm Hg	1.8×10^{-2}
Surface tension at 77° F, dyne/cm	23
Viscosity at 100° F, cp	9.0
Viscosity at 160° F, cp	3.8

The dispersion tests were run in the same manner as described above with kerosene. Different surfactants used and results obtained are listed in table 14.

In general, the longer settling times are due to differences in viscosity and density of Fluorolube FS-5 and kerosene. From Stokes' Law, the settling rate is proportional to the density difference between the solid and the liquid and inversely proportional to the viscosity of the fluid. With the density of magnetite being about 5.0 gm/cc, the density difference for the Fluorolube is 3.1 gm/cc as compared to 4.2 gm/cc for the kerosene. At room temperature, the viscosity of Fluorolube is about 12 cp versus 2 cp for kerosene. Under otherwise equivalent conditions, the settling times in Fluorolube FS-5 should be eight times longer.

TABLE 14. – SEDIMENTATION OF MAGNETITE IN FLUOROLUBE FS–5

Tube No.	Additive	Level	Settling characteristics
F-1	Perfluoro-octanoic acid	0.12 gm	Some suspension after three days
F-2	Perfluoro-octanoic acid	.05 gm	Some suspension after three days
F-3	Perfluoroacetic acid	.10 cc	Settled over weekend hazy supernatant
F-4	FC-176 surfactant (fluorinated nonionic surfactant (3-M)	.10cc	Less than 14 minutes
F-5	L-79, silicone surfactant Union Carbide Corp.	.10 cc	Less than 70 minutes
F-6	Perfluorobutyric acid	.10 cc	Settled over weekend clear supernatant
F-7	Oleic acid	.10 cc	Settled over weekend clear supernatant
F-8	L-527 silicone surfactant Union Carbide Corp	.10 cc	Less than 14 minutes
F-9	Z-6020 surfactant Dow-Corning Chemical Co	.10 cc	Less than 14 minutes formed big flocs
F-10	Tenlo 70 surfactant Nopco Chemical Co	.10 cc	Less than 70 minutes
F-11	Calcium naphthanate	.10 cc	Less than 70 minutes
F-12	Blank	---	Less than 14 minutes

TABLE 14

The surfactants used were chemicals which were believed to be compatible with fluorocarbons and that would absorb on the surface of the particles so that an entropic barrier would be developed around the particles in this liquid much in the manner of oleic acid in kerosene. Perfluoronated carboxylic acids were an obvious choice. Other fluorinated compounds presently available in the laboratory were also tried. Little is known about the behavior of silicones in fluorocarbons. Therefore, a number of silicone surfactants were tried as well. To show the specificity of surface active agents, Tenlo 70 and oleic acid, which were satisfactory suspending agents in kerosene, were also tried even though it was believed that they would not prove to be satisfactory.

The results of the tests were as follows. The silicones were not compatible with this system. The hydrocarbon surfactants were not as poor as the silicones, but did not compare with the perfluorinated compounds in their suspending activity. Oleic acid was the best of this lot. Of the perfluorinated compounds, perfluoroacetic acid was better than perfluorobutyric acid, but not as good as perfluoro-octanoic acid. This could be due to the partial ionization of the perfluoroacetic acid, a strong acid, with the partial formation of a double layer around the particles leading to some stabilization.

The best results were obtained with the perfluoro-octanoic acid. This is the longest chained perfluorinated carboxylic acid that is presently on hand. The solubility of this material appeared limited. In both cases not all the acid went into solution. Grinding of magnetite in Fluorolube FS-5 with the addition of perfluoro-octanoic acid was tried in the attritor (A-14). There was no colloid formation. This was considered due to the limited solubility of the surfactant in this solvent. Longer chained perfluorinated surfactants should be considered next since they should be more soluble in the medium.

Dispersion of Elemental Metals. - The elemental metals iron, nickel, cobalt as well as some of their alloys have saturation magnetizations that are higher by a factor of 3 to 4 than the magnetite or other ferrites used in the studies. Hence, there is considerable inherent interest to these materials and so a number of runs were made with elemental iron in kerosene using different surfactants.

Grinding 1 μ iron particles obtained by decomposition of iron carbonyl in the presence of Emulphor EL 620, a polyoxyethylated vegetable oil used as a dispersant for iron powders in the manufacture of magnetic coupling fluids, did not result in colloid formation (G-14).

An opaque, black, clean colloid of low viscosity with a slight magnetic response, was obtained after 15 days when this iron powder was ground in the presence of oleic acid. After 33 days the material after centrifugation

had a saturation magnetic moment of 5.6 gauss. A sample of this material in a beaker was exposed to the air overnight which resulted in a lowering of the magnetic moment by a factor of 2. Another sample heated momentarily to the boiling point in the presence of air lost its magnetism completely. The iron particles were undoubtedly oxidized to a nonmagnetic oxidation state. Due to the enormous surface area of these colloidal particles oxidation is rapid, hence this behavior is not unexpected.

A further attempt to incorporate elemental iron was made using Tenlo 70 as the grinding agent (Run G-53), special precautions being taken to eliminate oxygen contamination; kerosene was first refluxed over molecular sieves to eliminate dissolved gases and moisture and the system then handled under a nitrogen atmosphere.

After 609 hours of grind the material was dark but nonmagnetic and after 927 hours, it was slightly magnetic but not worth measuring. After 1727 hours, a dark colloidal suspension that had a magnetic moment of 20 gauss in a 10 000 gauss applied field and a density of 0.834 gm./cc was obtained. These numbers yield the following values for the volume fraction solids in suspension:

Assuming

$$M_{iron} = 21\,200 \text{ gauss when } H = 10\,000 \text{ gauss},$$

then

$$\epsilon_M = 0.095 \text{ percent, and}$$

$$\epsilon_D = 0.50 \text{ percent.}$$

Evidently not all the material in suspension is magnetic. Due to the precautions taken there should not have been any oxidation due to the presence of atmospheric oxygen or humidity. There is a good chance that the surfactant Tenlo 70 might have reacted with the powder. The contents of the mill were under a positive pressure when opened. The vent gases from the glove bag in which the mill was opened reeked of ammonia -- which could only have come from decomposition of the surfactant. Tenlo 70 contains both amine and alcohol groups which could have reacted with the nascent iron to form oxides or nitrides which are nonmagnetic. The rate of grind in both iron runs was slower than for magnetite. The rate constant for both runs G-13 (small mill) and G-53 (large mill) was approximately 2×10^{-4} hr^{-1} based on magnetization. This slower apparent rate of grind is partially due to a slower attrition of the iron powder itself; iron is a ductile material while magnetite is hard and brittle. It might also be partially due to chemical decomposition of the iron particles when they react with a stabilizing agent.

Further work is required in the formulation of metal dispersions; in particular in trying to find a stabilizer that does not decompose.

Dispersal of Coated Iron-Cobalt Particles. - The production of ultrafine, elemental, magnetic particles for incorporation into permanent magnets has reached a high level of sophistication at the hands of Luborsky and his colleagues and employs a technique of electrodeposition into mercury (ref. 5).

Now the prospect of incorporating such elemental particles into a ferrofluid has always been tantalizing since these particles possess a magnetic moment per unit volume which is three to four times greater than the ferrite material which now composes the magnetic portion of the organic ferrofluids. However, the dispersal of elemental ferromagnetic particles into a carrier liquid is known from our past work as well as from general considerations to lead to a rapidly oxidizable mixture whose magnetic properties are only transient in existence (G-13). It is therefore of interest to note that recently production has been made by Falk (ref. 6) of $CoFe_2O_4$ coated iron-cobalt particles, and that such particles are resistant to air oxidation.

In response to our request Mr. Falk has kindly furnished samples of two kinds of ferrite coated particles (LODEX-55). Their characteristics are given in table 15.

TABLE 15. – CHARACTERISTICS OF FERRITE-COATED IRON-COBALT PARTICLES

Elongated particles	Round particles
Diameter = 100 Å	Diameter = 500 to 1000 Å
Length = 1000 Å	Weight % O_2 = 10 to 12%

A sample of the round particles agitated in a test tube in the presence of kerosene and oleic acid produced, at once, a trace of colloidally dispersed material. This was intensified by heating the mixture although the resultant colloid was not magnetically responsive. Next a mixture of 300 cc decane, 50 gm magnetic powder, and 25 cc oleic acid was charged in the attritor mill (Run A-7) and after approximately 5 days of grinding at 505 rpm produced a gel which later broke to a magnetically responsive colloid whose ferric induction, however, was not exceptionally high. It was hypothesized that this

grinding may have led to particle fracture (pure iron powder is grindable to colloidal dimensions) and further oxidation rather than just the breaking of particle-to-particle contacts. Finally then, to overcome this possible disadvantage, attempt was made to produce a dispersion by ultrasonic means employing a Branson Sonifier having an immersible element. The input of ultrasonic energy was sufficient to bring to a boil the contents of a 50 cc beaker within a few minutes. Accordingly a water-cooled copper container was constructed which eliminated this problem. Subsequent ultrasonic irradiation for 4 days with elements having in turn flat, pointed, and wedge geometries produced just a tea-colored liquid without a noticeable magnetic response.

The elongated particles were then ultrasonically irradiated without any noticeable magnetic response.

MODIFICATION OF FERROFLUIDS

The colloidal dispersions obtained by grinding are dilute suspensions of magnetic materials (about 2 to 3 volume-percent solids). For many applications, fluids with different properties than those attainable with the fluids fresh from a mill and centrifuge were desired. Techniques were developed to concentrate the solids by removing some of the solvent; to substitute one liquid carrier for another, modify the properties of the carrier, and to a limited extent; replace a surfactant by another, thus changing the nature of the stabilizing layer; and to modify the particle size distribution of solids in suspension.

Concentration of Fluids

The magnetic strength of a ferrofluid is proportional to the volume concentration of magnetic solids in suspension. Fluids of increased magnetic strength are obtained by removal of the carrier. It was possible to obtain suspensions that contained over 20 volume-percent solids from the original suspensions by vacuum evaporation. This was successfully accomplished in a Rinco vacuum evaporator. (See fig. 17.) In this apparatus there is controlled vaporization on a continually renewed low temperature film. Thin film evaporation under vacuum was necessary in order to prevent the fluids from overheating, since as discussed in the section on Stability of Ferrofluids, the ferrofluids are temperature sensitive. For example, an oleic acid stabilized ferrofluid will irreversibly flocculate if heated above 95° C. Since kerosene (the standard carrier) has a boiling range of about

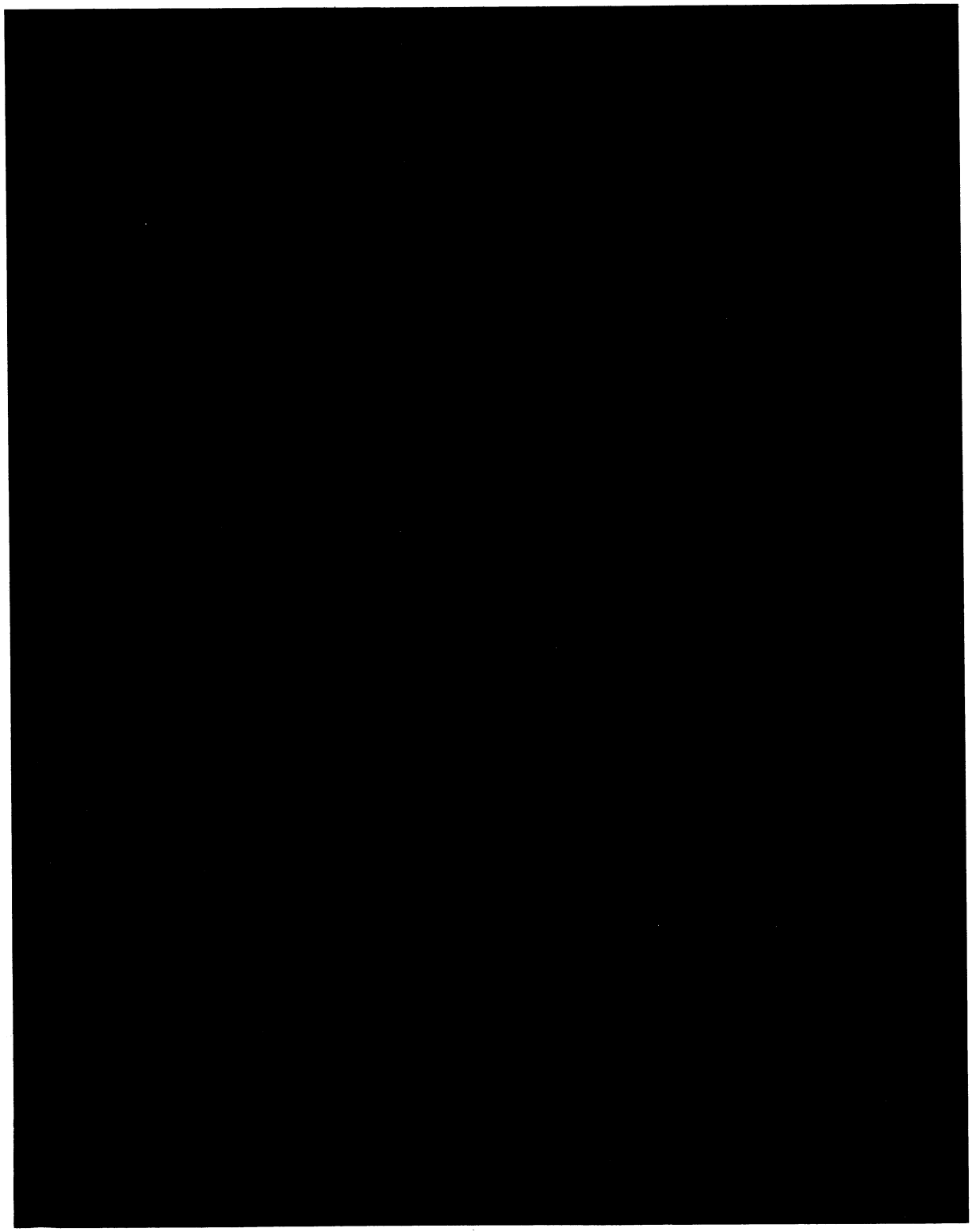

Figure 17. – Rotary Vacuum Evaporation Apparatus to Concentrate Ferrofluids through Uniform Heating of Thin Liquid Films, by Removal of Solvent

Top

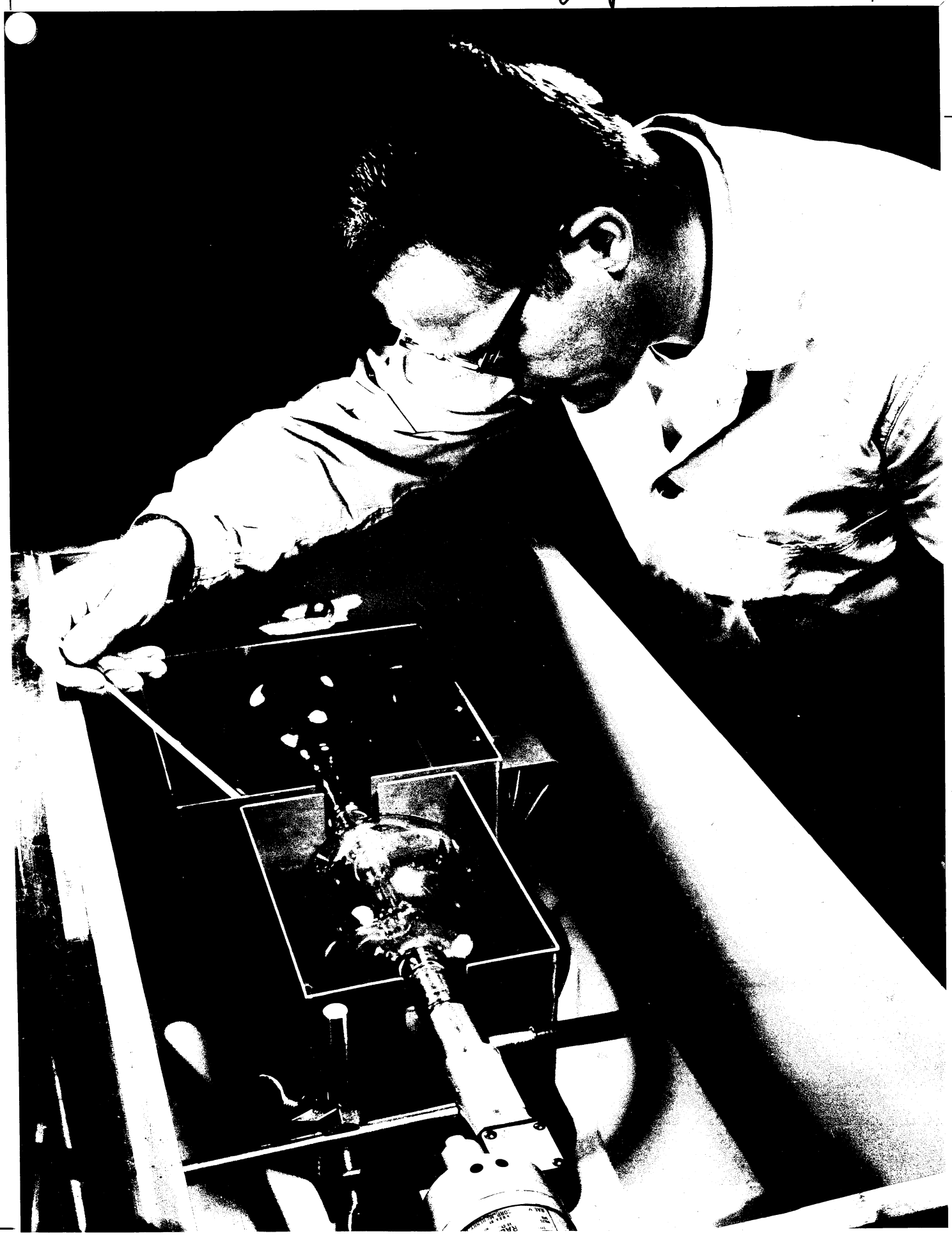

Fig 17 Pg 61 T-89 FIG 17

210 to 220° C at atmospheric pressure, these fluids had to be treated under vacuum in order to have a boiling range which is lower than the critical temperature of the fluid. Thin film evaporation was necessary in order to obtain reasonable heat transfer and minimum overheating with concentrated suspensions which tend to be very viscous. Typical operating conditions for the concentration of a kerosene-based ferrofluid were a reboiler temperature of 70° C at an operating pressure of 0.1 mm Hg.

Ferrofluids prepared by grinding in other carrier fluids could be concentrated in the same manner. If a very volatile carrier fluid was used, such as heptane, concentration could be carried out at a much lower temperature. In fact, it was possible to evaporate a heptane base fluid to dryness at room temperature. The residue was a brown, waxy solid that redispersed spontaneously in other hydrocarbons to give different ferrofluids.

Carrier Exchange

It was not necessary to go all the way to a solid residue in order to change carrier fluids. Ferrofluids were successfully modified in a number of cases by adding a nonvolatile liquid to a ferrofluid with a more volatile carrier and then evaporating as described above. The original carrier fluid is removed preferentially, leaving behind a ferrofluid dispersed in the new carrier. For example, a silicone base ferrofluid was made in this manner. An aryl-alkyl silicone oil, L-43 (Union Carbide Corp), was added in predetermined amounts to a kerosene base ferrofluid, G-44. This mixture was then treated in the Rinco unit. Kerosene was preferentially removed, the residue now being a dispersion of magnetite in the silicone oil. This ferrofluid had different properties than the original kerosene base fluid, for example, high viscosity at low magnetization.

Carrier Gelling

Another method of changing the properties of a ferrofluid was to incorporate an additive in the system that modified the properties of the carrier fluid without otherwise changing the system. Aluminum salts of long chained carboxylic acids are thickening and gelling agents for hydrocarbons. Aluminum naphthanate was found to be a compatible gelling agent for ferrofluids. It should be noted that in low concentrations this material was also found to be a grinding agent. Addition of 5 percent aluminum naphthanate (by weight) transformed a ferrofluid from a free flowing liquid to a rigid, thixotropic gel that resisted flow at low shear rates, but flowed under high shear. Smaller amounts of aluminum soap gave intermediate properties.

Flocculation/Redispersion

It was found that the addition of an excess of a polar solvent that was miscible with the carrier fluid, such as acetone or iso-propyl alcohol resulted in flocculation. The particles separated from the liquid phase. After separating the solids from the supernatant, it was observed that the solids would redisperse spontaneously in fresh solvent or fresh solvent to which a small amount of stabilizing agent was added. Thus, it was also possible to modify the ferrofluids by this alternate technique. By adding less carrier fluid to the flocculated material, it was possible to concentrate the system. By changing carrier fluids, solvent interchange occurred. By this technique, it was possible to replace kerosene as a carrier by other hydrocarbons, such as decane or toluene, for example, or halocarbons such as trichloroethylene or carbon tetrachloride, as well as miscellaneous other organic compounds.

Modification of the Stabilizing Layer

As is discussed in detail in the section on the stability of ferrofluids, if the flocculated solids are washed repeatedly with fresh polar solvent, it is observed, sooner or later depending upon the particular surfactant used, that the flocculated solids do not redisperse spontaneously in kerosene or similar hydrocarbons. These solids do redisperse spontaneously in kerosene that contains surfactant. The ease of redispersion decreases with increasing washing of the solids, samples of flocculated solids would not redisperse if systematically extracted for a long period of time.

The experiments indicate that repeated washing of the solids removes part of the original stabilizing layer. Since it is not necessary to use the same surfactant to obtain redispersion after flocculation, it was possible to obtain ferrofluids that were stabilized by a mixture of surfactants which could be very different in structure. For example, ferrofluids were made that contained mixed layers of oleic acid and Tenlo 70, oleic acid and dodecyl amine. Very little has been done except to demonstrate the feasibility of modifying ferrofluids in such a manner. The properties of colloidal dispersions containing two or more surfactants have not been studied. This is a most complex area which should prove to be of long term interest.

Modification of Particle Size Distribution

The magnetic fluids produced by ball milling contain a distribution of particle sizes. As is discussed in greater detail in following sections on the properties of ferrofluids, it is thought that the smaller particles ($d < 50$ Å) do not contribute to the magnetic moment of the mixture in proportion to their

size as do the larger particles due to the greater thermal disorientation of the smaller particles. At the same time the small particles contribute excessively to the colloid viscosity due to the greater volume of the stabilizing layer around the particle per unit of particle volume. Hence, various means were devised for removing small particles.

Centrifugal Classification. - Centrifugal classification attempts to separate particles of different sizes by utilizing the difference in sedimentation velocity. The fluids treated in these experiments previously had oversize and undispersed materials removed by centrifuging so in the additional centrifuging, material is merely moved from one fluid region to another and no material leaves the fluid.

Initially a sample of fluid holds particles of all sizes throughout its volume. After centrifuging, the bottoms contain an excess of large particles in mixture with at least as great a concentration of small particles as in the original, while the top of the tube contains a mixture which is deficient in large particles. Thus, the top fraction will be more nearly monodisperse than the bottom but it is not the size range of interest here. This is an *a priori* disadvantage of this method. Two bottom fractions may be combined and recentrifuged in which case the second bottoms so obtained should be somewhat more monodispersed in large particles than before. Sufficient tests were conducted, as described below, to determine the magnitude of the effect.

Initial tests indicated that dilution is necessary to obtain any appreciable separation, probably due to hindered settling effects. Subsequently, dilution of G-1, -2, -3 material with an equal volume of kerosene was done prior to spinning which then required an additional vacuum evaporation step later on. Material was centrifuged for 1 hour at 17 000 g, with the results shown in table 16.

TABLE 16. – EFFECT OF CENTRIFUGATION ON COMPOSITION OF A FERROFLUID

Sample	M_s	ρ	ϵ, percent
Top fraction	34.9	0.856	1.43
Bottoms	53.5	.882	2.05

The concentration of tops, bottoms, and original fluid were then varied by evaporation and dilutions and properties measured to determine the effect

on viscosity. Sufficient data were obtained to plot curves from which the values in table 17 could be interpolated.

TABLE 17. – VISCOSITY OF PORTIONS OF CENTRIFUGED FERROMAGNETIC FLUIDS AS A FUNCTION OF THEIR SATURATION MAGNETIZATION

Saturation magnetization, M_s, gauss	Viscosity, η, centipoise (T = 30° C)			
	Tops	Original	First Bottoms	Second bottoms
10	2.1	2.0	2.0	1.95
20	3.2	2.3	2.3	2.2
40	4.0	3.2	3.0	2.9
80	22.0	6.5	6.5	5.5

The data of table 17 show, as expected, that the top fluid is degraded more-so than bottoms fluid is improved. In fact, no appreciable improvement in bottoms is noticeable until the second spinning. In conclusion, the improvement obtained here is not great and further work seems more promising along other lines when it is highly magnetic fluid of low viscosity that is desired.

Magnetodialysis. - Another possible means for obtaining the separation was a process of magnetically aided dialysis.

Ordinary dialysis relies on diffusion through a membrane to separate various species. The permeability of the membrane varies from species to species and permits their separation. In the magnetically aided dialysis the membrane is replaced by a magnetic field gradient through which a particle diffuses at a rate dependent on its magnetic moment. Since smaller particles experience less magnetic force than larger particles, they are expected to diffuse faster and hence permit the desired separation.

Initial experiments consisted simply of dipping a bar magnet into magnetic fluid, then suspending the bar magnet with its magnetic fluid coating in a volume of solvent (kerosene) in a beaker. It was observed that the field served to hold the magnetic fluid to the pole piece in a satisfactory

manner while diffusion proceeded. However, the system was very sensitive to vibration when removing the sample so that blobs of fluid were lost and in addition very little material could be processed at a time. Subsequently an improved system was devised as shown in figure 18 in which a finite region of magnetic field serves to separate reservoirs of any desired sizes. The attraction of the magnetic field and initial charge of fluid was such that the system could be inverted without loss of material. Thus, the fringing magnetic field served quite effectively as a nonmaterial membrane.

A theoretical description of the process is of interest for the purpose of interpreting the experiment and will now be developed. The model system consists of a semi-infinite slab region of fluid with faces at $y = 0, \ell$. The concentration of magnetic particles in the fluid at $y = 0$ is maintained at $n(0) = n_0$ while at $n(\ell) = 0$. The region is permeated by a magnetic field of constant gradient dH/dy that produces a force on each particle in the direction of smaller y. The particle flux N is determined by the superposition of a diffusive flux and a current as

$$N = - \mathcal{D} \, dn/dy + nu \tag{11}$$

where

$$\mathcal{D} = kT/3\pi\eta D \tag{12}$$

is the Einstein diffusion coefficient and u is the terminal velocity of a particle in the positive y direction due to magnetic force opposed by viscous drag. Assuming Stokes' Law of drag and that the magnetic force on a particle is unaffected by the magnetic field of other particles,

$$\frac{M}{4\pi} \frac{\pi D^3}{6} \frac{dH}{dy} = - 6\pi\eta \frac{D}{2} u \tag{13}$$

where η is viscosity of the suspending fluid and the equation is written in cgs units. For steady-state diffusion so that N is constant, equation (11) is a linear first order differential equation whose integrating factor is $e^{u\ell/\mathcal{D}}$. The solution subject to the boundary conditions given previously is

$$N = \mathcal{D} \frac{n_0}{\ell} \frac{u\ell/\mathcal{D}}{(e^{u\ell/\mathcal{D}} - 1)} \tag{14}$$

where, from equations (12) and (13),

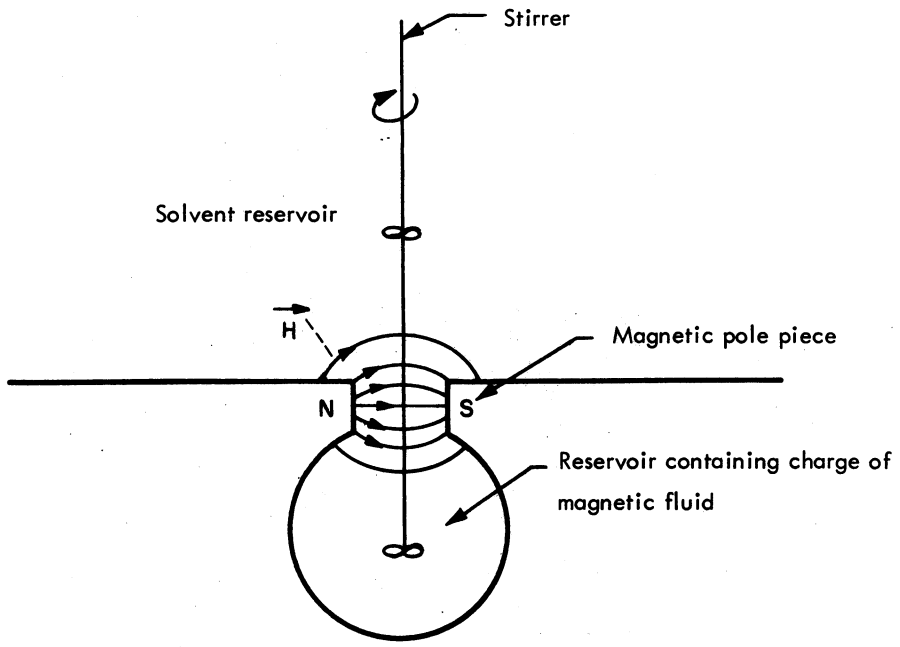

Figure 18. – Schematic Illustration of Magnetodialysis Apparatus

$$\frac{u\ell}{\mathcal{D}} = \frac{v M \frac{dH}{dy} \ell}{4\pi k T} \tag{15}$$

in which $v = \pi D^3/6$ is the particle volume. Since $\mathcal{D} n_o/\ell$ is the diffusion rate in the absence of magnetic forces, equation (14) is expressed as the product of that rate times a fractional factor that corrects for retardation of the rate due to the applied field. One curve in figure 19 is a plot of equation (14) for typical conditions identified in the legend. Another curve, entitled Dialysis, plots the diffusion rate versus particle size for diffusion in the absence of magnetic effects. It is seen that for a particle diameter which is less than about 50 Å the curves closely coincide. Above about 150 Å the particles are effectively prevented from escaping across the boundary $y = \ell$ by the magnetic field while in the absence of a magnetic field the diffusion flux of particles of this size would be appreciable. Hence the analysis gives hope that a fairly sharp separation might be obtained in which remaining fluid is composed of particles whose diameter is greater than $\mathcal{D} \simeq 100$ Å.

To estimate the importance of superparamagnetism (thermal disorientation) on the above calculations the effective value of magnetic moment per unit volume was recomputed for each particle size from the Langevin expression L(a) for use in equations (16) and (17)

$$L(a) = \coth a - \frac{1}{a} \tag{16}$$

$$a = \frac{v M_s H}{4\pi k T} \tag{17}$$

Here M_s is the saturation magnetization of bulk material and thus the effective value of magnetization is given by ML(a). A mean field of H = 2000 oersted was assumed for the estimate. It may be seen from the figure that the corrected curve is barely distinguishable from the original curve, hence the correction is unimportant in this case.

A 1000-hour experiment with 45 ml of oleic-acid-stabilized magnetite-in-kerosene ferrofluid (G-1, -2, -3) was performed the results of which are presented in table 18. The sample of dialyzed material was vacuum evaporated to yield the concentrated dialyzate. It is seen that the magnetization of 110 gauss is higher than that of the original material, 95 gauss, although the viscosity 5.4 cp is less than that of the original material, 8.5 cp. Hence, it may be concluded that the magnetodialysis did indeed benefit the

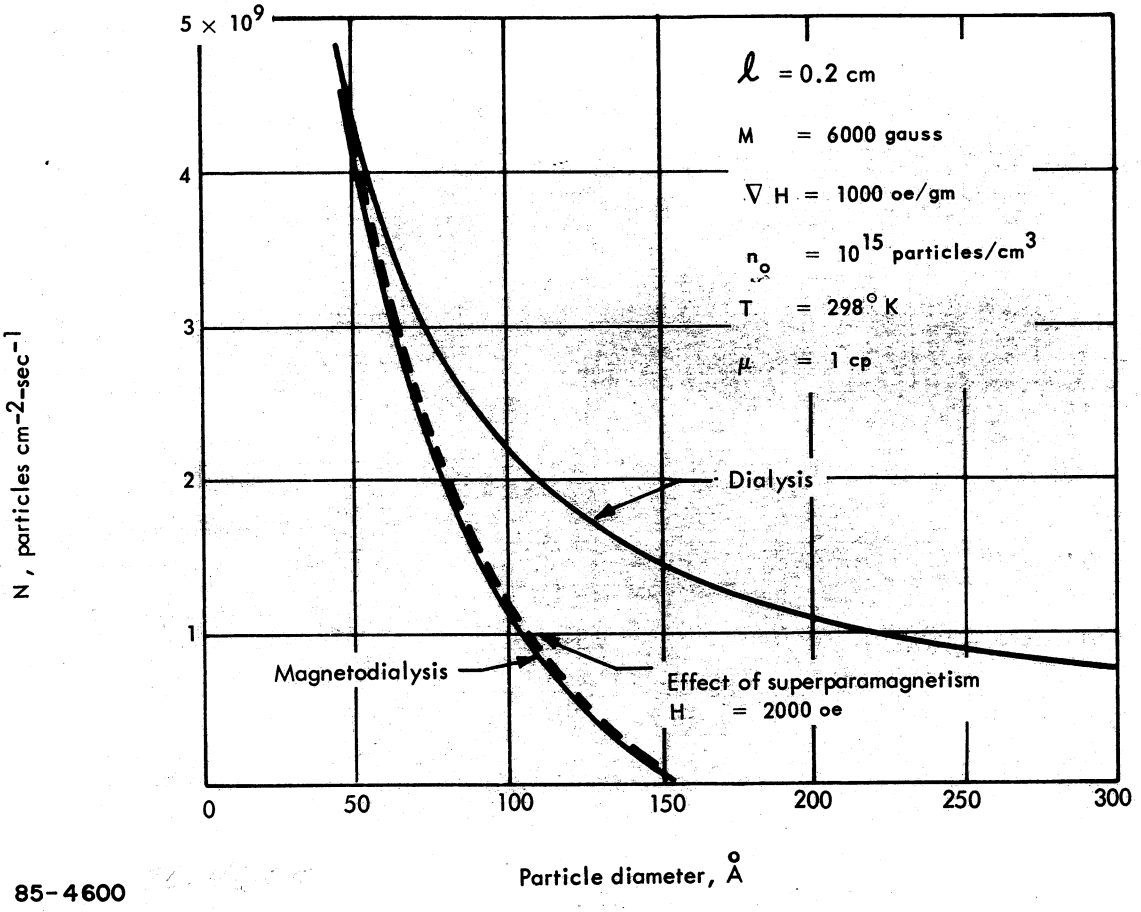

Figure 19. – Diffusional Flux Rates in Magnetodialysis Compared to Ordinary Dialysis as a Function of Particle Size

TABLE 18. – MAGNETODIALYSIS EXPERIMENTAL DATA

Sample	Magnetization; gauss (H = 10 000 oe)	Viscosity 30° C, cp	Density R. T. gm/cc
Fresh material (G-1, -2, -3)	95	8.5	0.953
Dialyzed material (1000 hours)	28	2.5	.836
Concentrated dialyzate	110	5.4	.946
Dilute G-1, -2, -3	71	5.4	.922

material and most probably did so by selective extraction of undersize material. As another comparison, the table shows that diluted starting material of viscosity 5.4 cp has a magnetization of only 71 gauss compared to 110 gauss for 5.4 cp concentrated dialyzate so that a 55 percent increase in magnetization at a constant viscosity was realized.

Substantial further work has to be done in the area of particle size distribution modification. In overall effectiveness, the most promising of the techniques appears to be magnetodialysis, especially if it were combined with a process of selective grinding.

METALLIC FERROFLUIDS

The initial objective of this phase of the work was to determine the feasibility of preparing a highly concentrated amalgam of low viscosity and high magnetization. For one application to energy conversion (ref. 7) the magnetization should be 10 000 gauss corresponding to a packing fraction of about 0.5 while the viscosity should be low enough, e.g., $\eta < 25$ centipoise, to prevent excessive wall friction in flow through small bore tubes.

Electrodeposition

Preparation of metallic ferrofluids was attempted by electrodeposition of a magnetic metal in mercury to form magnetic amalgams. This technique has received a great deal of attention in recent technology through the studies

TABLE 19. – ELECTRODEPOSITION OF IRON PARTICLES

Measured variables										Percent iron by volume calculated results		
Sample	Volume of mercury, cc	Electrolyte	Electrolyte concentration, molal	pH	Voltage, v	Current, amps	Time, min	Amalgam[a] density, gm/cc	Magnetic moment, gauss, at H = 10, 000 oe	Faraday, [d] percent	Density, [e] percent	Magnetic[f] moment, percent
ED-1	66.5[b]	$FeSO_4 \cdot 7H_2O$	1.6	---	3.2	4	145	---	---	1.9	---	---
ED-2[c]	66.5	$FeSO_4 \cdot 7H_2O$	1.6	2	3.4	4	161	13.17	---	2.1	6.5	---
ED-3	133	$FeCl_2 \cdot 4H_2O$	2.2	2	2.2	2	50	12.59	500	2.7	16.9	2.3
					4.0	5	150					
ED-4	66.5	$FeSO_4 \cdot 7H_2O$	2.0	2	4.5	4	150	---	210	1.0	1.8	1.0
ED-5	66.5	$FeSO_4 \cdot 7H_2O$	1.6	1	3.0	3	360	13.38	705	3.5	3.0	3.3
ED-6	66.5	$FeSO_4 \cdot 7H_2O$	1.6	1	1.4	0.5	960	13.45	---	1.6	1.8	---

[a] All samples were magnetically concentrated except ED-1 and ED-2.

[b] Contained 5.5 grams of dissolved 20 mesh tin.

[c] Subsequently electrolyzed with $SnCl_2\ 2H_2O$ at pH1; 4 volts and 0.5 amp for 8 hours.

[d] Assumes 100 percent cathodic efficiency.

[e] Calculated from densities as $(\rho_{Hg} - \rho_{amalgam})/(\rho_{Hg} - \rho_{Fe})$.

[f] Assumes magnetic moment of saturated iron of 21 580 gauss.

of Luborsky (ref. 5) and coworkers; in their work the subdomain particles are produced in elongated shapes for use in the production of permanent magnets. The method was known to Joule (ref. 8) who observed the general properties of iron amalgams resulting from the electrolysis of the sulfates and chlorides at mercury cathodes. A semisolid sample of a fluid amalgam, 1.39 percent by weight in iron, containing 1.2 grains of iron was attracted by a magnet with a force of 0.36 grain. A sample of iron weighing 3.06 grains placed in the same container was attracted by a force of 0.94 grain. Assuming the amalgam density is 13.5 gm/cc, iron density 7.87 gm/cc and iron magnetization of 21 580 gauss, the magnetization under the applied field was $\frac{3106\ (13.5)\ (0.36)\ (0.0139)\ (21\,580)}{12\ (7.87)\ (0.94)}$ = 502 gauss. As will be seen, this is comparable to the values obtained in the present work.

Duncan (ref. 9) gives a review with many references to the literature regarding the nature of iron amalgams.

In the present work an electrolysis cell was also constructed for the preparation of magnetic mercury colloid. The cell accommodated 50 to 150 milliliters of mercury in a flat pool which served as a cathode for electrolysis from aqueous solution. An Armco iron anode having the same area is positioned above the mercury surface to produce a uniform current density. The mercury is agitated by a stirrer to promote formation of spherical particles and the cell is immersed in a constant temperature bath.

The results of various electrodeposition experiments are listed in table 19. The amount of iron contained in the amalgam as determined from the Faraday equivalents to the total coulombs of charge that flowed is consistent with the amount calculated from the measured magnetic moment of the amalgam using the search coil technique. However, the content of iron determined by measurement using pycnometer technique leads to large overestimates at times. This indicates that simple additivity of volumes is not attained; the incorporation of iron into the mercury leads to an anamalous reduction in density.

The magnetic particles do not separate from the liquid carrier. However, the magnetic mercury is separable into a magnetic portion and a nonmagnetic portion. The magnetic portion is very viscous and usually displays a finite yield stress. Thus the free surface of a small pool of the material may be deformed after which the material fails to recover its shape. Measurements of the viscosity with a Brookfield viscometer show that apparent viscosity is a smoothly decreasing function of shear rate. Typical of the data for the following measurements obtained with ED3: η = 90 000 centipoise at 2 rpm, η = 40 000 at 4 rpm, η = 17 000 at 10 rpm, and η = 11 000 at 20 rpm at room temperature using spindle number 5.

A bismuth amalgam was prepared by electrolysis from $Bi(NO_3)_3 \cdot 5H_2O$ in dilute nitric acid using a platinum anode and 100 grams of mercury, running 1 ampere for 1/2 hour. A portion of the material was added to a portion of ED3 material and magnetically concentrated. The product was very magnetic, seemed to have a low viscosity and no longer displayed a yield stress such as mentioned above. However, a sequence of similar experiments using ED4 material resulted in a product more viscous than the original; hence, the material with vanishing yield stress is difficult to reproduce.

Addition of the mercury soluble additive to a magnetic amalgam reduces its viscosity. However, since the additive also increases the volume of the mixture there is some question as to the mechanism responsible for the decreased viscosity. On the one hand the reduction may be due to a change in the van der Waals attraction force between particles while on the other hand it may simply be due to the greater particle to particle separation that is brought about. To decide between the better of these two possibilities a series of experiments were performed in which portions were diluted first with indium, then with mercury. Indium rather than bismuth was chosen on the basis of its ready solubility in mercury. By comparing the viscosity of the indium sample of a given magnetization with the viscosity of a mercury-iron sample of the same (interpolated) magnetization a meaningful comparison could be made. These results are summarized in table 20.

TABLE 20. – VISCOSITIES OF MAGNETIC AMALGAMS

Material	Magnetization, gauss	Viscosity, cp
Initial amalgam	573	126×10^4
Amalgam + mercury	544[a]	36×10^4
Amalgam + 2.5 weight,% indium	544[a]	9.9×10^4

[a]Interpolated values.

The viscosity of these amalgams is a function of the strain rate which, however, was held constant in these experiments. Thus, amalgam viscosity was measured with a Brookfield viscometer using a cylindrical spindle (CLV No. 3) at a rotational speed that resulted in an applied strain rate of

0.18 sec^{-1}. It is seen that addition of indium reduced the viscosity by a factor of 3 to 4 times greater than occurred by equally diluting a sample with mercury. Therefore, it is concluded as more probable that the transmission of van der Waals forces was affected by the addition of indium which in turn led to a reduction of the force and a decrease in viscosity. By the same token the experiment indicates that magnetic interaction between particles was not solely responsible for the observed viscous behavior.

A recent patent (ref. 10) also describes the addition of metallic bismuth, magnesium, or aluminum to increase the colloid fluidity of magnetic, iron-containing mercury amalgam. A sample of this material was furnished to us by the inventor that we might determine its magnetic property and appearance. The material as furnished displayed good fluidity while its saturation ferric induction was 1190 gauss. The material, just like the material we have produced, would segregate in the gradient field of a permanent magnet. The magnetic portion removed from the excess mercury then assumed the characteristic semisolid or thixotropic form characteristic of a gel. In this state its saturation ferric induction was 2330 gauss, a rather high value. Again, it was evident that the material was not truly stabilized against flocculation even though it did possess good fluid behavior in the initial state.

Qualitative experimentation in the preparation of nickel amalgam gave end results similar to the iron amalgam. Although initially deposited nickel amalgam is not ferromagnetic, it becomes so when temperature is increased. Bates (ref. 11) gives 225° C for the transition temperature.

Status

It is concluded that ferromagnetic amalgam of the high concentration originally desired is unknown in the fluid state. The generally high viscosity of even the dilute amalgams suggests, in the light of viscometric consideration, that the dispersion of particles is structured as a network of chains in gel fashion. This follows in as much as monodisperse systems of the same concentrations have low theoretical viscosities.

Based on observation of the undesired tendency of magnetic amalgam of any concentration to segregate in an applied magnetic field gradient, these studies were not carried any further.

PROPERTIES OF FERROFLUIDS AND THEIR RELATION TO STRUCTURE

Size Distribution by Electron Microscopy

Basic parameters of any colloidal dispersion of solid particles are the size and size distribution of these particles. Direct measurements of the size and distribution of the ferrofluids were obtained by taking electron micrographs of samples of the suspensions.

Experimental. - The specimen for examination in the electron microscope is first dispersed on thin carbon films supported by copper grids. Specimens prepared by this technique provide shadowgraphs of the powder on a photographic plate from which information on particle size and shape are obtained.

The electron microscope used in these measurements is the 100 kV Siemens Elmiskope I. This microscope has a useful magnification range of 200 to 200 000 times with a resolution of 10 angstrom units. The resulting images are photographed on 6.5 x 9-centimeter glass plates from which 2X enlargements are obtained.

These photomicrographs provide images of the base solid particles. The electron bombardment in the microscope results in severe heating of the particles. Temperatures of 1000° C have been estimated for nonconducting particles. Since the specimen is under vacuum, the organic layer evaporates or chars, leaving a carbon residue which is transparent to the electron beam.

Four micrographs of G-44 fluid were obtained at two different magnifications, 160 000X and 320 000X. Two photographs were obtained from ground and centrifuged fluid and two others were obtained from samples that had then been flocculated and redispersed. These photomicrographs were obtained to characterize G-44 fluids, to show the effect of sampling on particle distribution by having four different samples, and to determine if there were any effects of flocculation on the particle size distribution of the solids in suspension.

A photomicrograph typical of the ferrofluids made from IRN 100 magnetite was obtained for runs G-4, -5, -6 and also for run G-21. A photomicrograph of fluid G-26 made with the Wright Industries magnetite was also obtained. So was a photomicrograph of fluid G-24 made with

Krystanel, 90 to 100° C Curie point, manganese-zinc ferrite. Particles forming the gel that resulted at the end of run G-46 were redispersed for another photomicrograph. The solid here was IRN 100 magnetite.

All the photographs resembled each other. A typical photograph is shown as figure 20. The ferrofluid particles are fairly compact, irregularly shaped masses. The particle size ranges from about 30 to 240 Å overall. The distribution is much narrower in the individual photographs however.

Particle Size Distribution Measurements. - Detailed particle distribution measurements were made in those instances where other physical measurements were made on the fluids under consideration and for which an absolute measure of particle size was necessary for analytical treatment.

Particle size distributions were obtained for the G-4, -5, -6, G-21, and G-44 fluids. The projected diameter of 250 particles was obtained from a photomicrograph by approximating the cross-sectional area of a particle to the area enclosed by a calibrated transparent circle. A single such determination was made for the G-21 and G-4, -5, -6 fluid. Four determinations, one from each of the four photomicrographs, were made for the G-44 fluid. This provided a method of determining the reproducibility of this measurement.

Histograms for the different particle counts are presented in figures 21 to 26. These distribution curves were replotted on logarithmic probability paper in figures 27 to 32. In these figures, the cumulative number fraction smaller than a given diameter on a probability graph is plotted against the logarithm of this diameter. Straight lines were obtained when the data was plotted in this manner. This indicates that the particle size distribution is log normal. According to this distribution law, it is not the differences of equal amount in excess or defect from a mean value which are equally likely but ratios of equal amount in excess or defect from a mean value. The log normal distribution is expressed by the following equation:

$$y = \frac{1}{\ell n\ \sigma_G \sqrt{2\pi}} \exp\left[- \frac{(\ell n\ D - \ell n\ \overline{D}_G)^2}{2\ \ell n^2\ \sigma_G} \right] \qquad (18)$$

where $\overline{D}_G$ = geometric mean diameter

σ_G = the geometric standard deviation, the standard deviation of the distribution of ratios around the geometric mean.

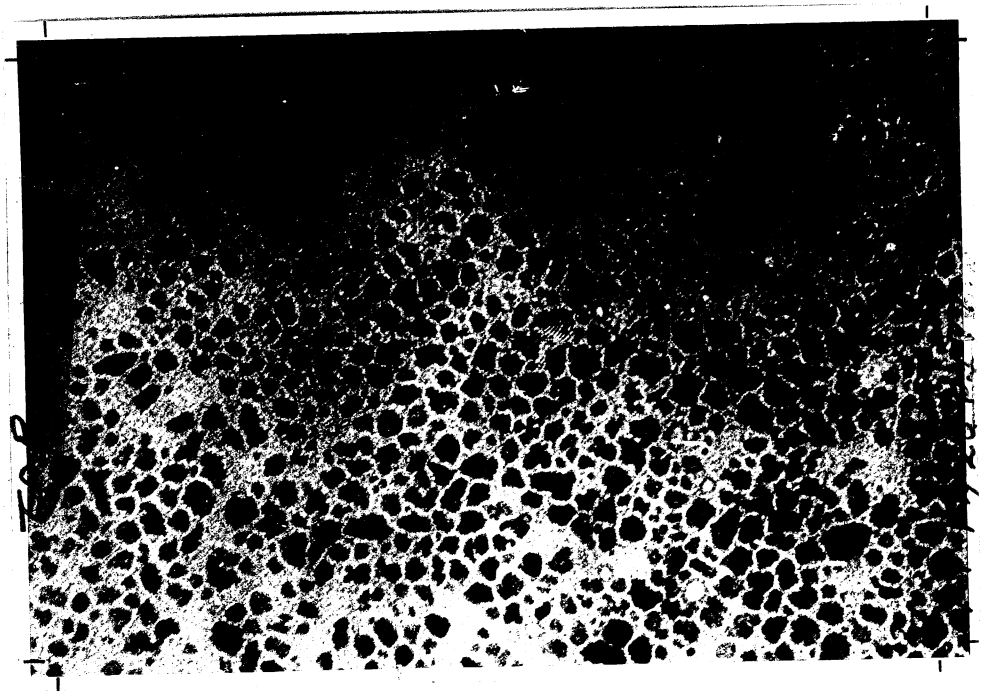

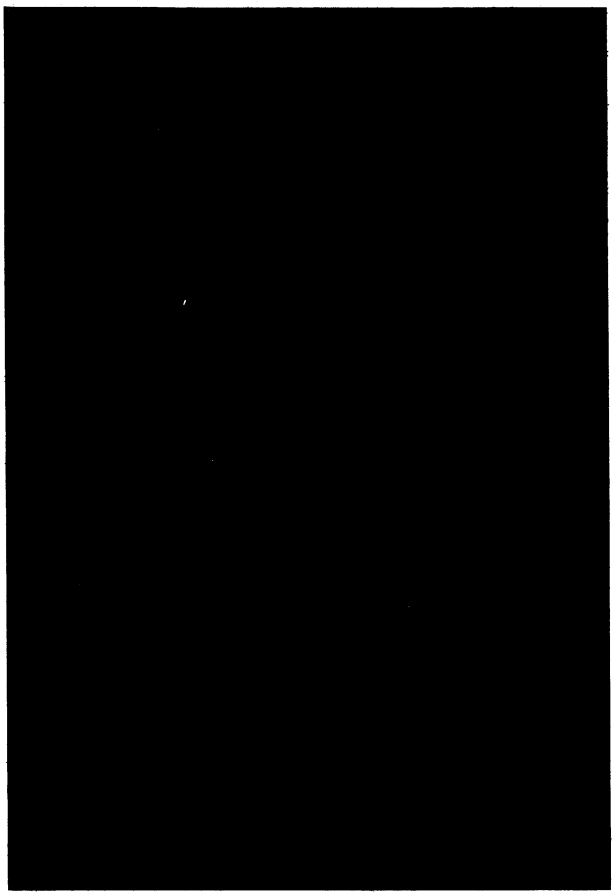

Figure 20. – Electron Micrograph (66881) of
G-4, -5, -6 Ferrofluid (240 000X)

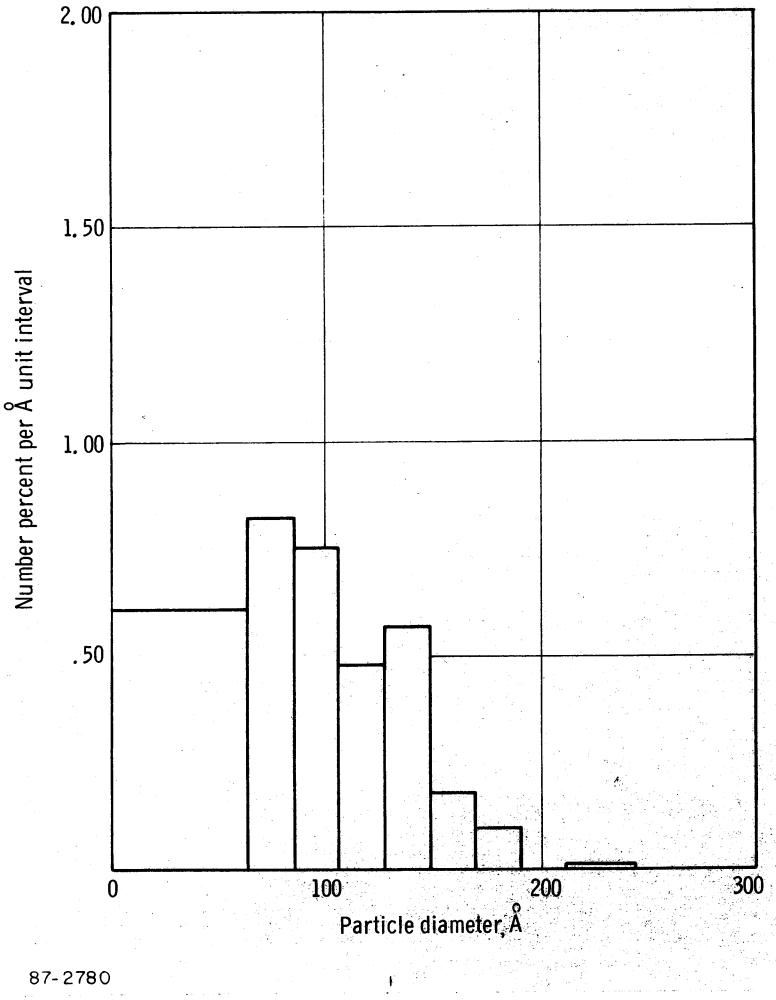

Figure 21. – Particle Size Distribution for G-44 Fluid Derived from Electron Micrograph 66891 (240 000X)

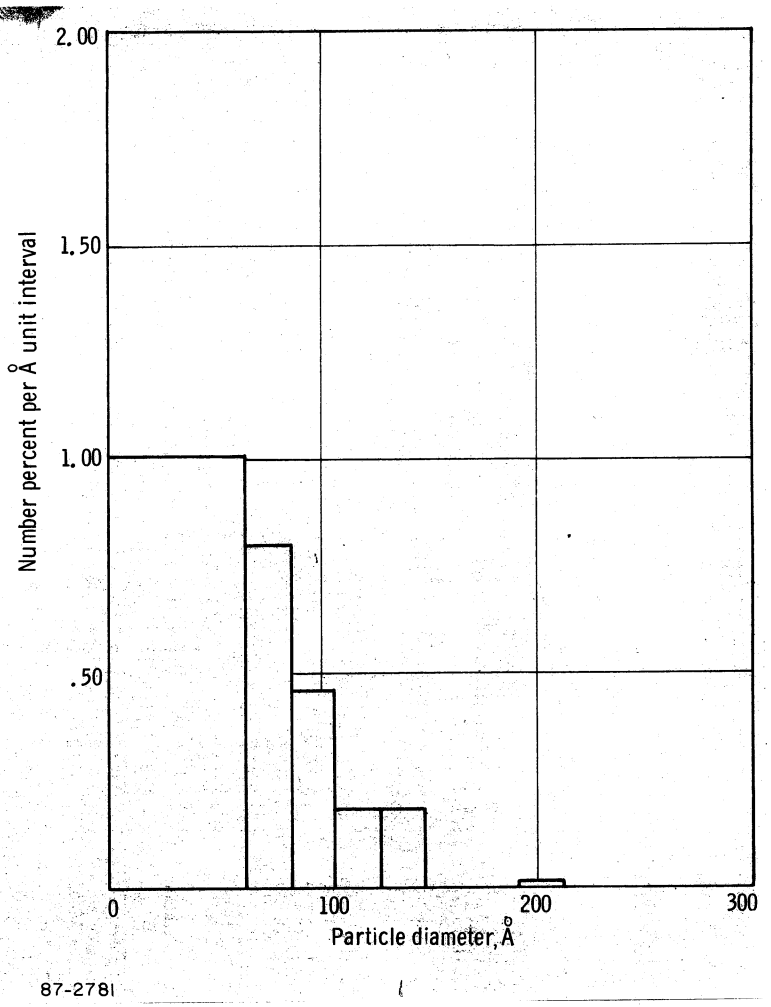

Figure 22. – Particle Size Distribution for G-44 Fluid Derived from Electron Micrograph 66905 (240 000X)

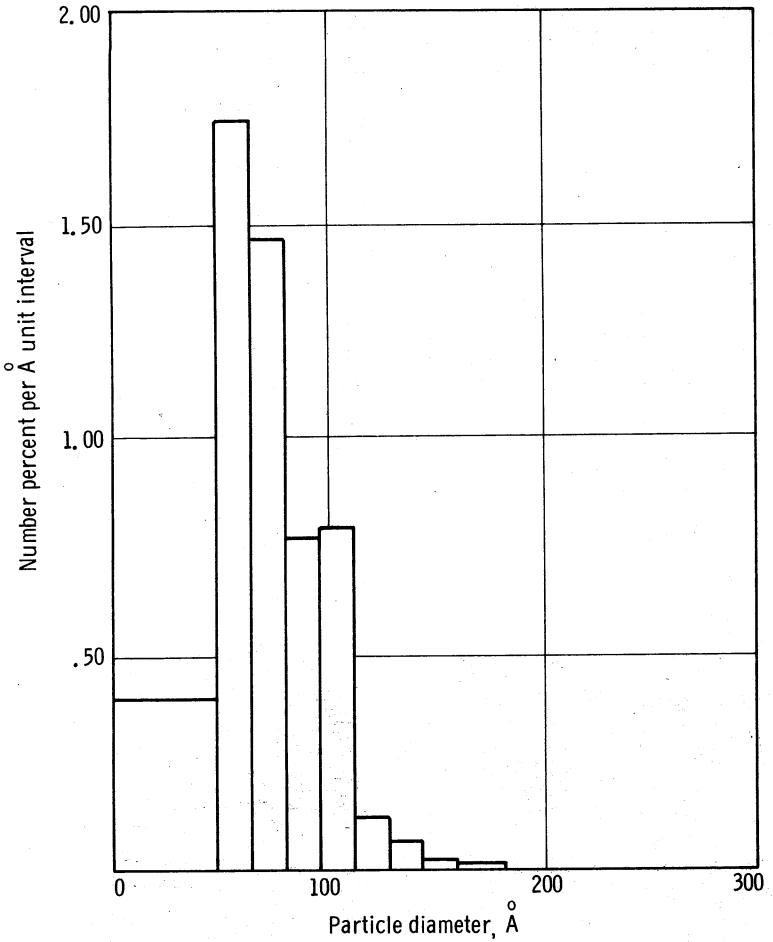

Figure 23. – Particle Size Distribution for G-44 Fluid Derived from Electron Micrograph 66892 (320 000X)

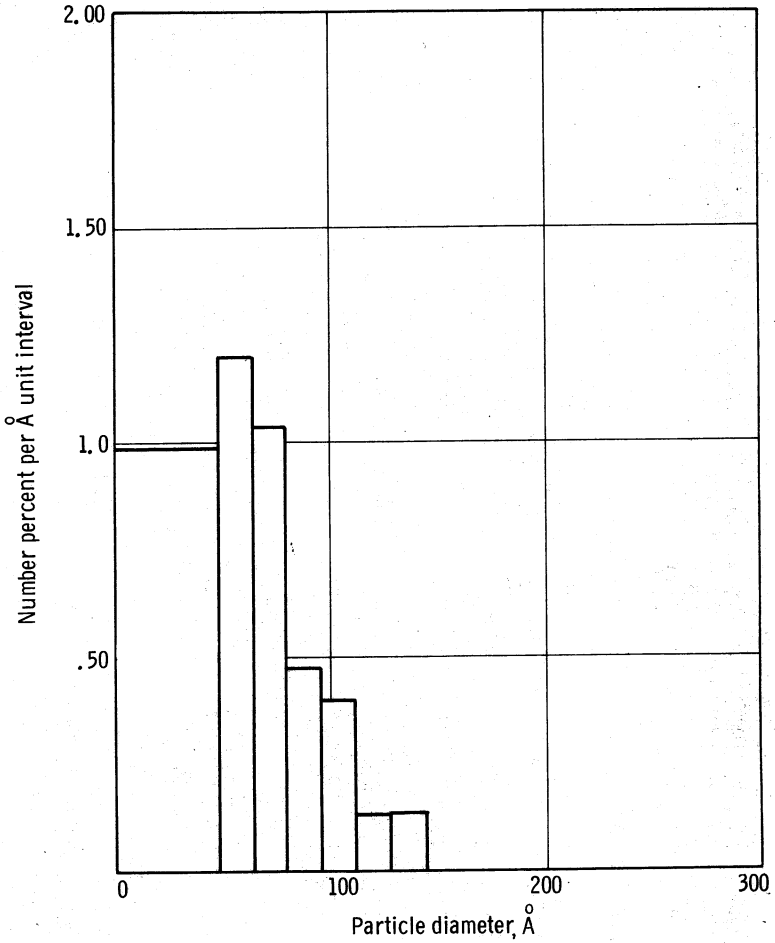

Figure 24. – Particle Size Distribution for G-44 Fluid Derived from Electron Micrograph 66906 (320 000X)

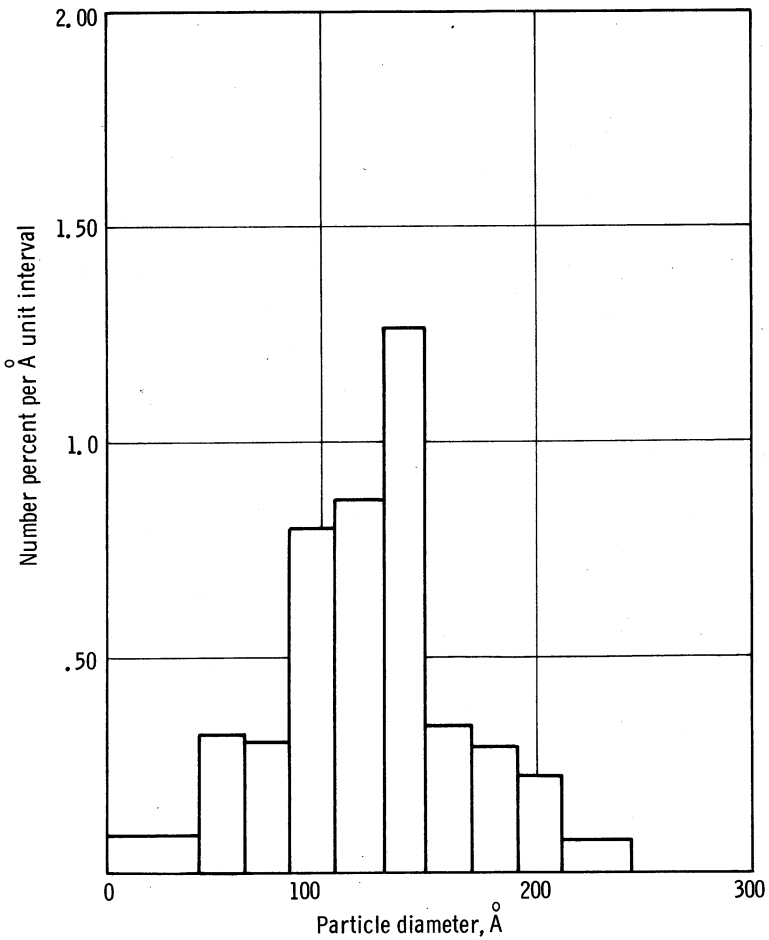

Figure 25. – Particle Size Distribution for G-21 Fluid -- 250 Count

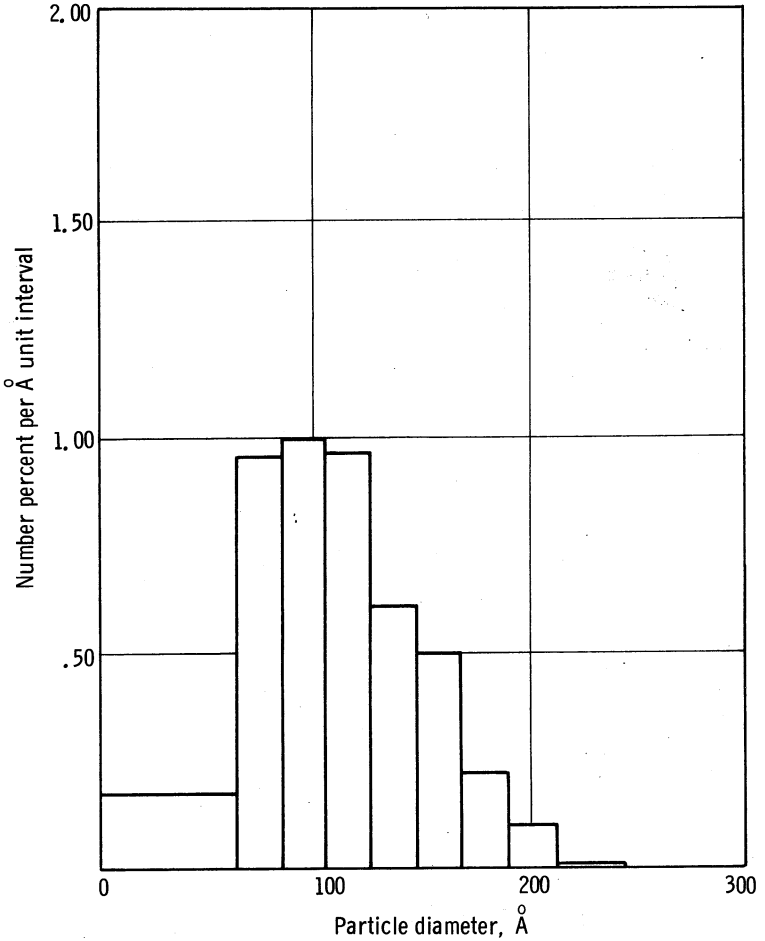

Figure 26. – Particle Size Distribution for G-4, -5, -6 Fluid -- 500 Count

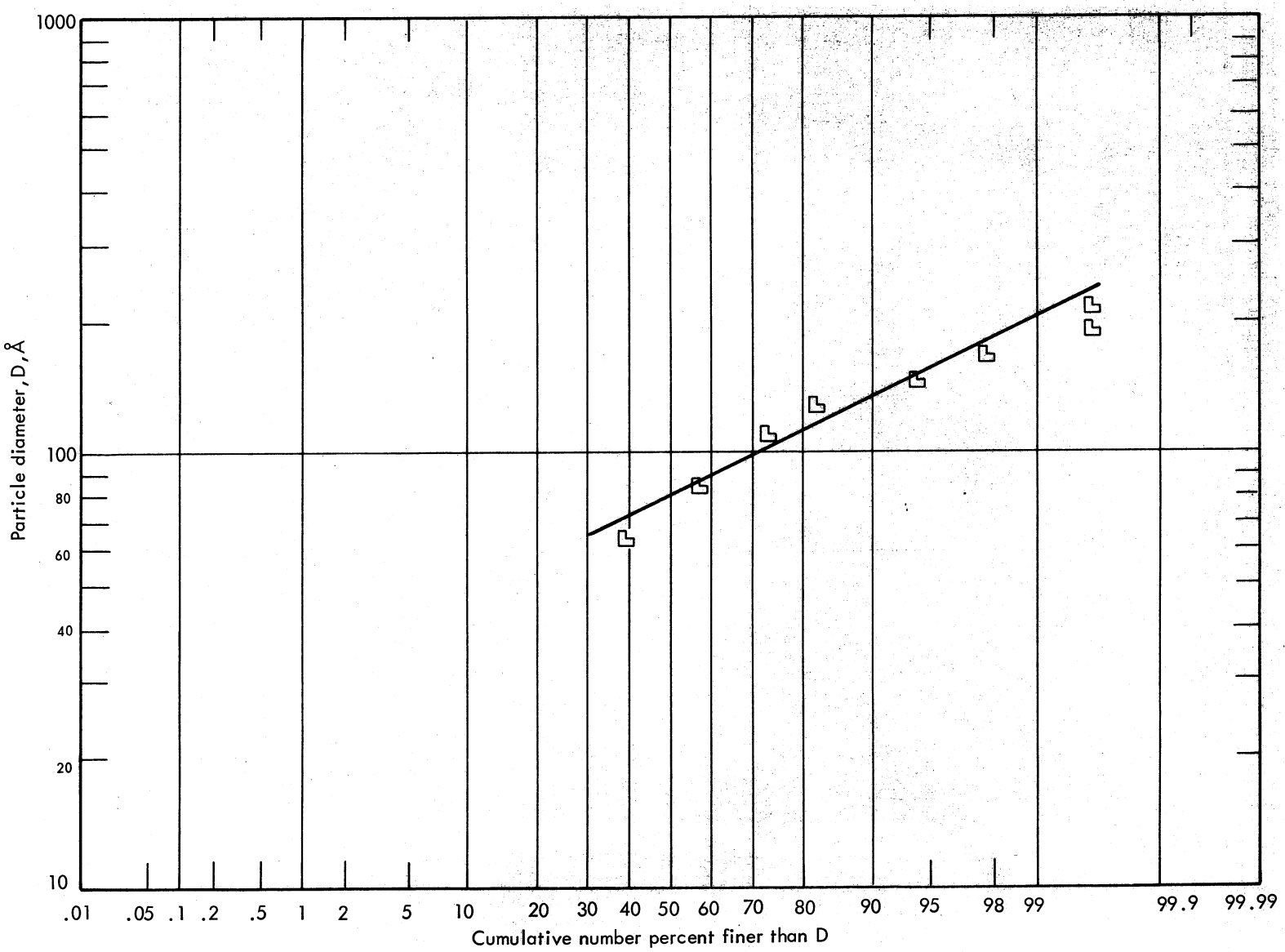

Figure 27. – Cumulative Particle Size Distribution of G-44 Fluid (Logarithmic Probability Plot)
Photograph 66891 (240 000X)

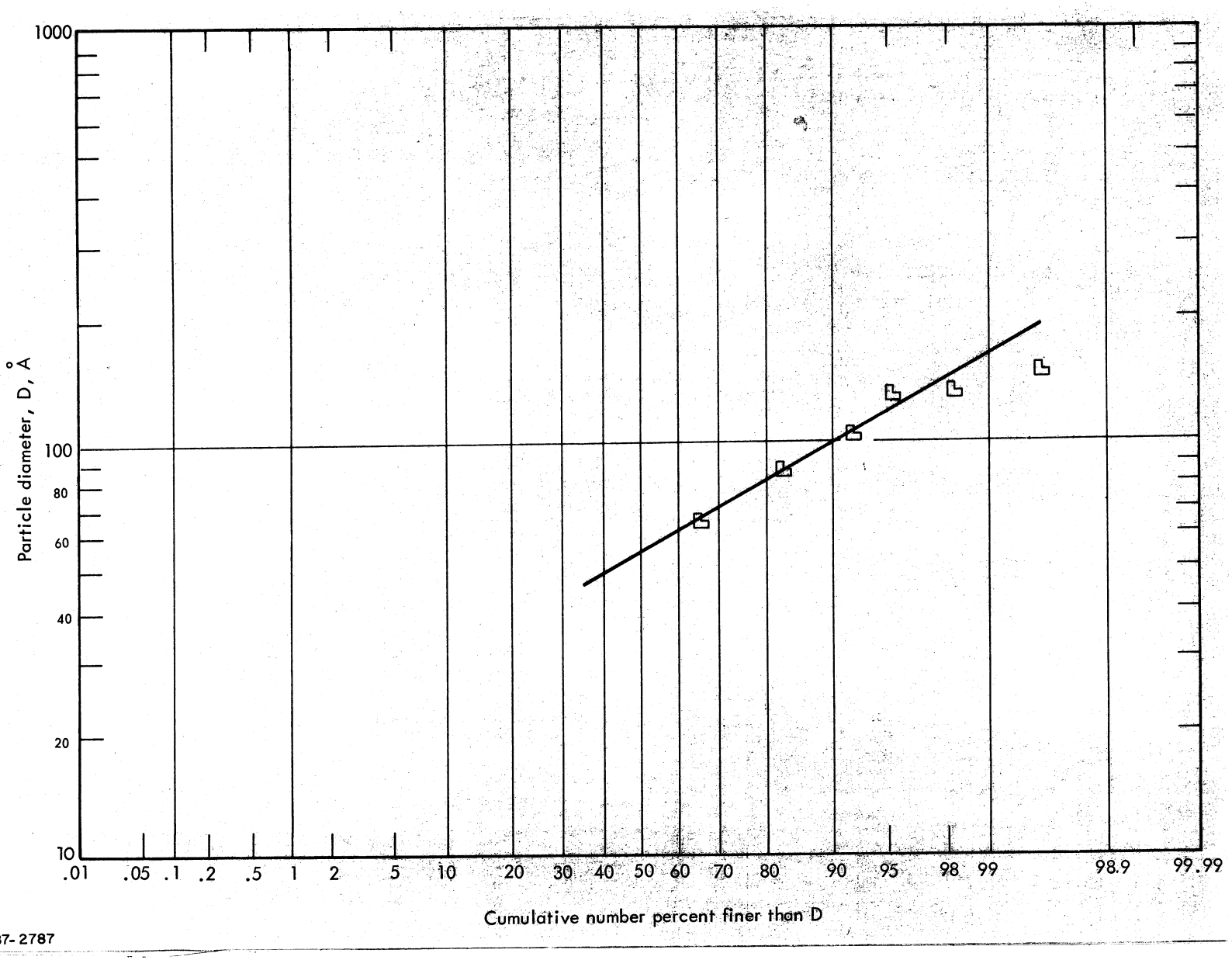

Figure 28. – Cumulative Particle Size Distribution of G-44 Fluid (Logarithmic Probability Plot)
Photograph 66905 (240 000X)

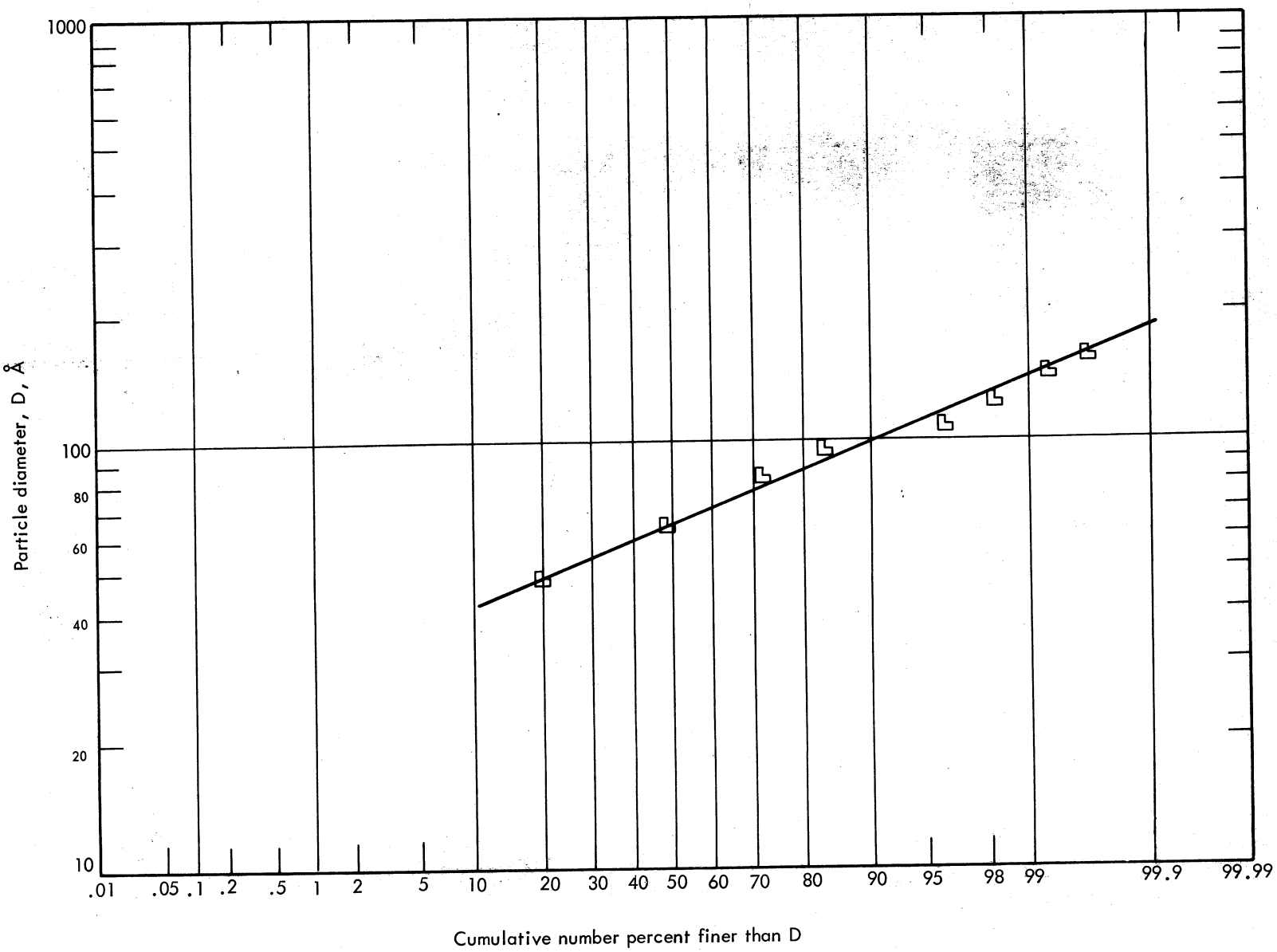

87-2788

Figure 29. – Cumulative Particle Size Distribution of G-44 Fluid (Logarithmic Probability Plot)
Photograph 66892 (320 000X)

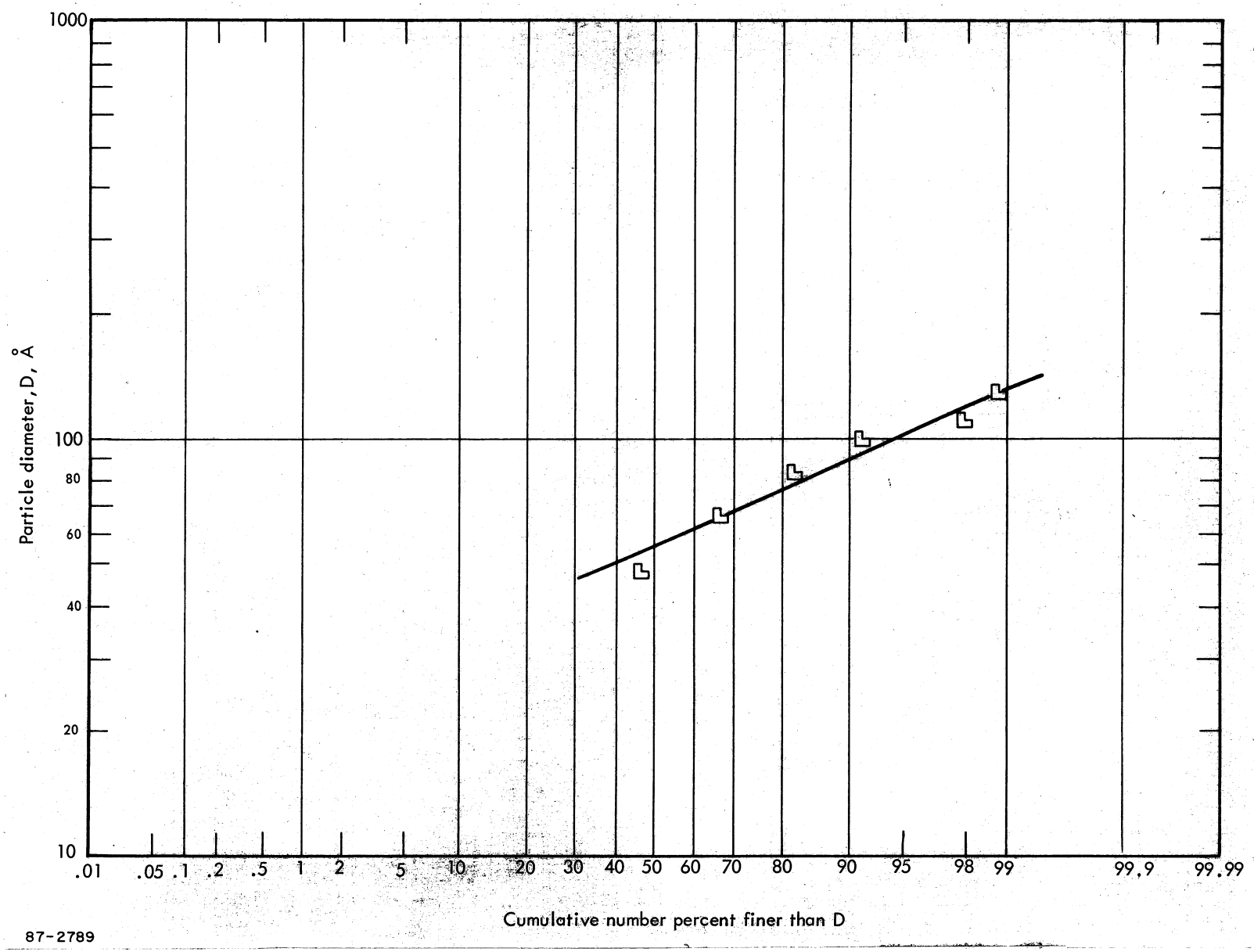

Figure 30. – Cumulative Particle Size Distribution of G-44 Fluid (Logarithmic Probability Plot)
Photograph 66906 (320 000X)

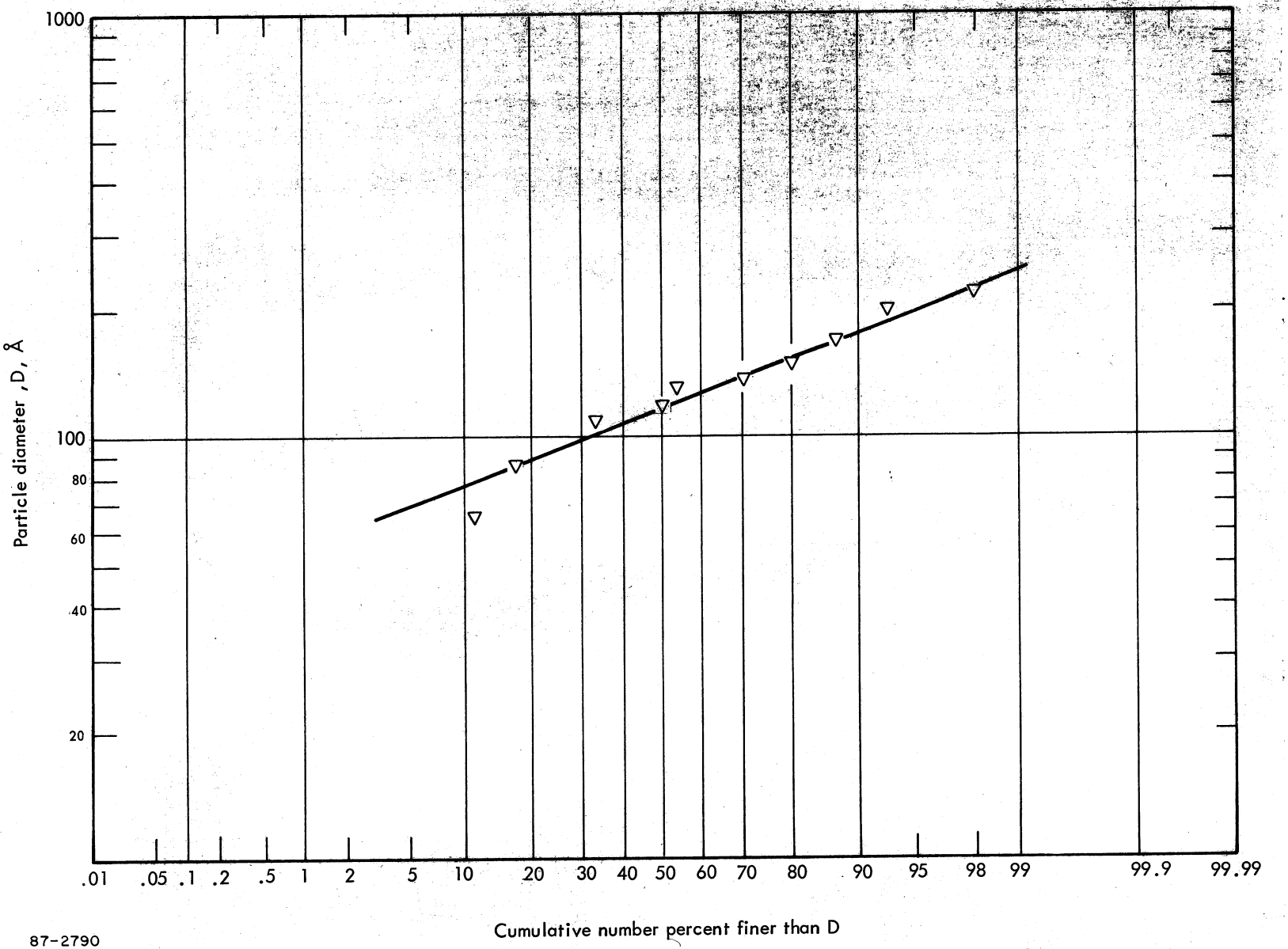

Figure 31. – Cumulative Particle Size Distribution of G-21 Fluid (Logarithmic Probability Plot)

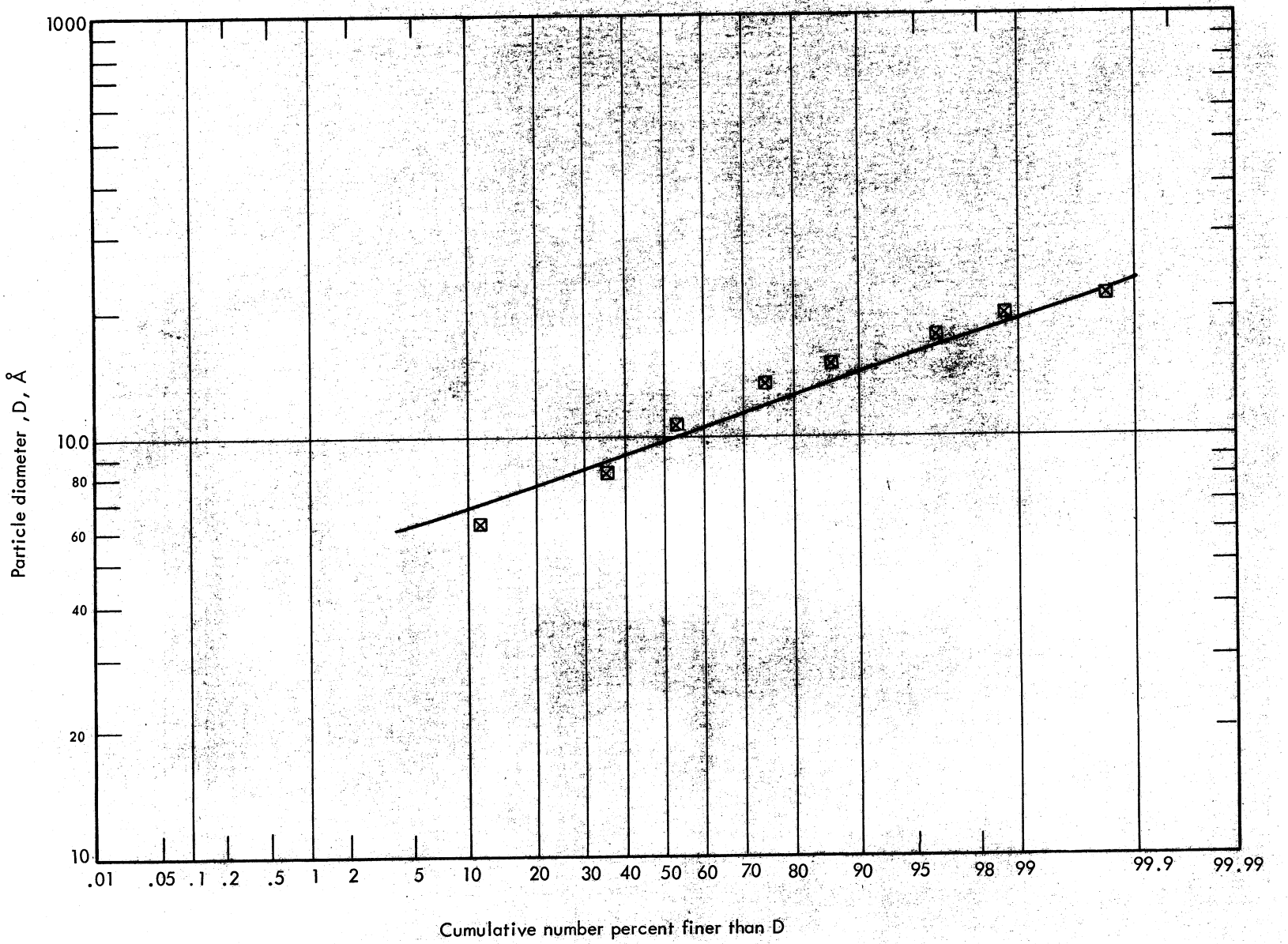

87-2791

Figure 32. – Cumulative Particle Size Distribution of G-4, -5, -6 Fluid (Logarithmic Probability Plot)

The log normal distribution often characterizes the distribution of particle sizes for systems subjected to grinding so that the results obtained here are not at all unusual.

As a rule if the number distribution of a given variable obeys a certain distribution, the normal probability distribution, for example, the weight distribution does not, and vice-versa. The log normal distribution is different. One of its properties is that if the number distribution is log normal, other distributions such as the weight distribution are also log normal and possess the same log standard deviation (ref. 12). The various averages are related to each other by the equations presented in table 21.

This is a useful property of this distribution, since the different mean diameters can be immediately calculated by formula once the basic particle diameter distribution is known. The basic distribution is easily obtained by plotting on logarithmic - probability paper, as was done in figures 27 to 32, where the cumulative number fraction smaller than a given diameter, D, is found on the X-axis (probability chart) and the corresponding diameter on the Y-axis (logarithmic chart). The geometric mean number diameter is obtained by drawing a horizontal projection at the 50 percent point on the line to the Y-axis. The log of the geometric standard deviation is obtained from the difference between logarithms of the particle size at the 84 percent level, which is obtained by drawing a horizontal projection of the line at 84 percent point to the Y-axis, and the logarithm of the geometric mean diameter.

$$\ell n\ \sigma_G = \ell n\ D_{84} - \ell n\ D_{50}$$

The different average particle diameters found for fluids G-4, -5, -6, G-21, and G-44 (individual counts and average of four counts) are presented in table 22. One common characteristic of these systems is the narrow particle size distribution.

The four measurements on G-44 fluids yielded the following parameters: $\overline{D}_{NG}$, mean value 63 Å with standard expectation 12 A; $\overline{\sigma}_G$, mean value 1.49, standard expectation 0.08.

A standard expectation of 20 percent for the mean diameter is good in view of the fact that two parameters were changed, namely, magnification and sampling technique. The flocculated samples yielded a smaller particle size while the magnification seemed to have an effect on the standard deviation of the dispersion. These effects were confounded in these measurements, however.

TABLE 21. – RELATION BETWEEN DIFFERENT PARTICLE STATISTICS FOR A LOG-NORMAL DISTRIBUTION

$$\ln \bar{D}_{VA} = \ln \bar{D}_{NG} + 3.5 \ln^2 \sigma_G$$

$$\ln \bar{D}_{VG} = \ln \bar{D}_{NG} + 3.0 \ln^2 \sigma_G$$

$$\ln \bar{D}_{SA} = \ln \bar{D}_{NG} + 2.5 \ln^2 \sigma_G$$

$$\ln \bar{D}_{LA} = \ln \bar{D}_{NG} + 1.5 \ln^2 \sigma_G$$

$$\ln \bar{D}_{NA} = \ln \bar{D}_{NG} + 0.5 \ln^2 \sigma_G$$

$\bar{D}_{VA}$ = Arithmetic volume average diameter = $\dfrac{\Sigma n_i D_i^4}{\Sigma n_i D_i^3}$

$\bar{D}_{VG}$ = Geometric volume average diameter = $\dfrac{\Sigma n_i \ln^4 D_i}{\Sigma n_i \ln^3 D_i}$

$\bar{D}_{SA}$ = Arithmetic surface average diameter = $\dfrac{\Sigma n_i D_i^3}{\Sigma n_i D_i^2}$

$\bar{D}_{LA}$ = Arithmetic length average diameter = $\dfrac{\Sigma n_i D_i^2}{\Sigma n_i D_i}$

$\bar{D}_{NA}$ = Arithmetic number average diameter = $\dfrac{\Sigma n_i D_i}{\Sigma n_i}$

$\bar{D}_{NG}$ = Geometric number average diameter = $\dfrac{\Sigma n_i \ln D_i}{\Sigma n_i} = \dfrac{\ln \Pi D_i^{n_i}}{N}$

σ_G = Geometric standard deviation; $\ln \sigma_G = \sqrt{\dfrac{\Sigma n_i \ln^2 D_i}{N} - \ln^2 \bar{D}_{NG}}$

TABLE 21

TABLE 22. – AVERAGE PARTICLE DIAMETERS FROM ELECTRON MICROGRAPHS FOR DIFFERENT FERROFLUIDS

Electron micrograph number	66881	66883	66892	66906	66891	66905	
Magnification, X	240 000	240 000	320 000	320 000	240 000	240 000	
Fluid	G-4, -5, -6	G-21	G-44	G-44 ppt	G-44	G-44 ppt	G-44 average
$\bar{D}_{NG} = D_{50}$, Å	98	115	64	56	80	54	63
$\sigma_G = D_{84}/D_{50}$	1.32	1.37	1.42	1.43	1.50	1.59	1.49
$\bar{D}_{VA}$ = Å	127	165	---	---	---	---	100
$\bar{D}_{SA}$ Å	119	145	---	---	---	---	87
$\bar{D}_{LA}$ Å	110	134	---	---	---	---	76
$\bar{D}_{NA}$ Å	102	120	---	---	---	---	67
Number of particles counted	500	250	250	250	250	250	---

Magnetic Properties of the Ferrofluids

Using a result of classical statistical mechanics it is possible to relate the magnetization curve of the ferromagnetic fluid to the particle size distribution provided it is assumed that particles do not interact with each other. A theoretical development follows.

Theoretical Development Relating Magnetization Curve to Particle Size and Particle Size Distribution. - The magnetic properties of the fluid are specifically due to the presence of the ferromagnetic particles in suspension, each particle contributing to the overall magnetic effects. Rosensweig et al.(ref. 1), analyzed the magnetic properties of a ferrofluid by terms of Langevin's classical theory.

It is assumed that each particle, regardless of its size or state of subdivision, retains the essential magnetic property of a domain. Bulk material, it will be recalled, is composed of an assemblage of domains in each of which the magnetic moment per unit volume is the saturation value appropriate to the temperature considered. The radius of a spherical domain is on the order of 150 Å for the common ferromagnetic oxides considered in this work. Hence, the particles of the solvents under present consideration are presumably essentially subdomain in size. When suspended in a fluid, each particle with its embedded magnetic moment, ν, is analogous to a molecule of a paramagnetic gas. At equilibrium the tendency for the dipole moments to aline with an applied field is partially overcome by thermal agitation. Provided that there is no particle to particle interaction, application of Langevin's theory leads to the following equation:

$$\frac{\bar{\nu}}{\nu} = \coth \frac{\nu H}{kT} - \frac{kT}{\nu H} \tag{19}$$

In this equation ν is the true magnetic moment per particle and $\bar{\nu}$ is the average moment that actually results. Unlike in its original application to paramagnetism, now the magnetic moment per particle in the Langevin equation is a function of temperature. The ferric induction of suspension, M, that results is related to M_s, ν, and $\bar{\nu}$, in the following manner provided the magnetic property increases linearly with volumetric concentration of magnetic particles, ϵ_M:

$$\frac{M}{M_s} = \frac{\epsilon_M \bar{\nu}}{\nu} \tag{20}$$

In the above equations, ν is a function of the size and shape of the particles in suspension. For a monodisperse system of spherical particles of diameter D

$$\nu = \frac{\pi D^3}{6} \frac{M_s}{4\pi} = v \frac{M_s}{4\pi} \tag{21}$$

where v = particle volume.

In high applied fields, equation (19) reduces to:

$$\frac{\bar{\nu}}{\nu} = \frac{M}{\epsilon M_s} = 1 - \frac{4\pi kT}{v M_s H} \qquad \frac{\nu H}{kT} \gg 1 \tag{22}$$

after substitution of equation (21).

In low fields, the following equation is obtained:

$$\frac{\bar{\nu}}{\nu} = \frac{M}{\epsilon M_s} = \frac{1}{3} \frac{v M_s H}{4\pi kT} \qquad \frac{\nu H}{kT} \ll 1 \tag{23}$$

Magnetization curves for different assemblies of equal sized spherical particles were calculated according to equation (19) and are presented in figure 33. The magnetization of such equal sized systems in a 10 000 oersted field as a function of particle size is presented in figure 34.

For a ferrofluid containing an arbitrary distribution of sizes the Langevin function is weighed by the size distribution in the general case:

$$\frac{M}{\epsilon M_s} = \frac{\sum_{i=1}^{\infty} \left[\coth \frac{v_i M_s H}{4\pi kT} - \frac{4\pi kT}{v_i M_s H} \right] n_i v_i}{\sum_{i=1}^{\infty} n_i v_i} \tag{24}$$

For high fields the above equation becomes

$$\frac{M}{\epsilon M_s} = \frac{\Sigma \left[1 - \frac{4\pi kT}{v_i M_s H} \right] n_i v_i}{\Sigma n_i v_i} = \frac{\Sigma n_i v_i - \Sigma \frac{4\pi kT}{M_s H} n_i}{\Sigma n_i v_i}$$

$$= 1 - \left[\frac{4\pi kT}{M_s H} \right] \frac{\Sigma n_i}{\Sigma n_i v_i} \tag{25}$$

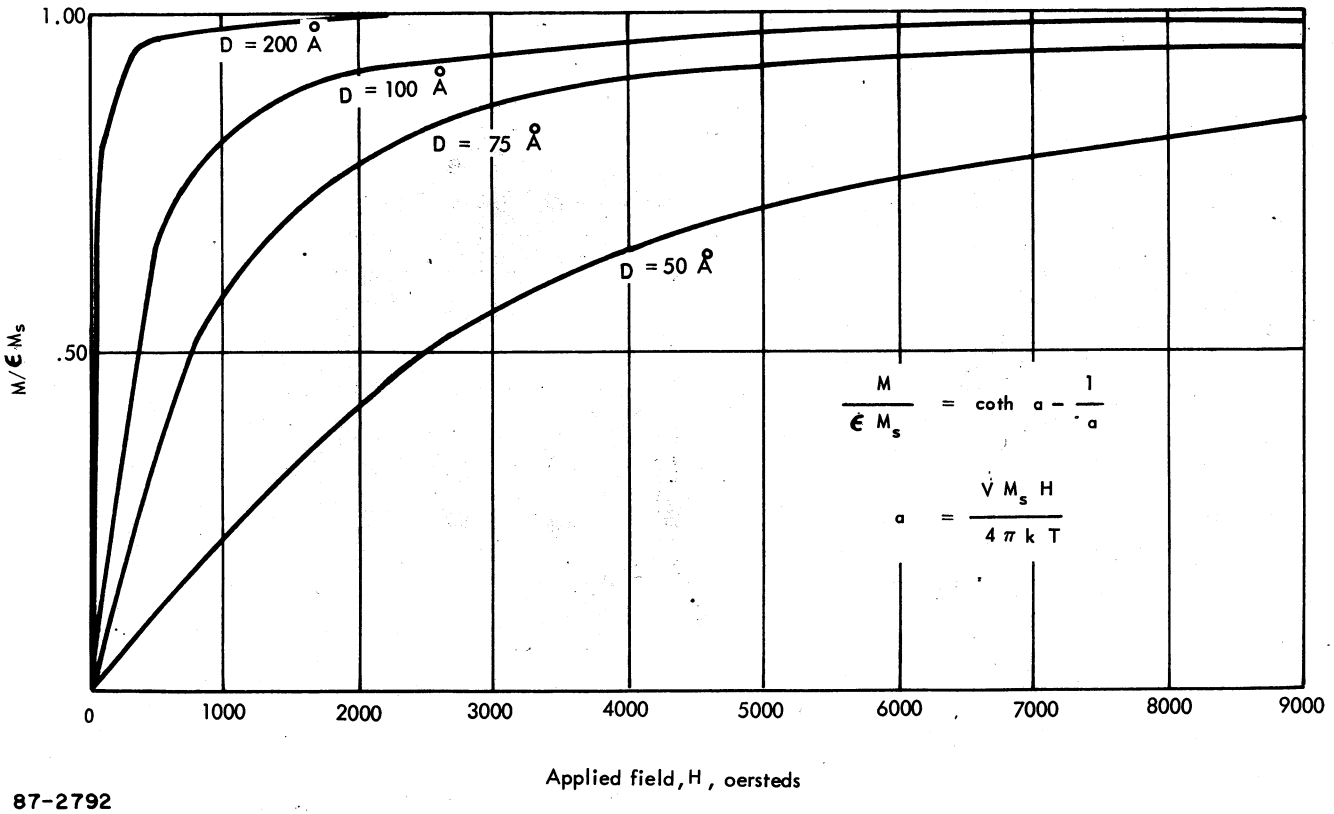

Figure 33. – Calculated Magnetization Curve for Monodisperse Spherical Magnetite Particles, M_{ss} = 5660 gauss

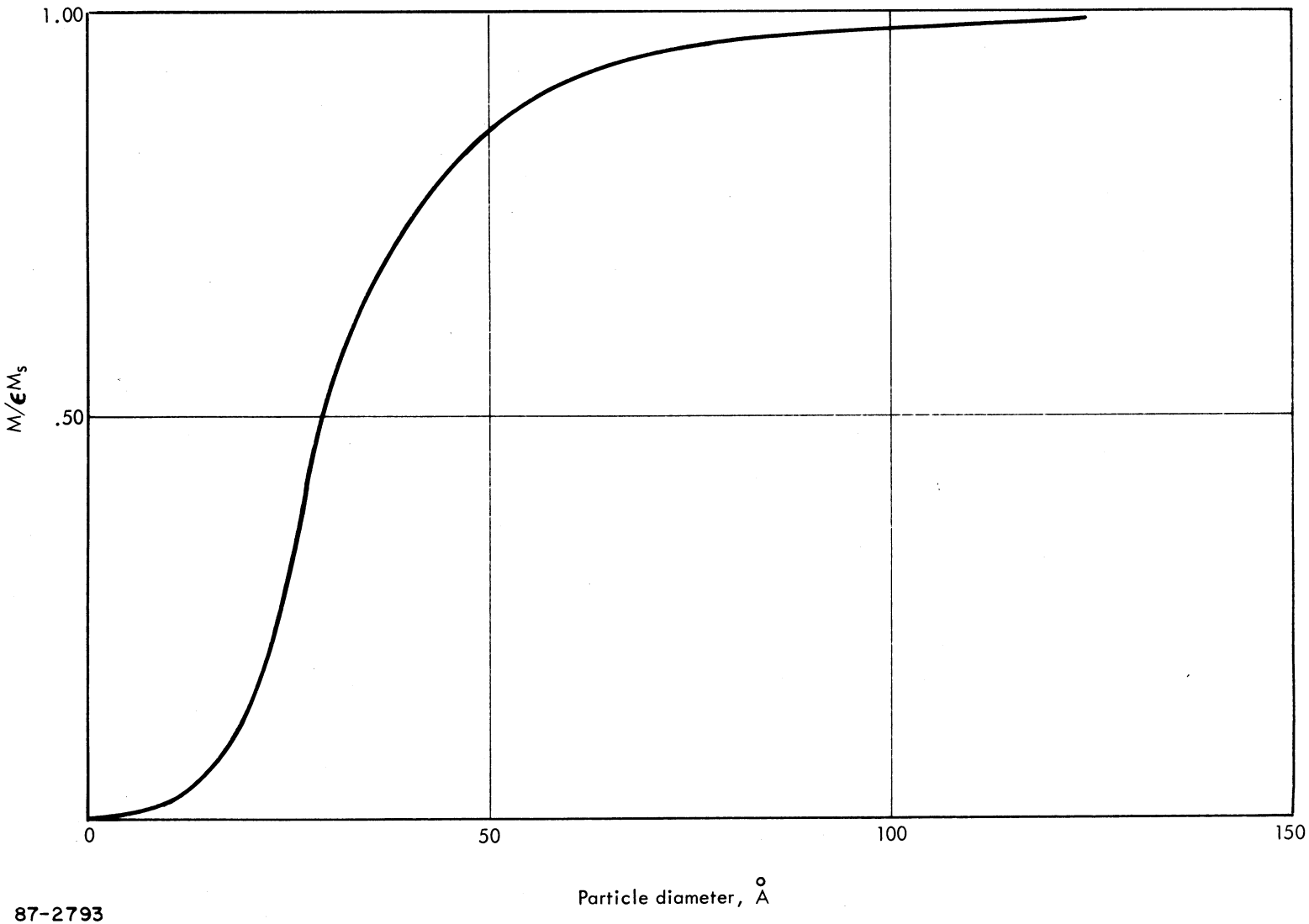

Figure 34. – Magnetization of Spherical Equal Sized Particles of Magnetite (M_{ss} = 5660 gauss) In a 10 000 Oersted Field as a Function of Particle Size

By definition $\frac{\Sigma n_i v_i}{\Sigma n_i} = \bar{V}_i$ the number average particle volume.

Therefore

$$\frac{M}{\epsilon M_s} = 1 - \frac{4\pi k T}{\bar{V}_i M_s H} \tag{26}$$

For low fields, equation (24) becomes

$$\frac{M}{\epsilon M_s} = \frac{\sum_{i=1}^{\infty} \left[\frac{1}{3} \frac{v_i M_s H}{4\pi k T} n_i v_i \right]}{\sum_{i=1}^{\infty} n_i v_i}$$

$$= \frac{1}{3} \frac{M_s H}{4\pi k T} \frac{\Sigma n_i v_i^2}{\Sigma n_i v_i} \tag{27}$$

The magnetization curve of a ferrofluid with a distribution of particle sizes will be a function of the mean particle volume in a high applied field, and of the first moment about the mean volume in low fields.

This magnetization of multidisperse ferrofluid is a function of both the average particle volume $\bar{v}$ and the standard deviation of particle σ_v, since by definition

$$\frac{\Sigma n_i v_i^2}{\Sigma n_i v_i} = \frac{\Sigma n_i v_i^2}{\Sigma n_i} \frac{\Sigma n_i}{\Sigma n_i v_i} = \frac{\sigma_v^2 - \bar{V}^2}{\bar{V}} \tag{28}$$

$$\frac{M}{\epsilon M_s} = \frac{1}{3} \left[\frac{M_s H}{4\pi K T} \right] \left[\frac{\sigma_v^2 - \bar{V}^2}{\bar{V}} \right] \tag{29}$$

If the particles are assumed to be spherical then $v_i = \frac{\pi}{6} D_i^3$
Therefore,

$$\frac{1}{\bar{V}} = \frac{\Sigma n_i}{\Sigma n_i v_i} = \frac{6}{\pi} \frac{\Sigma n_i}{\Sigma n_i D_i^3} = \frac{6}{\pi} \frac{\Sigma n_i}{\Sigma n_i D_i^3} \cdot \frac{\Sigma n_i D_i^2}{\Sigma n_i D_i^2} \cdot \frac{\Sigma n_i D_i}{\Sigma n_i D_i} \tag{30}$$

while in a low field

$$\frac{M}{M_s} = \frac{1}{3}\left[\frac{M_s H}{4\pi kT}\right]\left(\frac{\pi}{6}\right)\frac{\Sigma n_i D_i^6}{\Sigma n_i D_i^5}\cdot\frac{\Sigma n_i D_i^5}{\Sigma n_i D_i^4}\cdot\frac{\Sigma n_i D_i^4}{\Sigma n_i D_i^3}$$

$$= \frac{M_s H}{72\,kT}\left[\frac{\Sigma n_i D_i^6}{\Sigma n_i D_i^5}\cdot\frac{\Sigma n_i D_i^5}{\Sigma n_i D_i^4}\cdot\frac{\Sigma n_i D_i^4}{\Sigma n_i D_i^3}\right] \qquad (36)$$

Experimental Procedure. - The magnetic characteristics of a ferrofluid were obtained by a search coil technique. A Harvey Wells direct current regulated power supply is used to supply current to a 10 000 gauss electromagnet. This electromagnet has 2-3/4 inch pole pieces which are hollowed axially to accommodate the placement of test specimens in a search coil placed within the electromagnet. (See fig. 35.)

Magnetization measurements are obtained by rapidly removing the sample from the search coil and determining the deflection obtained on a Leeds and Northrup ballistic galvanometer for a given applied field. The ferrofluid is contained in tubular capsules 1.00-inch long by 0.25-inch diameter and 0.50-inch long by 0.125-inch diameter. The magnetization measurements are calibrated against standard pure iron and pure nickel samples. (See fig. 36.)

Measurements were performed on samples of ferrofluid using the search-coil ballistic galvonometer technique in which the sample and its holder were soaked at the desired temperature in an oven or a cold bath after which prompt measurement was made before the temperature could adjust to the ambient. There is some uncertainty in the data thereby obtained due to thermal expansion effects, so the data on fluids at the high temperature end may be about 10 percent lower than actual.

Experimental Results. - Magnetization curves were obtained at room temperature for a number of ferrofluids. Typical of these results are the curves for fluids G-44 (fig. 37 and table 23), G-4, -5, -6 (fig. 38 and tables 24 and 25), and G-21 (fig. 39 and tables 26 and 27). For the G-4, -5, -6, and G-21 fluids, curves were obtained at two concentration levels. The magnetization curve of the magnetic powder (IRN 100) used to prepare these fluids is presented in figure 40.

The saturation magnetization of the following systems was measured as a function of temperature.

since

$$\frac{\Sigma n_i D_i^3}{\Sigma n_i D_i^2} = \overline{D}_{SA}\ , \quad \frac{\Sigma n_i D_i^2}{\Sigma n_i D_i} = \overline{D}_{LA}\ , \quad \frac{\Sigma n_i D_i}{\Sigma n_i} = \overline{D}_{NA}$$

as defined in table 21,

$$\frac{1}{\overline{V}} = \frac{6}{\pi}\left[\frac{1}{\overline{D}_{SA}\ \overline{D}_{LA}\ \overline{D}_{NA}}\right] . \tag{31}$$

Similarly,

$$\frac{\Sigma n_i v_i^2}{\Sigma n_i v_i} = \frac{\Sigma n_i \left[\frac{\pi}{6} D_i^3\right]^2}{\Sigma n_i \frac{\pi}{6} D_i^3} = \frac{\pi}{6} \frac{\Sigma n_i D_i^6}{\Sigma n_i D_i^3} \tag{32}$$

$$= \frac{\pi}{6} \frac{\Sigma n_i D_i^6}{\Sigma n_i D_i^3} \cdot \frac{\Sigma n_i D_i^5}{\Sigma n_i D_i^5} \cdot \frac{\Sigma n_i D_i^4}{\Sigma n_i D_i^4} \tag{33}$$

The first moment of particle volume is equal to the product of the fifth, fourth and third moments of particle diameter times $\pi/6$ for spheres. In the case of a log normal distribution for which

$$\ell n \frac{\Sigma n_i D_i^k}{\Sigma n_i D_i^{k-1}} = \ell n\ \overline{D}_{NG} + [\ k + 0.5\ ]\ \ell n^2\ \sigma_G \tag{34}$$

the above moments can be determined easily from the distribution curve on a log normal probability plot.

In high fields therefore

$$\frac{M}{\epsilon M_s} = 1 - \frac{4\pi k T}{M_s H}\left[\frac{6}{\pi\ \overline{D}_{SA}\ ,\ \overline{D}_{LA}\ \overline{D}_{NA}}\right]$$

$$= 1 - \frac{24\ k\ T}{M_s\ H\ [\overline{D}_{SA}\ \overline{D}_{LA}\ \overline{D}_{NA}\ ]} \tag{35}$$

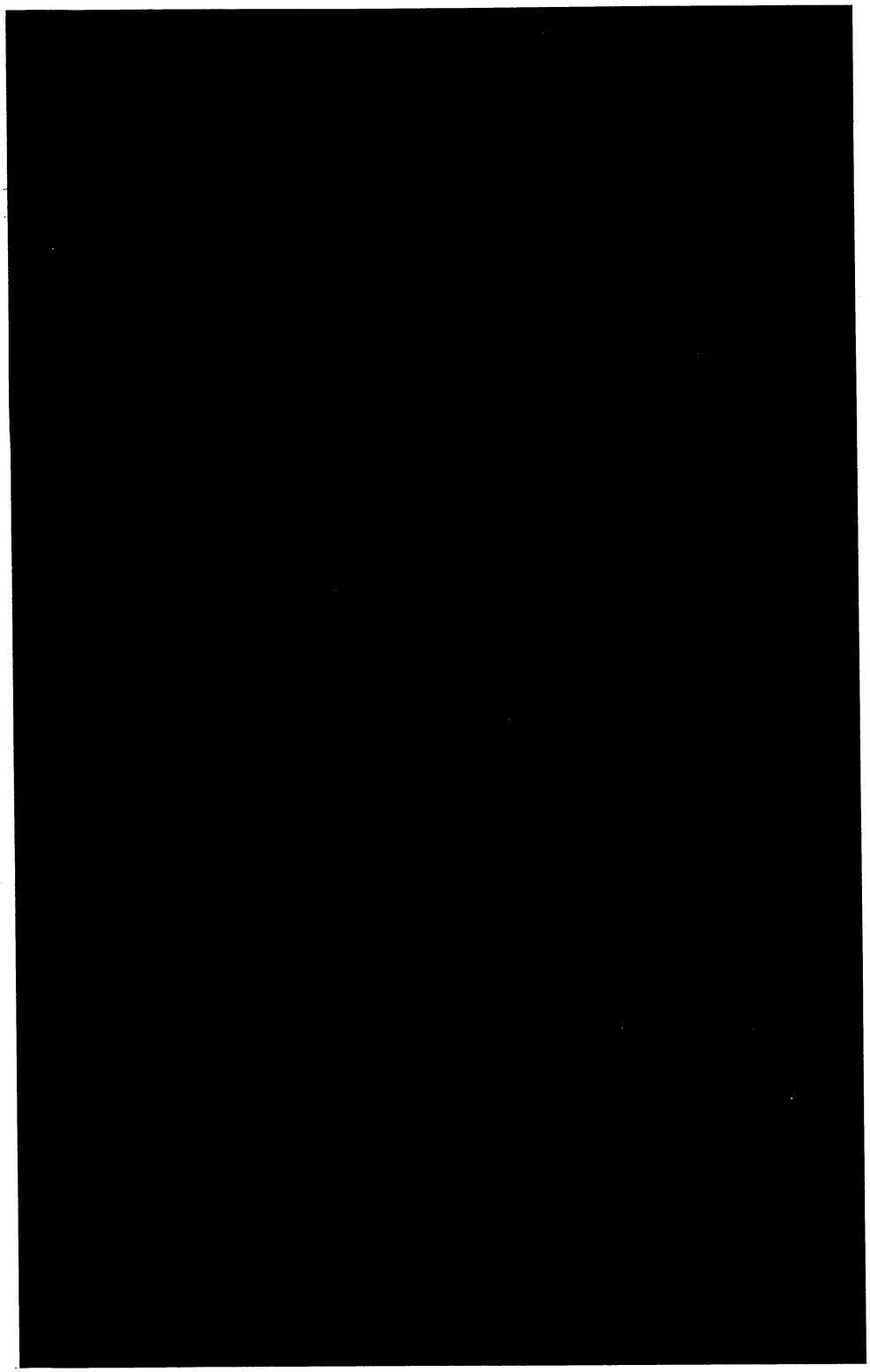

Figure 35. – View of Search Coil Mounted between Pole Pieces of an Electromagnet

Top

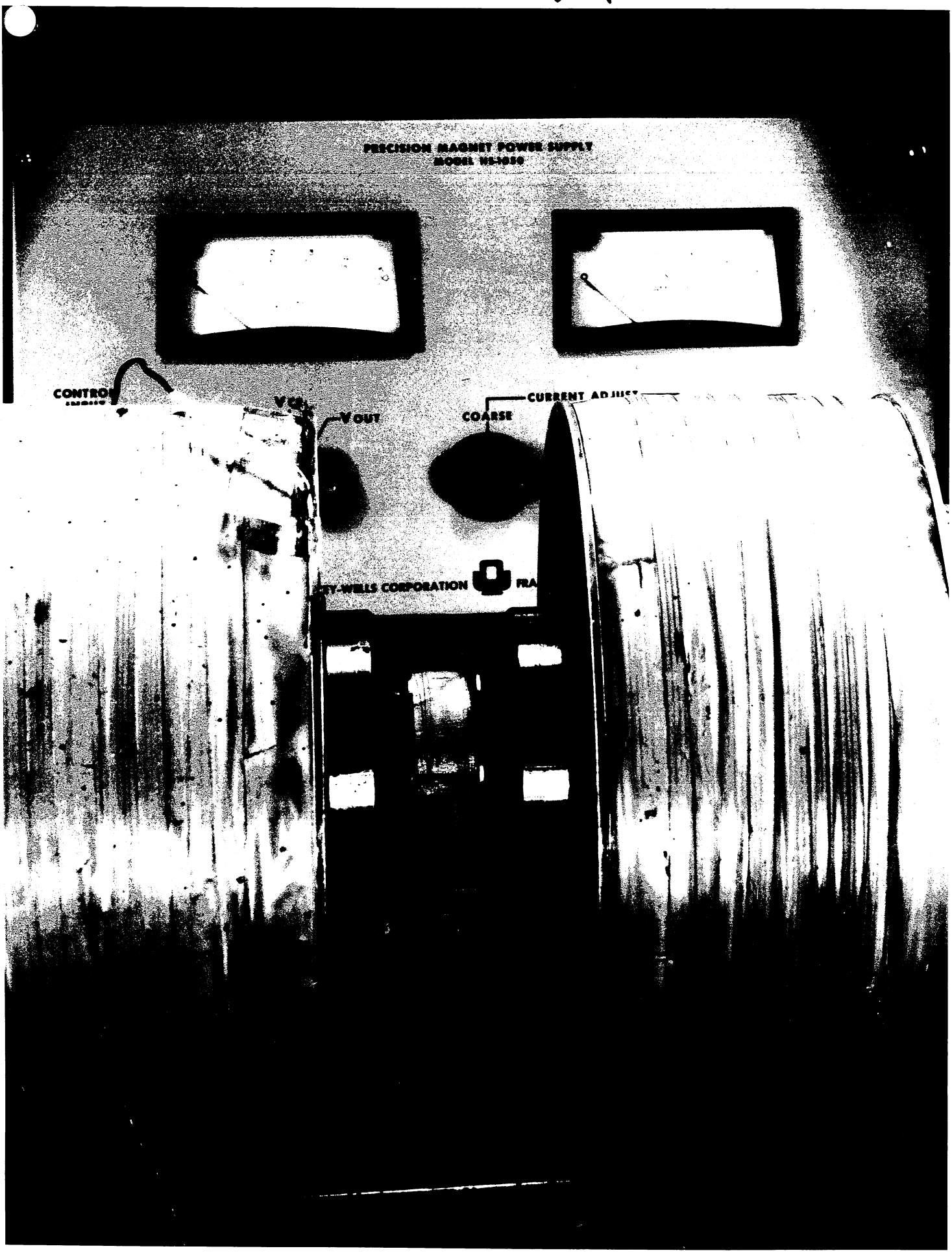

Fig 35 Pg 97

FIG 35 T-62

Top

Fig 36 Pg 98

Fig 36

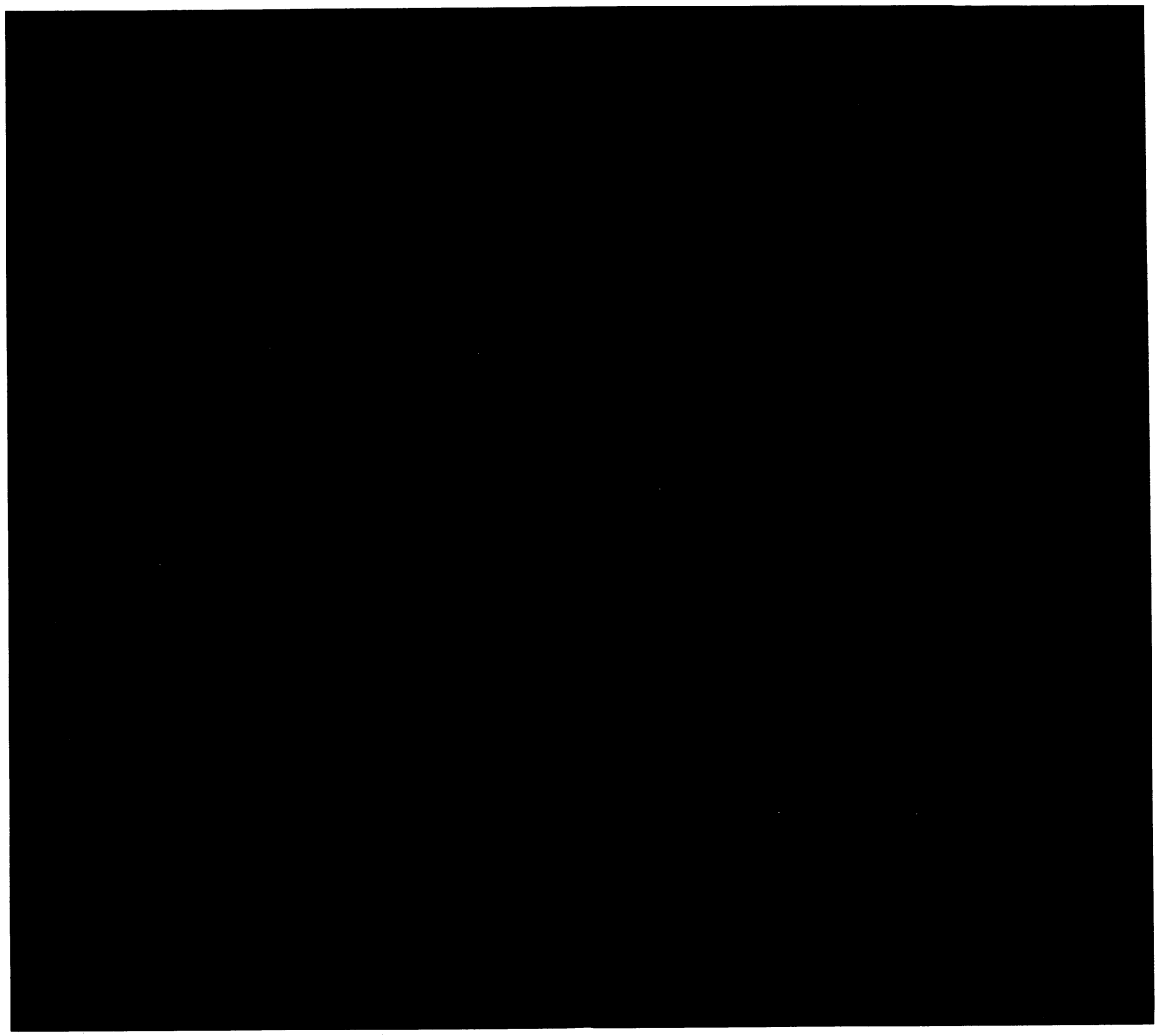

Figure 36. – Ballistic Galvanometer Determination of Ferrofluid Magnetic Properties (The ferrofluid is contained in a tubular sample holder which is withdrawn from the axially bored hole in the electromagnet during the course of the measurement)

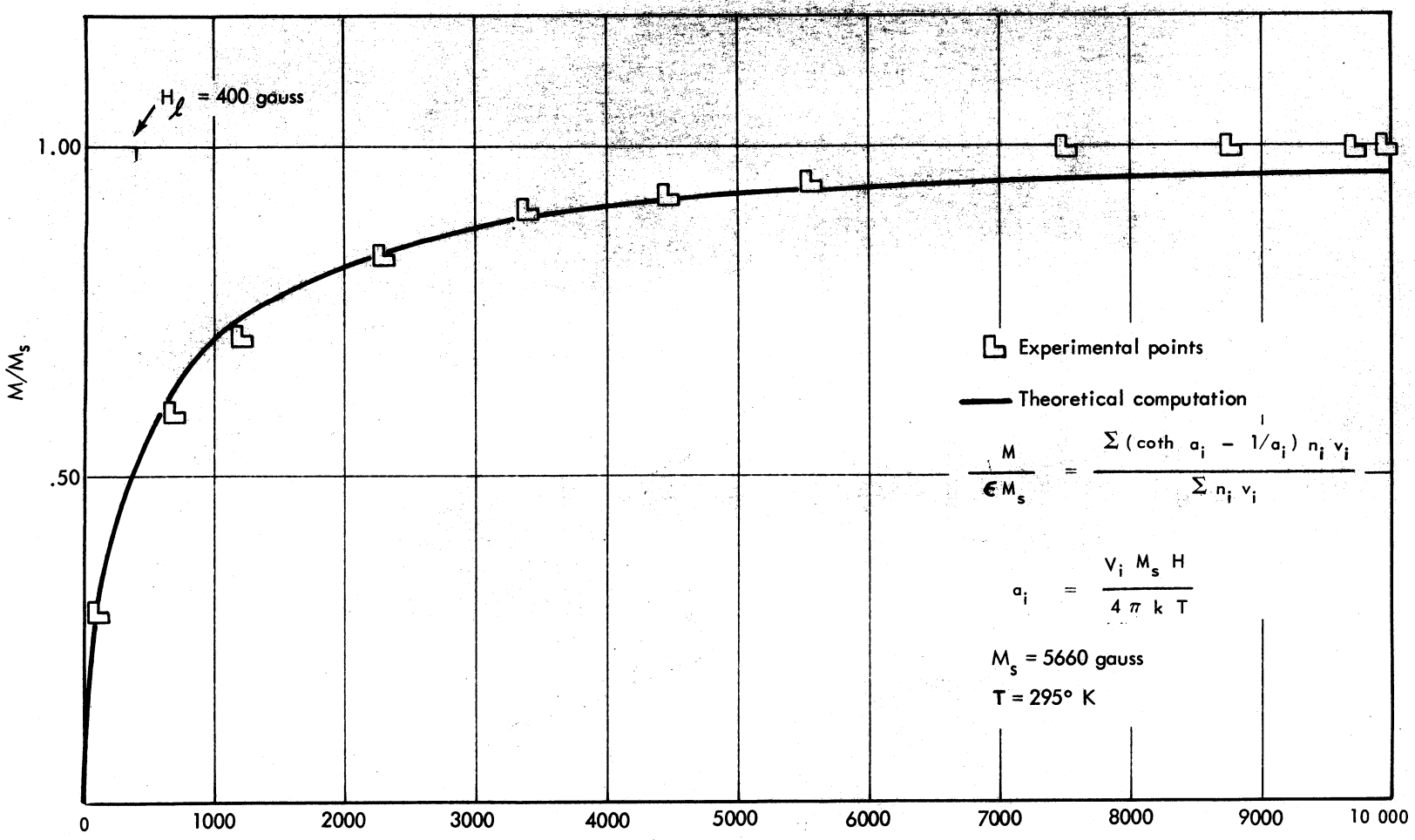

Figure 37. – Magnetization Curve for G-44 Fluid (M_s = 212 gauss)

TABLE 23. – MAGNETIZATION DATA FOR FERROFLUID G-44

Applied field, H, oersted	Fluid magnetization, M, gauss	$\frac{M}{M_s} = \frac{M}{\epsilon M_{ss}}$	1/H, oersted $^{-1}$	Fluid characteristics
116	61	0.288	8.62×10^{-3}	Density, $\rho = 0.953$ gm/cc
			2.28×10^{-3}	Total volume fraction solids,
			1.79×10^{-3}	$\epsilon_D = 0.0379$
---	126.5	.596	1.49×10^{-3}	Saturation magnetication of solids in suspension,
1200	151	.712	8.34×10^{-4}	$M_{ss} = 5660$ gauss
2300	177	.835	4.34×10^{-4}	Volume fraction magnetic
3400	191	.901	2.94×10^{-4}	solids, $\epsilon_M = \frac{M_s}{M_{ss}} = 0.0375$
4450	197	.927	2.25×10^{-4}	
7500	212	1.00	1.33×10^{-4}	Conversion, $K = \frac{\epsilon_M}{\epsilon_D} = 0.99$
8150				
8750	212	1.00	1.14×10^{-4}	
9500	212	1.00	1.05×10^{-4}	
9950	212	1.00	1.005×10^{-4}	

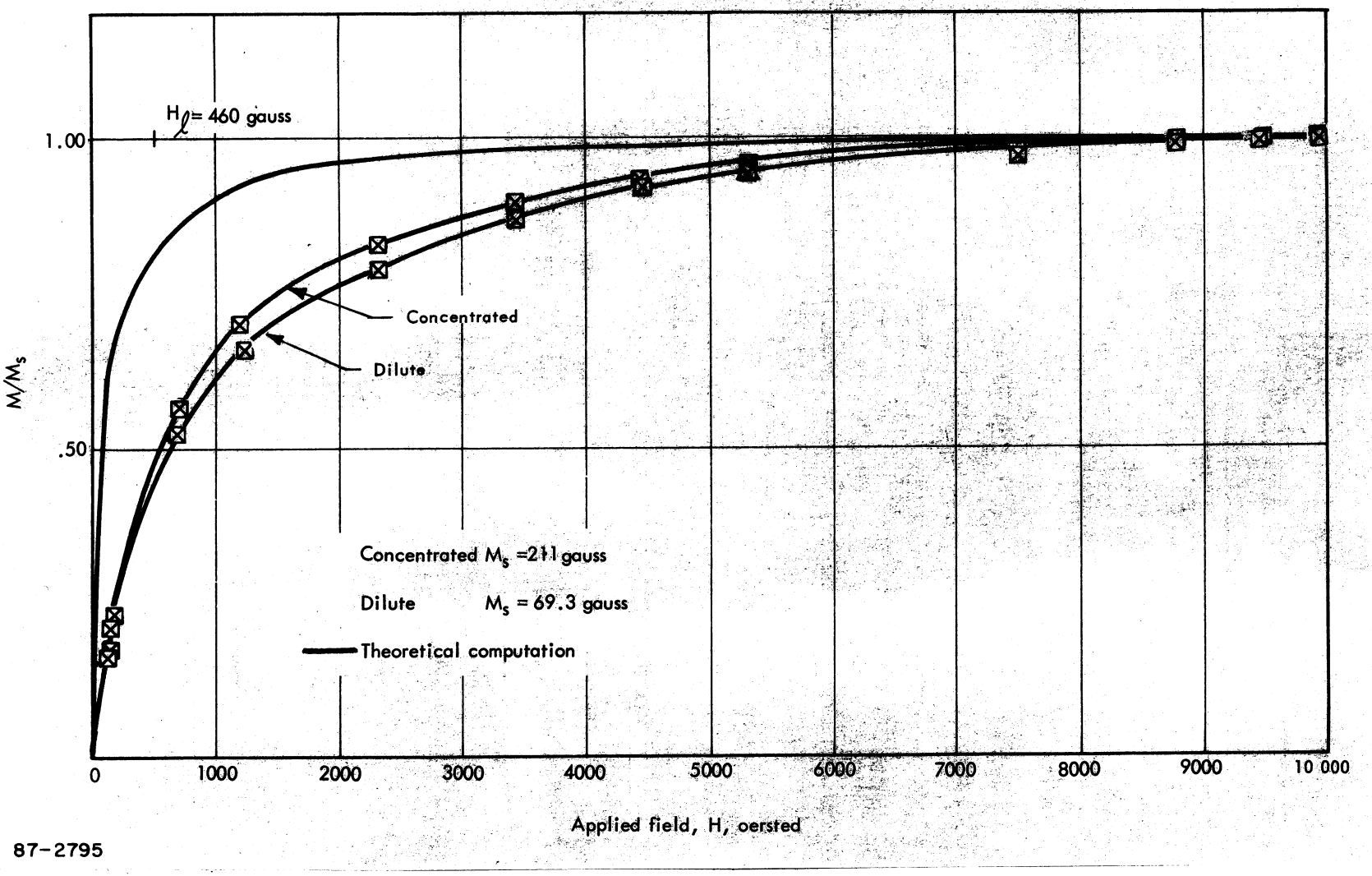

Figure 38. – Magnetization Curves for G-4, -5, -6 Fluids and Comparison with Theoretical Computation

TABLE 24. – MAGNETIZATION DATA FOR FERROFLUID DILUTE G–4, –5, –6

Applied field, H, oersted	Fluid magnetization, M, gauss	$\frac{M}{M_s} = \frac{M}{\epsilon M_{ss}}$	1/H, oersted $^{-1}$	Fluid characteristics
116	14.8	0.214	8.62×10^{-3}	Density, ρ = 0.859 gm/cc Total volume fraction solids, ϵ_D = 0.0165
670	36.5	.527	---	
1200	46.3	.668	8.34×10^{-4}	Saturation magnetization of solids in suspension, M_{ss} = 5660 gauss
2300	54.4	.785	4.34×10^{-4}	
3400	60.9	.878	2.94×10^{-4}	
4450	63.8	.922	2.25×10^{-4}	Volume fraction magnetic solids, $\epsilon_M = \frac{M_s}{M_{ss}} =$ 0.0122
5540	65.4	.943	1.81×10^{-4}	
7500	66.6	.963	1.33×10^{-4}	
8750	69.3	1.00	1.14×10^{-4}	Corversion, $K = \frac{\epsilon_M}{\epsilon_D} = 0.74$
9400	69.3	1.00	1.06×10^{-4}	
9950	69.3	1.00	1.005×10^{-4}	

TABLE 25. – MAGNETIZATION DATA FOR FERROFLUID CONCENTRATED G–4, –5, –6

Applied field, H, oersted	Fluid magnetization, M, gauss	$\frac{M}{M_s} = \frac{M}{\epsilon M_{ss}}$	1/H, oersted $^{-1}$	Fluid characteristics
80	38.4	0.182	1.25×10^{-2}	Density, ρ = 1.002 gm/cm^3
116	49.6	.236	8.62×10^{-3}	Total volume fraction solids, ϵ_D = 0.050
670	120	.569	1.49×10^{-3}	Saturation magnetization of solid in suspension, M_{ss} = 5660 gauss
1200	148	.704	8.34×10^{-4}	Volume fraction magnetic solids, $\epsilon_M = \frac{M_s}{M_{ss}}$ = 0.0372
2300	175	.829	4.34×10^{-4}	
3400	191	.905	2.94×10^{-4}	
4450	198	.940	2.25×10^{-4}	
5540	202	.958	1.81×10^{-4}	
7500	211	1.00	1.33×10^{-4}	Conversion, $K = \frac{\epsilon_M}{\epsilon_D}$ = 0.75
			1.23×10^{-4}	
8750	211	1.00	1.14×10^{-4}	
9500	211	1.00	1.05×10^{-4}	
9950	211	1.00	1.005×10^{-4}	

TABLE 25

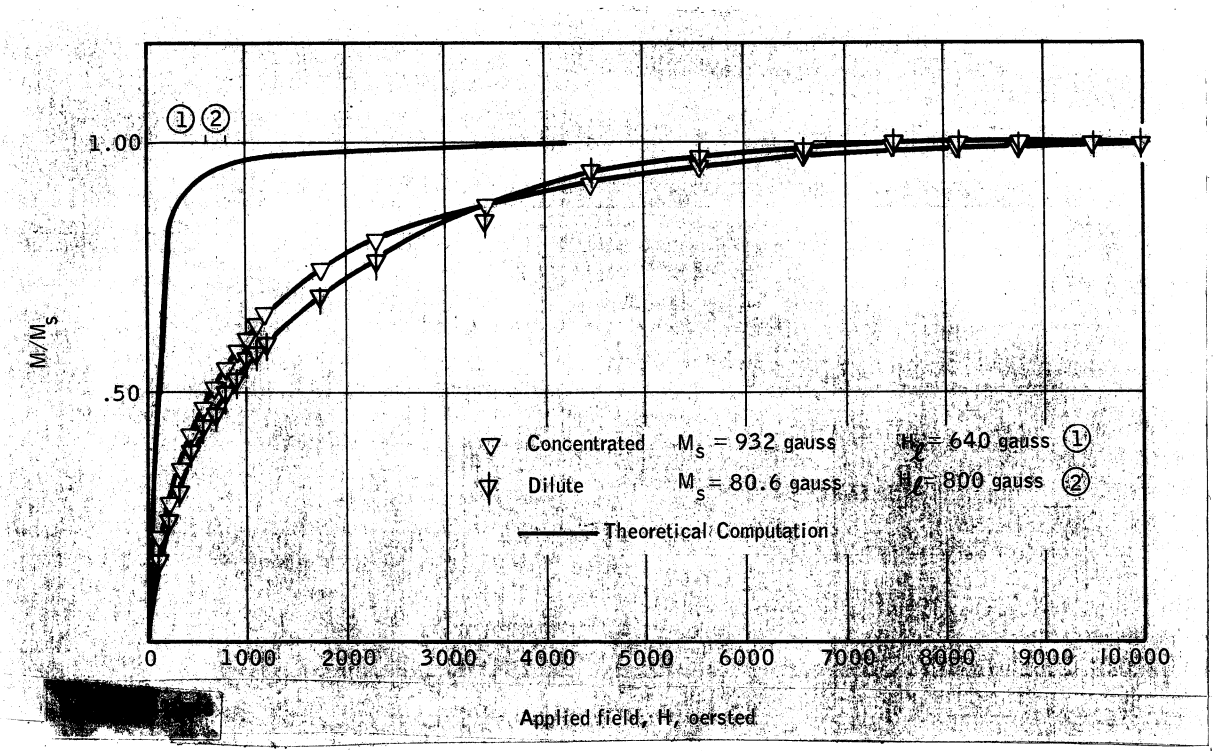

Figure 39. – Magnetization Curve for G-21 Fluids and Comparison with Theoretical Computation

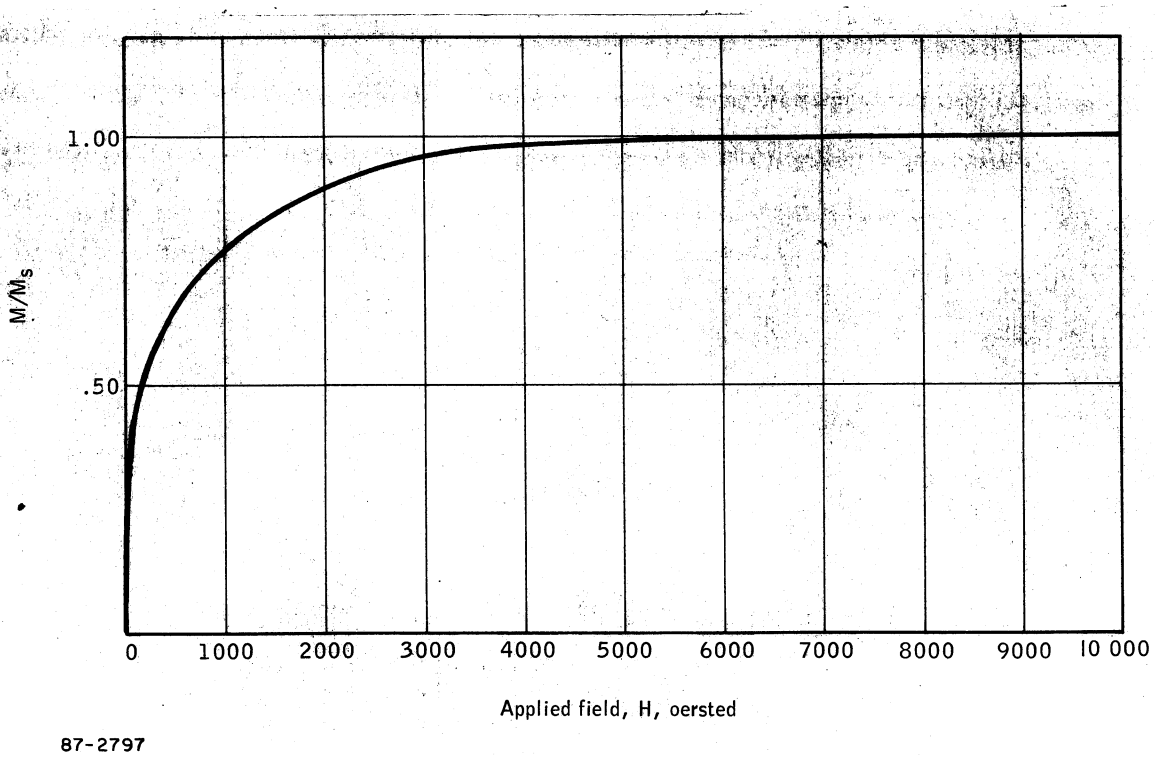

Figure 40. – Normalized Magnetization Curve for IRN 100 Magnetite Powder

TABLE 26. – MAGNETIZATION DATA FOR FERROFLUID DILUTE G-21

Applied field, H, oersted	Fluid magnetization, M, gauss	$\frac{M}{M_s} = \frac{M}{\epsilon M_{ss}}$	$1/H$, $(\text{oersted})^{-1}$	Fluid characteristics
116	14.8	0.167	8.62×10^{-3}	Density, $\rho = 0.895$ gm/cc
210	24.3	.274	4.76×10^{-3}	Total volume fraction solids, $\epsilon_D = 0.024$
330	27.0	.305	3.03×10^{-3}	
440	34.5	.389	2.28×10^{-3}	
560	38.2	.432	1.79×10^{-3}	Saturation magnetization of solid, $M_{ss} = 5660$ gauss
670	40.5	.958	1.49×10^{-3}	
780	44.2	.500	1.28×10^{-3}	
900	46.8	.528	1.11×10^{-3}	Volume fraction magnetic solids, $\epsilon_M = \frac{M_s}{M_{ss}} = 0.0156$
1000	50.5	.570	1.00×10^{-3}	
1100	51.6	.583	9.00×10^{-4}	
1200	53.0	.597	8.34×10^{-4}	
1750	61.5	.695	5.72×10^{-4}	
2300	67.6	.764	4.34×10^{-4}	Conversion, $K = \frac{\epsilon_M}{\epsilon_D} = 0.65$
3400	75.0	.846	2.94×10^{-4}	
4450	83.8	.945	2.25×10^{-4}	
5540	86.1	.972	1.81×10^{-4}	
6600	87.5	.987	1.52×10^{-4}	
7500	88.6	1.00	1.33×10^{-4}	
8150	88.6	1.00	1.23×10^{-4}	
8750	88.6	1.00	1.14×10^{-4}	
9200	88.6	1.00	1.09×10^{-4}	
9500	88.6	1.00	1.05×10^{-4}	
9950	88.6	1.00	1.005×10^{-4}	

TABLE 26

TABLE 27. – MAGNETIZATION DATA FOR FERROFLUID CONCENTRATED G–21

Applied field, H, oersted	Fluid magnetization, M, gauss	$\frac{M}{M_s} = \frac{M}{\epsilon M_{ss}}$	$1/H$, oersted^{-1}	Fluid characteristics
80	---	---	1.25×10^{-2}	Density, ρ = 1.85 gm/cc[a]
116	198	0.212	8.62×10^{-3}	
210	262	.281	4.76×10^{-3}	Total volume fraction Solids, ϵ_D = 0.252[a]
330	323	.346	3.03×10^{-3}	
440	390	.418	2.28×10^{-3}	
560	437	.469	1.79×10^{-3}	Saturation magnetization of solids in suspension, M_{ss} = 5660 gauss
670	478	.512	1.49×10^{-3}	
780	506	.544	1.28×10^{-3}	Volume fraction magnetic solids, $\epsilon_M = \frac{M_s}{M_{ss}}$ = 0.164
900	542	.582	1.11×10^{-3}	
1000	566	.607	1.00×10^{-3}	
1100	594	.636	9.00×10^{-4}	
1200	615	.659	8.34×10^{-4}	
1750	700	.750	5.72×10^{-4}	Conversion, $K = \frac{\epsilon_M}{\epsilon_D}$ = 0.65
2300	750	.805	4.34×10^{-4}	
3400	815	.874	2.94×10^{-4}	
4450	851	.913	2.25×10^{-4}	
5540	885	.947	1.81×10^{-4}	
6600	904	.969	1.52×10^{-4}	
7500	914	.979	1.33×10^{-4}	
8150	921	.987	1.23×10^{-4}	
8750	930	.997	1.14×10^{-4}	
9200	932	1.00	1.09×10^{-4}	
9500	932	1.00	1.05×10^{-4}	
9950	932	1.00	1.005×10^{-4}	

[a]Calculated from ϵ_M and K.

i. Magnetite-in-kerosene ferrofluid (run G-26) between -25 and + 100° C.

ii. Manganese-zinc ferrite in kerosene ferrofluid (heat engine fluid) between -25 and + 150° C.

iii. Manganese-zinc ferrite powder between -25 and + 150° C.

These results are presented in figure 41.

Discussion of Results.

Room Temperature Magnetization Curves. - The particular results presented concerning magnetization at ambient temperature were chosen because independent particle size distribution measurements were available in these cases. As a result it was possible to calculate in each of these cases the magnetization curve predicted by superparamagnetic theory using equation (24). These predicted values are also presented in figures 37 to 39 for each of the fluids.

The experimental curves are drawn on the basis of M/M_s where M is the magnetization of the fluid in a field H, M_s is the magnetization of the fluid in the maximum field available experimentally (H = 10 000 oersted). This presumes that the fluid is saturated in this field. The calculated values of $\left(\frac{M}{\epsilon M_s}\right)$ for each of the fluids at 10 000 gauss all approach a value of 1.0, confirming this assumption.

Examination of the different curves show them to be all very similar as evidenced by the fact that at H = 1000 oersted, $0.55 < \frac{M}{M_s} < 0.65$. In the two cases where fluids of different concentrations were examined, the normalized curve for the more concentrated fluid lies above the normalized curve for the more dilute system.

Examination of figure 37 for G-44 fluid shows excellent agreement between the experimental magnetization curve and the magnetization curve expected from superparamagnetic theory. The experimentally observed magnetic conversion of grind ($\epsilon_M = 0.98$) indicates that there are few non-magnetic contaminants in suspension. In fact that there might be essentially no foreign contaminants in this fluid since $\frac{M}{\epsilon M_s}$ at 10 000 oersted was found to be 0.97. These differences are within experimental error and cannot be differentiated.

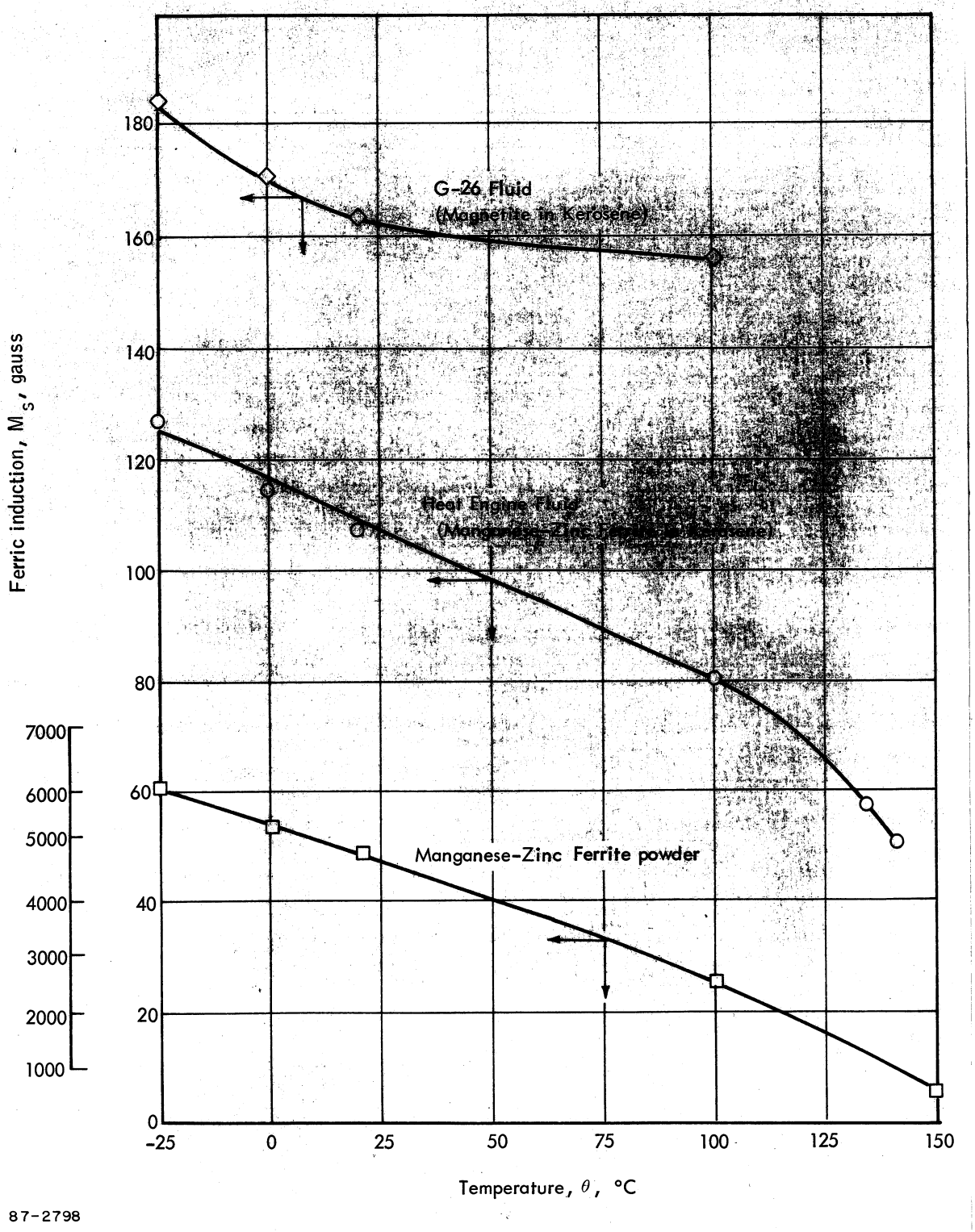

Figure 41. – Saturation Magnetization of Ferrofluids and a Ferrite versus Temperature

In the case of the other two fluids (G-4, -5, -6 and G-21) the experimentally observed curves rise much less rapidly than would have been predicted by superparamagnetic theory. The volume average particle size of fluids G-4, -5, -6 and G-21 were 127 and 165 Å, respectively, as compared to 98 Å for G-44 fluid. The magnetic conversion of G-4, -5, -6 was 74 percent and of G-21 was 65 percent. These low conversions cannot be explained in terms of partial magnetization in a 10 000-oersted field since $\frac{M}{\epsilon M_s}$ in these cases is asymptotic to unity. The presence of nonmagnetic impurities could account for the low conversion.

With both fluids, G-4, -5, -6 and G-21, increasing the concentration of the suspension raises the level of the normalized magnetization curve. This is an indication that there might be some association of the particles in suspension which would increase with increasing particle concentration. Association would transform individual small particles of low magnetic moment into a larger assembly of higher magnetic moment. Dawson and Haydon (ref. 13) found optical evidence for association of stabilized particles in fatty-acid stabilized suspensions of 50 Å titanium dioxide particles in benzene. Judged by the sensitivity of superparamagnetic effects to particle size (see fig. 34), the extent of association appears limited.

The effect of particle volume on the Langevin function can also be used to explain the findings of the Vitro powder grinding run. As was shown in figure 16, the magnetic moment of the fluid increased and then decreased with time while the solids content (as measured from the density of the suspension) increased towards an assymptotic value. After 12 days of grinding in the attritor, the volume fraction solids was 2.70 percent and the magnetic moment of the fluid was 46 ±4 gauss. After 28 days of grinding, the volume fraction solids had increased to 3.0 percent while the magnetic moment of the fluid had decreased to 36 gauss. Correcting for the differences in solids loading, there is reduction of 30 percent in the magnetic moment of the fluid unit volume fraction solids loading.

As a first approximation, it can be assumed that the saturation magnetization of γFe_2O_3 is equal to the saturation magnetization of Fe_3O_4. It can also be assumed that the particles in suspension can be considered to be a system of closely sized spheres. In terms of figure 34 therefore, the decrease in magnetization can be interpreted as a decrease in particle size from a region where $M/\epsilon M_s \longrightarrow 1$, namely above 70 Å in diameter, to a region where $M/\epsilon M_s \approx 0.70$, namely 30 to 40 Å in diameter. These numbers are not inconsistent with the fact that the Vitro powder before grinding had a specific surface area of 56 m^2/gm, which corresponds to a surface average particle diameter of 210 Å.

Initial Permeability of Ferrofluids. - The initial permeability of the ferrofluids provides a simple characterization that describes the magnetization in response to a weak applied field.

$$\mu_i = \left(\frac{\partial B}{\partial H}\right)_{H=0} \tag{37}$$

$$B = H + M \tag{38}$$

Thus,

$$\mu_i = 1 + \left(\frac{\partial M}{\partial H}\right)_{H=0} \tag{39}$$

According to superparamagnetic theory, by differentiating equation (23)

$$\left.\frac{dM}{dH}\right)_{H=0} = \frac{V \epsilon M_s^2}{4\pi kT} \tag{40}$$

so that

$$\mu_i = 1 + \frac{V \epsilon M_s^2}{4\pi kT} \tag{41}$$

For a system of equal sized noninteracting particles the initial permeability of a ferrofluid should increase with increasing particle size and particle concentration. μ_i is the maximum value of the permeability for a ferrofluid. The minimum applied field available using the search-coil ballistic galvanometer technique was 116 oersted. It was not feasible to measure lower applied fields with this apparatus. The initial permeabilities of the different fluids were approximated from the slope of a secant passing from the origin to the magnetization curve at a value of H = 116 oersted, the minimum value measured:

$$\mu_i - 1 = \left(\frac{\partial M}{\partial H}\right)_{H=0} \approx \frac{M_{(H=116)}}{116} \tag{42}$$

The average permeability obtained in this manner will be lower than the true initial value of the permeability. The results obtained are presented in figure 42. This figure incorporates data presented in figures 37 to 39, as well as further data on G-21 fluids presented in figure 42, and fluids G-10, G-47, and 5-23-66-1.

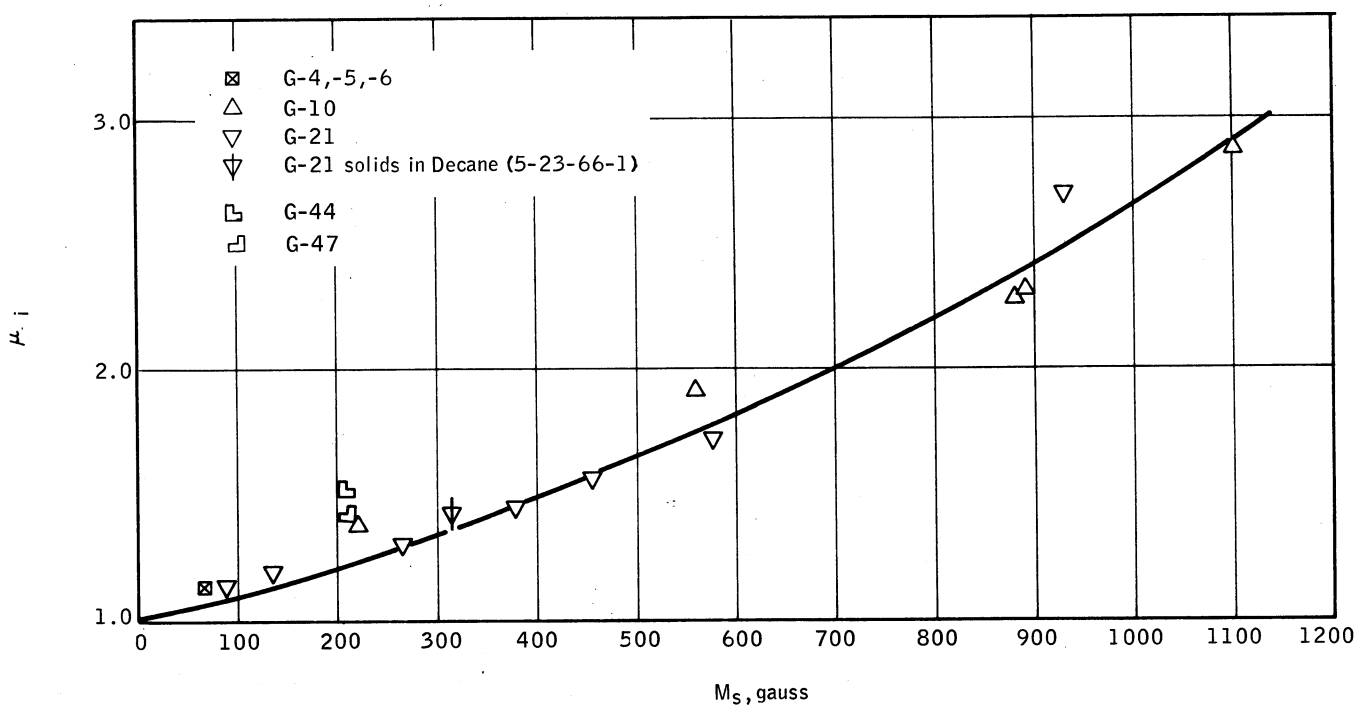

87-2799

Figure 42. – Initial Permeability of Magnetite Ferrofluids as a Function of Saturation Magnetization

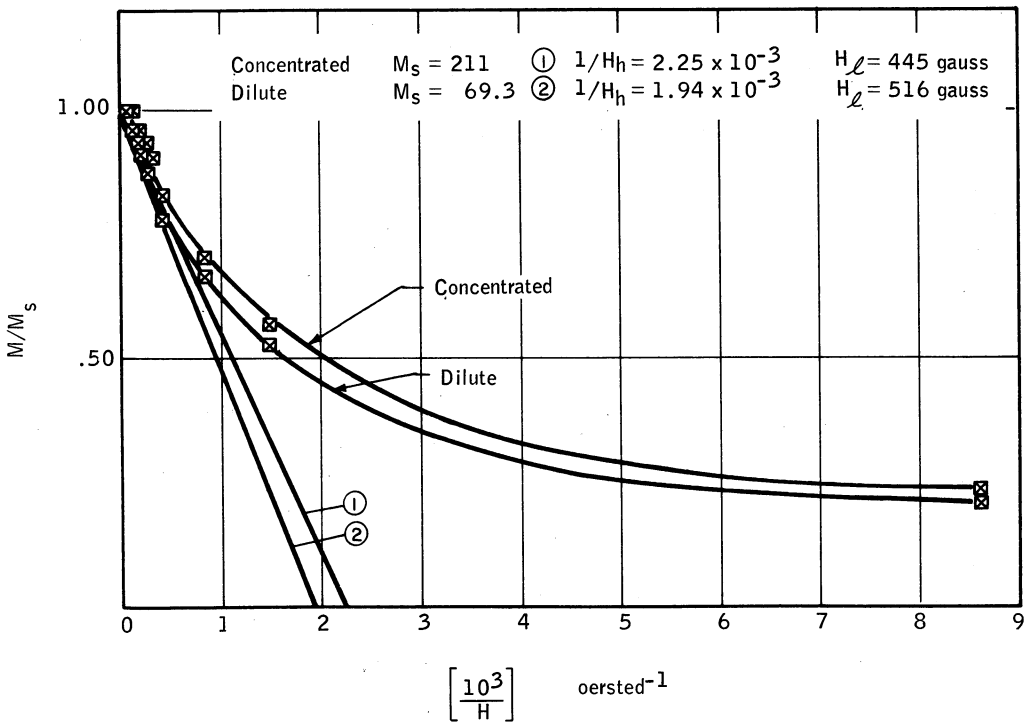

87-2800

Figure 43. – Magnetization of G-4, -5, -6 Fluids versus Inverse of Applied Field

The initial permeability of the fluids increases with increasing saturation magnetization of the fluid, i.e., with increasing magnetite concentrations in suspension and the increase is linear within the precision of the data.

Application to Particle Size Analysis. - According to the previous theoretical development, measurement of the variation of M of a ferrofluid as a function of the applied field H should yield information on the size distribution of the particles in suspension. Equation (25) can be rewritten as

$$\frac{M}{\epsilon M_s} = 1 - \frac{H_h}{H} \tag{43}$$

where

$$H_h = \frac{4\pi kT}{M_s \bar{V}} \tag{44}$$

Similarly, equation (29) can be rewritten as

$$\frac{M}{\epsilon M_s} = \frac{H}{H_\ell} \tag{45}$$

where

$$H_\ell = \frac{1}{3}\left[\frac{M_s(\bar{V})}{4\pi kT}\right]\overline{(V^2)} = \frac{\bar{V}^2}{3H_h} \tag{46}$$

$\overline{(V^2)}$ = mean square volume

The average particle volume is obtained if the experimental data are plotted with $\frac{M}{\epsilon M_s}$ as ordinate versus 1/H. A value of H_h will be obtained from the intersection of the tangent to the curve at 1/H equal zero with the abcissa. The average particle volume is then given by

$$\bar{V} = \frac{4\pi kT}{H_h M_s} \tag{47}$$

The statistical variance of particle volumes is obtained by determination of H_ℓ once H_h is known. H_ℓ is easily found from a graphical construction based on $M/\epsilon M_s$ plotted versus H_h, so that

$$\frac{[\overline{(V)^2} - \overline{(V^2)}\,]^{1/2}}{\bar{V}} = \left[3\,\frac{H_h}{H_\ell} - 1\right]^{1/2} \tag{48}$$

The data for fluids G-4, -5, -6, G-21, and G-44 presented in figures 37 to 39 were treated in this manner. Figures 43 to 45 are plots of normalized magnetization $\frac{M}{M_s}$ against the inverse of the applied field from which values of H_h were obtained. Values of H_ℓ were obtained from figures 37 to 39. The results are presented in table 28. The average particle volume was computed from the particle statistics ($\bar{D}_{NG}$ and σ_G) obtained from electron micrographs. The statistical variance of volume was calculated with the same statistics:

$$\frac{\Sigma n_i v_i^2}{\Sigma n_i v_i} = \frac{\Sigma n_i v_i^2}{\Sigma n_i}\,\frac{\Sigma n_i}{\Sigma n_i v_i} = \frac{\overline{(V^2)}}{\bar{V}}$$

$$\frac{\sqrt{\overline{(V)^2} - \overline{(V^2)}}}{\bar{V}} = \sqrt{\left[\frac{\Sigma n_i v_i^2}{\Sigma n_i v_i}\right]\frac{1}{\bar{V}} - 1} \tag{49}$$

There is very good agreement between the statistics obtained from the magnetic measurements and the electron micrography for the G-44 fluid, but poor agreement with the G-21 and G-4, -5, -6 fluids. The lack of accord is in part due to difficulties in obtaining values of H_h, and to some extent H_ℓ.

The ferrofluids are observed to be saturated at finite values of H that range between 5000 and 10 000 oersted. Due to the insensitivity of the measurements it is not possible to detect even smaller variations in M. There is also the problem of association of particles in suspension. Thus, the experimental magnetization versus inverse applied field curve has a horizontal slope at $1/H = 0$. A value of $1/H_h$ was obtained in each case by drawing a straight line through the point $\frac{\epsilon M}{M_s} = 1.0$, $1/H = 0$ that best fit the data in the region close to the ordinate. Depending on how one interpreted these measurements, as shown in figure 45 for G44 fluid, it is possible to generate different values of $1/H_h$, which in this case range from 1.9×10^{-3} to 3.0×10^{-3} (oersted)$^{-1}$. This corresponds to a variation of average volume of from 1.7×10^5 to 2.8×10^5 Å^3. For a fixed value of H_h, this also corresponds to a variation of from 2.9 to 1.5 for the statistical volume variance.

There is also some uncertainty in H_ℓ. Low field measurements below H = 116 oersted were not obtainable with the apparatus used. As was done with μ_i, H_ℓ was obtained from the secant passing from the origin to the point

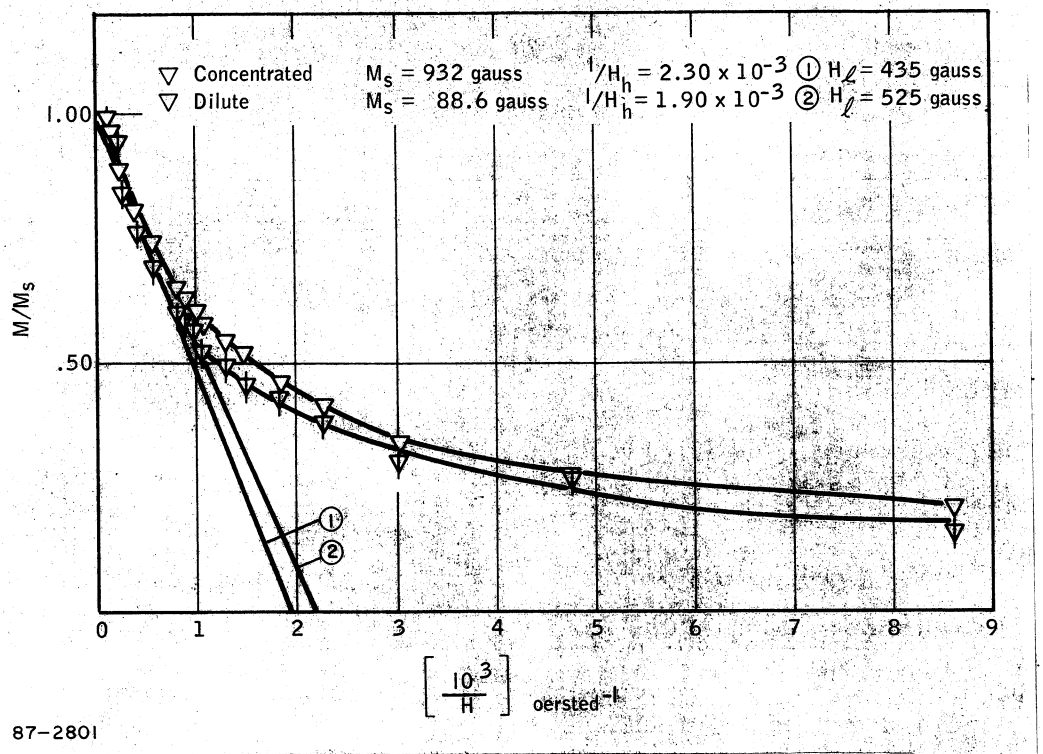

Figure 44. – Magnetization of G-21 Fluids versus Inverse of Applied Field

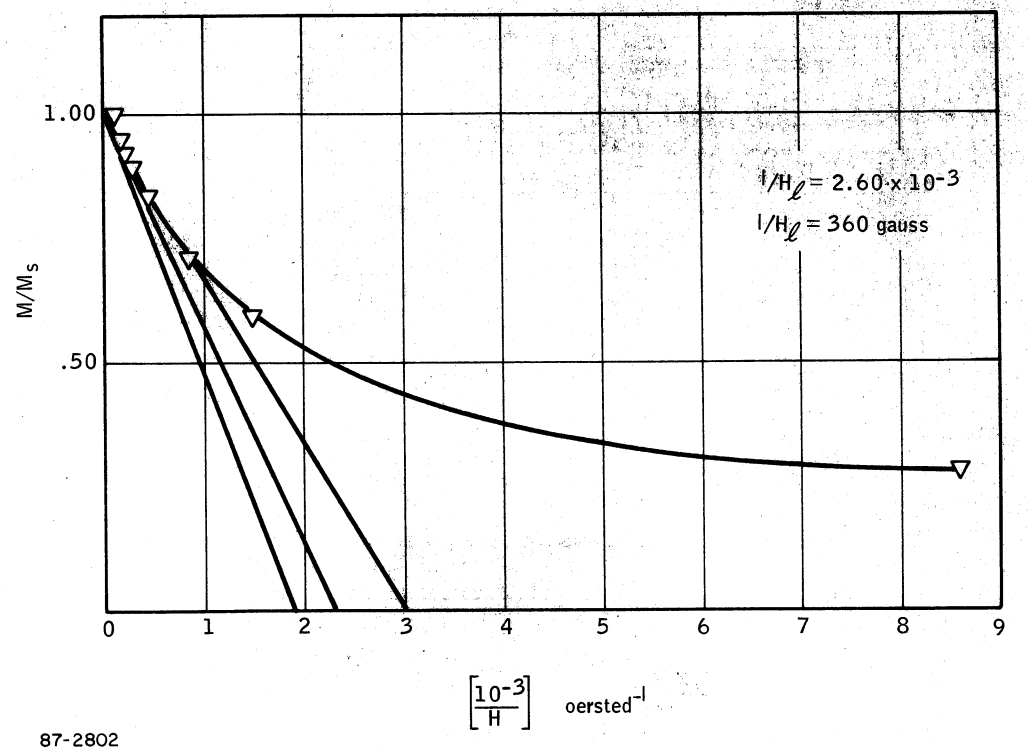

Figure 45. – Magnetization of G-44 Fluid versus Inverse of Applied Field, M_s = 212 gauss

TABLE 28. – COMPARISON OF PARTICLE SIZE DISTRIBUTION MEASUREMENTS FOR FERROFLUIDS

Fluid	G-4, -5, -6 concentrated	G-4, -5, -6 dilute	G-21 concentrated	G-21 dilute	G-44
Magnetic measurements $1/H_h$, oersted^{-1}	2.25×10^{-3}	1.78×10^{-3}	2.30×10^{-3}	1.90×10^{-3}	2.60×10^{-3}
H_h	445	516	435	525	360
H_ℓ	460	460	640	800	400
$\bar{V}$ $\mathring{A}^3 \times 10^5$	2.07	1.78	2.13	1.76	2.38
Statistical variance of volume = $= \frac{\sqrt{(\bar{V}^2) - (\bar{V})^2}}{\bar{V}} = 3\left[\frac{H_h}{H_\ell} - 1\right]$	1.9	2.4	1.0	1.0	1.7
Electron microscope measurements					
$\bar{D}_{NG}$, $\mathring{A}$	98		115		63
σ_{NG}	1.32		1.37		1.49
$\bar{V} = \frac{\pi}{6} \bar{D}_{SA} \bar{D}_{LA} \bar{D}_{NA}$, $\mathring{A} \times 10^5$	7.00		12.2		2.32
Statistical variance of volume = $\frac{\sqrt{(\bar{V}^2) - (\bar{V})^2}}{\bar{V}}$	.97		1.24		1.84

on the curve at H = 116 oersted. This overexaggerates the value of H_ℓ, but in a consistent manner.

It is concluded that this means for determining particle size and size distribution from knowledge of the magnetization curve is a valuable though somewhat rough tool. It does, however, result in a simple and rapid determination without the need of going to electron microscopy, which is expensive and time consuming.

Temperature Dependence of Ferrofluid Magnetization. - The saturation ferric induction as a function of temperature is important in order to estimate the performance of magnetocaloric heat engines or pumps for example, or in estimating the temperature sensitivity of any instrument which uses the ferrofluid.

As shown in figure 41 the ferric induction decreases with increasing temperature and this is generally typical of magnetic materials. The temperature dependence of the magnetic properties of a ferrofluid is a function of the magnetic solid component. Thus a magnetite base dispersion changes little at room temperature since magnetite has a Curie point of 570° C. Ferrofluids made with a ferrite that has a low Curie temperature exhibit relatively large changes in ferric induction. As can be seen from figure 41 with the manganese-zinc ferrite, the general decrease of ferric induction of the initial raw powder with temperature parallels that of the colloidal suspension containing ground powder. Within the limitations of the data, the Curie point seems to be unaffected by the grinding process.

The gradual decrease of magnetization with temperature is a handicap in a heat engine. There is hope in obtaining a true 90-100° C ferrite. According to Guilland (ref. 14) polycrystalline manganese zinc ferrite ($Mn_{1-x}\ Zn_x\ Fe_2O_4$) with $x = 0.50$ would have a saturation magnetization of 4000 gauss at room temperature (25° C) and a Curie point in the range of 90 - 100° C.

Viscosity of Ferrofluids

Viscosity is defined in absolute units as the ratio of the force per unit area (or shearing stress) required to maintain a unit velocity gradient (or rate of shear) in the fluid:

$$\eta = \frac{\tau}{\Gamma} \tag{50}$$

η = absolute viscosity, poises

τ = shear stress, dyne/cm^2

Γ = shear rate, sec^{-1}

For an ideal fluid, at a given temperature, η, is independent of the rate of shear. The viscosity at a given temperature, of such fluids called Newtonian fluids, is characterized by a single determination of the shear stress/shear rate relationship.

Many fluids, however, such as polymer solutions and concentrated colloidal suspensions are more complex. The viscosity for such non-Newtonian fluids is shear rate dependent. The only satisfactory way of characterizing them is by means of flow curves in which shear stress is plotted against rate of shear.

General Relationships on Viscosity of Suspensions. - Theoretical predictions are available for determining the viscosity of a fluid containing suspended particles. The earliest is that of Einstein which was derived by solving the flow field of pure strain perturbed by the presence of a sphere. The result related mixture viscosity, η_s, to solvent viscosity, η_o, and solids fraction, ϕ.

$$\frac{\eta_s}{\eta_o} = 1 + 2.5\,\phi \qquad (51)$$

This Einstein relationship, however, can be valid only for small concentrations such that the radius, r, of particles is small compared to the mean distance between them. For higher concentrations a procedure introduced by De Bruyn (see ref. 15) was modified by Rosensweig et al. (ref. 1) who assumed a functional relationship of the type:

$$\frac{\eta_s}{\eta_o} = \frac{1}{1 + a\phi + b\phi^2} \qquad (52)$$

For vanishingly small values of ϕ it is insisted that this equation reduce to equation (51) which determines a = -2.5. At some concentration ϕ_c, indicative of close packing of the particles, the fluid becomes rigid and so the fluidity, η_o/η_s, goes to zero. This determines the constant b as:

$$b = \frac{2.5\,\phi_c - 1}{\phi_c^2} = f(\phi_c) \qquad (53)$$

De Bruyn used the value $\phi_c = 0.74$ corresponding to hexagonal close-packed spheres. Further calculations indicate that the choice of a given numerical value of ϕ_c for values of $0.70 \leq \phi_c \leq 1.00$ is not critical since in this range $f(\phi_c)$ is essentially constant. It has a value of 1.55 ± 0.05, as shown in figure 46.

With $a = -2.5$, the denominator of Equation (52) is a perfect square if $b = -(1.25)^2 = -1.5625$. This is the value of $-f(\phi)_c$ for $\phi_c > 0.70$.

The solution viscosity can therefore be expressed as

$$\frac{\eta_s}{\eta_o} = \frac{1}{(1 - 1.25\,\phi)^2} \tag{54}$$

or in terms of a critical packing

$$\frac{\eta_s}{\eta_o} = \frac{1}{\left(1 - \frac{\phi}{\phi_c}\right)^2} \tag{55}$$

where $\phi_c = 1/1.25 = 0.80$, which is slightly higher than the value used by De Bruyn.

Application of General Relationship to Ferrofluids

Monodisperse Systems. - A ferrofluid is a three component system. In addition to the solid and liquid carrier, there is also the surfactant which is presumed to be adsorbed on the surface of the colloidal particles. The presence of an absorbed layer increases the effective volume of the solid particles in suspension. Uncoated spherical particles of the radius, r, when present in such quantity as to give a volume fraction, ϵ, will, when coated with a uniform layer of thickness, δ, occupy a fractional volume in the fluid of (see fig. 47):

$$\phi = \epsilon(1 + \delta/r)^3 \tag{56}$$

Equations (52) and (56) combined may be expressed as:

$$\frac{\eta_s - \eta_o}{\epsilon\,\eta_s} = 2.5\left(1 + \frac{\delta}{r}\right)^3 - \left(\frac{2.5\,\phi_i - 1}{\phi_i^2}\right)\left(1 + \frac{\delta}{r}\right)^6 \epsilon \tag{57}$$

Combining equations (54) and (56) also yields:

$$\eta_s = \frac{\eta}{\left[1.0 - 1.25\,\epsilon\left(1 + \frac{\delta}{r}\right)^3\right]^2} \tag{58}$$

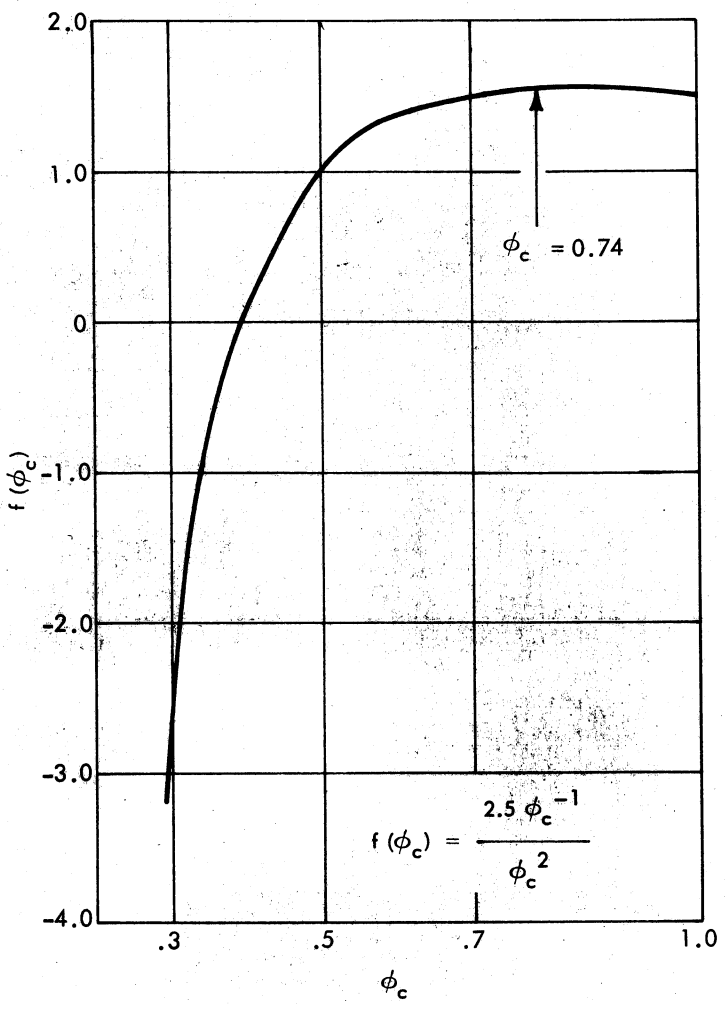

Figure 46. – Viscosity Law Coefficient as a Function of Volume Fraction Packing

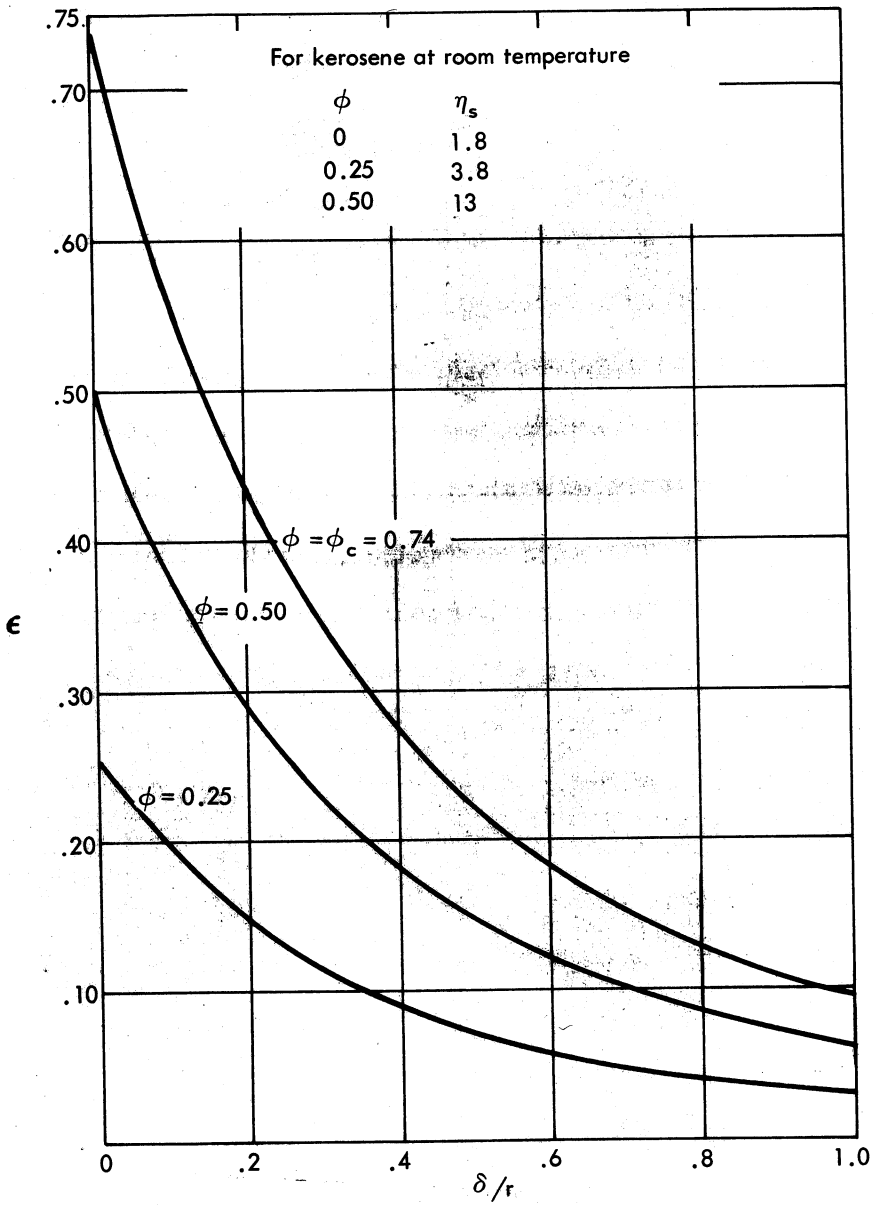

86-7651

Figure 47. – True Solids Volume Concentration as a Function of Relative Monolayer Thickness at Different Apparent Concentrations

is obtained experimentally from density or magnetization measurements, as previously discussed.

Multidisperse Systems. - The previous development assumed a system of equal sized spheres. In systems where there is a variation in particle size, the relation between the thickness of the stabilizing layer and the sizes of the particles is more complex and is better represented by the results of the following development.

The effective volume fraction solids in the system ϕ is equal to

$$\phi = \frac{4\pi}{3V} \Sigma n_i (r_i + \delta)^3 \tag{59}$$

where V = volume of the system. This assumes that the thickness of the stabilizing layer around a particle is constant and independent of particle size. Similarly, the true volume fraction solids in the system is

$$\epsilon = \frac{4\pi}{3V} \Sigma n_i r_i^3 \tag{60}$$

In the above equations, there are n_i particles of radius r_i in the system. The ratio of ϕ/ϵ is

$$\frac{\phi}{\epsilon} = \frac{\Sigma n_i (r_i + \delta)^3}{\Sigma n_i r_i^3} \tag{61}$$

Expanding the above equation yields

$$\frac{\phi}{\epsilon} = \frac{\Sigma n_i r_i^3}{\Sigma n_i r_i^3} + \frac{3\delta \Sigma n_i r_i^2}{\Sigma n_i r_i^3} + \frac{3\delta^2 \Sigma n_i r_i}{\Sigma n_i r_i^3} + \frac{\delta^3 \Sigma n_i}{\Sigma n_i r_i^3} \tag{62}$$

In the above equation, Term A is equal to 1. The volume to surface average particle diameter is defined by the following equations:

$$\bar{D}_{SA} = \frac{\Sigma n_i D_i^3}{\Sigma n_i D_i^2} = \frac{\Sigma n_i (2 r_i)^3}{\Sigma n_i (2 r_i)^2} = \frac{2 \Sigma n_i r_i^3}{\Sigma n_i r_i^2}$$

Term B is therefore equal to $\frac{6\delta}{\bar{D}_{SA}}$.

Term C can be multiplied in the denominator and the numerator by the term $\Sigma n_i r_i^2$

$$\frac{3\delta^2 \Sigma n_i r_i}{\Sigma n_i r_i^3} = 3\delta^2 \frac{\Sigma n_i r_i}{\Sigma n_i r_i^2} \cdot \frac{\Sigma n_i r_i^2}{\Sigma n_i r_i^3}$$

Now the length mean diameter of a particle is equal to

$$\bar{D}_{LA} = \frac{\Sigma n_i D_i^2}{\Sigma n_i D_i} \quad \frac{\Sigma n_i (2r_i)^2}{\Sigma n_i (2r_i)}$$

so that

$$\frac{\Sigma n_i r_i}{\Sigma n_i r_i^2} = \frac{2}{\bar{D}_{LA}}$$

Term C is therefore equal to $12\delta^2 / \bar{D}_{LA} \bar{D}_{SA}$

Term D can be expanded in a similar fashion by multiplying the numerator and denominator by the product $[\Sigma n_i r_i^2][\Sigma n_i r_i]$

$$\frac{\delta^3 \Sigma n_i}{\Sigma n_i r_i^3} = \delta^3 \frac{\Sigma n_i}{\Sigma n_i r_i} \cdot \frac{\Sigma n_i r_i}{\Sigma n_i r_i^2} \cdot \frac{\Sigma n_i r_i^2}{\Sigma n_i r_i^3}$$

The number mean diameter $\bar{D}_N$ is equal to:

$$\bar{D}_{NA} = \frac{\Sigma n_i D_i}{\Sigma n_i} = \frac{\Sigma n_i (2r_i)}{\Sigma n_i}$$

Substitution into the above equation yields

$$\frac{\delta^3 \Sigma n_i}{\Sigma n_i r_i^3} = \frac{8\delta^3}{\bar{D}_{SA} \cdot \bar{D}_{LA} \cdot \bar{D}_{NA}}$$

The ratio of ϕ/ϵ is therefore:

$$\frac{\phi}{\epsilon} = 1 + \frac{6\delta}{\bar{D}_{SA}} + \frac{12\delta^2}{\bar{D}_{SA} \bar{D}_{LA}} + \frac{8\delta^3}{\bar{D}_{SA} \cdot \bar{D}_{LA} \cdot \bar{D}_{NA}} \qquad (63)$$

The different average particle diameters in equation (63) can be obtained experimentally from particle size distribution measurements. ϕ can be obtained from viscosity measurements while ϵ is obtained from density measurements. Therefore it should be possible to calculate experimental values for δ using the above cubic equation.

No assumptions as to particle size distribution were made in equation (63). In the case of a log-normal particle size distribution where the different mean particle diameters are related, it is possible to simplify the relationship in terms of $\bar{D}_{NG}$ the geometric number mean particle size and σ_G the geometric standard deviation:

$$\frac{\phi}{6} = 1 + \frac{6\delta}{\bar{D}_{NG}\, e^{2.5}\, \sigma_G{}^2} + \frac{12\,\delta^2}{\bar{D}_{NG}{}^2\, e^{4.0}\, \sigma_G{}^2} + \frac{8\,\delta^3}{\bar{D}_{NG}{}^3\, e^{4.5}\, \sigma_G{}^2} \qquad (64)$$

Equation (63) is applied to the determination of surface layer thickness in the discussion of results.

Effect of Temperature. - According to equation (54) at any given temperature, the viscosity of a ferrofluid is a function of the viscosity of the base fluid and the effective volume fraction ϕ.

The base fluids used in these studies are simple, unassociated liquids that normally follow Andrade's rule:

$$\eta_o = A\, e^{-E/RT} \qquad (65)$$

where A and E are characteristic constants, R is the gas constant and T the absolute temperature.

ϕ is a function of δ, particle size and ϵ. Both particle size and can be considered not to depend on temperature except for second order effects due to changes in density. The thickness, δ, is undoubtedly a complex function of temperature since adsorption of molecules on a surface is temperature dependent.

Viscosity Measurements

Equipment. - The viscosity measurements were carried out using Fenske reverse flow capillary viscometers. (See fig. 48.) The viscometers are especially suited for determinations on opaque liquids. The viscometers are bathed in a controlled, constant temperature bath. The temperature of test could be controlled over a wide range.

Inherent in the use of a capillary viscosimeter is the assumption that the liquid under test is Newtonian in character. The mathematical analysis of viscosity data for complex systems is greatly simplified if the material under test is subjected to a uniform rate of shear. This cannot be accomplished with a capillary viscometer and can only be approached with the

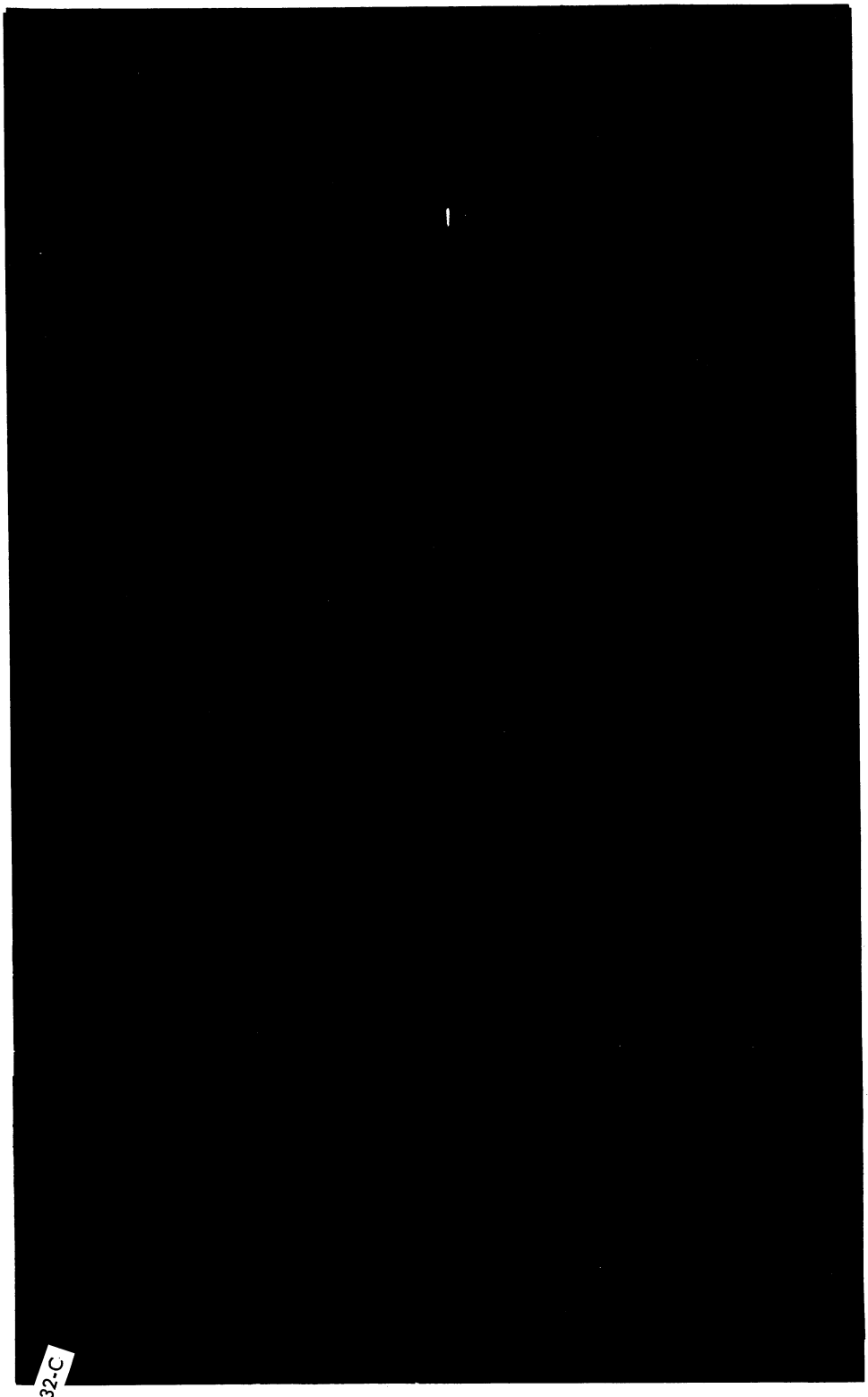

Figure 48. – Viscosimeter Tubes and Constant Temperature Bath (The tube at the left is a Fenske reverse flow type while the tube at the right is a conventional Ostwald design)

Top

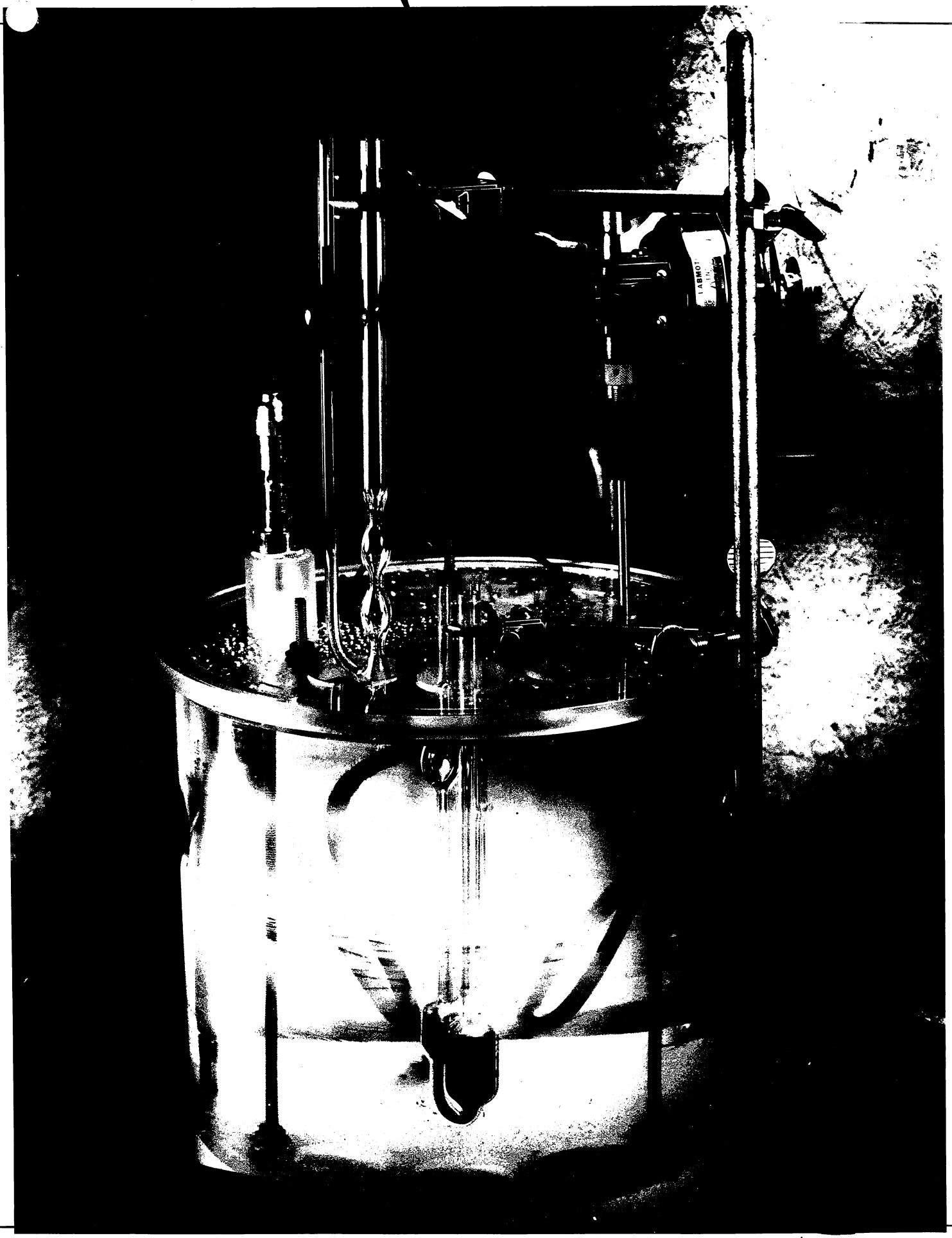

Fig 48 Pg 124 FIG 48 T-82

coaxial cylinder type for very small gapwidths and large diameter cylinders. The attempt to secure high rates of shear by using high speeds of rotation then courts serious errors arising from the generation of heat within the fluid.

Arrangements were made with Ferranti Electric, Inc for the use of a cone and plate viscometer for the testing of selected fluids of interest to this program. This was the Ferranti-Shirley viscometer which consists of a stationary flat plate and a slightly conical rotating disc driven by a variable speed motor. It provides a precise and rapid means of obtaining flow measurements on non-Newtonian fluids by subjecting the sample to definite uniform shear rates; for additional information see references 16 and 17.

The viscometer was operated with an automatic plate setting unit which controlled the position to an accuracy of better than 0.001 inch. The viscometer comes equipped with a cooling jacket for constant temperature operation but in these tests operation was at ambient temperature. An automatic flow curve recorder (X-Y recorder) displayed the data in response to a control unit that gave uniform acceleration of the cone up to maximum speed followed by deceleration to zero at the same selected rate. The data obtained are given in Figures 49 and 50; Table 29 provides a summary.

Experimental Results

Capillary Tube Measurements. - The effects of solids concentration, and thereby magnetization, on the viscosity of different ferrofluids prepared by grinding were obtained at room temperature. The different families of fluids tested are described in table 30. The results of these viscosity tests are presented in tables 31 through 34 and summarized in figure 51.

The effect of temperature on the viscosity concentration relationship was obtained for one set of ferrofluids obtained from grind G-21. These results are presented in table 35 and figure 52. The effect of base solvent was also examined. The viscosity-temperature characteristics of concentrated G-21 fluid rediluted with decane of constant magnetization ($M = 310$ gauss at room temperature) was measured. These results are presented in figure 53 and table 36. Table 36 also presents relevant properties of the fluid.

Discussion of Results

Variable Shear Rate Measurements. - As shown in figure 49(a), the silicone fluid DC 510 yielded a linear response under acceleration and deceleration. The slight decrease of viscosity with time could be due to viscous heating that would produce a viscosity decrease as observed. This is a

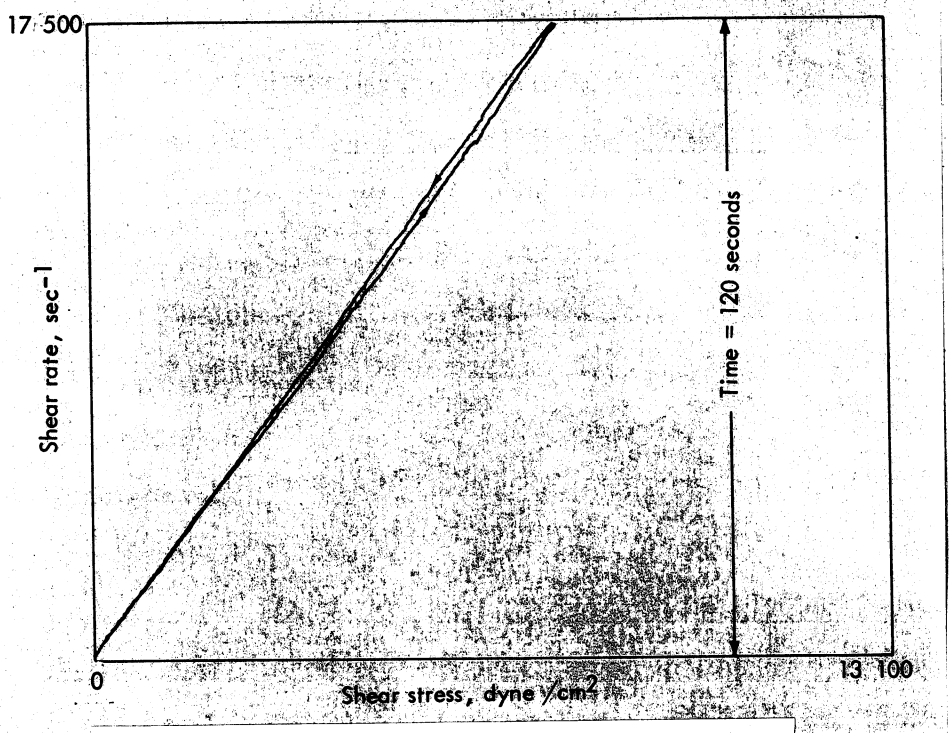

Figure 49a. – Shear Rate versus Shear Stress of Dow-Corning 510 Silicone Fluid (50 centistokes)

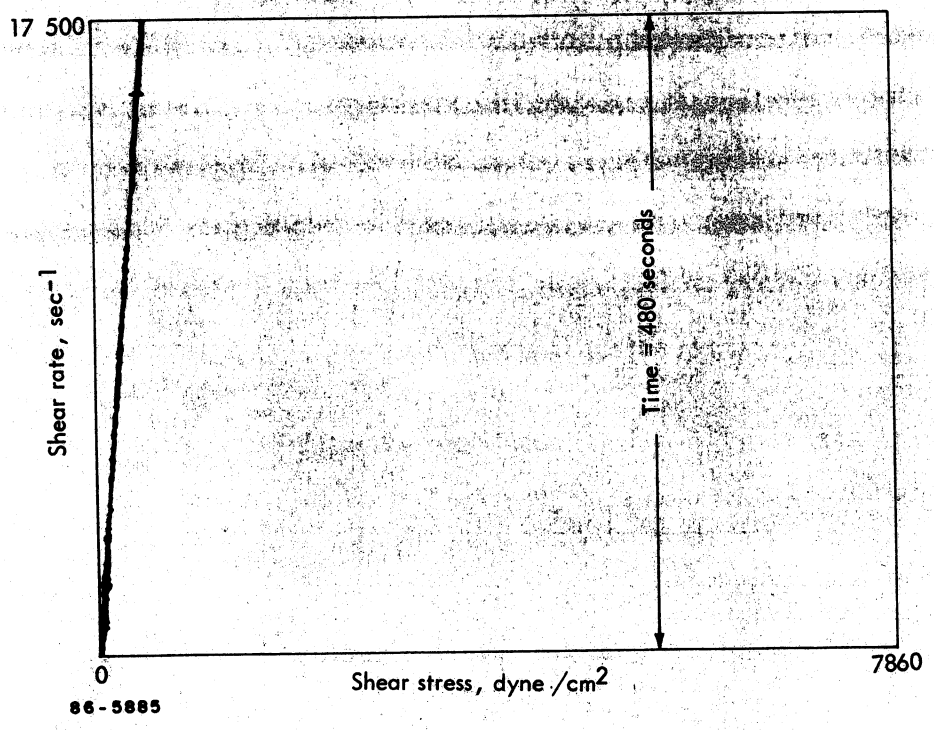

Figure 49b. – Shear Rate versus Shear Stress of Magnetite/Oleic Acid/ Decane Ferrofluid (M_s = 310 gauss, η = 2.8 centipoise)

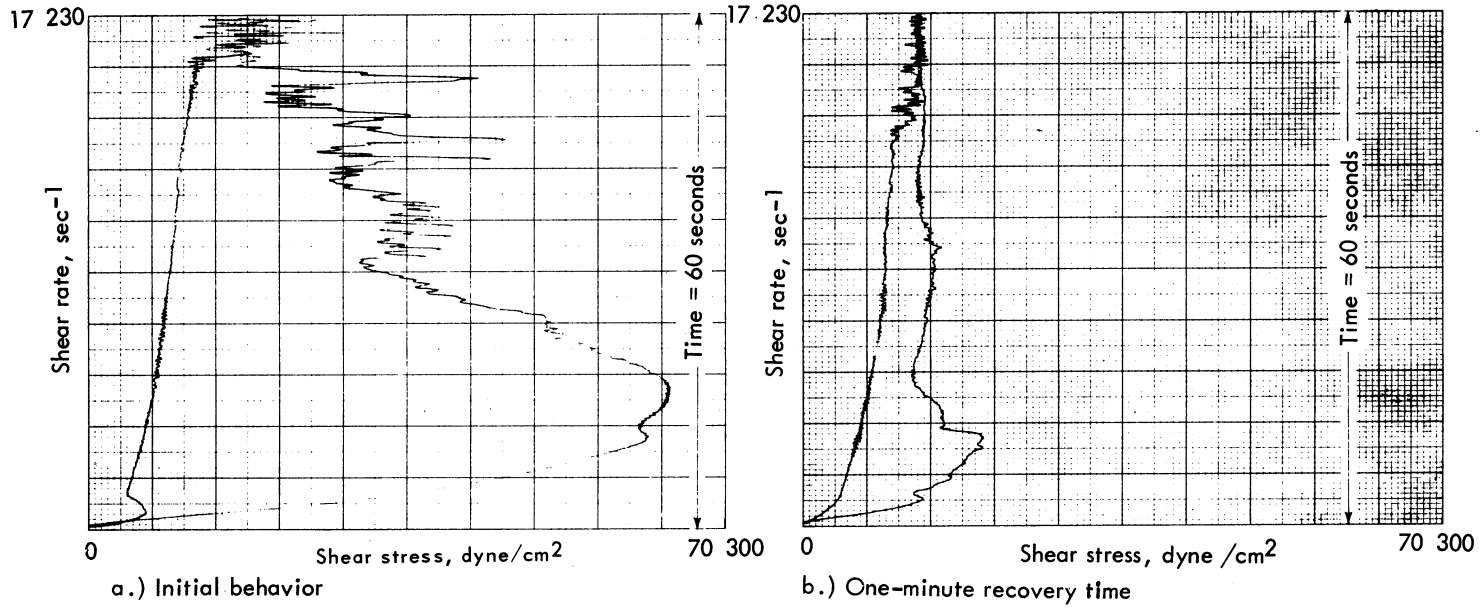

Figure 50. – Influence of Recovery Time on Shear Rate versus Shear Stress of Concentrated G-31 Ferrofluid (M_s = 1000 gauss, η = 2000 centipoise at Low Shear). (A) Initial Behavior; (B) One-Minute Recovery Time; (C) Five-Minute Recovery Time

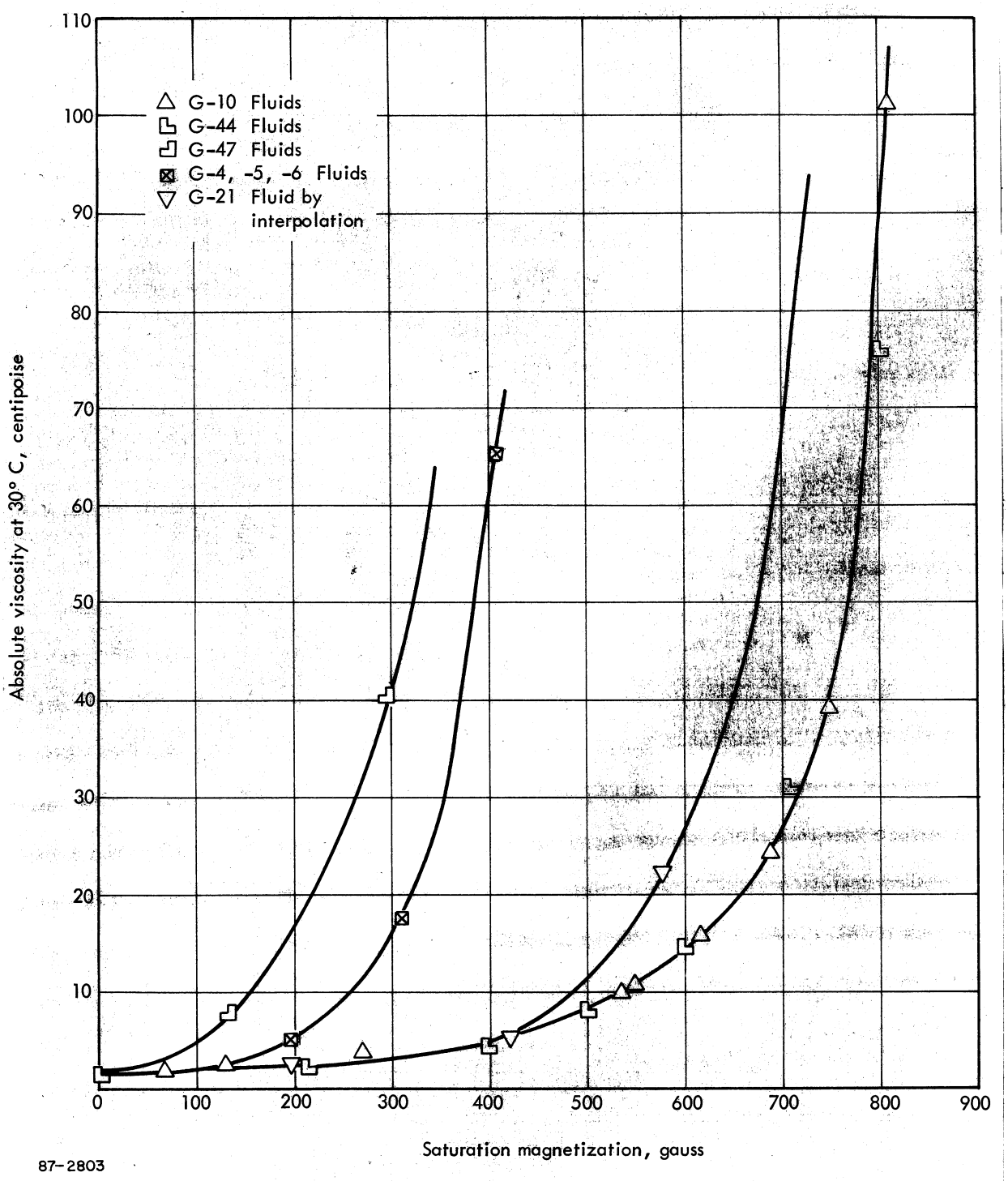

Figure 51. – Saturation Magnetization versus Viscosity for Different Ferrofluids

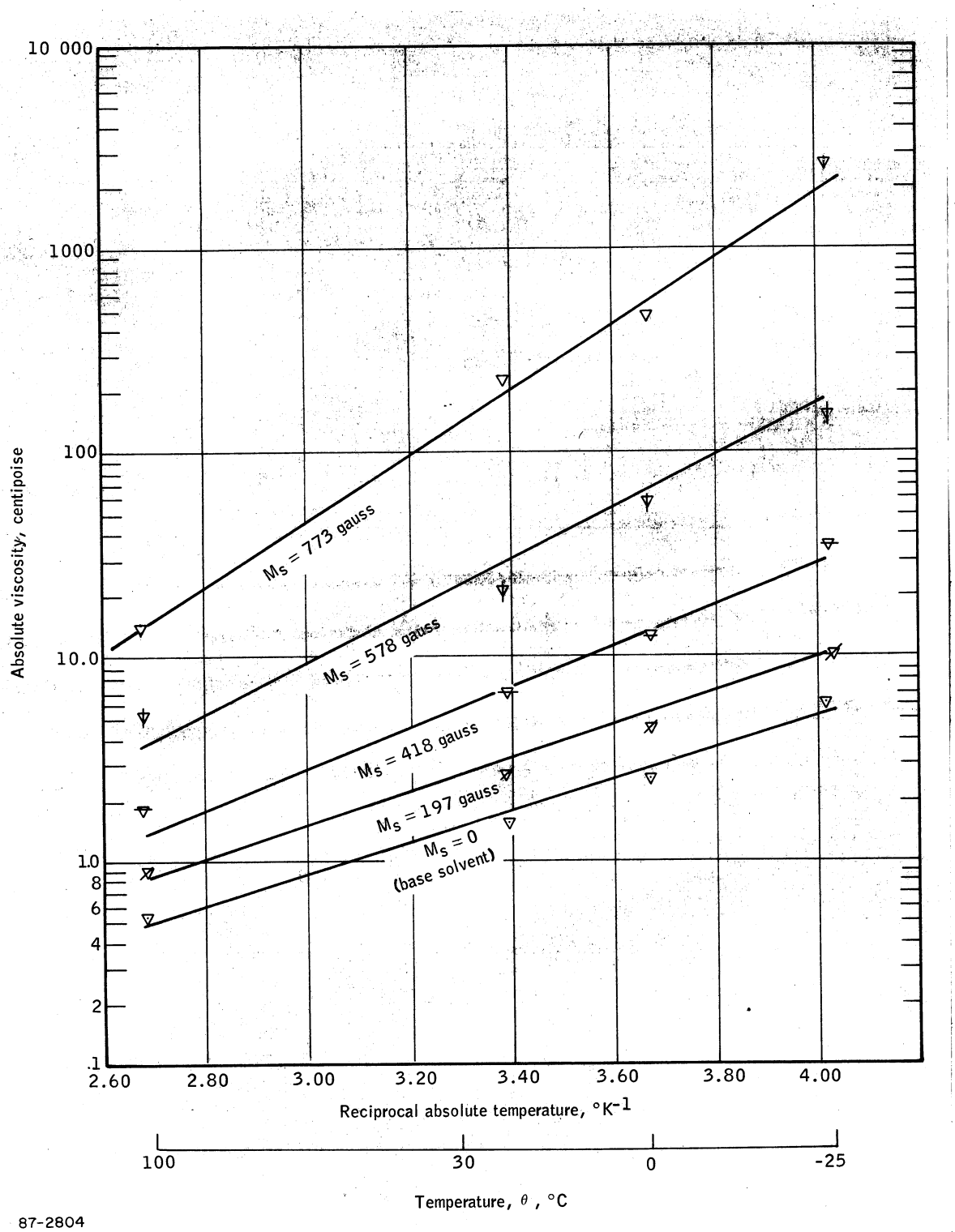

Figure 52. – Absolute Viscosity as a Function of Temperature and Magnetization for G-21 Kerosene-Based Fluids

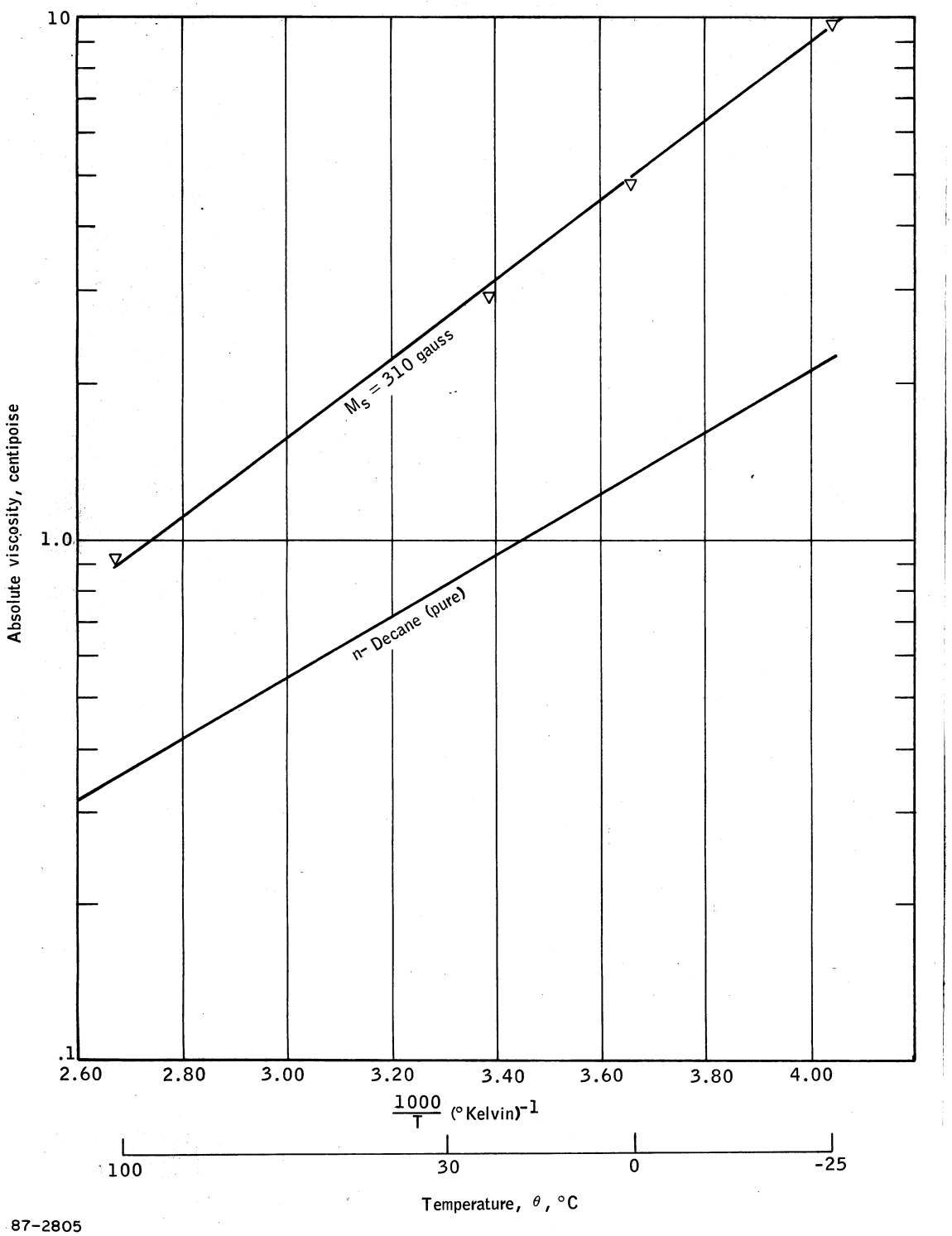

Figure 53. – Viscosity of Decane-Based Ferrofluid (M_s = 310 gauss) versus Temperature

TABLE 29. – SUMMARY OF RHEOLOGICAL TESTS CONCERNING SHEAR RATE VERSUS SHEAR STRESS

Figure	Fluid	Saturated ferric induction, gauss	Nominal viscosity	Cone and plate viscosity, cp	Maximum shear rate, sec^{-1}	Acceleration time, seconds	Comments
57a	Dow-Corning 510 silicone fluid	---	50 cs (label value)	44	17 500	120	Noncolloidal reference fluid
57b	Magnetite/oleic acid/decane, run G	310	2.5 cp (capillary tube determination)	2.8	17 500	480	This tests a dilute ferrofluid of high fluidity
58a	G-21, run 1	1000	---	2000 (at low shear)	17 230	60	These tests determined thixotropic nature of a very concentrated ferrofluid
58b	G-21, run 2	1000	---	2000 (at low shear)	17 230	60	Approx 1 minute of recovery time between runs 1 and 2
58c	G-21, run 3	1000	---	2000 (at low shear)	17 230	60	Five minutes of recovery time between runs 2 and 3

TABLE 30. – SUMMARY OF VISCOMETRY TESTS

Grind No.	Magnetic solid	Surfactant	Surfactant concentration, cc/gm solid	Carrier fluid	Arithmetic vol. average particle size (from electron micrograph)	Test temperature, °C	Magnetization range, gauss	Viscosity range, cs (at room temperature)
G-4, -5, -6	Magnetite	Oleic acid	0.50	Kerosene	127	30	63 - 510	2.65 - 633
G-10	Magnetite	Oleic acid	.50	Kerosene	---	30	67 - 975	2.03 - 1000
G-21	Magnetite	Oleic acid	.35	Kerosene	165	-25/+100	197 - 773	2.69 - 224
G-44	Magnetite	Tenlo 70	.50	Kerosene	98	30	212 - 1057	2.45 - 7400
G-47	Magnetite	Aerosol	.50	Kerosene	---	30	135 - 575	7.08 - 3130
G-21	Magnetite	Oleic acid	.50	Decane	165	-25/+100	310	3.00

TABLE 31. – MAGNETIZATION, VISCOSITY, AND DENSITY OF G–4, –5, –6 FLUIDS OF VARIOUS CONCENTRATIONS

(ϵ_M/ϵ_D = K = 0.74)

Magnetization, M, at H = 10 000 oe	Absolute viscosity, η at 30° C, cp	Density ρ, gm/cc	Volumetric[a] loading, ϵ_D, percent	Volumetric[b] loading, ϵ_M, percent	$\frac{\eta_s - \eta_o}{\eta_s}$	$\left[\frac{\eta_s - \eta_o}{\eta_s}\right]\frac{1}{\epsilon}$ Reduced viscosity
510	835	1.320	12.5	9.02	0.997	7.96
405	65.2	1.206	9.80	7.15	.978	9.96
307	17.6	1.105	7.40	5.42	.906	12.3
197	5.20	.992	4.68	3.48	.720	14.5
63.2	2.27	.859	1.52	1.12	.269	17.7
0	1.66	.744	---	---	---	---

[a]Based on density measurement: $\epsilon_D = \frac{\rho - \rho_L}{\rho_s - \rho_L}$ ρ_s = 5.0 gm/cc

[b]Based on magnetization measurement: $\epsilon_M = \frac{M_s}{M_{ss}} = \frac{M_s}{5660}$

TABLE 32. – MAGNETIZATION, VISCOSITY, AND DENSITY OF G–10 FLUIDS OF VARIOUS CONCENTRATIONS

(ϵ_M/ϵ_D = K = 0.89)

Magnetization, M, at H = 10 000 oe	Absolute viscosity, η, at 30° C, cp	Density, ρ, gm/cc	Volumetric[a] loading, ϵ_D, percent	Volumetric[b] loading, ϵ_M, percent	$\frac{\eta_s - \eta_o}{\eta_s}$	$\left[\frac{\eta_s - \eta_o}{\eta_s}\right]\frac{1}{\epsilon}$ Reduced viscosity
975	No flow	1.63	19.8	17.2	---	---
810	106	1.467	16.0	14.3	0.984	6.14
747	39.0	1.404	14.5	13.2	.954	6.58
688	24.5	1.360	13.5	12.1	.926	6.86
616	15.7	1.304	12.2	10.9	.886	7.25
548	10.8	1.250	10.9	9.7	.832	7.65
535	9.82	1.243	10.7	9.46	.815	7.65
269	3.87	1.021	5.4	4.85	.532	9.9
129	2.46	.896	2.5	2.28	.260	10.4
67	2.03	.838	1.1	1.18	.105	10.0
0	1.82	.79	---	---	---	---

[a] Based on density measurement: $\epsilon_D = \frac{\rho - \rho_L}{\rho_s - \rho_L}$ ρ_s = 5.0 gm/cc

[b] Based on magnetization measurement: $\epsilon_M = \frac{M_s}{M_{ss}} = \frac{M_s}{5660}$

TABLE 33. – MAGNETIZATION, VISCOSITY, AND DENSITY OF G-44 FLUIDS OF VARIOUS CONCENTRATIONS
(ϵ_M/ϵ_D = K = 0.98)

Magnetization, M, at H = 10 000 oe	Absolute viscosity, η at 30° C, cp	Density, ρ, gm/cc	Volumetric[a] loading, ϵ_D, percent	Volumetric[b] loading, ϵ_M, percent	$\frac{\eta_s - \eta_o}{\eta_s}$	$\left[\frac{\eta_s - \eta_o}{\eta_s}\right]\frac{1}{\epsilon}$ Reduced viscosity
1057	7430	1.613	19.3	18.7	0.999	5.18
918	325	1.500	16.6	16.2	.994	5.98
800	76.0	1.420	14.7	14.1	.980	6.69
707	31.2	1.340	12.8	12.5	.953	7.44
600	14.69	1.257	10.9	10.6	.904	7.95
501	8.10	1.180	9.20	8.85	.822	8.92
397	4.97	1.098	7.20	7.00	.706	9.86
212	2.45	.953	3.99	3.74	.408	10.7
0	1.45	.794	---	---	---	---

[a]Based on density measurement: $\epsilon_D = \frac{\rho - \rho_L}{\rho_s - \rho_L}$ ρ_s = 5.0 gm/cc

[b]Based on magnetization measurement: $\epsilon_M = \frac{M_s}{M_{ss}} = \frac{M_s}{5660}$

TABLE 34. – MAGNETIZATION, VISCOSITY, AND DENSITY OF G–47 FLUIDS OF VARIOUS CONCENTRATIONS

(ϵ_M/ϵ_D = K = 0.97)

Magnetization, M, at H = 10 000 oe	Absolute viscosity, η, at 30° C, cp	Density, ρ, gm/cc	Volumetric[a] loading, ϵ_D, percent	Volumetric[b] loading, ϵ_M, percent
575	3130	1.256	10.9	10.1
457	183	1.153	8.50	8.06
194	40.2	1.016	5.24	5.18
135.2	7.09	.897	2.42	2.39
0	1.81	.80	---	---

[a]Based on density measurement: $\epsilon_D = \dfrac{\rho - \rho_L}{\rho_s - \rho_L}$ $\rho_s = 5.0$ gm/cc

[b]Based on magnetization measurement: $\epsilon_M = \dfrac{M_s}{M_{ss}} = \dfrac{M_s}{5660}$

TABLE 35. – VISCOSITY-TEMPERATURE CHARACTERISTICS OF G-21 FERROFLUIDS AT DIFFERENT SOLIDS LOADINGS

Magnetite/oleic acid/kerosene ferrofluid, 0.35 cc oleic acid per gram of magnetite (G-21 fluid)					
Room temperature magnetization, M_s, gauss, at H = 10 000 oe	773	578	418	197	0
Volume fraction solids, $\epsilon_M = M_s/3600$[a]	.214	.161	.116	.0547	---
θ = - 25° C					
Kinematic viscosity, ν, cs	1460	106	28.0	11.1	7.00
Calculated suspension density, ρ, gm/cc	1.73	1.51	1.29	1.06	.83
Absolute viscosity, η, cp	2520	160	3.62	11.8	5.80
θ = 0° C					
Kinematic viscosity, ν, cs	286	32.4	10.3	4.70	3.00
Calculated suspension density, ρ, gm/cc	1.70	1.47	1.25	1.02	.79
Absolute viscosity, η, cp	486	61	12.9	4.80	2.57
θ = 22° C					
Kinematic viscosity, ν, cs	134	15.1	5.58	2.69	2.01
Calculated suspension density, ρ, gm/cc	1.67	1.45	1.23	1.00	.77
Absolute viscosity, η, cp	224	21.9	6.86	1.69	1.54
θ = 100° C					
Kinematic viscosity, ν, cs	8.81	2.93	1.54	0.96	0.76
Calculated suspension density, ρ, gm/cc	1.62	1.40	7.18	.93	.71
Absolute viscosity, η, cp	14.3	4.93	1.82	.89	.54

[a]Based on conversion K = 0.65; KM_s = (0.65) (5660) = 3600 gauss TABLE 35

TABLE 36. – VARIATION OF VISCOSITY OF 5-23-66-1 MAGNETIC FLUID (G-21 SOLIDS DILUTED WITH DECANE)
M_s = 310 GAUSS

θ Temperature, °C	γ_s Kinematic viscosity, cs	ρ [a] Suspension density, gm/cc	η_s Absolute viscosity, cp	η_o [b] Carrier absolute viscosity, cp	η_s/η_o
-25	8.77	0.764	9.75	2.245	4.33
0	4.35	.745	4.80	1.304	3.68
22	2.76	.728	3.00	.93	3.23
100	.88	.668	.91	.37	2.46

TABLE 3C

[a] Calculated $\rho = \epsilon(\rho_s - \rho_L) + \rho_L$

where:

ϵ = 0.0843

ρ_s = 5.0 gm/cc

ρ_L = ρ_{decane} at θ

[b] Pure decane.

reference graph which shows the behavior of a fluid known to be Newtonian in flow characteristics.

The low viscosity ferrofluid (G-40) produces curves (figure 49(b) which show high frequency variations (grassy appearance) compared to the silicone fluid. Aside from this the fluid exhibited the reversible linear behavior of a Newtonian liquid.

These results show that this ferrofluid is well dispersed. There is essentially no gross interaction between the particles as evidenced by the overall Newtonian behavior of the system. There might be some local particle association as exemplified by the clumping of particles to form limited agglomerates. The disruption of these elements which increasing shear could account for grassy oscillations along the principal line.

Associative tendencies are much more pronounced with the concentrated G-21 ferrofluid, as evidenced by figures 50(a) to 50(c).

This material is concentrated to the verge of being dry. From the magnetization measurements, the volume fraction solids is at least 17.6 percent. This does not include the nonmagnetic inclusions which should raise the true volume fraction of all solids in suspension to above 20 percent. As will be discussed further in more detail, for the more dilute ferrofluids of the G-21 family, $\phi/\epsilon = 5.0$ at room temperature. If there is no compression of the boundary layer in this very concentrated system, one obtains over 100 percent for the effective volume fraction solids in the system. This system consists of particles with their stabilizing layer distorted and with essentially no free fluid between the particles.

The curves presented in figures 50(a) to 50(c) exhibit thixotropy, the isothermal gel-sol-gel transformation in a substance subjected to increasing then decreasing shear. The area bounded by the up and down curves results from the temporary breakdown of the gel like structure of the material. The enclosed area of the "hysteresis loop" is seen to be determined by the maximum rate of shear, by the total shearing time, and by the recovery time elapsed between runs.

All three curves reveal a smooth increase of shear rate versus shear stress beginning from zero shear rate to about 3000 sec^{-1}. From 3000 to 17 230 sec^{-1} (the maximum shear rate) there is an oscillating decrease in shear stress. As the rate of shear decreases from its maximum value the shear stress decreases with some oscillations returning to the initial smooth curve in the last stages of deceleration.

At low shear rates, this fluid behaves in pseudo-Newtonian fashion in which individual lubricated particles slip by each other in the whole particle mass. At higher shear rates, there is progressive breakdown in structure wherein assemblies of particles of ever decreasing size are rent assunder (the oscillations are evidence of the progressive breakdown).

The fluid can be envisioned as an assembly of lubricated ball bearings. At low shear rates, the fluid behaves in pseudo-Newtonian fashion. A viscosity of 2000 cp is obtained from the initial point of the curve. At these low shear rates the whole assembly deforms "en masse" with slippage of individual elements past each other. With increasing shear rates, the particles cannot slip past each other rapidly enough so that the whole assembly is progressively torn apart into smaller and smaller subgroups. With decreasing shear rate, the system regains its structure. However, as the variation of area of the hysteresis loop shows, the recovery of structure is a kinetic process which is about 1/3 completed in 1 minute and about 2/3 completed in 5 minutes.

From these variable shear rate measurements, it can be concluded that the ferrofluids behave as Newtonian fluids at low shear rates even at solids loading of 20 percent. At lower solids concentration, the ferrofluids behave in a Newtonian manner to shear rates as high as 17 000 sec^{-1}.

The shear rate in the capillary tube viscometers was of the order of 10 inverse seconds and had been varied by a factor of 2. At this shear rate, all the ferrofluids studied are Newtonian. The viscosity data obtained in the capillary tubes can therefore be validly analyzed in terms of the equations which presented in the theoretical development. Except for the very viscous fluids where $\phi \rightarrow \phi_{max}$, the ferrofluid should be essentially Newtonian over wide range of shear rates. The capillary tube measurement characterizes the viscosity of these fluids. In those cases where $\phi \rightarrow \phi_{max}$, the capillary tube measurement will only be representative at low shear rates.

Capillary Tube Viscosity Measurements. - As presented in figures 51, 52, and 53, the viscosity of a ferrofluid increases nonlinearly with increasing saturation magnetization of the fluid, increases with decreasing temperature, varies with the nature of the carrier liquid, varies with its method of preparation. Ferrofluids obtained from different grinds have a different viscosity/magnetic moment characteristics.

These results were analyzed in terms of equations (57), (63), and (65), from which it was possible to draw conclusions on the structure of the ferrofluids.

Relations between Magnetization and the Viscosity of a Multidisperse Ferrofluid. - The viscosity of a suspension of coated spherical particles of radius r and stabilizing layer thickness δ, is related to the volume concentration solids in suspension by equation (57). For multidisperse systems, the equivalent equation is:

$$\frac{1}{\epsilon}\left(\frac{\eta_s - \eta_o}{\eta_s}\right) = 2.5\left(\frac{\phi}{\epsilon}\right) - \left(\frac{2.5\,\phi_c - 1}{\phi_c^2}\right)\left(\frac{\phi}{\epsilon}\right)^2 \epsilon \qquad (66)$$

The ratio of ϕ/ϵ is defined by equation (63) and is constant for a given system at constant temperature. Thus if this equation is obeyed a plot of measured values of $(\eta_s - \eta_o)/\eta_s$ versus ϵ should yield a straight line. Straight lines are obtained when such plots are constructed for different kerosene based ferrofluids as shown in figure 54.

The data from run G-47 are not presented in this figure. This fluid was an Aerosol TR stabilized dispersion of magnetite in kerosene. While quite stable in the absence of air, the fluid tended to form a separate solid phase at the air-liquid interface. This phase separation occurred in the capillary tubes during the viscosity measurements. The combination of high viscosity at low solids loading and phase separation discouraged any further investigations on fluids containing Aerosol TR.

The viscosity of a ferrofluid increases with increasing magnetization of the fluid as a result of the corresponding increase in concentration of solids in suspension, ϵ. For a given set of ferrofluids of varying M_s obtained from a specified grinding operation, M_s is directly proportional to

$$M_s = K M_{ss} \epsilon_D \qquad (67)$$

where $K = \epsilon_M/\epsilon_D$ = conversion, a constant for a given grind. In the above equations, M_{ss} is the saturation magnetization of the magnetic solid in suspension, (for magnetite, M_{ss} = 5660 gauss), ϵ_M is the volume fraction magnetic solids in suspension. ϵ_M is smaller than ϵ_D because of the presence of non-magnetic solid impurities that are also present in suspension as a result of the grinding operation. For the runs presented in tables 31 to 34 K = 0.65 to 0.98.

Viscosity of a Ferrofluid as a Function of the Physical Parameters of Its Components. - The viscosity measurements provide valuable insight on the structure of the stabilizing layer around the individual colloidal particles. They also provide information on the effect of size of the particles, the nature of the stabilizing agent and the viscosity of the base fluid.

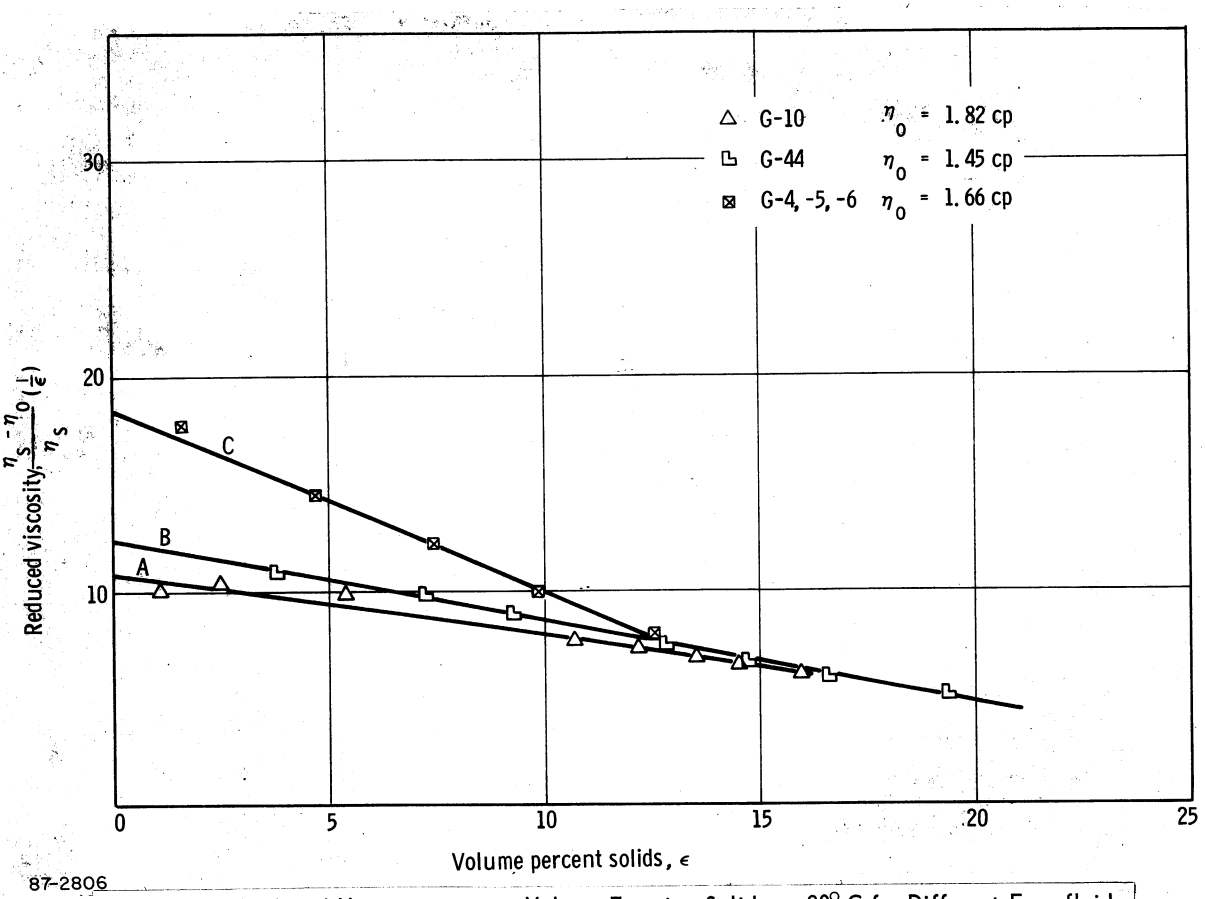

87-2806

Figure 54. – Reduced Viscosity versus Volume Fraction Solids at 30° C for Different Ferrofluids

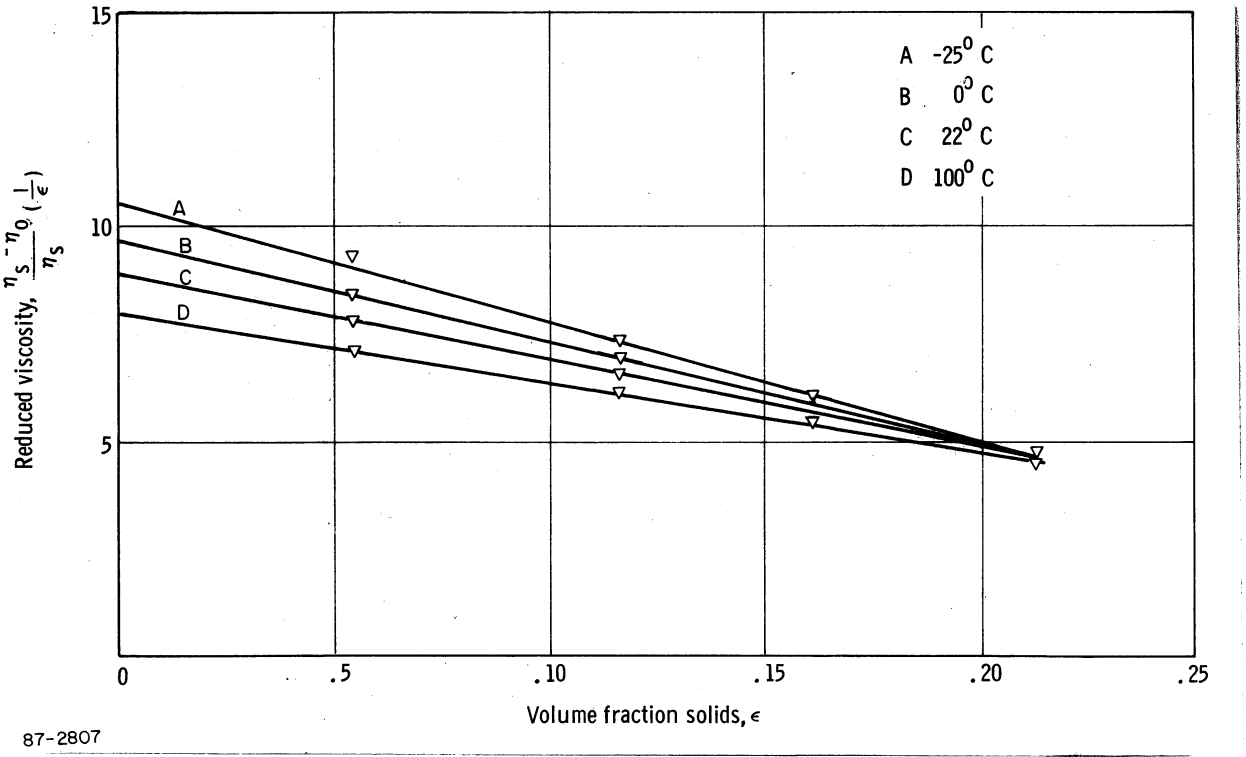

87-2807

Figure 55. – Reduced Viscosity versus Volume Fraction Solids at Different Temperatures for G-21 Fluids

Figure 54 which was presented in the previous section is a plot of the reduced viscosity $\left(\frac{\eta_s - \eta_o}{\eta_s}\right)\frac{1}{\epsilon}$ as a function of the solids concentration for different families of ferrofluids at room temperature. Each family originated a grinding run. The members of a given family differ only in the relative concentration of carrier fluid. The other components, the solid particles and the surfactant are identical in kind and relative total amounts.

Each of these lines has a characteristic slope and intercept. According to equation (66), $f(\phi_c)$ is obtained numerically from the slope and ϕ/ϵ from the intercept. Inserting these results and the appropriate average particle diameters in equation (63) yields a calculated value of δ, the thickness of the stabilizing layer.

The values of $f(\phi_c)$, ϕ/ϵ and δ obtained for these different ferrofluids are presented in tables 37 and 38. The values for grind G21 at 30°C are obtained by interpolation from figure 55. This figure presents the reduced viscosity versus concentration for G-21 fluids at different temperatures. These results are discussed in further detail in a following section.

The function $f(\phi_c)$ is found to be constant. This is the expected behavior. The critical volume fraction in suspension should be the same for all dispersions that have similar size distribution characteristics. The electron micrographs of the different suspensions all indicate a log normal distribution of particle sizes for a given grind. The value of ϕ_c corresponding to the values of $f(\phi_c)$ found experimentally are in the range where it is insensitive to ϕ_c in the expected range of 0.70 to 0.80 which corresponds closely to the volume of close packed equal sized spheres ($\phi = 0.74$).

The values obtained here for the thickness of the stabilizing layer of well dispersed suspensions range from 30 Å for a Tenlo 70 stabilized dispersion to 35 Å and 55 Å for two oleic acid stabilized dispersions in kerosene.

It has been previously considered that the thickness of the stabilizing layer around a particle is equal to the length of an oriented extended surfactant molecule. These findings indicate a more complex structure for the stabilizing layer since the thickness of a monolayer of surfactant would not exceed 20 to 25 Å.

Oleic acid is a typical surfactant which is well characterized. The structure of this molecule is easily visualized through a Fisher-Hirschfelder-Taylor atomic scale model. In this model, internuclear distances and the

TABLE 37. – EXPERIMENTAL VALUES OF ϕ/ϵ, $f(\phi_c)$, AND δ AT 30° C FOR DIFFERENT KEROSENE BASE FERROFLUIDS

Ferrofluid	ϕ/ϵ	$f(\phi_c)$	δ, angstrom units
G-4, -5, -6	7.36	1.55	55
G-10	4.16	1.60	---
G-21[a]	3.52	---	37
G-44	4.48	1.55	30

[a] Interpolated from figure 55.

TABLE 38. – EXPERIMENTAL VALUES OF ϕ/ϵ, $f(\phi_c)$, AND δ FOR G-21 FLUID AS A FUNCTION OF TEMPERATURE

Temperature, θ, °C	ϕ/ϵ	$f(\phi_c)$	δ, angstrom units
-25	4.22	1.61	43
0	3.90	1.52	41
22	3.60	1.64	38
100	3.02	1.59	32

atomic dimensions are on a scale of 10^8 to 1, with correct bond angles. Thus a centimeter length measured on the model corresponds to one angstrom unit length on the true molecule. In its normal configuration, oleic acid has a length of about 20 Å. It can extend its length to a maximum of about 25 Å and can contract to about one half of its extended length. The cross-sectional area of the molecule is about 20 $Å^2$. Figures 56 and 57 illustrate an oleic acid molecule in its most extended and retracted positions respectively.

The fractional coverage of the particle surface by the surfactant molecule is of interest. (See table 39.) The specific surface area of the particles, A_s is given by the equation

$$A_s = 6/\rho_s \bar{D}_{SA} \tag{68}$$

where

ρ_s = particle density = 5.0 gm/cc

$\bar{D}_{SA}$ = volume/surface average particle diameter

A value of $\bar{D}_{SA}$ for both fluids is obtained from the electron micrograph particle count. The specific oleic acid surface coverage is obtained from the initial oleic acid magnetite ratio in the preparation, the relative amounts magnetic solids and nonmagnetic solids and the cross sectional area of an oleic acid molecule. The fractional coverage is the ratio of the specific oleic acid coverage to the specific surface area of the particles. If the cross sectional area of an oleic acid molecule is taken to be 20 $Å^2$, the fractional coverage is 1.13. If the cross sectional area of this molecule is assumed to be 18 $Å^2$ the fractional coverage is 1.01.

These numbers indicate that the particle surfaces are covered with at least a monolayer of oleic acid since it is expected that the distribution coefficient for oleic acid in magnetite hydrocarbon systems would be high. The distribution coefficient, K, is defined as

$$K = \frac{\text{Millimoles surfactant adsorbed per unit surface area of solid}}{\text{Millimoles surfactant in solution per unit volume of liquid}}$$

These numbers further indicate that there is not sufficient oleic acid present to form a second layer of oleic acid molecules around the particles, assuming equal distribution among all particles in the system.

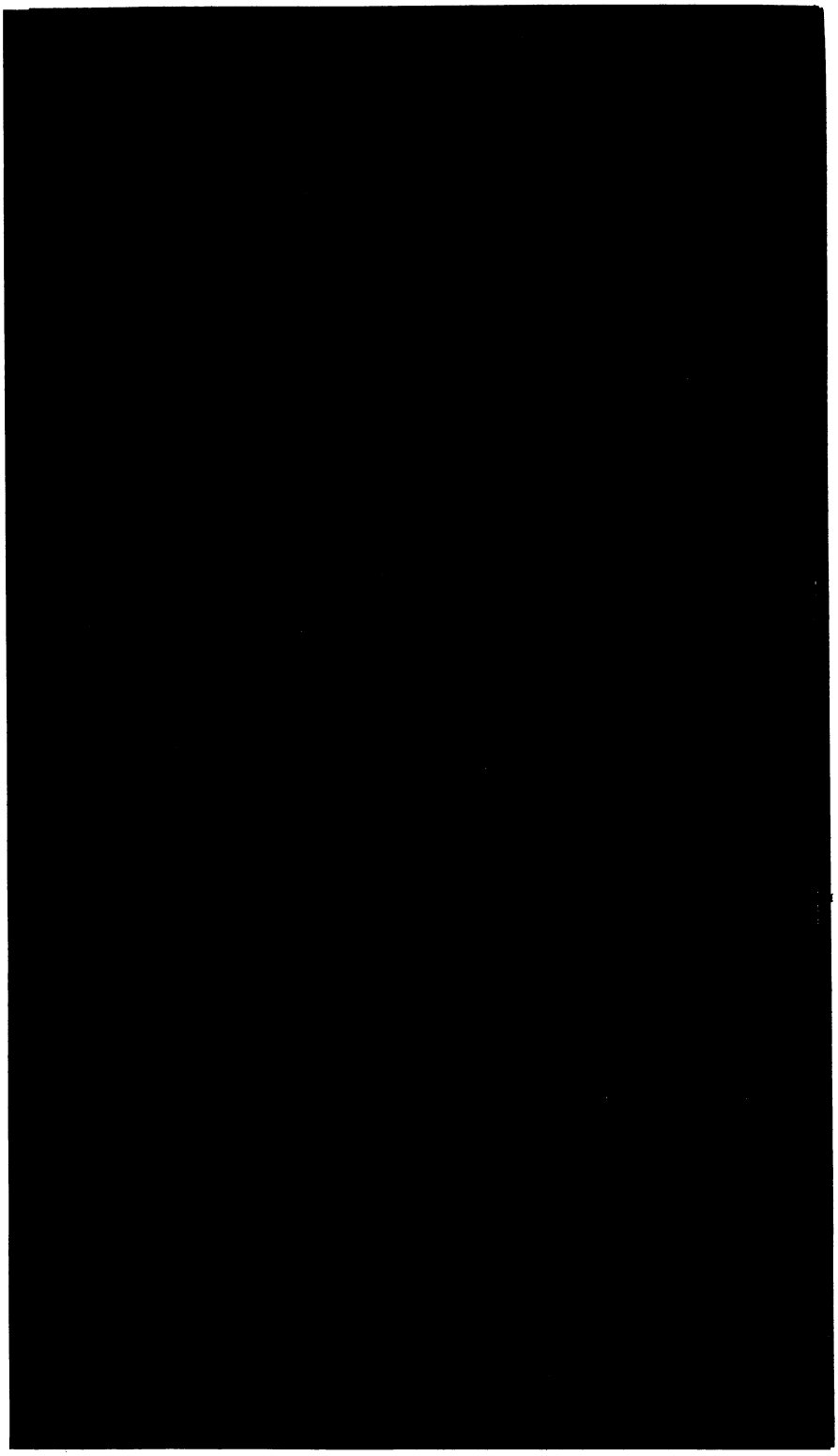

14746-H

Figure 56. – Molecular Model of Oleic Acid (Extended Configuration)

Top

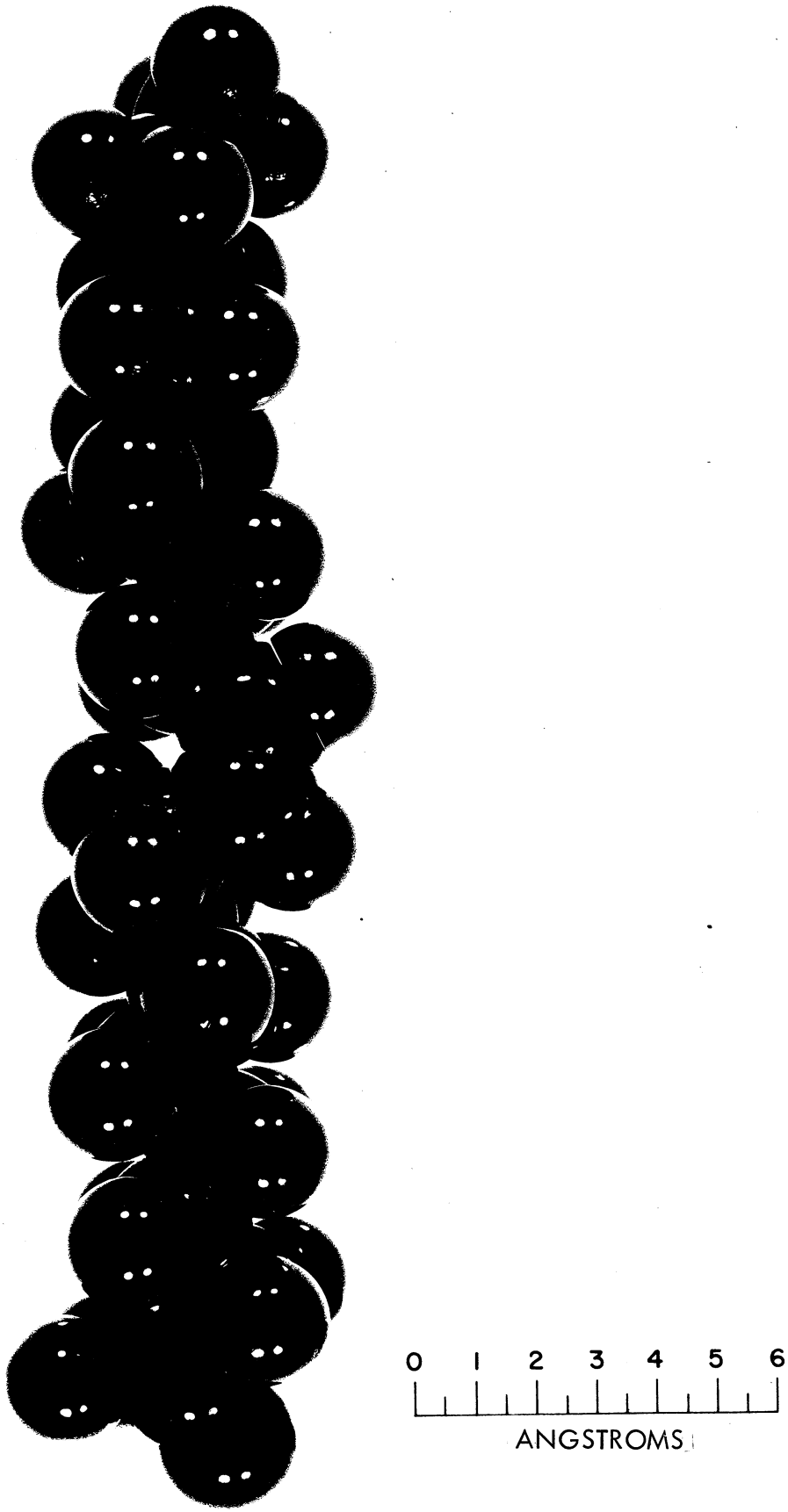

Fig 56 Pg 154 FIG 56 T-86

Top

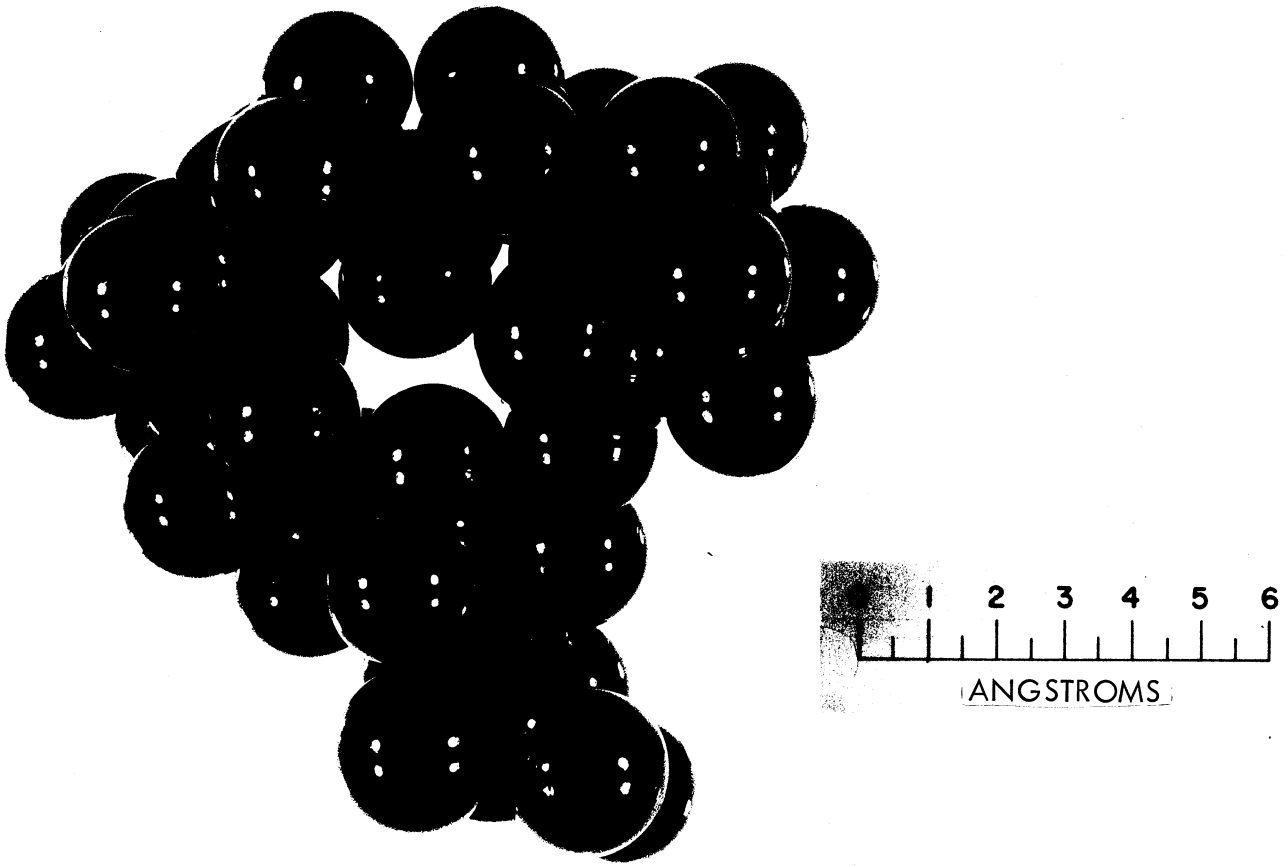

T-92

Fig 57 Pg 146

FIG 57

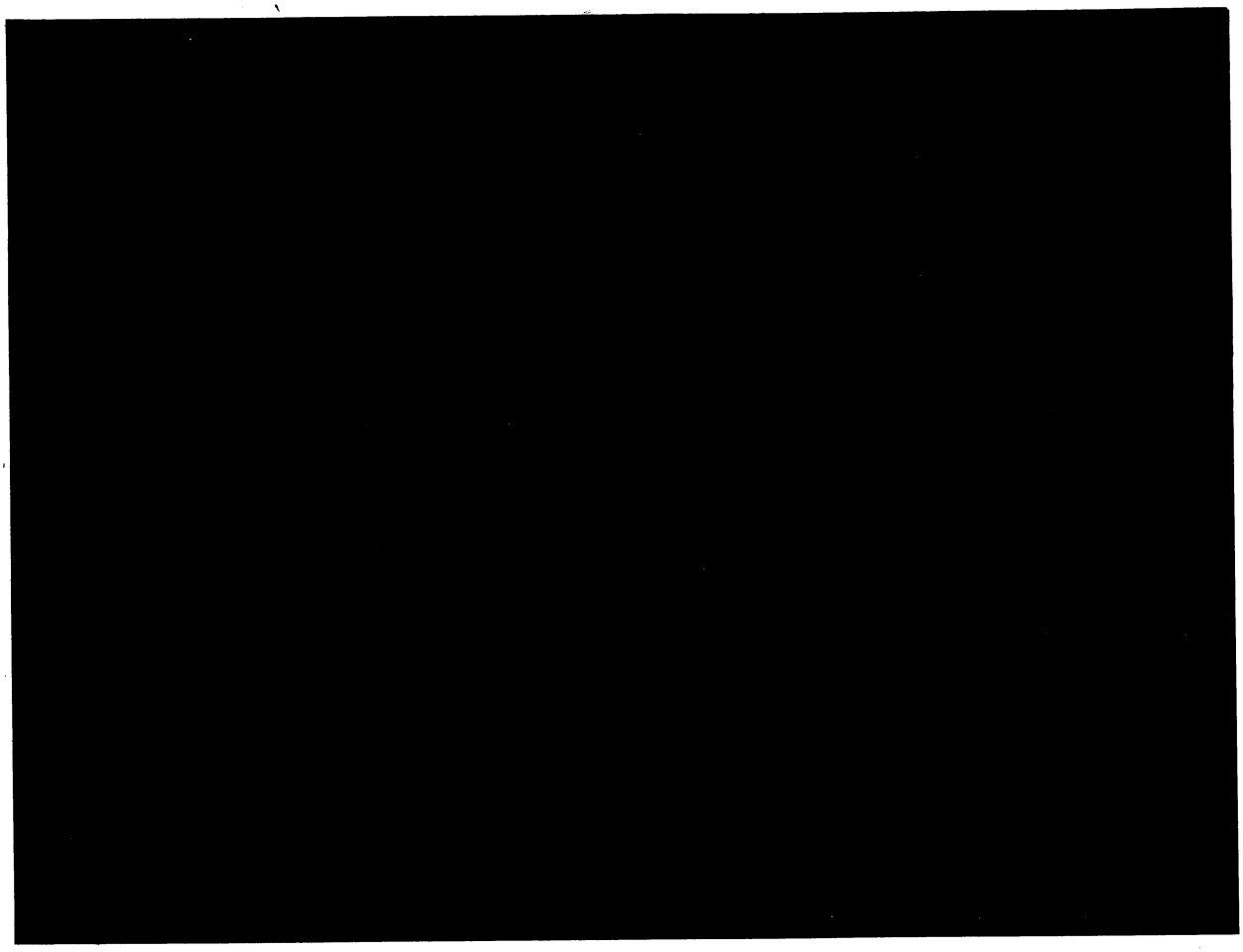

14746-G

Figure 57. – Molecular Model of Oleic Acid (Retracted Configuration)

TABLE 39. – SURFACE COVERAGE OF FERROFLUID PARTICLES BY OLEIC ACID

Grid No.	G-4, -5, -6		G-21	
Average surface/volume particle diameter, $\bar{D}_{SA}$ (from electron micrograph count)	120 Å		148 Å	
Specific surface of particles, $m^2/gm = 6/\rho_s \bar{D}_{SA}$	120 m^2		76 m^2	
$K = \frac{\text{Magnetic solids in suspension}}{\text{Total solids in suspension}}$	.75		.65	
Oleic acid concentration $\frac{\text{millimoles}}{\text{gram total solids}}$	1.14		.71	
Cross-sectional area of one oleic acid molecule, $Å^2$	20	18	20	18
Surface covered by oleic acid present, m^2/gm	137	123	85	77
Fractional surface coverage	1.14	1.02	1.12	1.01

In order to account for the thickness of the stabilizing layer it is necessary to consider the co-adsorption of solvent molecules on the particles. Doyle and Ellison (ref. 18) recently studied the simultaneous adsorption of carbon - 14 labeled stearic acid and tritium labeled octadecane on different metal surfaces. This is a system in many ways analogous to the acid-kerosene-magnetite system. They found very strong evidence for multilayer co-adsorption, as pictured in figure 58.

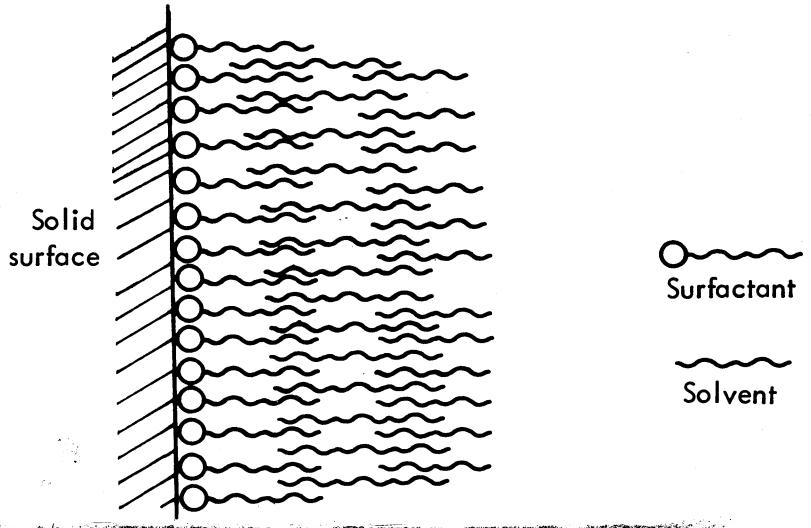

Figure 58. – Idealized Multilayer Absorption of Surfactant and Solvent

A monolayer of surfactant adsorbs on the solid surface. This first layer forms an anchor for a second layer which consists of adsorbed solvent molecules which dovetail between the hydrocarbon tails of adsorbed surfactant. In turn a third layer which also consists of more weakly adsorbed solvent molecules is formed, anchoring itself in the spacings of the second layer. Such a multilayer sheath with possibly more than 3 layers would account for the values of δ obtained from the viscosity measurements. It is difficult to explain why different thicknesses were obtained in the two fluids, especially since G-21 in decane exhibits a stabilizing layer that is about 50 Å thick.

The results presented in figure 53 and table 39 were for a ferrofluid made by diluting concentrated G-21 solids with decane. Assuming the base solvent to be decane, values of ϕ, ϕ/ϵ and δ were calculated using the simplified correlation, (eq. 54) at each temperature. These results are presented in table 40. By interpolation δ for oleic acid/decane is about 50 Å at 30° C.

These experimental results indicate an effect of the solvent on the thickness of the boundary layer which up to now was neglected. If this model

TABLE 40. – THICKNESS OF STABILIZING LAYER OF DECANE BASE FLUID (5-23-66-1)

Temperature, θ, °C	η_s/η_o	ϕ	ϕ/ϵ	δ, angstrom units
-25	4.33	0.518	6.16	58
0	3.68	.476	5.66	54
22	3.23	.440	5.23	51
100	2.46	.362	4.32	44

applies, differences in boundary layer thicknesses might be found with carriers of differing molecular structure with the same surfactant. Evident parameters include molecular weight of the molecule, straight chain versus branched molecules and aliphatic versus aromatic molecules.

The surfactant used also has an effect on the thickness of the stabilizing layer. For example, the results indicate that Tenlo 70 results in a thinner layer than oleic acid. Unfortunately, Tenlo 70 is a complex mixture of a number of hydroxy-amines and thus does not lend itself to analytical treatment.

The presence of a monolayer of oleic acid in both fluids G-21 and G-4, -5, -6 implies that the grinding operation is limited by the surfactant concentration. In order to obtain particles of a certain size there has to be sufficient surfactant present in the solution to coat the particles completely.

The possibility of having a stable ferrofluid in which the particles are coated with less than a monolayer of surfactant exists. However, within the limited scope of the present data, ferrofluids have not been made for which there is evidence of less than monolayer coverage of surfactant. It is known that grinding does not proceed in the absence of surfactant. It is also known that certain runs which initially formed dispersed colloids resulted in gel formation after prolonged grinding; and that these gels broke upon the addition of more surfactant but rarely upon the addition of more carrier fluid (Run G-46 as an example - figure 28).

The presence of a gel is indicative of the formation of a network within the liquid structure. This network is a result of association of small, solvated elements of the system. These elements in the systems presently being considered can only be the surfactant or the solid particles. In those cases where the surfactant is completely miscible with the carrier fluid, as is the case with oleic acid, the gel has to be due to the association of the solid particles present. Such gel formation can best be explained in terms of partial flocculation of the particles.

Physically, this partial flocculation is visualized as follows: when there is insufficient surfactant present in solution, the average thickness of the stabilizing layer has decreased to such a level that two sheathed particles coming into contact will tend to adhere to each other. The particles are still separated by the finite thickness of the stabilizing layer which determines the minimum approach and limits the forces of attraction between the particles. The presence of a solvated layer geometrically prevents close packing of the particles. The result is the formation of a weakly bound network of particles which gives the system "body" - thus a gel.

The findings that surfactants smaller than twelve carbon atoms in length do not result in the formation of a stable colloidal dispersion can be interpreted in another fashion in view of these results. it has been previously considered that the small molecules did not provide enough separation between two particles to prevent particle to particle interaction, the particle separation being equal to twice the length of the adsorbed molecules. Another interpretation is that the smaller molecules do not provide a suitable anchor for the carrier molecules which also form part of the stabilizing sheath.

Effect of Temperature on Viscosity of a Ferrofluid. - The viscosity of different G-21 ferrofluids was measured at different temperatures. These results were presented in table 35 and figure 60. In this figure, the log of the viscosity is plotted against the inverse absolute temperature. Each fluid of the G-21 family yields a straight line whose slope increases with increasing magnetization or increasing concentration solids. There is a greater effect of temperature on viscosity with increasing solids concentration.

In figure 55 the reduced viscosity $\frac{1}{\epsilon}\left(\frac{\eta_s - \eta_o}{\eta_s}\right)$ is plotted against ϵ for each of the different G-21 ferrofluids. At any given temperature the data fall on a straight line with the slopes of the lines increasing with decreasing temperature. Values of ϕ/ϵ and $f(\phi_c)$ were calculated from each of these lines. These results are presented in table 38. As can be seen from this table the critical concentration function $f(\phi_c)$, and therefore ϕ_c as well, is invariant with temperature. The implication of these results is that the idealized ferrofluid model developed by Rosensweig et al.(ref. 1) is valid over a wide temperature range.

The value ϕ/ϵ increases with decreasing temperature. Since the particle size remains constant this means that the stabilizing layer has increased in thickness. The variation of ϕ/ϵ with temperature is correlated by the following equation:

$$\phi/\epsilon = 1.75\, e^{215/T} = 1.75\, e^{425/RT} \qquad (69)$$

The variation of δ (in angstroms) with temperature is correlated by the following equation:

$$\delta = 18.0\, e^{235/T} = 18.0\, e^{465/RT} \qquad (70)$$

The increase in δ with decreasing temperature can best be explained in terms of increasing adsorption of the carrier molecules with decreasing temperature, δ increasing with the amount of solvent adsorbed for particle. The exponential relationship and the low value of the exponent of e, which can be looked upon as an activation energy, are indicative of a physical adsorption process.

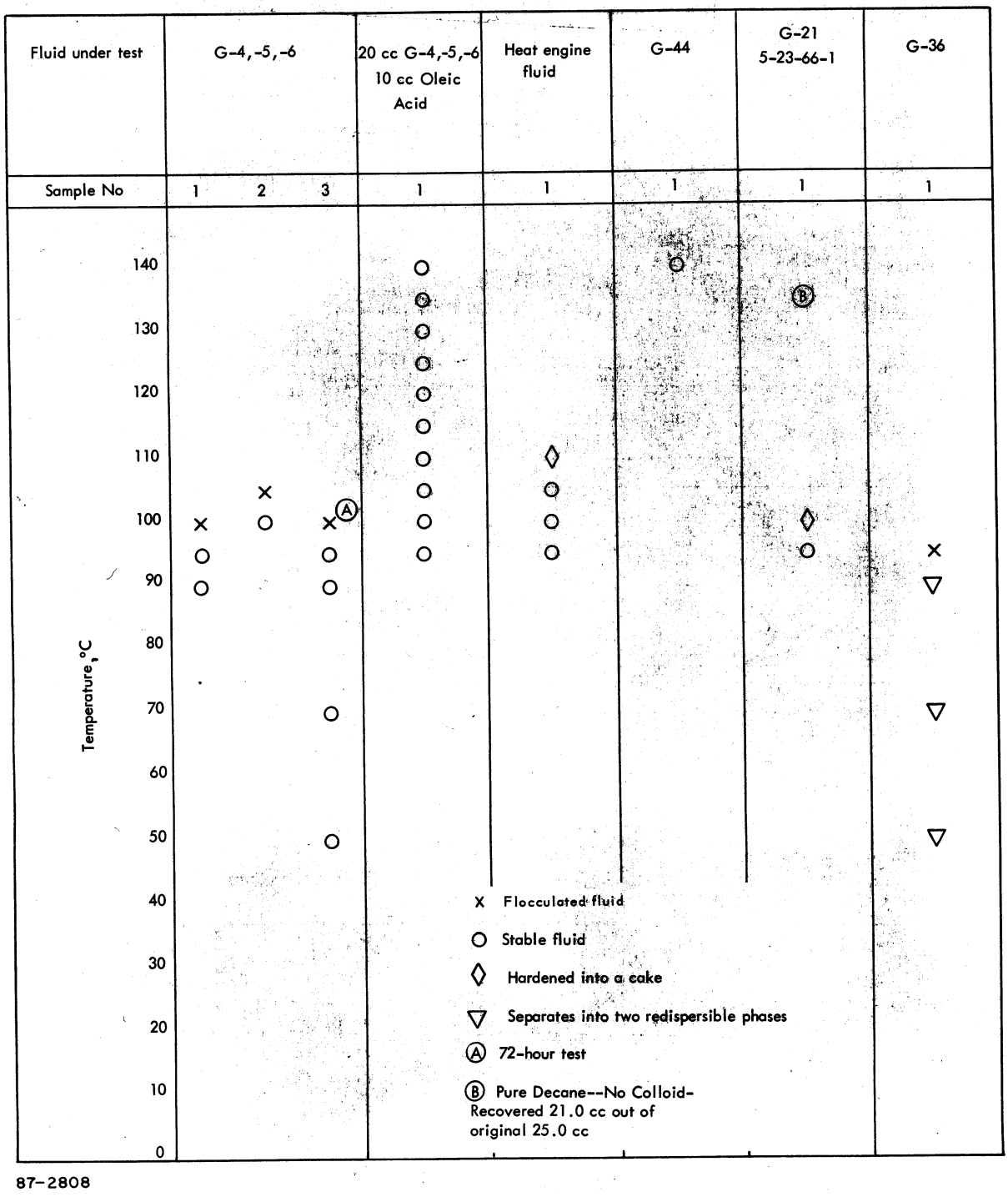

Figure 59. – Thermal Stability of Ferrofluids (24-hour Test)

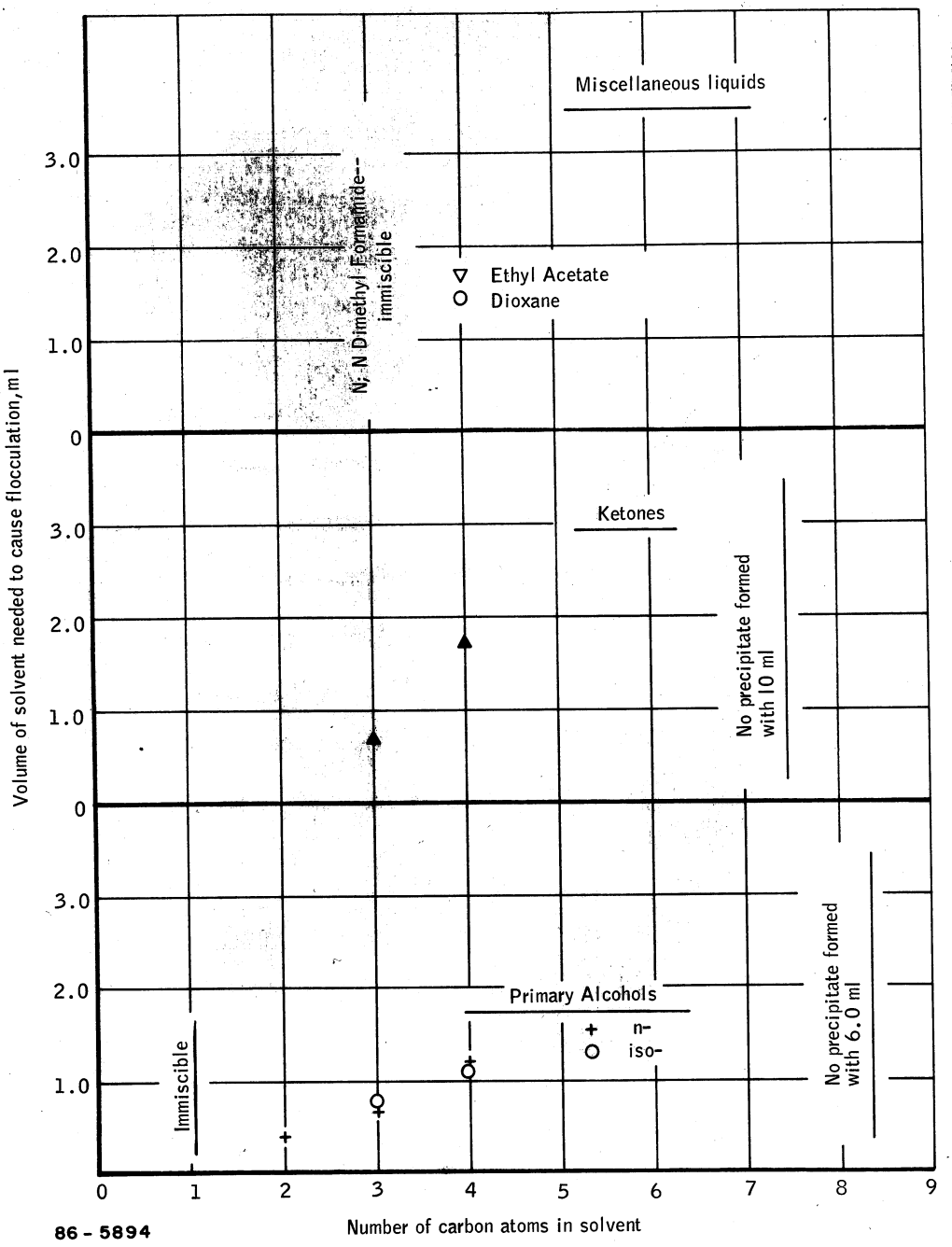

Figure 60. – Flocculating Amounts of Alcohols, Ketones, and Miscellaneous Liquids as a Function of the Number of Carbon Atoms

Effect of Carrier Fluid. - A simple way to lower the viscosity of a ferrofluid according to the present development is to lower the viscosity of the carrier fluid. The viscosity of a ferrofluid is proportional to the viscosity of the carrier fluid. The viscosity at 30° C of a ferrofluid made with G-21 solids that had been concentrated to near dryness and then rediluted with n-decane to M_s = 310 gauss is compared to the viscosity at the same temperature of a G-21 fluid of equal magnetic strength in table 41. The ratio of the viscosities of the two ferrofluids is essentially equal to the ratio of the viscosities of the base solvents.

The effect of temperature on the thickness of the stabilizing layer in the decane fluid is essentially the same as in the kerosene fluid. In the decane fluid it was found that

$$\delta = 25\, e^{415/RT} \tag{71}$$

Electrical Properties of Ferrofluids

Little is presently known concerning the electrical properties of the ferrofluid. This discussion is concerned with measurements of a ferrofluid having a carrier which is an organic liquid.

The specimen studied here was G-44 material with a saturation ferric induction of 200 gauss. The G-44 material consists of magnetite in kerosene with the Tenlo 70 dispersing agent. The measurements were performed by A. Harvey at Chalk River Nuclear Laboratories, Atomic Energy of Canada Limited in Ontario.

To perform a dielectric strength measurement a standard VDE cell was constructed as described in ASTM D1816-60T, together with a small cell, modified from an ASTM D-877 cell. With the first cell it was determined that the breakdown strength of the kerosene was 28 kV for a 0.081-inch gap, at 70° F. The intent then was to measure the breakdown strength of ferrofluid in the small cell but the ferrofluid was found to be too conductive. Its volume resistivity, at 60 Hz, was 1.16×10^8 ohm-cm.

The capacitance of the cell changed from 4 pf with air to 6 pf with the ferrofluid in it, so that the dielectric constant could be taken as approximately 1.5. A value which is corrected for the fact that ferrofluid occupied only the cylindrical volume between two, round flat-faced electrodes is estimated to be over 2.

TABLE 41. – COMPARISON OF VISCOSITIES OF KEROSENE G–21 FLUID (M_s = 310 GAUSS) AND DECANE BASE G–21 FLUID (M_s = 310 GAUSS) AT 30° C

	G-21 regular	5-23-66-1 fluid
T	30° C	30° C
M_s	310 gauss	310 gauss
η_o	1.50 cp	.82 cp
η_s	4.5 cp	2.6 cp
η_{o1}/η_{o2}	1.83	
η_{s1}/η_{s2}	1.73	

Colloidal Stability of Ferrofluids

It has been observed that changes in the environments of the ferrofluids can result in flocculation of the particles. In some cases it has been possible to peptize the particles, in other cases, an irreversible change had occurred.

The ferrofluids under consideration in the following discussion are all magnetite or ferrite dispersions in a hydrocarbon carrier fluid stabilized by the presence of a surfactant such as oleic acid.

The stability of these dispersions, as reported in detail by Rosensweig et al. (ref. 1) is considered to be due to entropic repulsion of interacting molecules adsorbed on the particle surfaces. The adsorbed surface active molecules result in the formation of a sheath around each particle that prevents these particles from coming close enough to permit secondary valence and magnetic forces of attraction to become large enough to result in coalescence or flocculation of the particles.

Effect of Time. - Ferrofluids prepared by grinding in the presence of a surfactant and then centrifuged at 17 000 g in general proved to have long term stability at room temperature. There was no noticeable sedimentation or segregation of the magnetic particles, with one exception. A sample of G-21 ferrofluid that had been centrifuged but not otherwise modified, was observed to have flocculated, after approximately 8 months shelf storage in a pyrex reagent bottle. The magnetization of the original fluid was M_s = 190 gauss. The magnetization of the stored fluid was M_s = 18 gauss. At the same time, however, G-21 fluid that had been concentrated by partial removal of the base solvent proved to be quite stable during the same period of time.

These results are tentatively explained in terms of a decrease in suspension stability with increasing particle size and an increase of surfactant surface concentration (at a fixed solids/surfactant ratio) with increasing solids concentration.

Grind G-21 differed from most of the other lfuids in that only 0.35 cc of oleic acid per gram of magnetite was used in its preparation as compared to the usual loading of 0.50 cc of surfactant per gram of solid powder. As a result, the particles obtained from this grind were larger, as evidenced by photomicrographs ($\bar{D}_{VA}$ = 165 Å) than the particles obtained in grinds which contained a higher concentration of surfactant. The agglomerative tendency for these fluids is therefore higher than for the fluids which contain a higher initial concentration of surfactant.

The dilution of the fluid will effect the surface concentration of surfactant. For a given liquid-powder system, there is an equilibrium distribution coefficient K that relates the surface concentration of surfactant adsorbed on the solid surface to surfactant in solution. Since the surface area and total amount of surfactant are invariant in a family of ferrofluids of varying solids concentration (magnetization), there can be transfer of surfactant from the solid surface to the liquid phase with increasing dilution of the ferrofluid. As a result the coverage of the stabilizing layer decreases. The combination of larger particle size and decreased coverage of the stabilizing layer is believed to be the cause of the observed flocculation of the dilute G-21 fluids.

Effect of Temperature. - The temperature stability of the ferrofluids was studied by heating liquid samples in glass flasks equipped with vertical water-cooled condensers. The flasks were heated in a controlled temperature electric furnace. The liquid samples were observed periodically to note any apparent change in physical appearance.

The experimental results are presented in figure 59. The compositions of the fluids are presented in table 3. Heat engine fluid is a fluid of 90 to 100° C Curie point ferrite stabilized with Aerosol OT. Fluid No. 5-23-66-1 is described in table 36. In figure 59, each point represents a sample heated to the temperature of test for 24 hours. If the sample was stable, the temperature was then raised to the next level for 24 hours. This procedure continued until flocculation was observed.

The most stable fluid was G-44 a suspension stabilized with Tenlo 70. This was stable up to 140° C. The oleic and stabilized dispersions were stable up to about 95 to 100° C. Time was a factor as evidenced by sample No. 3 (G-4, -5, -6) which was stable at 100° C for 24 hours, but flocculated after 72 hours. Adding an excess of surfactant (oleic acid) resulted in higher temperature stability. The fluid to which oleic acid was added was stable to 140° C.

The stability of a ferrofluid, in general, depends on

i. the presence of a monolayer,

ii. the nature of entropic repulsion, and

iii. the nature of van der Waals attraction.

If this picture is accepted then the further criterion is that the entropic repulsion energy curve when algebraically summed with the attraction energy

curve must produce an energy hump of at least several kT units of thermal energy to prevent thermal motions from bringing colloidal particles into hard contact. Now the London model for van der Waals attraction shows no dependence on temperature while the model for entropic repulsion gives an energy proportional to the absolute temperature T. Then it can be deduced that the energy hump is displaced to smaller separation distances while, at the same time its magnitude increases. Since thermal energy of the individual particles also increases in direct proportion to absolute temperature the two effects tend to cancel.

Flocculation can be considered to occur when the surface concentration of surfactant falls below a minimum value needed to form a stabilizing sheath. The decrease in sol stability with increasing temperature is believed to be due to desorption of the surfactant with increasing temperature due to increased thermal motion or a reversal of the reaction holding the stabilizing agent to the particle surface. The distribution coefficient decreases with increasing temperature. Increasing the concentration of the surfactant in the system tends to a result in higher temperature stability because a higher temperature is needed to decrease the surfactant concentration to the initial value.

It was observed that it is possible to heat a fluid to a given temperature for a short period of time without flocculation occurring yet prolonged heating at the same temperature will cause flocculation. This is due to the fact that adsorption and desorption processes occur at a finite rate. In a short period of time, insufficient amounts of surfactant desorb to result in flocculation which would occur however, were the system allowed to reach equilibrium conditions.

Effect of Additives and Flocculation. - Aliphatic and aromatic hydrocarbons can be added in any desired excess to kerosene base ferrofluids without resulting in flocculation. Thus benzene, toluene, heptane, decane, tetradecane could be used as diluents or substitutes for kerosene. Similarly, carbon tetrachloride and trichlorethylene did not result in flocculation when added to the ferrofluid. It was also observed that L-43, an aryl-alkyl silicone oil manufactured by Union Carbide Corp. could be incorporated without flocculation.

The addition of a number of hydrocarbon soluble liquids results in the flocculation of the ferrofluids. The solids come out of suspension with the liquid losing its opaqueness and, of course, its magnetic properties.

It has been observed that an excess of such compounds as acetone, dioxane, the lower aliphatic alcohols, carboxylic acids such as propionic

acid, butyric acid, octanoic acid as well as oleic acid, butylamine, poly (dimethyl silicone oils) (Dow-Corning 200 and Union Carbide Corp. L-45 fluids of greater than 10 cs viscosity) poly (phenyl methyl silicone oils) such as Dow-Corning 510 and Dow-Corning 710 fluids, poly (diamyl silicone oil) (Union Carbide Corp. L-42 fluid), resulted in flocculation.

The addition of high polymers such polyisobutylene (Enjay Vistanex LM-MS; Staudinger M. W. = 8700 to 10 000) to a kerosene base ferrofluid and of polystyrene to a toluene base ferrofluid resulted in flocculation.

The stability of an oleic acid stabilized suspension of magnetite in kerosene (G-4, -5, -6 fluid) in the presence of other liquids was studied quantitatively by adding the other solvent drop by drop from a 10 ml buret to 1.0 ml of G-4, -5, -6 fluid in a test tube until a precipitate separated from the solution in the field of a permanent magnet brought to the side of the test tube. The solvents studied were 1-4-dioxane, acetone methylethyl ketone, 4-heptanone, ethyl acetate, N-N dimethyl formamide, methanol, ethanol, isopropanol, propanol-1, isobutanol, butanol-1, allyl alcohol and octanol-1.

The results obtained are presented in figure 60. Each point is an average of at least two determinations. The amount of fluid needed to cause precipitation for any homologous group increases with the number of carbon atoms, i.e., with decreasing polarity of the molecules until the higher homologues such as octanol-1 and 4-heptanone appear to be completely compatible with the ferrofluids. However, very polar solvents such as methanol and dimethyl formamide are immiscible with the ferrofluid and also do not result in flocculation.

Flocculation was reversible in these studies. For example, 1.0 ml of fresh ferrofluid was added to a mixture of isobutanol ferrofluid that had some precipitate in it just past the end point. The precipitate disappeared. It reappeared upon the further addition of isobutanol, when the initial isobutanol concentration was again reached.

The stabilizing layer in the original carrier (kerosene) is a compatible well solvated layer of absorbed material. Addition of a liquid that is similar in all properties to the original carrier does not alter the structure of the layer to a significant degree. Molecules of the additive can be substituted for molecules of the original carrier without effecting the structure of the stabilizing sheath.

Flocculation occurs if the solvated layer is disrupted in some manner by the addition of a different component to the system. The main possibilities for the physical mechanisms underlying flocculation include:

i. Desorption of the coating of surfactant around the particle, thereby destroying the stabilizing sheath.

ii. Displacement of the adsorbed surfactant by small polar molecules that are too short to provide a sufficiently thick adsorbed layer.

iii. Retraction or coiling of the surfactant molecules when these are not compatible with the principal liquid phase, leading to poor solvation and a very thin stabilizing layer of reduced effectiveness.

iv. Bridging of particles by the simultaneous adsorption of polymeric molecules on more than one particle, leading to the formation of a continuous network.

The sensitivity of the ferrofluid to various additives can be explained in terms of the above.

An attempt has been made to classify fluids in terms of the liquid solubility parameter and hydrogen bonding classification in order to provide guide lines that can characterize those liquids that can be added to a given ferrofluid without resulting in flocculation. From a theoretical point of view, the solubility parameter of a material, Δ is the square root of the cohesive energy density which is the energy of vaporization per unit volume

$$\Delta = \sqrt{\frac{\Delta E}{V_M}} \tag{72}$$

where

ΔE = energy of vaporization per mole

V_M = molar volume of the liquid

The solubility parameter can be calculated from physical properties of the solvent. From thermodynamics,

$$\Delta E = \Delta H - RT \tag{73}$$

where

ΔH = latent heat of vaporization per mole

R = gas constant

T = absolute temperature.

The molal volume is simply the ratio of the molecular weight of the fluid, MW, to the density of the fluid at the temperature under consideration, ρ.

Therefore

$$\Delta = \sqrt{\frac{\rho(\Delta H - RT)}{MW}} \tag{74}$$

Small (ref. 19) published a list of molecular attraction constants which permit the calculation of solubility parameter from chemical structure by the use of the following equation

$$\Delta = \frac{\rho \Sigma G}{MW} \tag{75}$$

The individual molar attraction constants, G, are additive over an entire structural formula and ΣG represents the sum of all the atoms and groupings in a unit molecule. The calculation procedure is not too reliable for strongly hydrogen-bonded products (alcohols, amines, and carboxylic acids) except in those cases where the hydrogen-bonded group comprises only a minor part of the molecules. This method of obtaining a Δ value is quite accurate for the molecules of simple solvents. However, its real value lies in its applicability to polymers for which heats of vaporization and boiling points are not readily measureable. In computing a solubility parameter by this procedure, the repeating unit of the polymer chain is made the basis for the calculation. Values of G are presented in table 42.

The other parameter used to characterize likeness is hydrogen bonding. This parameter is still qualitative at the moment, the hydrogen-bonding strength being considered as low, medium or high. In general, the more polar the medium, the greater the hydrogen bonding.

The distribution of some of the more common solvents by solubility parameter and hydrogen-bonding strength is presented in table 43. The closer the match of solubility parameter and hydrogen-bonding strength of two liquids, the more alike they are. Note that in going from lower left to the upper right of table 43, one progresses from nonpolar to polar liquids.

TABLE 42. – MOLAR ATTRACTION CONSTANTS AT 25° C

Group	G	Group	G
Single-bonded carbon		H (variable)	80-100
$-CH_3$	214	O (ethers)	70
$-CH_2-$	133	Cl (mean)	260
$-CH-$	28	Cl (single)	270
$-\overset{|}{\underset{|}{C}}-$	-93	Cl (twinned as in $-CCl_2-$)	260
Double-bonded carbon		Cl (tripled as in $-CCl_3$)	250
$=CH_2$	190	Br (single)	340
$=CH-$	111	I (single)	425
$=C-$	19	S (sulfides)	225
Triple-bonded carbon		CO (ketones)	275
$CH \equiv C-$	285	COO (esters)	310
$-C \equiv C-$	222	CN	410
Conjugation	20-30	CF_2 (n-fluorocarbon)	150
Cyclic structures		CF_3 (n-fluorocarbon)	274
Phenyl	735	SH (thiols)	315
Phenylene (o, m, p)	658	ONO_2 (nitrates)	ca. 440
Naphthyl	1146	NO_2 (aliphatic nitro-compounds)	ca. 440
Ring (5-membered)	110	PO_4 (organic phosphates)	ca. 500
Ring (6-membered)	100	OH (hydroxyl)	ca. 320[a]

TABLE 42

[a]Not originally presented in Small's listing (ref. 22) of molar attraction constants; an empirically derived value.

TABLE 43. — DISTRIBUTION OF SELECTED COMMON SOLVENTS BY SOLUBILITY PARAMETER AND BY HYDROGEN BONDING CLASSIFICATION

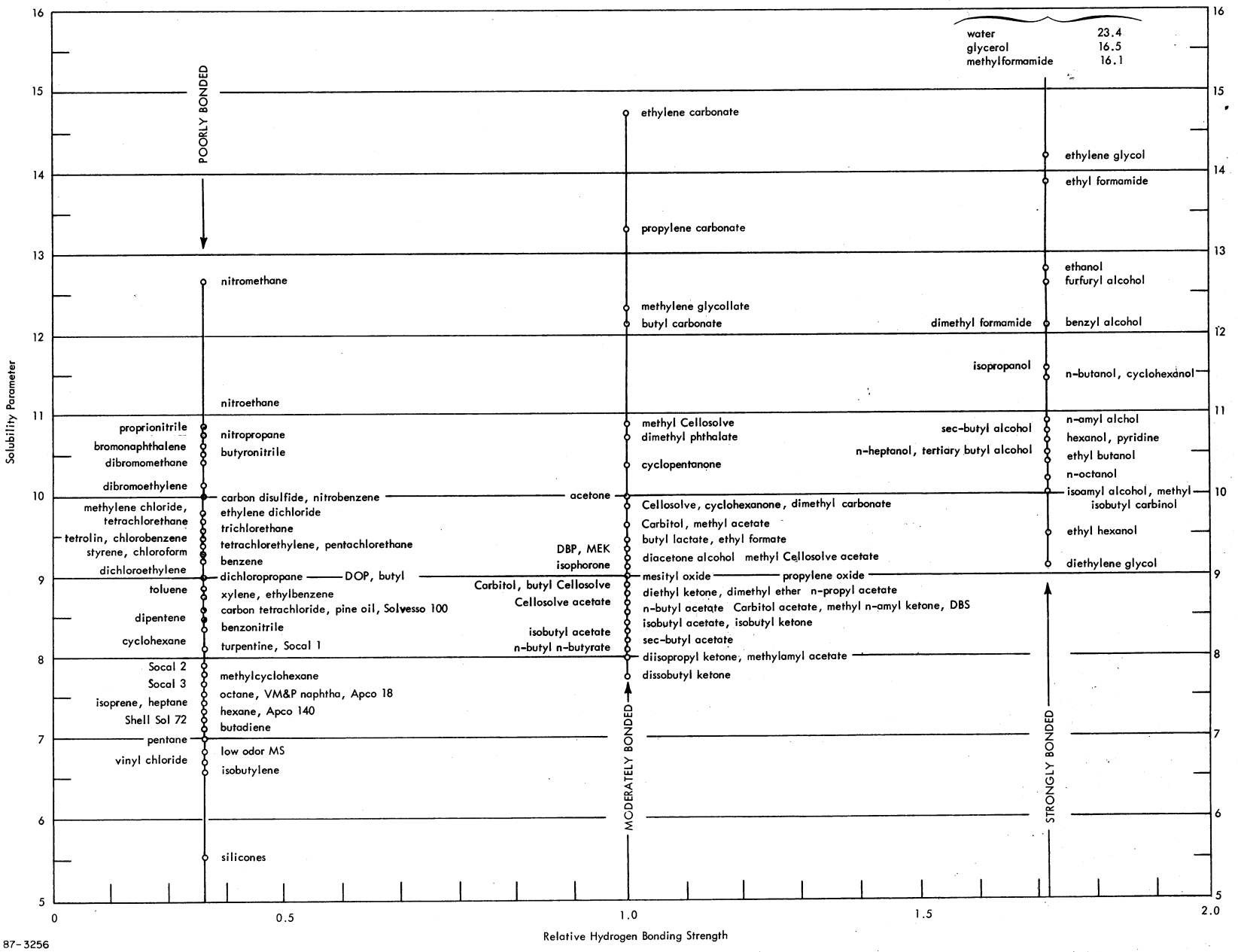

87-3256

Kerosene has a solubility parameter of about 8. It is poorly bonded in regards to hydrogen-bonding interaction. All the other compounds that were compatible with kerosene base ferrofluids have amalgams values of these parameters. Hexane, carbon tetrachloride, toluene, ethylene trichloride all have similar hydrogen bonding characteristics and solubility parameters that range from about 7 to less than 9.

The behavior of the various silicone oils is understandable in terms of the compatibility and other mechanisms.

The stability parameter of the dimethyl silicone oils decreases with increasing chain length. Little and Singleterry (ref. 20) calculated values of the solubility parameter for different dimethyl siloxanes. These values are presented in table 44.

TABLE 44.– SOLUBILITY PARAMETER OF DIMETHYL SILOXANES

Solvent	Solubility parameter, Δ
Siloxane octamer	4.72
Siloxane hexamer	5.0
Siloxane pentamer	5.2
Siloxane dimer	6.5

The lower homologues of the dimethyl siloxane families are more similar to the hydrocarbons than the higher molecular weight compounds thus tend to be more compatible. The low solubility parameter of the dimethyl siloxanes is due to the presence of the methyl groups. These also have a low interaction energy of interaction with CH_2 groups that predominate in hydrocarbons as pointed out by Crowl (ref. 21). The dimethyl silicone molecules tend to ball up individually rather than interact with the hydrocarbon - surfactant masses. Evidence for this is the low variation of viscosity of these liquids with temperature.

In addition to the above, in the case of the higher molecular weight homologues flocculation can also occur as a result of interparticle bridging by simultaneous absorption of the polymer molecule on two or more particles. The repeating unit of a siloxane chain, $\left[\begin{array}{c} CH_3 \\ | \\ -Si- \\ | \\ CH_3 \end{array} -O-\right]$, has a molecular weight

of 74 and a length of about 2 Å. Thus a polymer with a molecular weight of 100 000 has a molecular length of about 2700 Å. Since the average particle in suspension is about 100 Å in diameter, the possibilities after entanglement are evident.

The analogous behavior of the phenyl-methyl silicones (DC 510 and DC 710 fluids) can be explained in the same manner.

There was one silicone oil that was completely compatible with the ferrofluids. This was Union Carbide Corp silicone oil L-43. Thus is an an aryl alkyl silicone oil which contains long pendant hydrocarbon side chains. As a result this compound is much more similar to the normal hydrocarbon than the silicones with short side chains.

The flocculating activity of the low molecular polar additives can be considered to occur as a result of both retraction of the surfactant molecules adsorbed on the surface and displacement of these molecules by the polar solvent molecules. Such a mechanism has been proposed by Garrett and Lawrence (ref. 22) to explain the flocculation of polar oxide suspensions in neoprene-solvent adhesives.

In terms of liquid similarity, the smaller molecules in a homologuous group tend to have a higher value of the solubility parameter than the large molecules as evidenced by table 43. A smaller concentration is required of the additive to cause a given change in the properties of the solvent which leads to flocculation.

At the same time, it is possible to consider flocculation to be due to adsorption of these polar molecules which causes a collapse in the sheath. Low molecular weight compounds are more effective flocculents than the higher homologues because they are shorter in length and also because a given volume of fluid contains a greater number of small molecules than large molecules molecules.

The flocculating effect of polyisobutylene and polystyrene can be explained in terms of interparticle bridging as in the case of the higher molecular weight silicone oils.

Extraction of Ferrofluids. - Flocculated solids were washed with the precipitating solvent repeatedly in order to attempt the removal of the stabilizing layer.

An efficient method of systematically washing a solid material with a small amount of liquid is to use a Soxhlet Extractor (fig. 61). The material to be extracted is placed in a porous thimble usually made of paper. This

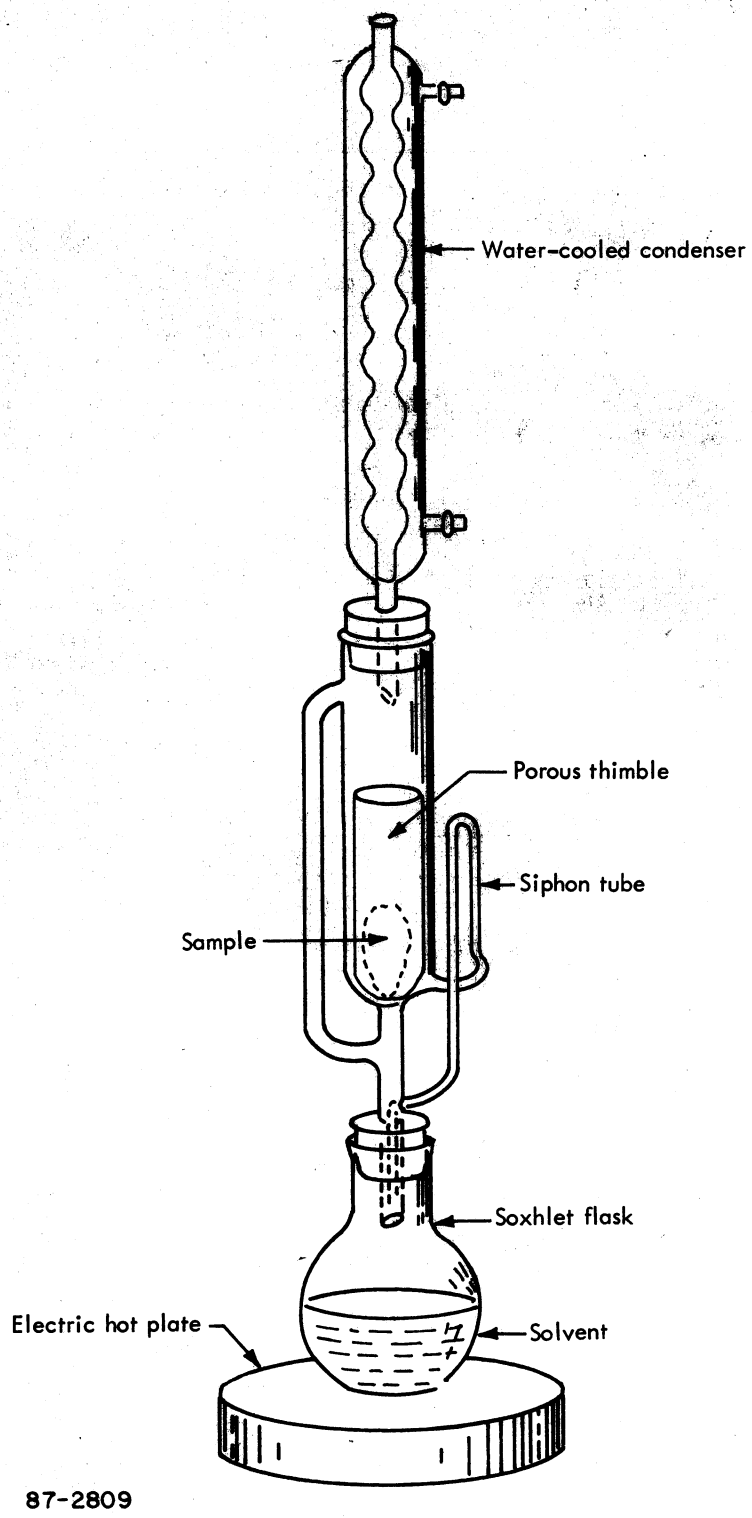

Figure 61. – Soxhlet Extraction Apparatus

thimble in turn is placed inside an extraction tube above which there is a water-cooled condenser and below which there is attached a round flask which can be heated. The extraction tube is provided with a vapor bypass and syphon tube. The solvent is placed in the flask and is gently boiled. The vapors flow through the bypass to the condenser where they are condensed. The resulting liquid drops into the thimble where it comes into contact with the sample to be extracted. The liquid level builds up in the extractor to a height slightly higher than the top of the syphon tube at which time all the liquid in the extractor is returned into the reboiler flask, carrying with it a fraction of the dissolved substance. The process repeats itself automatically and is allowed to continue until the removal of the adsorbed substance from the solid is believed complete.

The solid placed in the extractor can be analyzed before and after extraction, or the solvent can be analyzed after extraction to determine the efficiency of the operation.

The materials extracted were:

i. G-15 solids: This was the residue of an oleic acid stabilized colloidal dispersion of magnetite in heptane which remained after evaporation of the heptane. This material contains all the oleic acid initially added to the grinding batch, namely 0.45 gm of oleic acid per gram of magnetite.

ii. This was the residue obtained by flocculating 100 ml of G-44 ferrofluid, a Tenlo 70 stabilized dispersion of magnetite in kerosene, with 800 ml of acetone. From magnetization and density measurements (see table 11), the original fluid contained 19.5 grams of solids. After drying, the flocculated solids weighed 22.1 grams. Assuming no loss of solids during the operation and complete precipitation, the solids also contained 2.6 grams of other material that was presumed to be the surfactant, Tenlo 70, which is a nonvolatile compound. In the preparation of the original grind, 0.50 ml of surfactant was used per gram of magnetite. These results indicate that in the case of Tenlo 70 stabilized suspensions, a considerable fraction of the surfactant is removed during the initial flocculation step.

Small amounts of these solids were extracted with different polar solvents for varying periods of time. These experiments are listed in table 45.

TABLE 45. – EXTRACTION OF FERROFLUID SOLIDS

Extraction run	1	2	3	4	5
Extraction liquid	Hexamethyl disilane[a]	Acetone	Isopropanol	Ethanol	N-Propanol
Liquid volume, cc	75	175	80	100	100
Time of extraction, hrs	96	64	340	48	140
Solids / Grind No.	G-15	G-15	G-15	G-44	G-44
Surfactant	Oleic acid	Oleic acid	Oleic acid	Tenlo 70	Tenlo 70
Initial surfactant/ magnetite ratio	.50 cc/gm	.50 cc/gm	.50 cc/gm	.50 cc/gm	.50 cc/gm
Initial weight solids, gm	9.97	6.34	1.61	3.66	5.82
Final weight solids, gm	---	5.60	1.28	2.89	4.20
Weight loss, gm	---	.74	.33	.77	1.62
Calculated initial weight surfactant (based on initial ratio), gm	---	1.97	.50	1.14	1.80
Surfactant removed, %	---				
1. $\frac{\text{Weight loss}}{\text{Initial weight surfactant}}$		37.6	66.0	68.5	90.0
2. $\frac{\text{Weight loss}}{\text{Initial weight surfactant}} \left[1 - \frac{MW_{so}}{MW_s}\right]^b$	---	47	89	---	---

[a] Dow-Corning 200 Fluid, 0.65 cs

[b] MW_{so} = molecular weight solvent; MW_s = molecular weight surfactant.

In all cases, the extracted material had a different appearance than the initial material. The initial solids, in particular the G-15 solids, were a shiny deep brown color and had a waxy feel to the touch. The extracted solids had a dull gray sheen. The weight of the extracted solids was less in all cases than the weight of the initial material, indicating removal of some material.

After extraction, the originally water white liquid in the reboiler was yellow colored, except in the case of extraction run No. 1 with hexamethyl disilane as the extracting fluid. In this case, the liquid was ferrofluid brown in color. The thimble of the extractor was also stained deep brown indicating that partial redispersion had occured, as was observed during the initial parts of the run. Since material was carried over into the reboiler, it was not possible to calculate an extraction efficiency for this run.

The weight loss that is observed is considered due to the removal of surfactant from the surface of the particles. The oleic acid appears to be more firmly bound to the surface of the particles than the Tenlo 70. It was not possible to remove all the oleic acid even in two weeks of extraction while it appears that all the Tenlo 70 is removed in a week. Taking into account the replacement of oleic acid by the solvent molecules on the surface of the particles, maximum removal of oleic acid was found to be less than 89 percent (Extraction run No. 3). Not knowing the molecular weight of Tenlo 70, this second calculation could not be made, however, from the results of run No. 5, it appears quite likely that all the surfactant was removed in this case.

Repeptization. - It was observed that it was possible to redisperse the solids obtained by flocculating oleic acid stabilized ferrofluids with acetone or similar solvents, by decanting the supernatant acetone/kerosene mixture and then adding fresh kerosene. The particles went back into suspension with a minimum amount of stirring. Flocculation/redispersion proved to be a simple method of concentrating an oleic acid stabilized ferrofluid or of changing the carrier, since the solvent in which redispersion took place could be different in amount and nature than the original carrier. One further interesting observation was that when water was added to a test tube containing flocculated magnetite solids in the presence of the acetone-kerosene supernatant, repeptization occurred spontaneously.

The ease of redispersion decreased with increased washing of the solids with the flocculating solvent.

Attempts were made to redisperse freshly extracted G-15 solids from the acetone extraction. These solids did not readily redisperse when

kerosene was added. They did however redisperse upon prolonged standing (at least 48 hours). Addition of carboxylic acids, such as proprionic acid, butyric acid and octanoic acid as well as oleic acid resulted in a number of interesting effects. Addition of a few drops of oleic acid to a freshly prepared mixture of kerosene and extracted magnetite resulted in rapid dispersion of the material. The resulting ferrofluid was a stable colloidal suspension. Adding other carboxylic acids of shorter chain length also resulted in rapid redispersion of the particles. The resulting suspensions however were not stable and flocculated within a few days. This occurred with proprionic acid, butyric acid and octanoic acid.

It was believed that the concentration of the added carboxylic acid might be varied in order to minimize flocculation. The concentration of octanoic acid was therefore varied over a wide range. One gram of extracted magnetite was added to 10 cc of kerosene in a graduated centrifuge tube. The initial bulk volume of the powder was about 1.0 cc. Octanoic acid was added to different tubes in varying amounts: 0, 0.046. 0.096, 0.20 0.42 and 0.80 cc. The rate of initial dispersion increased with increasing octanoic concentration. However, all these octanoic suspensions were not stable over a prolonged period of time and flocculated. The blank ultimately redispersed under similar conditions without flocculation.

If the same extracted solids are oven dried, ground in a mortar and pestle and stored at room temperature for a period of time, it becomes more difficult to redisperse these solids in kerosene. Results of attempts at redispersing the products of two extraction runs that were treated in this manner, including the acetone extracted product used in the experiments just described, are presented in table 46 and table 47. In these tests, 0.1 gram of solids were added to a test tube containing 1.0 cc of liquid and a small amount of stabilizing agent. In these tests, there was no redispersion whatsoever in the absence of additives, even after 6 weeks contact time. Even in the presence of different additives, including oleic acid, the original stabilizing agent, the solids did not redisperse to any substantial extent. Only in the presence of octyl amine and dodecyl amine did substantial redispersion take place.

Solids from G-44 grind that was stabilized with Tenlo 70 were more difficult to redisperse than oleic acid stabilized solids after similar treatment. As shown in table 48 simply flocculated G-44 material did not redisperse spontaneously in kerosene in the absence of additives. These solids however redispersed in the presence of a number of additives, complete redispersion occurring when Tenlo 70 or oleic acid were added. There was also extensive, but not complete redispersion, in pure butanol-1 and proprionic acid. Results for ethanol extracted, dried, ground and aged G-44 solids are presented in table 49. This material did not redisperse

TABLE 46. – REDISPERSION OF ISOPROPANOL–EXTRACTED G–15 SOLIDS

Carrier liquid	Volume, cc	Dispersant	Amount, cc	Color of supernatant fluid contact time			
				0	1 day	1 week	6 weeks
Kerosene	1.0	Blank	---	---	Clear	Clear	Clear
Kerosene	1.0	Oleic acid	0.15	---	Light yellow	Brown	Yellow brown
Kerosene	1.0	10-undecenoic acid	.15	---	Clear	Clear	Clear
Kerosene	1.0	Octanoic acid	.15	---	Light yellow	Yellow	Yellow brown
Kerosene	1.0	Propionic acid	.15	---	Clear	Clear	Clear
Kerosene	1.0	Octylamine	.15	Immediate	Ferrofluid	Ferrofluid[a]	Ferrofluid[a]
Kerosene	1.0	Dodecylamine	.30[b]	Redispersion	Ferrofluid	Ferrofluid	Ferrofluid
Kerosene	1.0	Tenlo 70	.15	---	Light yellow	Yellow	Brown
Propionic acid	1.0	---	---	---	Light yellow	Brown	Brown
Butanol-1	1.0	---	---	---	Clear	Clear	Clear

[a]Complete redispersion.

[b]30 percent solution in kerosene.

TABLE 47. – REDISPERSION OF ACETONE-EXTRACTED G–15 SOLIDS

Carrier liquid	Volume, cc	Dispersant	Amount, cc	Color of supernatant fluid contact time			
				0	1 day	1 week	6 weeks
Kerosene	1.0	Blank	---	Clear	Clear	Clear	Clear
Kerosene	1.0	Oleic acid	0.15	Clear	Clear	Clear	Clear
Kerosene	1.0	10-undecenoic acid	.15	Clear	Clear	Clear	Clear
Kerosene	1.0	Propionic acid	.15	Clear	Clear	Clear	Clear
Kerosene	1.0	Octylamine	.15	Clear	Yellow	Brown	Deep brown
Kerosene	1.0	Tenlo 70	.15	Clear	Clear	Yellow	Brown
Kerosene	1.0	Octanoic acid	.15	Clear	Clear	Clear	Clear
Propionic acid	1.0	---	---	---	Yellow	Brown	Brown
Butanol-1	1.0	---	---	---	Clear	Clear	Clear

TABLE 48. – REDISPERSION OF ACETONE-FLOCCULATED G–44 SOLIDS

Carrier liquid	Volume, cc	Dispersant	Amount, cc	Color of supernatant fluid contact time			
				0	1 day	1 week	6 weeks
Kerosene	1.0	Blank	---	Clear	Clear	Clear	Clear
Kerosene	1.0	Oleic acid	0.05	Ferrofluid	Ferrofluid	Ferrofluid[a]	Ferrofluid[a]
Kerosene	1.0	Oleic acid	.15	Ferrofluid	Ferrofluid[a]	Ferrofluid[a]	Ferrofluid[a]
Kerosene	1.0	Tenlo 70	.05	Brown	Ferrofluid	Ferrofluid[a]	Ferrofluid[a]
Kerosene	1.0	10-undecenoic acid	.05	Brown	Ferrofluid	Ferrofluid	Ferrofluid
Kerosene	1.0	10-undecenoic acid	.15	Brown	Ferrofluid	Ferrofluid[a]	Ferrofluid
Kerosene	1.0	Proprionic acid	.05	Clear	Clear	Clear	Clear
Kerosene	1.0	Proprionic acid	.15	Clear	Clear	Pale yellow	Pale yellow
Kerosene	1.0	Tenlo 70	.15	Brown	Ferrofluid[a]	Ferrofluid[a]	Ferrofluid[a]
Kerosene	1.0	Ethanol	.15	Clear	Dark brown	Ferrofluid	Ferrofluid
Ethanol	1.0	---	---	Clear	Light yellow	Yellow	Yellow
Butanol	1.0	---	---	Clear	Deep yellow	Ferrofluid	Ferrofluid
Propionic acid	1.0	---	---	Ferrofluid	Ferrofluid	Ferrofluid	Ferrofluid

[a]No precipitate left - complete redispersion - magnetic liquid.

in kerosene, even in the presence of a number of additives. There was slight redispersion in pure proprionic acid. Similar results were obtained with the solids of the n-propanol extraction run.

Redispersion of the colloidal particles occurs when a stabilizing sheath can form around the particles. In the case of the oleic acid stabilized suspensions flocculated with acetone, removal of the acetone by either replacement of the acetone-kerosene mixture with pure kerosene or by extraction with water, results in the reformation of the stabilizing sheath. In the above case, it is apparent that relatively little oleic acid is removed by the acetone and that flocculation is due to a contraction of the stabilizing sheath in the presence of acetone. If the flocculation step removes a substantial amount of the surfactant, as is the case with the Tenlo 70 stabilized materials, then there is not enough stabilizing agent left on the particles to form the foundation of a sheath and the particles remain undispersed. Addition of more stabilizing agent, which can be a different surfactant than Tenlo 70, allows the sheath to form and repeptization then occurs.

The greater the extent of removal of the initial surfactant the greater the difficulty in redispersing the solids subsequentially. In fact, if too much surfactant is removed, redispersion will not occur at all, even in the presence of excess surfactant in the carrier fluid used as the suspending medium. This is an indication that unless there is an organic barrier, two particles in contact will adhere to each other. Cold welding of these particles is a distinct possibility. The particles will be arranged in an assembly will not be disrupted by the addition of stabilizing agent under conditions of gentle shaking. The greater the extent of removal of the surfactant, the greater the probability of having two bare particles in contact. The effect of time on the ease of redispersion of the extracted solids is a further indication of possible cold welding.

Redispersion depended on the nature of the surfactant added. Oleic acid and Tenlo 70 were quite effective if there was not substantial stripping of the initial stabilizer. The shorter chain carboxylic acids were not as effective. If redispersion occurred, there was no long term stability. This is considered to be due to the short chain length of these molecules leading to a stabilizing sheath that is not thick enough. Surprisingly two relatively short chain amines, octylamine and dodecylamine proved to be the most effective redispersants in these tests. Stable ferrofluids were not formed which had pure octylamine stabilizing layers, but ferrofluids were formed which presumably had mized stabilizing layers (octylamine plus Tenlo 70 or octylamine plus oleic acid). This is an interesting finding particularly since it was not possible to form ferrofluids by grinding in the presence of octylamine, and while it was possible to form ferrofluids in the presence of dodecylamine, the rate of grind was slow with this surfactant. These

results indicate that a good grinding agent is not necessarily the best redispersant, and vice-versa. This is most probably due to the fact that there are different possible sites for adsorption on the surface of the particles, as was shown by Dintenfass (ref. 23) who showed that the adsorbability of surface active agents on the surface of inorganic pigments in toluene was a function of the polar group. Agents with different polar groups could be adsorbed independently from each other, while agents with the same polar group competed for the same sites. With solids originally prepared in the presence of, say oleic acid, a number of the acid adsorbing sites are already taken up by the residual oleic acid that was not removed by extraction. The amines since they attack different sites function in a different manner and thus can act more rapidly.

Further findings of some interest were the redispersion of the particles in very polar organic solvents such as butanol and proprionic acid. Redispersion in these suspensions was presumed to have occurred as a result of electrostatic repulsion rather than entropic repulsion as was the case in the nonpolar hydrocarbon media. These polar solvents have a higher dielectric constant and conductivity so that an electrostatic double layer could be formed. These are analogous to the results of Koelmans and Overbeek (ref. 24) on the stability of suspensions in polar nonaqueous media.

Surface Tension (Conventional Determination)

The surface tension of ferrofluid was obtained by both the drop weight method and the tensiometer method. An instrument known as a stalagmometer used in the drop weight determination is a volumetric pipette which contains a known volume of liquid. It differs from the standard pipettes in that it has a capillary bore and a wide, ground flat tip. This results in the slow formation and full development of drops. Each pipette is calibrated in terms of the number of drops formed by water which has a surface tension of 72 dyne/cm^2.

The weight of a drop W formed at the tip of the tube of radius r by a liquid of surface tension, γ, according to Harkins and Brown (ref. 25) is:

$$W = 2\pi r \gamma \, f(r/c) \tag{76}$$

where c is a capillary constant and $f(r/c)$ is a unique function of r/c.

The number of drops $\mathcal{N}$ formed by a volume of liquid, V, is

$$\mathcal{N} = V\rho/W = V \rho_L / 2\pi r \gamma \, [1/f(r/c)] \tag{77}$$

TABLE 49. – REDISPERSION OF ETHANOL–EXTRACTED G–44 SOLIDS

Carrier liquid	Volume, cc	Dispersant	Amount, cc	Color of supernatant fluid contact time			
				0	1 day	1 week	6 weeks
Kerosene	1.0	Blank	---	Clear	Clear	Clear	Clear
Kerosene	1.0	Oleic acid	0.05	Clear	Clear	Clear	Clear
Kerosene	1.0	Oleic acid	.15	Clear	Clear	Clear	Clear
Kerosene	1.0	Tenlo 70	.05	Clear	Clear	Clear	Clear
Kerosene	1.0	10-undecenoic acid	.05	Clear	Clear	Clear	Clear
Kerosene	1.0	10-undecenoic acid	.15	Clear	Clear	Clear	Clear
Kerosene	1.0	Propionic acid	.05	Clear	Clear	Clear	Clear
Kerosene	1.0	Propionic acid	.15	Clear	Clear	Clear	Clear
Kerosene	1.0	Octylamine	.15	Clear	Clear	Clear	Clear
Kerosene	1.0	Dodecylamine	.15	Clear	Clear	Clear	Clear
Propionic acid	1.0	---	---	Clear	Light yellow	Yellow	Yellow brown
Ethanol	1.0	---	---	Clear	Clear	Clear	Clear
Water	1.0	---	---	Clear	Clear	Clear	Clear

where ρ_L = liquid density.

The instrument is designed in such a way that f (r/c) is invariant over large ranges of values of γ. The surface tension of a given liquid γ_1, is easily obtained from the following equation

$$\gamma_1 = \mathfrak{N}_r \gamma_r / \rho_{Lr} \cdot \rho_{L1} / \mathfrak{N}_1 \tag{78}$$

where

ρ_{L1} = density of the liquid gm/cc

$\mathfrak{N}_1$ = number of drops formed by the liquid

$\mathfrak{N}_r$ = number of drops formed by a reference liquid

γ_r = surface tension of reference liquid dynes/cm^2

ρ_{Lr} = density of reference liquid gm/cc

The above method was used to obtain the surface tensions of pure kerosene, a solution of oleic acid in kerosene (1 part oleic/10 parts kero sene), pure oleic acid and of G-4, -5, -6 ferrofluid (magnetite - kerosene, oleic acid). These results are presented in table 50.

The value of 30.4 dyne/cm^2 for the surface tension of oleic acid obtained in these tests is slightly lower than standard published value at 20° C of 32.5 dyne/cm (ref. 26). Kerosene is not a pure compound but a mixture of a number of components, and the published values vary between 23 and 30 dyne /cm at 20° C.

It is concluded from the data obtained above that the surface tension of a ferrofluid against air is not significantly different than the surface tension of the base liquid.

As a check on the stalagmometer results and to determine concentration effects, another series of surface tension measurements and a number of interfacial tension measurements as well were determined using a Cenco-Du Nouy tensiometer. The tensiometer was equipped with a platinum ring which was cleaned by heating to incandescence before each change to a new fluid. The data of these tests relate to the tension of ferrofluids of varying particle concentration. However, the proportion of oleic acid to magnetic solids is constant. The data and test conditions are presented in table 51 and values of surface tension are plotted in figure 62. As seen there, a number of comparative results verify the general consistence of the data.

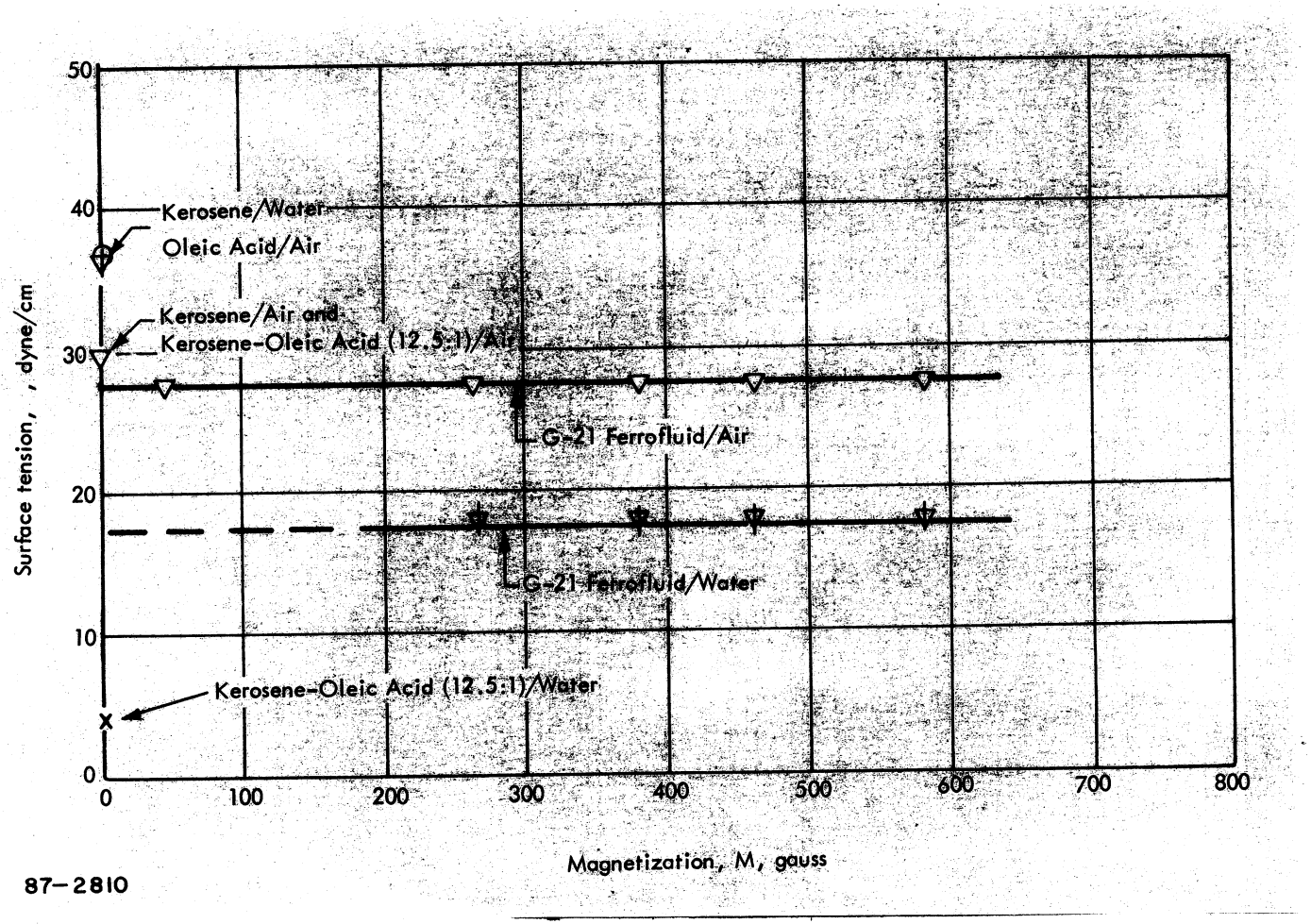

Figure 62. – Surface Tension of Ferrofluids in Absence of Applied Magnetic Field versus Saturation Magnetization

TABLE 50. – SURFACE TENSION MEASUREMENTS BY STALAGMOMETER TECHNIQUE

Fluid	Pure kerosene	Oleic acid	Oleic acid/ kerosene 1 part/10	G456 ferrofluid, 75 gauss
Temperature	22° C	22° C	22° C	22° C
Density, gm/cc	0.78	0.89	0.79	0.859
Number of determinations	4	4	4	3
Average number of drops	73.9	52.6	72.1	85.8
Standard deviation in drop number	.1	.7	.2	.3
Number of drops of water at 20° C	34.7	24.9	34.7	34.7
Surface tension water at 20° C	← 72 dyne/cm^2 →			
Density of water at 20° C	← 1.0 gm/cc →			
Measured surface tension, dyne/cm^2	26.4	30.4	27.4	25.0

TABLE 50.

TABLE 51. – SURFACE TENSION MEASUREMENTS BY TENSIOMETER TECHNIQUE
(TEMPERATURE 22° C; NUMBER OF DETERMINATIONS 5)

(fluid)/(medium)	(H_2O)/(air)	(Kero)/(H_2O)	(Oleic)/(air)	(Kero)/(air)	[a] K-O/air	[a] K-O/H_2O	(G-21)/(air) M_s = 264	(G-21)/(air) M_s = 378	(G-21)/(air) M_s = 460	(G-21)/(air) M_s = 578	(G-21)/(water) M_s = 264	(G-21)/(water) M_s = 378	(G-21)/(water) M_s = 460	(G-21)/(water) M_s = 578
Fluid density, gm/cc	72.00	0.78	0.89	0.78	0.79	0.79	1.100	1.206	1.295	1.476	1.100	1.206	1.295	1.476
Measured surface tension, dyne/cm	1.00	37.4	36.0	29.0	29.3	4.0	27.5	27.6	27.6	27.5	17.0	16.9	17.3	17.9
Standard deviation in surface tension, dyne/cm	.00	.05	.05	.06	.05	.00	.08	.04	.00	.04	.07	.04	.05	.07

[a] 1.25 volumes kerosene to 1 volume oleic acid.

A number of salient points are observed, as follows:

i. The tension of ferrofluid against air or water is independent of particle concentration, at least for the range studied.

ii. The interfacial tension of ferrofluid against water is lower than against air.

iii. The interfacial tension of ferrofluid against water is intermediate to the interfacial tension of (kerosene)/(water) and (kerosene-oleic acid)/(water) where the mixture of kerosene with oleic acid is in the proportion initially present in standard ferrofluid.

These points indicate that interfacial tension potentially furnishes a potent means for the determination of distribution coefficients and related information concerning the relative amount of a dispersant found in the carrier liquid of a ferrofluid compared to the amount adsorbed on the surface of the particles. It should be noted that mere determination of tension against air does not qualify as a tool for such adsorption studies since the tension is essentially unaffected by the dispersant concentration. The specificity of the test against water is undoubtedly related to the affinity of organic acid groups to the polar water medium. The utility of the technique would rely, in part, on the fact that solubility of oleic acid in water is quite small and so is the water/ferrofluid interfacial area compared to the area present on particle surfaces.

Surface Tension[1]
(Relationship to Surface Stability of Magnetizable Fluid in the Presence of a Uniform Magnetic Field)

The material of this section deals with the peculiar liquid spikes which are observed under appropriate conditions at the interface between magnetic fluid and a nonmagnetic fluid medium. A theoretical treatment is developed that predicts the sudden onset of the phenomenon, and relates the value of the critical magnetic field and geometrical spacing to properties of the media. Experimental determinations are made of the critical parameters in which the density difference is varied by more than a factor of 10 and a satisfactory comparison is found with the theory. The data are then utilized to determine surface and interfacial tensions.

[1] The theory, developed in all its essentials by M. D. Cowley, has been cast into its present form by a present author (R.E.R.). The experimental determinations were performed at the Avco Laboratories. The development here is in cgs units.

During the course of this work it was discovered that when a magnetic fluid possessing sufficiently great magnetic polarizability is brought into a given region of steady magnetic field, a free surface that is initially smooth will under certain conditions deform spontaneously to a corrugated configuration. (See figure 63.) Experimentation reveals that the corrugations are formed in response to a normal component of field at the surface, there being no formation when the applied field is wholly parallel to the surface. The phenomenon is reduced to its essentials in a laboratory configuration where a vertical, uniform magnetic field is applied normal to a pool of magnetic fluid. When the field is increased, a point is reached where the surface is suddenly perturbed to a pattern with hexagonal symmetry, that is the tips of the incipient protuberances are located on triangular centers.

As the field is increased to higher values, the protuberances are observed to grow taller and spike-shaped although their spacing remains sensibly constant. The tips of the spikes are then sharply pointed although the fluid nature of the medium remains and is readily proven by stirring.

In the absence of a polarizing field a fluid will ordinarily tend to minimize its surface area and hence the surface energy, but in the present case there is a spontaneous increase of surface area. Accordingly, it could be concluded that the increase of surface energy is accompanied by a decrease of magnetic field energy such that the sum of all energies including gravitational energy attains a minimum value.

Method of Attack. - The following presents a theory of the stability of the magnetic liquid surface which is based directly on consideration of force equilibrium. Equations and boundary conditions are developed for the small perturbation of a uniform field in the magnetic medium. A general periodic solution is derived where the standard practice is followed of applying boundary conditions at the unperturbed position of the surface. The treatment is for deep liquid although the analysis may be extended to liquid of finite depth. This linear theory can only purport to describe conditions at the onset of the phenomenon. However, it is empirically observed that the spacing of the spikes is insensitive to an increase of field although the length of spikes continues to increase.

Summary is given of alternate forms of the force law assuming a linear isotropic medium, with the surface conditions appropriate to each. Linearized forms for two of the easiest forms are given; one in this particular problem eliminates the surface condition.

Next the neutral stability condition is obtained by balancing the effect of gravitational forces, surface tension, and magnetic forces. The condition is satisfied for a given magnetization by two wave numbers of surface perturbation above a critical level of magnetization.

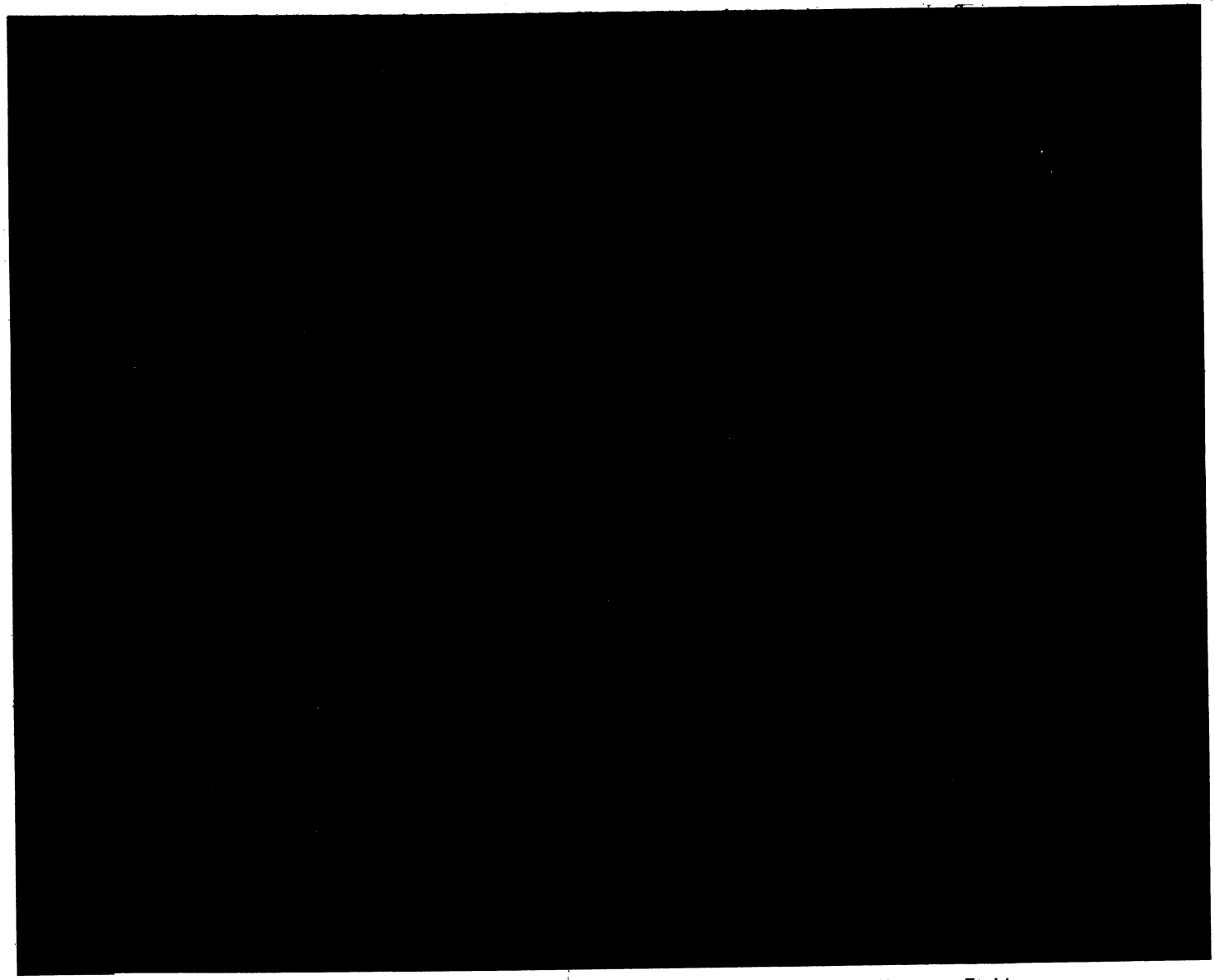

Figure 63. – Appearance of Fluid Surface in Response to Uniform, Normally Applied, Magnetic Field with Intensity in Excess of the Critical

Finally, comparison is made with experiment. The ratio of the square of critical field to critical spacing is a crucial test because it can be expressed in terms of just permeability and density. The comparison of interfacial tension is another important test. In addition to qualitative correspondence with the observed behavior, the theory has predicted with good agreement the quantitative features of the phenomenon.

The Magnetic Field Problem. - The field equations relevant to this problem are

$$\nabla \cdot \vec{B} = 0 \tag{79}$$

$$\nabla \times \vec{H} = 0 \tag{80}$$

where $\vec{B}$ and $\vec{H}$ are related through the defining equation

$$\vec{B} = (\vec{H} + \vec{M}) \tag{81}$$

The boundary conditions at an interface are

$$[H_t] = 0, \quad [B_n = 0] \tag{82 a, b}$$

where the subscript t denotes tangential component, n the normal component and brackets signify the jump or difference in quantity across the interface. It will be assumed that the vectors are parallel according to

$$\vec{B} \;//\; \vec{H} \;//\; \vec{M} \tag{83}$$

As the constitutive relationship, assume the medium is isotropic with a constant permeability, μ.

$$\vec{B} = \mu \vec{H} \tag{84}$$

The initial, unperturbed fields are specified by

$$\vec{B}_0 = (0, 0, B_0) \quad \vec{M}_0 = (0, 0, M_0) \quad \vec{H}_0 = (0, 0, H_0) \tag{85a, b, c}$$

while the perturbed fields for small variations are given by

$$\vec{B} = (b_x, b_y, B_0 + b_z) \quad \vec{M} = (m_x, m_y, M_0 + m_z) \quad \vec{H} = (h_x, h_y, H_0 + h_z) \tag{86a, b, c}$$

Since this is a linearized theory, the magnitudes may be approximated as follows:

$$B^2 = B_0^2 + 2 b_z B_0 + b_x^2 + b_y^2 + b_z^2$$
$$\simeq B_0^2 (1 + 2 b_z / B_0) \qquad (87a, b, c)$$

Thus,

$$B \simeq B_0 + b_z$$

$$M \simeq M_0 + m_z$$

$$H \simeq H_0 + h_z$$

The direction cosines $\vec{B} = (b_x/B_0, b_y/B_0, 1)$ and similarly for the others. The components of the perturbed field are related according to

$$b_z = \mu h_z \qquad m_z = \chi h_z \qquad (88a, b, c, d, e, f)$$

$$b_y = \mu h_y \qquad m_y = \chi h_y$$

$$b_x = \mu h_x \qquad m_x = \chi h_x$$

where $\mu = (1 + \chi)$ with χ the susceptibility.

Equation (80) permits the field $\vec{h} = \vec{H} - \vec{H}_0$ to be expressed in terms of a scalar potential function ϕ,

$$\nabla \phi = \vec{h} \qquad (89)$$

Then from (79) $\nabla \cdot (\mu \phi) = 0$ so the potential satisfies Laplace's equation

$$\frac{\partial^2 \phi}{\partial x^2} + \frac{\partial^2 \phi}{\partial y^2} + \frac{\partial^2 \phi}{\partial z^2} = 0 \qquad (90)$$

A general expression for the unit normal to the surface $z_0(x, y)$ is

$$\vec{n} \left[1 + \left(\frac{\partial z_0}{\partial x} \right)^2 + \left(\frac{\partial z_0}{\partial y} \right)^2 \right]^{1/2} = \left(- \frac{\partial z_0}{\partial x}, - \frac{\partial z_0}{\partial y}, 1 \right)$$

or to the accuracy of the linearization,

$$\vec{n} \simeq \left(- \frac{\partial z_0}{\partial x}, - \frac{\partial z_0}{\partial y}, 1 \right) \qquad (91)$$

Then $B_n = B \cdot n = B_0 + b_z$ so the interface condition (82b) becomes $[B_0 + b_z] = 0$ but $[B_0] = 0$ and hence $[b_z] = 0$ or

$$\left[\mu \frac{\partial \phi}{\partial z} \right] = 0 \qquad (92)$$

Next the consequence of the tangential condition of (82a) is determined. At the surface the tangential component vector of $\vec{H}$, denoted $\vec{H}_t$ is given by $\vec{H}_t = (\vec{n} \times \vec{H}) \times \vec{n}$; this vector lies in the plane of the vectors $\vec{n}$ and $\vec{H}$.

Carrying out the vector operations and preserving only the first order terms gives

$$\vec{H}_t = \left(H_0 \frac{\partial z_0}{\partial x} + h_x,\ H_0 \frac{\partial z_0}{\partial y} + h_y,\ 0 \right)$$

so the vector is entirely horizontal. From continuity of the two finite components across the boundary, it follows then that

$$\left[H_0 \frac{\partial z_0}{\partial x} + h_x = \right] 0$$

$$\left[H_0 \frac{\partial z_0}{\partial y} + h_y \right] = 0$$

Multiplying by dx, dy , respectively, and adding gives upon recognition of the property of a perfect differential that $[H_0 z_0 + \phi] = 0$ and since $[B_0] = 0$,

$$[\phi] = z_0 [M_0] \tag{93}$$

which describes the jump in the potential across the boundary. Denote the region above the surface as (2) and below the surface as (1). Then for the potential consider solutions which are periodic in x, y .

$$\phi_1 = \Phi_1 (x, y)\, e^{k_1 (z - z_0)} \qquad z < 0$$

$$\phi_2 = \Phi_2 (x, y)\, e^{-k_2 (z - z_0)} \qquad z > 0 \tag{94a, b}$$

Substitution into (90) gives

$$\frac{\partial^2 \Phi_1}{\partial x^2} + \frac{\partial^2 \Phi_1}{\partial y^2} + k_1^2 \Phi_1 = 0$$

$$\frac{\partial^2 \Phi_2}{\partial x^2} + \frac{\partial^2 \Phi_2}{\partial y^2} + k_2^2 \Phi_2 = 0 \tag{95a, b}$$

From the normal boundary condition, equation (92), using (94a, b) and evaluating quantities at $z = z_0$,

$$\mu_2 k_2 \Phi_2 + \mu_1 k_1 \Phi_1 = 0 \tag{96a}$$

Similarly, from the tangential condition of (93)

$$\Phi_2 - \Phi_1 = z_0 (M_0^{(2)} - M_0^{(1)}) \tag{96b}$$

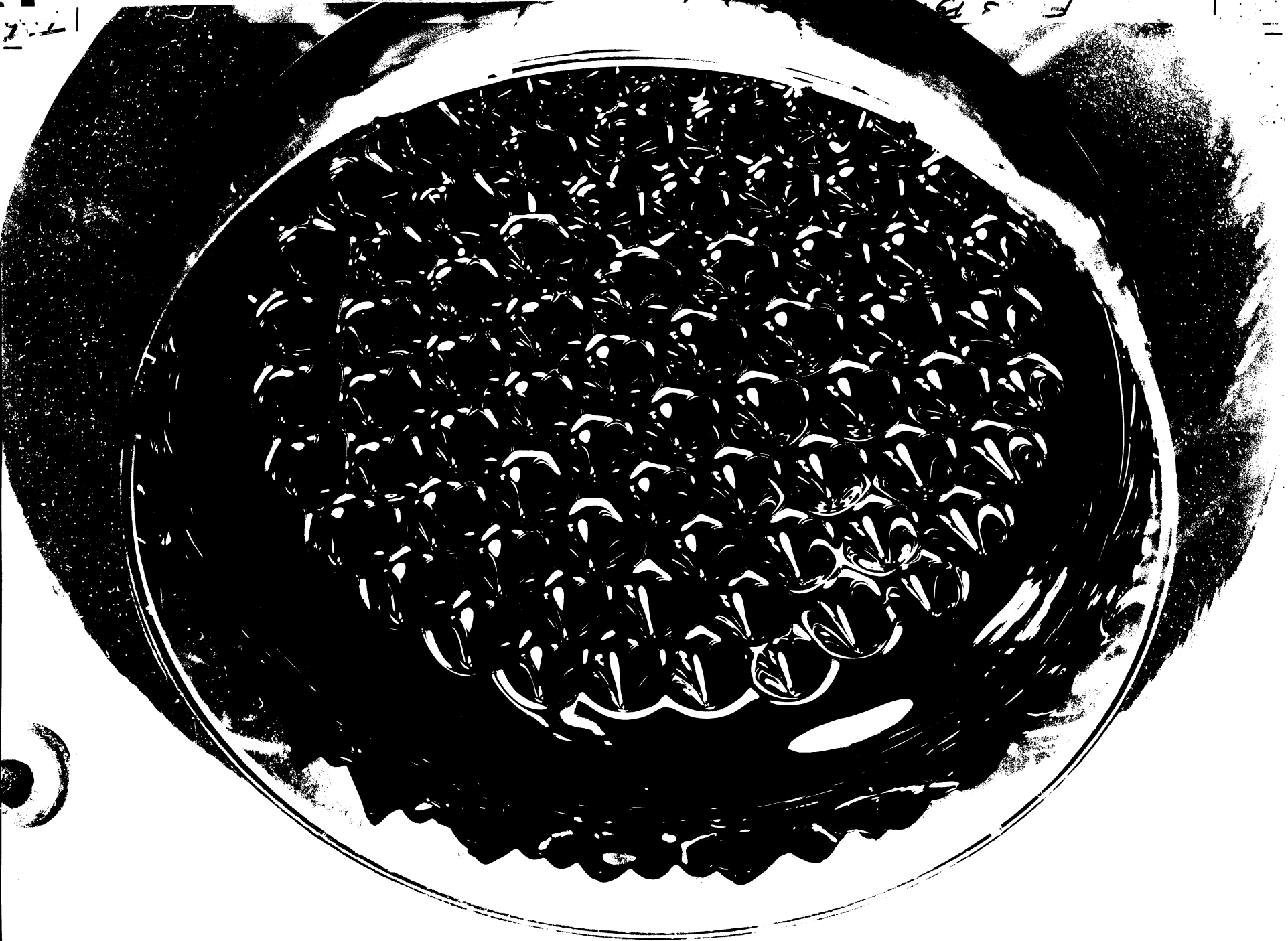

Equations (96a, b) solved simultaneously reveal that both Φ_1, and Φ_2 are directly proportional to z_0.

$$\Phi_1 = z_0 \frac{(M_0^{(1)} - M_0^{(2)})}{1 + \mu_1 / \mu_2}$$

$$\Phi_2 = z_0 \frac{(M_0^{(2)} - M_0^{(1)})}{1 + \mu_2 / \mu_1} \qquad (97a, b)$$

Thus (95a, b) becomes

$$\frac{\partial^2 z_0}{\partial x^2} + \frac{\partial^2 z_0}{\partial y^2} + k_1^2 z_0 = 0$$

$$\frac{\partial^2 z_0}{\partial x^2} + \frac{\partial^2 z_0}{\partial y^2} + k_2^2 z_0 = 0$$

and these give k_1, k_2 from the shape of the free surface. Since the free surface is unique, $k_1 = k_2 = k$,

$$k = -\left(\frac{\nabla^2 z_0}{z_0}\right)^{1/2} \qquad (98)$$

where $\nabla^2 z_0$ is two dimensional.

Expressions may now be found using (97a, b) and (98) for the components of the perturbation field $\vec{h}$ at $z = z_0$ in terms of the shape of the free surface.

Thus,

$$h_{1z} = \left(\frac{\partial \phi_1}{\partial z}\right)_0 = (-z_0 \nabla^2 z_0)^{1/2} \frac{M_0^{(1)} - M_0^{(2)}}{1 + \mu_1 / \mu_2}$$

$$h_{2z} = \left(\frac{\partial \phi_2}{\partial z}\right)_0 = (-z_0 \nabla^2 z_0)^{1/2} \frac{M_0^{(1)} - M_0^{(2)}}{1 + \mu_2 / \mu_1}$$

$$h_{1x} = \left(\frac{\partial \phi_1}{\partial x}\right)_0 = \frac{M_0^{(1)} - M_0^{(2)}}{1 + \mu_1 / \mu_2} \frac{\partial z_0}{\partial x}$$

$$h_{2x} = \left(\frac{\partial \phi_2}{\partial x}\right)_0 = \frac{M_0^{(2)} - M_0^{(1)}}{1 + \mu_2 / \mu_1} \frac{\partial z_0}{\partial x}$$

The nature of the solution may be sketched in the vicinity of a sinusoidal interface based on the results above and it may be shown that the field lines of $\vec{h}$ are closed loops whose extent never exceeds half the wavelength. If one extremity of a loop is at the knee of a crest, the other extremity is found at the nearest toe of a trough.

The Magnetic Force. - An equation of motion may be written of the following form and is applicable to any small volume element.

$$\rho \frac{D\vec{q}}{Dt} = - \nabla p^* + \vec{F} - \rho g \hat{z} \tag{99}$$

where

$$\frac{D}{Dt} = \frac{\partial}{\partial t} + \vec{q} \cdot \nabla$$

$\vec{q}$ = velocity

p^* = scalar quantities defined below

$\vec{F}$ = body force per unit volume due to magnetic origin

ρ = mass density

g = acceleration due to gravity

$\hat{z}$ = unit upward vector.

Here it will be assumed in accord with the field treatment presented in the previous section that permeability, μ, is constant ($\mu = B/H$). It will also be assumed that an appropriate expression for the body force is that given by Stratton (ref. 27); namely, the result of a derivation from energy principles first attributed to Korteweg and Helmholtz. The formulation has received extensive application in the work of Melcher (ref. 4) while an experimental support for the formulation was provided by Hakim and Hingham (ref. 28) who measured by optical means the influence of the stress field on the value of local mass density. This force density is given by

$$\vec{F} = -\frac{1}{8\pi} H^2 \nabla\mu + \frac{1}{8\pi}\nabla\left(\rho H^2 \frac{\partial \mu}{\partial \rho}\right) \tag{100}$$

and is to be used with the meaning that

$$p^* = p^\circ$$

where p° is the thermodynamic pressure. The expression for force density seems paradoxical since one might reasonably assume the existence of a medium in which $\frac{\partial \mu}{\partial \rho} = 0$ so the second term on the right side vanishes. Then the force density is proportional to $\nabla\mu$ and since μ is, we will suppose, a function only of two thermodynamic variables for example, pressure and temperature, then at constant conditions it is spatially constant within a medium and the force density vanishes. However, the force density is to be used with the understanding that its integration is to be carried out not only through the medium but across the surface of the medium as well. In that manner, the occurrence of surface stresses make an appearance and as a result a whole body can experience, a net force. Before proceeding further there are two other points to be mentioned. The term containing $\frac{\partial \mu}{\partial \rho}$ is known as the striction term, but if it were omitted at the outset, there would be no effect on the incompressible problems considered here. This is a consequence of the fact that it appears as the gradient of a scalar quantity and hence can be lumped into the pressure term. The other point is that alternate formulations for conjugate pairs p^* and $\vec{F}$ may be found by mathematical rearrangement of the Korteweg-Helmholtz formulation. Thus, it may be verified that the following formulations are all equivalent.

i. $$\vec{F} = -\frac{1}{8\pi} H^2 \nabla\mu + \frac{1}{8\pi}\nabla\left(\rho H^2 \frac{\partial \mu}{\partial \rho}\right)$$

$$p^* = p^\circ, \text{ thermodynamic pressure}$$

ii. $$\vec{F} = M\nabla B$$

$$p^* = p^\circ + \frac{1}{8\pi}\left(MB - \rho \frac{B^2}{\mu^2} \frac{\partial \mu}{\partial \rho}\right)$$

iii. $\vec{F} = M\nabla H/4\pi$

$$p^* = p^\circ + \frac{1}{8\pi}\left(MH - \rho H^2 \frac{\partial \mu}{\partial \rho}\right)$$

Each formulation, however, will lead to a different expression for surface stress, relations that are developed below.

Surface Stress Difference. - Expressions for the surface stress differences corresponding to the alternate formulations may be found by integrating the force density over the volume of a pill box element encompassing an interface. (See fig. 64.)

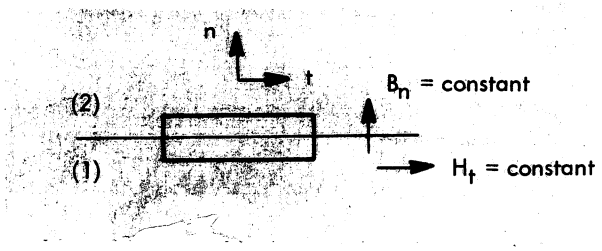

The normal force on an element of unit area at the surface is given in all cases by

$$\text{Normal stress} = \text{Lim} \int_0^{\delta_n} (-p^* + \vec{F} - \rho g \hat{z}) \cdot \hat{n}\, dn \qquad \delta_n \to 0$$

$$= \text{Lim} \int_0^{\delta_n} \left(-\frac{\partial p^*}{\partial n} + F_{\hat{n}} - \rho g \hat{z} \cdot \hat{n}\right) dn \qquad \delta_n \to 0$$

$$= -[p^*]_1^2 + \int_0^{\delta_n} F_n\, dn \qquad \delta_n \to 0$$

Thus the problem reduces to an evaluation of $\int_0^{\delta_n} F_n \, dn$ for each case.

For the various formulations, we have:

i. $$\int F_n \, dn = - \int \frac{1}{8\pi} H^2 \frac{\partial \mu}{\partial n} \, dn + \left[\frac{1}{8\pi} \rho H^2 \frac{\partial \mu}{\partial \rho} \right]$$

$$\int H^2 \frac{\partial \mu}{\partial n} \, dn = \int \left(\frac{B_n^2}{\mu^2} + H_t^2 \right) d\mu$$

$$= \left[- \frac{B_n^2}{\mu} + \mu H_t^2 \right]$$

$$= [- B_n H_n + B_t H_t] \qquad (101)$$

since,

$$H^2 = H_n^2 + H_t^2 , \quad [B_n] = 0 \quad \text{and} \quad [H_t] = 0.$$

Thus,

$$\text{Lim} \int_0^{\delta_n} F_n \, dn = \frac{1}{8\pi} \left[\rho H^2 \frac{\partial \mu}{\partial \rho} + B_n H_n - B_t H_t \right]$$

ii. $$\int F_n \, dn = \frac{1}{4\pi} \int M \frac{\partial B}{\partial n} \, dn = \frac{1}{8\pi} \int \frac{M_t}{B_t} \frac{\partial B_t^2}{\partial n} \, dn$$

$$= \frac{1}{4\pi} \int \left(B_t - H_t \right) d B_t$$

$$= \frac{1}{4\pi} \left[\frac{1}{2} B_t^2 - B_t H_t \right]$$

(102)

Hence,

$$\text{Lim} \int_0^{\delta n \to 0} F_n \, dn = \left[\frac{1}{8\pi} \, M_t^2 \right]$$

iii. $$\int F_n \, dn = \frac{1}{4\pi} \int M \frac{\partial H}{\partial n} \, dn = \frac{1}{8\pi} \int \frac{M_n}{H_n} \frac{\partial H_n^2}{\partial n} \, dn$$

$$= \frac{1}{4\pi} \int M_n \, d H_n = \frac{1}{4\pi} \int M_n \, d M_n$$

$$= \left[- \frac{1}{8\pi} \, M_n^2 \right]$$

Thus,

$$\text{Lim} \int_0^{\delta n \to 0} F_n \, dn = - \left[\frac{1}{8\pi} \, M_n^2 \right] \tag{103}$$

Having stated the force expressions and developed the corresponding expressions for surface stress, it is now possible to obtain linearized expressions for both which will be useful to the problem under consideration.

Linearized Forces and Boundary Conditions. - Formulation leads to complicated forms and will not be stated. There is advantage to working out both forms (ii.) and iii.), however, as they afford a choice which is not obvious at the start. For ii there follows

$$\vec{F} = \frac{M_0}{4\pi} \nabla b = \frac{1}{4\pi} \nabla \, (M_0 \, b_z)$$

and

$$\text{Normal stress} = \left[\frac{1}{8\pi} \, M_t^2 \right] = \frac{1}{8\pi} \left[M_0^2 \left\{ \left(\frac{\partial z_0}{\partial x} \right)^2 + \left(\frac{\partial z_0}{\partial y} \right)^2 \right\} \right.$$

$$+ 2 M_0 \left(m_x \frac{\partial z_0}{\partial x} + m_y \frac{\partial z_0}{\partial y} \right)$$

$$\left. + m_x^2 + m_y^2 \right] = 0$$

since all terms are small quantities of the second order.

For formulation (iii),

$$\vec{F} = \frac{M_0}{4\pi} \nabla h_z = \frac{1}{4\pi} \nabla (M_0 h_z)$$

and

$$\text{Normal stress} = -\left[\frac{1}{8\pi} M_n^2\right] = -\left[\frac{1}{8\pi} (M_0 + m_z)^2\right]$$

$$= \text{unperturbed stress} - \left[\frac{M_0 m_z}{4\pi}\right]$$

Now it can be seen there is an advantage to form (ii) where the unperturbed stress vanishes as does the perturbed stress to the order of this approximation. Thus, using the formulation $\vec{F} = \frac{1}{4\pi} M \nabla B$, only the surface tension is effective in supporting differences of stress across the interface and the difference of stress is simply $-[p^*]$.

Criterion for Neutral Stability on a Horizontal Surface. - The nomenclature of the system is illustrated in figure 65. As decided above, use will be made of the formulation $\vec{F} = \frac{M \nabla B}{4\pi}$ which implies that $p_2^* - p_1^*$ represents the downward acting stress across an element of interface. If there is a static

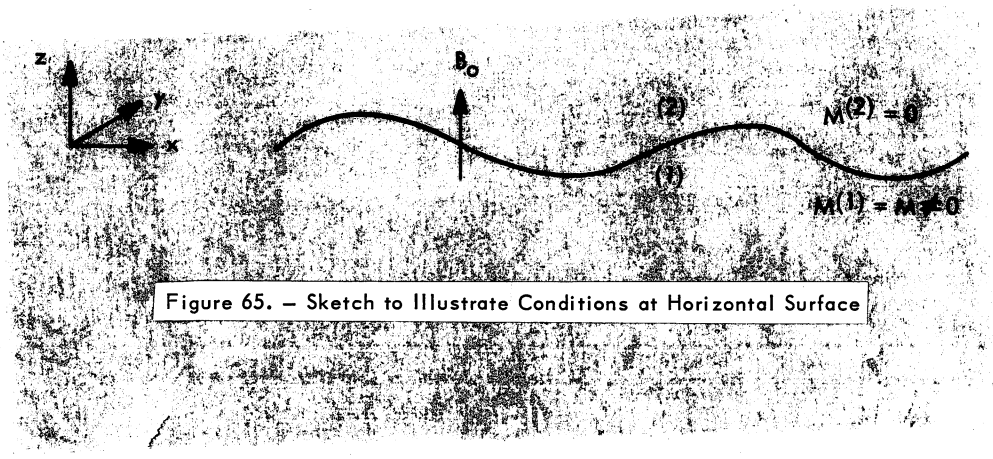

Figure 65. – Sketch to Illustrate Conditions at Horizontal Surface

equilibrium, then it is due to the effect of surface tension γ such that the tension applied upon the perimeter of an element is $-\gamma\nabla^2 z_0$ per unit area of the element with the stress acting in the downward direction

$$p_2^* - p_1^* - \gamma\nabla^2 z_0 = 0 \tag{104}$$

This is the stress boundary condition and again $\nabla^2 = \frac{\partial^2}{\partial x^2} + \frac{\partial^2}{\partial y^2}$. Now according to the formulation which has been selected, for both regions (i) and (ii) in the absence of motion,

$$-\nabla p^* - \rho g \hat{z} + \frac{M}{4\pi} \nabla B = 0$$

$$p^* = p^\circ + \frac{1}{8\pi}\left(MB - \rho \frac{B^2}{\mu^2} \frac{\partial \mu}{\partial \rho}\right)$$

Hence in (ii) where $M = 0$

$$\nabla p^* + \nabla (\rho g z) = 0$$

or

$$p_2^* + \rho_2 g z_2 = \text{const.}$$

while in (i)

$$p_1^* + \rho_1 g z_1 - \frac{M_0 b_z}{4\pi} = \text{const.}$$

When $z_2 = z_1 = 0$ at all x and y, $b_z = 0$, the interface is flat, and surface tension effects are absent. Then $p_2^* = p_1^*$ so it follows that the constants must be equal. The previous two expressions may now be combined and applied to the interface $z_1 = z_2 = z_0$ together with the stress boundary condition to give

$$p_2^* - p_1^* = (\rho_1 - \rho_2) g z_0 - \frac{M_0 b_z}{4\pi} = \gamma\nabla^2 z_0$$

as the condition for equilibrium. For a given deformation of the interface, there will be tendency to lower crests and raise troughs provided $(p_2^* - p_1^*) > \gamma \nabla^2 z_0$, hence the condition for stability may be written

$$\gamma \left(- \frac{\nabla^2 z_0}{z_0} \right) + (\rho_1 - \rho_2) g > M_0 \frac{b_z}{z_0}$$

From the solution for the magnetic field developed earlier, we have

$$b_z^{(1)} = \mu_1 h_z^{(1)} = \mu (- z_0 \nabla^2 z_0)^{1/2} \frac{M_0}{1 + \mu}$$

so that

$$\gamma \left(- \frac{\nabla^2 z_0}{z_0} \right) + (\rho_1 - \rho_2) g > \mu \left(- \frac{\nabla^2 z_0}{z_0} \right)^{1/2} \frac{M_0^2 / 4\pi}{1 + \mu} \qquad (105)$$

and this expresses the condition for stability entirely in terms of independent variables and the shape of the free surface. The expression may be simplified through the introduction of the nondimensional quantities

$$k_0^2 = - \frac{\nabla^2 z_0}{z_0} \frac{\gamma}{(\rho_2 - \rho_1) g} \qquad (106a, b)$$

$$\mathfrak{M}_0^2 = \frac{M_0^2 / 4\pi}{\sqrt{T (\rho_2 - \rho_1) g}}$$

Then in terms of the nondimensional wave number of surface perturbation k_0, the stability criterion is:

$$\frac{\mathfrak{M}_0^2}{1 + \mu} = k_0 + \frac{1}{k_0} = f(k_0) \qquad (107)$$

A plot of the function $f(k_0)$ defines a line above which lies the region of instability, below which is the stable region, and on which there is neutral equilibrium. The function passes through a minimum point at $k_0 = 1$, $f(k_0) = 2$. For values of the left hand side of the stability criterion less than 2 the condition is not satisfied by any k_0. Thus the onset of instability is

when $\frac{\mathcal{M}_0^2}{1+1/\mu} = 2$ and this occurs when $k_0 = 1$. This qualitative prediction is in accord with the facts of experimentation, that

i. a fluid having less than a critical value of saturation magnetization does not produce spikes under any arbitrarily high applied field, and

ii. a fluid having more than a critical value of saturation magnetization produces spikes only when the applied field exceeds a critical value.

Shape of Disturbance Pattern and Prediction of Critical Parameters. The shape of the disturbance pattern is not predicted by the theory but we may incorporate the empirical observation that most frequently the pattern is hexagonal, that is the spike peaks are on triangular centers. Corresponding to the distribution of Christopherson

$$z_0\ (x, y) = \xi \left(2 \cos \frac{\sqrt{3}}{2} kx \cos \frac{1}{2} ky + \cos ky \right) \qquad (108)$$

where ξ is a small constant and the distance between peaks is

$$\text{distance} = \frac{4\pi}{\sqrt{3}\, k}$$

Hence, from equation (98),

$$\text{distance} = \frac{4\pi}{\sqrt{3}} \left(- \frac{z_0}{\nabla^2 z_0} \right)^{1/2}$$

$$= \frac{4\pi}{\sqrt{3}\, k_0} \sqrt{\frac{\gamma}{(\rho_1 - \rho_2)\, g}}$$

where the last equality follows from the definition of k_0. Recalling that the condition for neutral stability at minimum $\mathcal{M}_0$ is $k_0 = 1$ then gives directly the critical distance between peaks.

$$\ell_c = \frac{4\pi}{\sqrt{3}} \sqrt{\frac{\gamma}{(\rho_1 - \rho_2)\, g}} \qquad (109)$$

It is noted that the critical distance is independent of the magnetization of the medium. The value of the critical magnetization in turn depends on surface tension, desnity difference, the acceleration due to gravity, and the permeability as follows

$$M_c = \left[2\left(1 + \frac{1}{\mu}\right)\right]^{1/2} \left[\gamma\,(\rho_2 - \rho_1)\,g\right]^{1/4} \qquad (110)$$

The corresponding critical field is $B_c = \dfrac{1}{1 - \dfrac{1}{\mu}}\, M_c$.

Comparison with Experiment. - A comparison of the theory with experiment has been accomplished and is reported in the following. Magnetic fluid contained in a glass vessel of 100-mm diameter was subjected to a spatially uniform magnetic field provided by a pair of air core solenoids. The conditions of the tests are noted in table 52. Four concentrations of magnetic fluid were employed each having a different density and magnetization curve. Table 53 lists the conversion of magnetic property from bulk solid to colloid as may be calculated from density and saturation magnetization. Since the fluids were dilutions of the same materials, the conversion should be invariant. The 1.4 percent standard deviation of the values is indicative of the general precision of the measurements.

Observation was made of critical spacing and critical applied field corresponding to the first appearance of the protuberances. Spacing was measured with a nonmagnetic divider to an estimated accuracy of ± 0.3 mm. The applied field was measured in the absence of the liquid using a Hall effect probe with the result that a linear calibration curve (not shown) was established corresponding to 37 gauss per ampere of applied current. Current was supplied by a regulated power supply and measured with an accurate ammeter. An important parameter, the density difference between phases across the perturbed interface, was varied by nearly a factor of 15 in the tests. This was accomplished by running against distilled water as well as air. The immiscible water layer, less dense than the magnetic liquid layer in each case, was floated over the magnetic liquid. There was a possibility that interfacial tension would require a period of equilibrium to achieve a steady value. Accordingly test 6 was repeated after the fluid phases had been in contact for two days; as the result there was no change in the experimental value of critical length or critical field.

A complete verification of the theory requires individual comparison of predicted and observed values of critical length and critical field. However, there is uncertainty in the values of surface tension and interfacial tension due to possible dependence upon the presence of the applied magnetic field. Hence it was chosen to first evaluate the ratio B_c^2/ℓ_c since this quantity

TABLE 52. – EXPERIMENTS TO DETERMINE THE SURFACE STABILITY OF MAGNETIZABLE FLUID[a] IN THE PRESENCE OF A UNIFORM MAGNETIC FIELD

Test No.	Ferrofluid depth, mm	Ferrofluid density, gm/cc	Nonmagnetic medium	Density of nonmagnetic medium, gm/cc	Critical magnetic field, B_c, gauss	Critical length, ℓ_c, mm	Comments
1	18	1.100	Air	0.001	463	12	Hexagonal array changes to square array at B = 655 gauss
2	18	1.100	Water	.998	148	~25	Container too small to display complete hexagonal array
3	16	1.206	Air	.001	317	10	37 spikes
4	16	1.206	Water	.998	155	21	ℓ_c measured at B = 167 gauss. Water depth = 25 mm
5	18	1.308	Air	.001	249	10	Very abrupt transition (± 1 gauss). ℓ_c was invariant to increase of field. Full coverage at B = 270 gauss
6	18	1.308	Water	.998	145[b]	17[b]	Central spike plus six others in perfect hexagon
7	20	1.476	Air	.001	181	9.5	54 spikes at full coverage
8	20	1.476	Water	.998	126	14	Very abrupt transition

[a]G-21 ferrofluid.

[b]No change after two days of equilibration.

TABLE 53. – EXAMINATION OF THE CONSTANCY OF THE CONVERSION

ρ, gm/cc	ϵ_D, %[a]	M_s, gauss	$\epsilon_D M_{ss}$[b]	$\frac{M_s}{\epsilon M_{ss}}$, % = Conversion
1.476	16.3	602	923	65.5
1.309	12.3	459	697	65.8
1.206	9.86	359	558	64.3
1.100	7.33	264	415	63.6

[a] $\epsilon_D = \frac{\rho - \rho_L}{\rho_s - \rho_L}$

ρ_L = 0.792 (kerosene)

ρ_s = 5.0 (magnetite)

[b] M_{ss} = 5660 gauss (magnetite)

DATE 53

is theoretically independent of γ. This is shown from combination of equations (109) and the expression for B_c which follows equation (110).

$$\frac{B_c^2}{\ell_c} = f(\mu) \frac{\sqrt{3}}{2\pi} g(\rho_1 - \rho_2) \tag{111}$$

where

$$f(\mu) = \frac{\mu(1+\mu)}{(\mu-1)^2}$$

This expression was used to compute theoretical values of (B_c^2 / ℓ_c) in table 54. The magnetization curves of the fluids were determined by the search coil technique using a cylindrical sample having a four-to-one length-to-diameter ratio. Consideration of demagnetization factors for this shape revealed that the correction to the applied field was only on the order of 3 percent and this was ignored. Figure 66 presents the measured magnetization curves. These curves are not linear in the experimental region. To obtain values of r for the analysis a chord slope was chosen which corresponds to (1 + M/H) where the values of M and H are found on the magnetization curve where $(M + H) = B_c$. To find these points, lines of constant B were superposed on the graph of the figure.

Table 54 presents the comparison with theory. It is seen that the agreement is reasonably good in all cases (+19%, -18%).

Finally, it is noted that equation (109) may be used to estimate values of surface and interfacial tension. Solving the equation for the tension gives,

$$\gamma = \frac{3\ell_c^2}{16\pi^2} g(\rho_1 - \rho_2) \tag{112}$$

Calculated values are listed in table 55. Surface and interfacial tensions of the various fluids were independently determined with a Cenco-Du Nouy tensiometer with the values in general agreement to those derived from the observation of stability. These values are listed in table 55. As an additional check on the work the surface and interfacial tensions of the ferrofluid of test 1 were independently determined by the drop-weight method in which liquid forms drops which fall off the end of a capillary tube; other determinations were done with the ring technique using a Du Nouy tensiometer. The values of tension determined by drop-weight technique are of good precision and so are the tensiometer values although the observed disparity between the two indicates the difficulty of obtaining an absolute value. Both the stability experiment and the conventional measurement of interfacial tension

Figure 66. – Magnetization Curves of Magnetic Fluid Utilized in the Stability Experiments (G-21 Material)

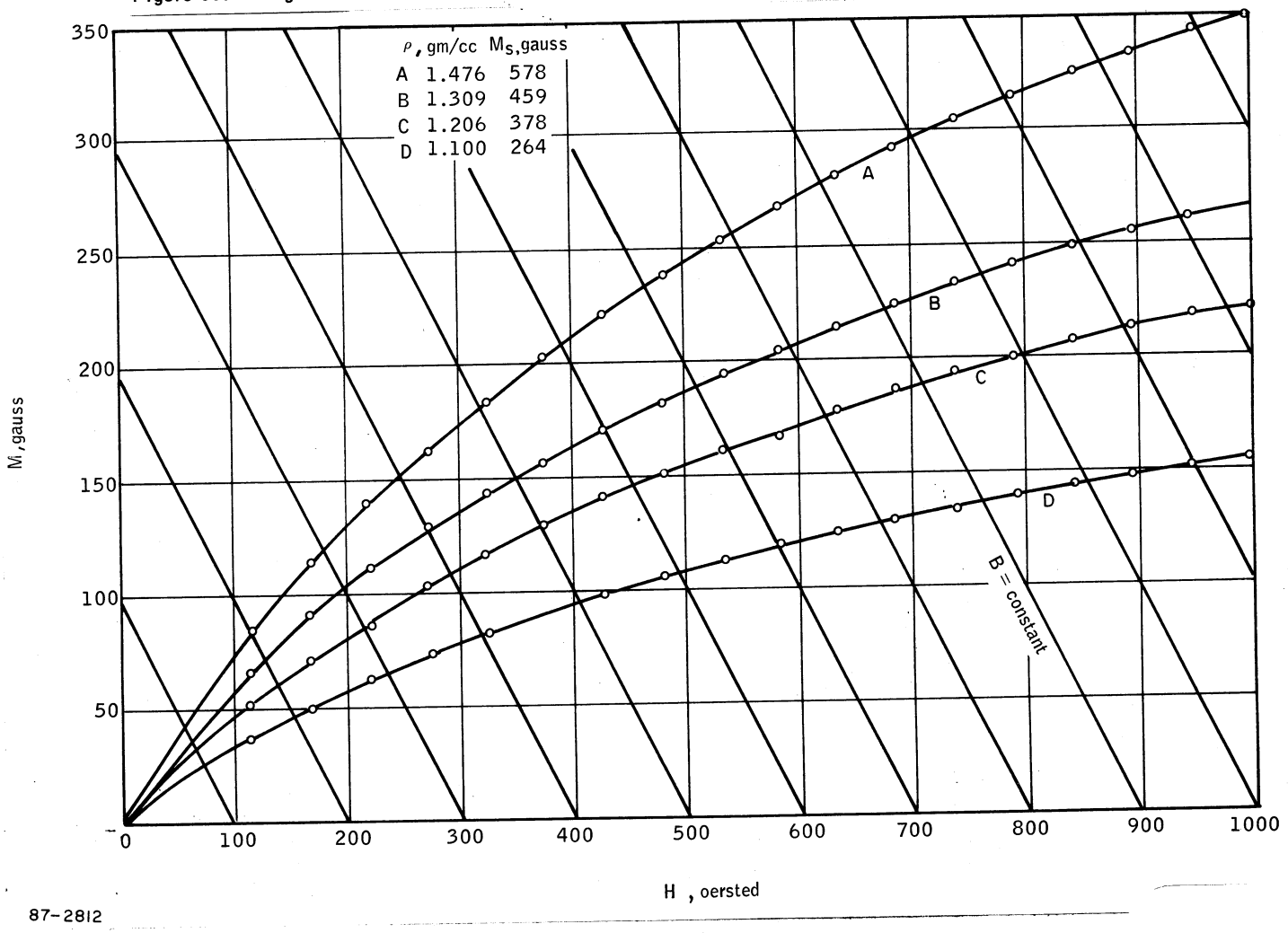

87-2812

TABLE 54. – TREATMENT OF DATA OF TABLE 52 AND COMPARISON WITH THEORY

Test No.	$\Delta\rho$, gm/cc	M_c, gauss	μ	(B^2/ℓ) theory	(B^2/ℓ) exptl,	Error, %
2	0.102	36	1.32	0.0104 gauss^2/cm	0.0088 gauss^2/cm	+15
4	.208	48	1.45	.0124	.0114	+8
6	.310	54	1.61	.0121	.0124	-2
8	.478	52	1.80	.0130	.0113	+15
1	1.099	90	1.23	.192	.179	+7
3	1.205	92	1.41	.0820	.100	-8
5	1.307	88	1.53	.0623	.062	0
7	1.475	80	1.77	.0425	.0345	+19

TABLE 5a

TABLE 55. – ESTIMATION OF TENSION, γ, FROM THE STABILITY EXPERIMENTS

Test No.	Contact medium	$\Delta\rho$, gm/cc	ℓ_c, cm	$\gamma_{stability}$	$\gamma_{tensiometer}$ [b]	$\gamma_{drop\text{-}weight}$ [c]
2	Water	0.102	~2.5	a	17.0	18.6
4	Water	.208	2.1	17	16.9	----
6	Water	.310	1.7	17	17.3	----
8	Water	.478	1.4	17.5	17.9	----
1	Air	1.099	1.2	29.5	27.5	22.5
3	Air	1.205	1.0	22.5	27.6	----
5	Air	1.307	1.0	24	27.6	----
7	Air	1.475	.95	25	27.6	----

[a] Doubtful value due to uncertainty in ℓ_c (~12 dyne/cm).

[b] Average of five determinations; standard deviation $\sigma < 0.1$.

[c] Average of three determinations; standard deviation $\sigma < 0.2$.

are in accord, however, that the tension is reduced in contact with water compared to contact with air.

Error Analysis. - Assuming the theory is correct, one must still admit to imprecision in its application. This, in turn, is due to imprecision in the variables used in making calculations based on a theoretical formula. The formula for B_c^2/ℓ_c may be easily analyzed for sensitivity to errors through the use of logarithmic differentiation. Assuming g, ρ_1, and ρ_2 are known exactly so that the major source of error is in the value of μ this gives

$$\frac{d(B_c^2/\ell_c)}{(B_c^2/\ell_c)} = g(\mu)\, d\mu/\mu$$

$$g(\mu) = (1 + 3\mu)/(1 - \mu^2)$$

which shows that the errors are magnified more so, the closer μ is to unity. The lowest value of μ occurred in Test No. 1 where $\mu = 1.23$ giving $g(\mu) = -9.2$. Now if the value of permeability scales directly with the magnetization-at-saturation, then

$$d\mu/\mu = dM/M \qquad (113)$$

Table 53 provides information on the accuracy of the values of M, see the last column. Since the fluids used in all the tests were simply different dilutions of the same particles in a given carrier fluid, the "conversion" should be invariant. Actually, due to uncertainty in the reported measurement of magnetization, the computed values of conversion produce a standard deviation of 2.1 percent. Thus the computations of B_c^2/ℓ_c are known only to about 9.2 (2.1) = 19 percent.

For the computations of surface and interfacial tensions of table 55, it may be shown in the same way that

$$d\gamma/\gamma = 2\, d\ell_c/\ell_c \qquad (114)$$

The values ℓ_c were measured with an estimated error of 5 percent so that the percentage error in tension is 10 percent.

In view of both the foregoing it appears that the theoretical predictions have proven correct within the accuracy of the data.

CONCLUSION

The main body of this report described the means for synthesis and modification of ferrofluids and presented the results of physical measurement. The observations and data were utilized to draw an improved mechanistic picture of the ferrofluid and then various aspects of macroscopic behavior were studied in which the fluid responds as a homogeneous medium. At this point it is in order to summarize the current state-of-art and indicate the relationship to foreseeable ultimate limits.

Figure 67 illustrates, in terms of the body forces generated, the current state-of-art as well as some theoretical limits upon the magnetic strength of a ferrofluid. The figure was computed from the relationship

$$\text{force/volume} = 1/4\pi \, \epsilon M_{ss} \, dH/ds \text{ (cgs units)} \tag{115}$$

in which M_{ss} is the saturation ferric induction of the solid, magnetic constituent of the colloid (expressed in gauss); s denotes distance and other quantities are identified on the figure.

Other data and considerations utilized in the construction of figure 67 are as follows. Considering ferrofluids constituted of magnetite (Fe_3O_4) as the magnetic component the saturation ferric induction is 5660 gauss. The maximum volumetric loading that has been obtained is 20 percent or $\epsilon = 0.2$. The known limit upon a solid's magnetization is 24 600 gauss corresponding to the alloy of iron with 35-percent cobalt (iron has a magnetization of 21 580 gauss at 20° C). The theoretical limit chosen for packing fraction of $\epsilon = 0.74$ corresponds to close-packed spheres. If needle geometry is assumed, or if a hierarchy of smaller particles are assumed to occupy the interstices, then the upper limit for packing fraction may approach unity so in this respect figure 67 is conservative in its choice of maximum limit for ϵ. As the figure emphasizes, the most magnetic ferrofluid produced so far has a ferric induction of about 1000 gauss, while the theoretical limit subject to the assumptions stated above is in excess of 20 000 gauss.

Figure 67 also illustrates that the body force developed in the possible magnetic liquids is comparable to a number of forces from technology. As examples, elemental liquid mercury experiences a body force of 843 lb/ft^3 under normal Earth gravitational attraction and this force is exceeded in current fluids. In the case of a plasma thrustor, an MPD (magnetoplasmadynamic) engine is considered where typically the current density is 10^3 amperes per square centimeter (10^7 amp/m^2) and magnetic field is 2000 gauss (0.2 W/m^2), so that specific force is $0.2 \times 10^7 = 2 \times 10^6$ Newtons/m^3,

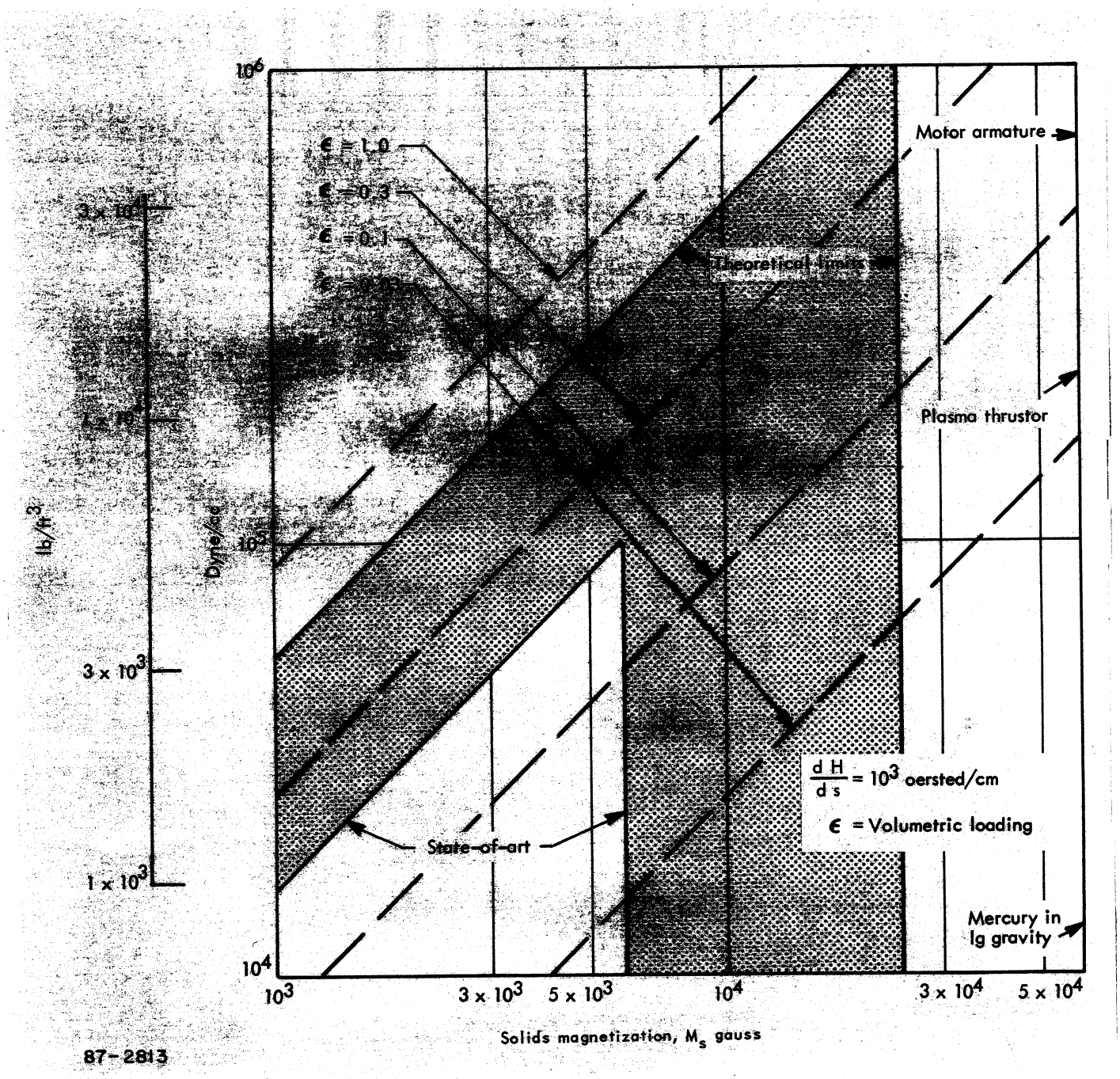

Figure 67. – Body Force in Magnetic Liquids as a Function of Solids Magnetization and Loading with Illustration of Current State-of-Art and Theoretical Limits

or 2×10^5 dyne/cm^3. The specific force on the rotor of an electric motor taken as 8×10^5 dyne/cm^3 is reckoned from a field gradient of 10^3 oersted/cm acting upon iron that is nearly saturated. These latter two examples illustrate forces beyond those presently obtained in the magnetic liquid but within the realm of theoretical possibility.

Further gain in the strength of magnetic fluid is to be obtained from increasing the packing fraction ϵ and increasing the solids' magnetization, M. Oxidation in the presence of air poses a severe problem to the use of elemental ferromagnetic particles while the ferrite materials employed in these studies are representative of the maximum magnetization available from non metallic materials. Increasing the packing fraction requires principally the ability to minimize the volume occupied by an adsorbed monomolecular layer of dispersing agent, and it seems likely that more immediate progress will result from work in this direction.

From time to time reports are circulated of the existence of a true ferromagnetic fluid consisting of other than particles suspended in a liquid. Such a material would be of tremendous scientific and technological interest. There it would be well to distinguish between a true solution and a pure fluid which is ferromagnetic. There is no sharp dividing line between a true solution and the ultrafine colloidal dispersions produced in this work. For example, the dry powder resulting from evaporation of solvent from oleic acid coated magnetite particles dispersed in heptane is observed to spontaneously redisperse in fresh solvent. A pure fluid should evaporate with no residue.

Although ferromagnetism is often associated only with solid materials having an ordered structure, it is of interest to note a statement by Gubanov (ref. 29):

"All theoretical and experimental investigations on ferromagnetism that have been treated in the literature refer to crystalline bodies. Ferromagnetism, however, is caused by exchange, interaction for the most part, between neighboring atoms, and it would seem there is no need to have a rigorous periodicity in the distribution of atoms. Liquid ferromagnetics have evidently never been observed, only on account of the melting temperature for ferromagnetics lying above the Curie point, but amorphous or vitreous substances can exist at temperatures low enough that when they contain the right atoms we have reason to believe they will be ferromagnetic!"

The challenge to the materials scientist is evident.

LIST OF REFERENCES

1. Rosensweig, R.E.; Nestor, J.W.; and Timmins, R.S.: Proceedings of the Symposium on Materials Associated with Direct Energy Conversion. A.I.Ch.E. - I.Chem.E. Meeting, London, 1965, Symposium Series No. 5, pp. 104-118. Published by the Institution of Chemical Engineers, 16 Belgrave Square, London S.W.1.

2. Papell, S.S., U.S. Patent 3,215,572., 2 November 1965

3. Papell, S.S.; and Faber, O.C.: Zero- and Reduced-Gravity Simulation On A Magnetic -Colloid Pool-Boiling System. NASA TN D-3288, February 1966.

4. Melcher, J.R.: Field-Coupled Surface Waves. M.I.T. Press, Cambridge, Massachusetts, 1963.

5. Luborsky, F.E.: The Formation of Elongated Iron and Iron-Cobalt Particles by Electrodeposition Into Mercury in Ultrafine Particles. W.E. Kuhn ed., John Wiley & Sons, Inc., New York, 1963, pp. 236-261.

6. Falk, R.B.: A Current Review of Lodex Permanent Magnet Technology. Journal of Applied Physics, Vol. 37, No. 3, 1 March 1966, pp. 1108-1112.

7. Resler, E.L., Jr.; and Rosensweig, R.E.: Magnetocaloric Power. AIAA Journal, Vol. 2, 1964, pp. 1418-1422.

8. Joule, J.P.: J. Chem. Soc., London, 16, 1863, p. 378.

9. Duncan, B.C.: Surface Chemistry in the System Iron-Mercury. Ph.D. Thesis in Chemistry, State College of Washington, 1957. Available through University Microfilms, Ann Arbor, Michigan (publication No. 25,052).

10. Flindt, M.: U.S. Patent 3,130,040. 1964.

11. Bates, L.F.; and Baker, C.J.W.: Proc. Phys. Soc., Vol. 52, 1940, p. 425.

12. Herdan, G.: Small Particle Statistics. 2nd Edition, Academic Press, Inc., New York, 1960, p. 84.

LIST OF REFERENCES (Cont'd)

13. Dawson, P.T.; and Haydon, D.A.: Kolloid Z., 1965, pp. 133-138.

14. Guilland, C.; and Creveaux, M.: Comptes Rendus. Acad. Sciences, Vol. 230, 1950, p. 1458. See: Handbook of Microwave Ferrite Materials. Wilhelm H. von Aulock, ed., Academic Press, New York, 1965.

15. Kruyt, M.R.: Colloid Science. Vol. I, Elsevier Publishing Co., New York, 1952, p. 351.

16. Slattery, J.C.: Analysis of the Cone-Plate Viscometers. Journal of Colloid Science, Vol. 16, No. 4, August 1961, pp. 431-437.

17. McKennel, R.: Cone-Plate Viscometer, Comparison with Coaxial Cylinder Viscometer. Analytical Chemistry, Vol. 28, November 1956, pp. 1710-1714.

18. Doyle, W.P.; and Ellison, A.H.: Advances in Chemistry. Series 43, 1964, pp. 268-274.

19. Small, P.S.: J. Appl. Chem. Vol. 3, 1953, p. 71.

20. Little, R.C.; and Singleterry, C.R.: J. Phys. Chem., Vol. 68, 1964, p. 3460.

21. Crowl, V.T.: Research Association of British Paint, Colour, and Varnish Manufacturers. Bulletin 64, Vol. 13, No. 1, March 1962.

22. Garrett, R.R.; and Lawrence, R.D.: Adhesive Age. October 1966, pp. 22-26.

23. Dintenfass, L.: Kolloid Z. Vol. 155, 1957, p. 121.

24. Koelmans, H.; and Overbeek, J.: Discussions of the Faraday Society. Vol. 18, Ch.G., 1954, p. 52.

25. Harkins, W.; and Brown, F.E.: J. Am. Chem. Soc., 1919, p. 499.

26. International Critical Tables, Vol. 2, 1933, p. 146.

27. Stratton, J.A.: Electromagnetic Theory. McGraw-Hill Book Company, Inc., New York, 1941, p. 145.

28. Hakim, S.S.; and Higham, J.B.: An Experimental Determination of the Excess Pressure Produced in a Liquid Dielectric by an Electric Field. Proc. Phys. Soc., Vol. 80, 1962, p. 190.

29. Gubanov, A.I.: Quasi-Classical Theory of Amorphous Ferromagnetics. Soviet Physics, Solid State, Vol. 2, 1960, p. 468. For a reduction to practice see: Mader, S.; and Novick, A.S.: Metastable Co-Au Alloys: Example of an Amorphous Ferromagnet. Applied Physics Letters, August 1965, p. 57.

30. Patton, T.C.: Paint Flow and Pigment Dispersion. Interscience Publishing Company, Inc., New York, 1964.

BIBLIOGRAPHY

A number of other publications have resulted during the course of this work and are cited below with a few comments relating to each.

Rosensweig, R.E.: Magnetic Fluids. International Science and Technology, July 1966. Provides an overview of the entire field of ferromagnetic fluid technology, covering nature of the fluid, behavior in applied magnetic fields, and potential for application in devices, processes, and scientific studies.

Rosensweig, R.E.: Buoyancy and Stable Levitation of a Magnetic Body Immersed in a Magnetizable Fluid. Nature, Vol. 210, No. 5036, 7 May 1966, pp. 613-614. Stresses generated within a magnetic fluid in response to a source of magnetic field interior to the fluid are demonstrated by the levitation of a body whose density is greater than that of the fluid.

Rosensweig,R.E.: Fluidmagnetic Buoyancy. AIAA Journal, Vol. 4, October 1966, No. 10, pp. 1752-1758. Quantitative treatment of levitation phenomena and comparison with experiment.

Neuringer, J.L.: Magnetic Effects on the Diffusion of Ferromagnetic Colloidal Particles Dispersed in a Current-Carrying Fluid Medium. The Physical Review, Vol. 145, No. 1, 6 May 1966, pp. 64-71. Bears on the question regarding uniformity of a ferrofluid in the presence of a magnetic field and illustrates in a quantitative fashion the establishment of a colloid-particle concentration gradient that serves to maintain an equilibrium. A

curious prediction is the migration of magnetic particles from a region of high field to a region of lower field, opposite the normal trend. The situation arises in the conduction of current through a hypothetical ferrofluid possessing electrical conductivity and can be understood physically in terms of forces on the ends of elementary dipoles, represented by the particles, in the presence of a purely azimuthal field.

Neuringer, J. L.: Some Viscous Flows of a Saturated Ferrofluid Under the Combined Influence of Thermal and Magnetic Field Gradients. Int. J. Non-Linear Mechanics, Vol. 1, 1966, pp. 123-137. The analysis develops analytical techniques for treating problems encountered in the boundary layer flows of ferromagnetic liquids. The magnetic moment of the fluid is taken as temperature dependent and this couples the flow field to the thermal field.

Rosensweig, R. E.: Litte, R. and Gelb, A., Magnetic Fluid Support Technique and Application to Accelerometers. To appear in Proceedings of the Symposium on Unconventional Inertial Sensors, Fourth Symposium (Washington, D. C.), 1966. The ferrohydrodynamic levitation phenomenon is proposed in the form of a slide bearing characterized by complete freedom from sticking. The bearing is analyzed in the form of an integrating accelerometer.